A CRITICAL EVALUATION OF WIND TURBINE TECHNOLOGY, LEADING TO THE DEVELOPMENT OF 20MW MULTI ROTOR SYSTEMS.

Michael J. Branney

2017

For the Degree of

Doctor of Philosophy

Centre for Doctoral Training in Wind Energy Systems

Department of Electronic and Electrical Engineering

University of Strathclyde

Signed:

Date:

Foreword

The following thesis presents the culmination of nearly five years of work into novel wind energy conversion systems and specifically the multi rotor system. This investigation and subsequent output would not have been possible without the continued support, patience and pearls of wisdom provided by Peter Jamieson and Professor Bill Leithead, both truly experts in the field.

Special thanks goes also to Robert Harries and David Witcher (formerly of GL Garrad Hassan) for their help and assistance through the loads aspect of this project. Thanks also goes to Chris Hornzee-Jones (Aerotrope) for his early work on the multi rotor system which provided a very solid basis for further development.

This work was also complemented late on by the work of both Takis Chaviaropoulos (CRES) and Spyros Voutsinas (NTU Athens) through their development of several aspects of the multi rotor concept under the Innwind Project which provided excellent supporting material for the development of this project.

I gratefully acknowledge the funding for this research provided by the Engineering and Physical Sciences Research Council (EPSRC) grant number: EP/G037728/1.

Lastly I would like to thank my good friends and colleagues from the DTC (especially the Dolphins.) for making my last years at University so enjoyable.

This is for Claire. For helping me get through thick and thin over the last 5 years and being a constant presence at my side.

Abstract

The development of the conventional wind turbine from conception to modern day has been based on evolutionary and incremental design changes. Current existing commercial horizontal axis machines have yet to breach the 6MW power rating without significant cost penalties. The reason for this is primarily due to the negative effects of the square cubed law which shows that any increase in turbine diameter will lead to a cubic increase in turbine mass for only a square increase in power output. Unfortunately, this universal truth can only be delayed and not ignored by advances in wind energy systems and it is therefore probable that conventional machines are nearing their power rating limits.

This project is focused firstly on a concerted review and evaluation of the wind energy design space followed by a more detailed study of those systems which theoretically should scale well with size and which may allow the wind industry to move to individual ratings of 10MW and beyond. Multi rotor systems with ratings of 20MW and above have been identified as serious contenders when considering cost of energy - the reduction of which, is a primary objective of the wind industry. Detailed cost analysis, conducted after extensive development of the multi rotor concept has found that multi rotors can provide cost of energy at around 85% of conventional 10MW single rotor machines and around 82% of a conventional 20MW machine in a far-offshore environment.

More specifically, this thesis details the development of the multi rotor system from initial concept, considering all the main engineering points and presenting them in a useful way to alleviate concerns and pioneer the way for future research into the concept.

CONTENTS

NOMENCLATURE

Acronyms

AC – Alternating Current

BTU - British Thermal Unit

CoE - Cost of Energy

CB – Circuit Breaker

CHS – Circular Hollow Section

DLC – Deterministic Load Case

DC – Direct Current

DFIG – Double Fed Induction Generator

ECD – Extreme Gust with Change of Direction

ETM – extreme turbulence model

EOG – Extreme Operating Gust

EWM – Extreme Wind Model

EWEA - European Wind Energy Academy

EU - European Union

GCT – Gravity Compression Turbine

HAWT - Horizontal Axis Wind Turbine

IEC – International Electrotechnical Commission

kW – kilo Watt

LIDAR – LIght Detection and Ranging.

MRS – Multi Rotor System

MTTR – Mean Time to Repair

MW – Mega Watt

mW – milli Watt

NTM – normal turbulence model

NWP – Normal Wind Profile.

O&M – Operation and Maintenance

p.d.f – Probability Density Function

UK - United Kingdom

UoS – University of Strathclyde

VAWT - Vertical Axis Wind Turbine

VSC – Voltage Source Controller

W – Watt

WEC – Wind Energy Conversion

Variables

Latin

A – Swept area (m^2)

A - abnormal safety factor (1.1)

C_P – Coefficient of Power *(dimensionless)*

C – Specific Heat Capacity (J/kg.K)

C_L – Coefficient of Lift *(dimensionless)*

C_D – Coefficient of Drag *(dimensionless)*

F - Force (N)

F_x – Force in X-direction (N)

F_y – Force in y-direction (N)

F_z – Force in z-direction (N)

I – Current (A)

M – Mass (kg)

N - normal safety factor (1.35)

P – Power (W)

R – Resistance (Ω)

R – Radius (m)

T – Temperature (K)

U – Incident wind velocity (m/s)

U - ultimate load (N)

V – *Voltage (V)*

Z – Height (m)

Z_0 – Surface Roughness Length (m)

Greek

$\acute{\alpha}$ – Angle of attack (degrees)

ρ – density of fluid (kg/m^3)

Ω – *Rotational Speed (rad/s)*

σ - *Rotor Solidity (dimensionless)*

σ^2 - *Variance (dimensionless)*

π – Pi (dimensionless)

λ – Tip speed ratio (dimensionless)

T – Torque (N/m)

ω - Rotor speed (rad/s)

Φ – Diameter (m)

CHAPTER I - INTRODUCTION

1.1 INTRODUCTION

The objective at the beginning of this thesis was to identify whether or not the conventional single rotor wind turbine scales well beyond current industry trends (>10MW). The trend to increase individual unit ratings is pushed by a desire to lower cost of energy (CoE) in an offshore environment – which is increasingly becoming the de facto for new wind farms.

Material limits are increasingly restricting the once rapid growth of individual wind turbine ratings with current trends indicating a plateau in the region of 7-10MW. While technology advances had previously hidden the effects of the 'square cubed' law - which relates to increases of mass as the cube of diameter – this is no longer the case. Modern blades are increasingly constructed from carbon fibre to achieve manageable weight/strength ratios and the cost of wind turbine plant is increasing, negating many of the advantages of large single units in CoE.

Logically, the same square cubed law which penalizes larger machines should benefit smaller machines when applying the same "advanced" technologies. It is conceivable that wind energy conversion (WEC) devices that previously fell by the way-side due to immature technology or a lack of research may once again be well placed to exploit the desire for a large power output at a single maintenance site.

The objective of this research was to conduct a broad technology review which encompasses a very wide variety of different wind energy conversion concepts from electro-hydrodynamic machines to lighter than air (airborne) rotors. From this, a single concept was identified as a competitive alternative to the conventional horizontal axis turbine from a CoE perspective. This concept is the multi rotor system.

1.2 SYNOPSIS

The bulk of the research into multi rotor systems and presented in this thesis is new and novel – with very little previous research on the concept beyond the initial theory having been conducted. It is expected that this research will pave the way for future development and research into the concept. In regards to multi rotors this thesis addresses the following issues by chapter:

A general introduction to the wind industry and the need for energy is presented in Chapter 2 along with more justification as to why an evaluation of the wind energy design space is required.

Chapter 3 makes a detailed evaluation of a whole host of different types of wind energy conversion devices. This literature review was very broad in scope and considered almost any type of device for which information was publically available or which has seen published work. The most promising designs and those for which the most information is available were evaluated in more depth to provide a solid comparative study. Numerous parameters are compared such as cost/weight, cost/power, weight/power and efficiency are considered. From this it is clear that the conventional rotor far exceeds any of the competitors in almost all the metrics.

This idea is built on in Chapter 4, where the multi rotor concept is first introduced. The multi rotor system takes advantage of all the metrics of the conventional rotor but instead of having multiple sites, locates all the turbines on a single structure. This avoids the punitive square cubed law for rotor scaling allowing large unit ratings at a single maintenance site – an essential component of keeping CoE low in an offshore environment. In addition, it introduces the additional benefits such as increased redundancy, more options for power optimisation/load alleviations and additional energy capture potential at the expense of a costlier structure.

Chapter 5 tackles the concept in more depth in order to arrive at a notional design that is feasible based on today's technology. The basis of the work is carried out with respect to the IEC-61400 standards for the design of wind turbine systems in order to

provide a real world basis for the concept. The objective of this part of the project was to arrive at a design that minimised both weight and cost while adhering to strict structural and loading requirements so as to not cancel out any cost saving benefits achieved through other means. These loading experiments also highlight a very interesting area of multi rotor development which allows such systems to be operated in such a way to minimize operational and fatigue loading through a combination of both control and electrical layout.

The electrical layout and one option for load alleviation is further developed in Chapter 6. This chapter attempts to lay the ground work for how each turbine would be interconnected, making suggestions as to transformer location, protection systems, cable redundancy and collection voltages. The consideration once again being to minimize cost and also structural weight.

Chapter 7 briefly revisits the structural design on the basis of the previous work conducted and new external work conducted as part of the European partnership, Innwind EU project. The structural design is not much changed and only further refined at this stage.

Lastly, taking the full multi rotor system and considering such aspects such as an improved maintenance regime, economies of scale and so on, the multi rotor is costed in comparison to single rotors of equivalent rating: 5MW, 10MW, 20MW in Chapter 8. The findings are that the multi rotor system can make significant mass and likely significant cost savings in comparison to conventional machines of equivalent rating and can do so without the years of research and development or advanced manufacturing methods those concepts are privy too.

1.3 ORIGINAL CONTRIBUTIONS

The original work presented in this thesis to which the author made significant contribution to is as follows:

Chapter 3: The consolidation of a large number of different devices from a wide variety of different sources (3.4-3.7). The taxonomy of these devices into a simplified classification system for easy referencing (3.8). An in-depth parametric analysis of 5 different systems including an update of the concepts based on current best available technology.

Chapter 4: The development of scaling laws and economies of scale when dealing with a 20MW multi rotor based on 444kW machines (4.2). The initial 45 rotor, 20MW multi rotor concept its layout and configuration (4.4). The downscaling of a pitch-regulated 444kW machine model for Bladed from a standard 5MW design (4.4). The modelling of a 45-rotor, multi-member system in Bladed and subsequent structural design (4.5).

Chapter 5: The application of the IEC-61400 standard in relation to multi rotor systems for which they are not designed (5.3). A detailed analysis and simulation of the MRS in a wide variety of environmental conditions in association with these standards (5.4 & 5.5). The strategies for load alleviation in the multi rotor system related to staged shutdowns (5.6). The strategy for yaw alleviation and rotor thrust yawing available only to multi rotor systems. The identification of the critical design load case in DLC 2.3 for the MRS (5.7). The identification of the fact that the multi rotor is well suited to turbulent wind while the large single rotor is not and which is therefore the opposite of normal convention (5.7).

Chapter 6: The parametric analysis of the optimum cabling routing system for a 45-rotor MRS (6.2). The negative effect of clustering on power capture

(6.3). A cost analysis of different types of collector array and power systems configuration including protection systems (6.4).

Chapter 7: The analysis of the effects of the use of low resolution wind files on fatigue calculations in comparison to high resolution wind files – a hardware limitation that may have proved problematic (7.2). Re-optimisation of the MRS structure for optimum weight to strength ratios (7.3)

Chapter 8: A study of the effects of different wind profiles on the energy capture in the MRS, for example shear (8.1)

Chapter 9: An investigation into maintenance strategy for O&M minimization for the MRS using existing models (9.5). A detailed cost analysis of the multi rotor system, arriving at representative costs, energy capture estimates and CoE of the MRS in comparison to equivalently rated single rotor systems (9.6).

In addition, the conclusions drawn throughout this work are entirely those of the author.

1.4 LIST OF PUBLICATIONS

Posters

- **Branney, M. and Jamieson, P.** (2013) *Multi rotors as a Means to Reduce Design Driving Loads of 20MW Wind Energy Systems.* European Wind Energy Academy Conference 2013. (Vienna, Austria)

Conference Articles

- **Branney, M. and Jamieson, P.** (2012) *Multi rotors: A Solution to 20MW and Beyond.* Deepwind 2012 (Trondheim, Norway).
- **Branney, M. and Jamieson, P.** (2013) *Structural Considerations of a 20MW Multi rotor Wind Energy System.* Making Torque from Wind 2013. (Oldenheim, Germany).
- **Jamieson, P., Branney, M., et.al.** (2014) *The Structural Design and Preliminary Aerodynamic Evaluation of a Multi rotor System as a Solution for Offshore Systems of 20MW or more Unit Capacity.* European Wind Energy Academy Conference 2014. (Barcelona)

Reports

- **Innwind.EU** (2014) *Innovative Turbine Concepts - Multi rotor System.* Deliverable Report for Innwind.EU Task 1.33.

Other publications stemming from this work

- **Jamieson, P., Chaviaropoulos, P. K., and Voutsinas, S.** (2015) *Large Scale Offshore Wind Energy Systems, the Multi rotor Solution.* EWEA Offshore 2015.

CHAPTER II – GENERAL BACKGROUND

2.1 THE NEED FOR ENERGY

Humans consume more energy today than they ever have in the history of mankind. World primary energy usage, as tracked by the World Bank, currently runs at 1835 kg of oil equivalent per capita per annum [1]. There is no doubt that as the world's population increases and developing countries continue to move towards more energy demanding economies that this level will continue to rise relatively unchecked. Indeed, the U.S Department of Energy and Energy Information Administration predict that the yearly energy usage will have doubled from 355 quadrillion Btu (1990 levels) to 739 quadrillion Btu by 2035 [2]. These values are inconceivable and lend credence to the suggestion that most of the world's Governments can only react to ever-increasing energy demands rather than plan for them.

The majority of consumed energy is provided by non-renewable sources such as fossil fuels: coal, oil and gas. In fact, although alternative sources of energy (including nuclear and renewables) are steadily increasing their share of the energy market each year they still accounted for less than 20% of total energy production by end of 2010 [3]. Yet there can be no doubt that without increased usage of such alternative sources, the world will face a severe energy crisis by the end of the 21st century.

One of the most promising solutions to the world's energy requirements lies within the wind, a source of power that has been used by humans for millennia almost without thought and which is regenerative, clean and free. There is evidence which suggests that as early as 3500 B.C, wind energy was being utilised by ancient Egyptians in order to propel watercraft along the river Nile and by around 640 A.D the Persians were using something a-kin to a rotating windmill to grind grain [4][5]. These civilisations clearly realised the potential that wind energy had in making a positive change to their society and this fact is no less true today.

2.2 HISTORICAL DEVELOPMENT OF WIND ENERGY

The modern wind energy industry seen today can be traced back to the end of the 19th century and the construction of a 10m high wind turbine in Marykirk, Scotland 1889. This was the first known instance of a wind turbine being used to generate electricity and was built by Professor James Blyth of the former Andersonian Institute in Glasgow. His design was very simple in nature, being described by the engineer as of *"tripod design, with a 33 foot wind shaft, four arms of 13 feet with canvas sails, and a Burgin dynamo driven from the flywheel using a rope"*. It was used to charge a set of batteries and light his small holiday home (the residents of the small town would not accept his offer of free excess electricity for fear that it was "the work of the devil".) [6]. By the beginning of the 20th century the greatest users of wind power were the US Midwest and the Danes (In the UK such power was not considered commercially feasible until the 1960s). By the early 1900s the Danish had in excess of 2000 devices that extracted energy from the wind either to pump water or mill grain and by the beginning of WW1 they had 250 electricity producing wind turbines (half of which were connected to power stations). The largest of these devices had towers standing 24m tall with 4-bladed 23m diameter rotors, though all were sub-100kW rated [7].

Perhaps one of the most significant advances came with the construction of the Smith-Putnam machine in the USA, which was a WW2-era 1.25MW rated horizontal axis wind turbine that attempted to apply all the latest advances in technology from the electrical, aerodynamic, mechanical and metrology fields. Apart from its size (it held the record in terms of rating until the late 80s), it was notable for being made from steel, having full-span pitch control and also flapping blades to reduce loads. This machine was really at the cutting edge of technology, having a C_P value of around 0.4 and which has only recently been matched by modern machine. Unfortunately, it failed in late 1946 due to a catastrophic blade failure caused by blade fatigue (which in hindsight is not surprising.)

Throughout this time, wind energy was never considered a commercially viable product for large scale energy production. Its predominant use was in widely spaced

communities or regions where no main electricity grid existed but where access to electricity was still required. This also meant that that majority of constructions were relatively small affairs using local material and expertise, likely highly inefficient and prone to mechanical failure. Indeed, it was not until the late 1960s and the oil crisis in the 70s and Californian energy dash that concerted work really began on standardising any type of system [8].

2.3 THE 'DANISH CONCEPT'

The first real success story of conventional wind engineering research (and the beginning of modern machines) came in 1956 with the construction of the Gedser wind turbine. The Gedser machine was stall regulated and rated at 200kW, had 3-blades, used an AC Asynchronous generator and made user of innovative centrifugally operated aerodynamic tip brakes to reduce aerodynamic loading in the case of over speed. It managed to run for nearly 11 years without any major maintenance until a bearing failure occurred in the late 1960s. The Gedser machine had finally proven that wind machines could be reliably built and run for longer than a decade - a crucial stepping stone [9].

After this, Danish engineers seemed primarily concerned with the production of scaled-down versions of the Gedser machine – with many designs rated well below 50kW. There was significant interest in the machines both politically and publicly during the 1970s when the energy crisis forced most of the West to consider alternatives to oil. Companies such as Vestas, Nordex, Bonus very quickly became the country leaders and eventually world leaders in wind turbine manufacturing [10].

The Danes and in particular Risø (the Danish research institute) by this point continued to focus on relatively small machines, whereas both the British and the Americans were experimenting on turbines in the MW scale. By focusing on smaller machines, the Danish gave their manufacturers a chance to further perfect and develop the engineering concepts on a smaller scale.

Eventually by 1980, the Danes began experimenting on larger 650kW stall and pitch regulated machines and later 1MW designs (although all were deemed commercially unviable). This stable development process meant that the Danes were well placed to take advantage of the California energy rush. It followed that a large proportion of the turbines built in California were imported from Denmark due to the strong Danish track record of building consistently reliable turbines. This financial windfall ensured that the Danish manufacturers had the economic might and technical know-how to dictate the wind turbine standard for the following two decades [11][12].

2.4 THE PRESENT

During the period 2009-2014, The Siemens 3.6MW pitch regulate variable speed machine was by far the most common rating for UK offshore wind (accounting for over 68% of installed capacity) [12]. The reasons for this are several; a competitive capital cost (driven down by economies of scale), a familiarity and comfortableness operating with a common machine both on an individual and operational basis and the use of a well-developed and understood technology with a good amount of existing operational data.

Individual wind turbine ratings of 7-10MW have been touted since 2014 but these constructions are on a relatively low scale on the European continent. The 2012 European Wind Energy Academy (EWEA) wind energy review [13] found that the average European rating for turbines installed in 2012 was 4MW and that there was no indication that this would rise in the following two years. The average instantaneous wind turbine rated power output in 2012 around Europe was 271MW, which would represent something in the region of 75-100 individual turbine sites typically.

Plotting the ratings of offshore wind farm individual ratings by year (Figure 2.1) shows a plateau in terms of rating. Given that increasing individual power ratings on single site is the single largest contributor to reductions in cost of energy it is likely that wind energy will not see another step change downwards in CoE unless a radical change occurs. This radical change could take the form of a change in design tact,

with a move towards a system better suited for larger individual site ratings (i.e. 20MW) in an offshore environment.

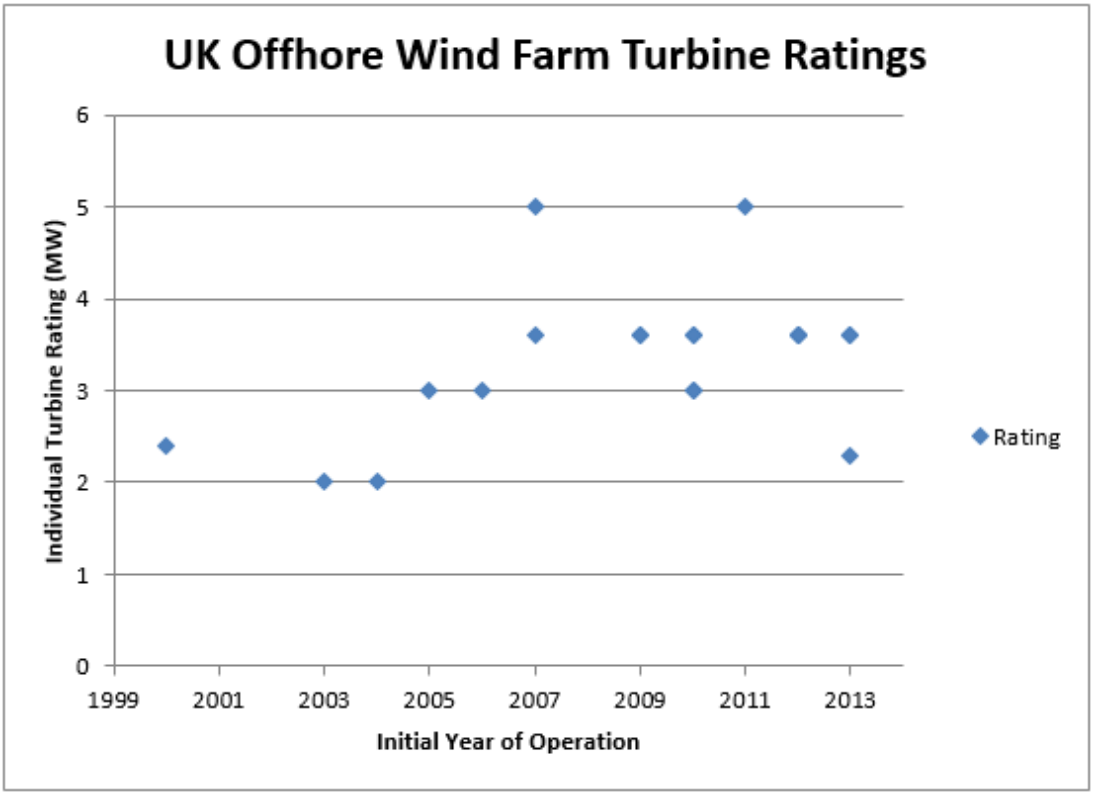

Figure 2.1 - UK Offshore Wind Farm Total Ratings as of June 2014

2.5 REDUCING COST OF ENERGY

One of the overriding objectives of current wind energy research and development is to make wind energy amongst (if not the) most competitive source of renewable energy both onshore and offshore. Current research activities in wind turbine can be categorised under two paths:

1. Incremental innovation, through economies of scale along with improvement manufacturing and installation techniques.
2. Breakthrough innovation, creation of innovative products such as significantly up-scaled turbines.

The ultimate aim is to maximize energy capture potentials by obtaining 20% of EU electricity demand by 2020 and up to 33% of demand by 2030 (up from 5% in 2011) [13]. In order to achieve these targets realistically, wind energy needs to be more

competitive than other renewables and close to fossil fuels in terms of CoE. Part of this commitment is likely to be met by upwards of 150GW of offshore wind by 2030. In order to meet even this relatively small number there are a series of technological challenges, including the up-scaling of wind farms and individual turbines as well as new deployment of electrical infrastructure.

UPWIND is one of the most recent and most advanced projects to ever be conducted for the development of large-scale wind energy conversion devices. The project ultimately led to arguments which support the development of rotors up to 250m in diameter and with individual turbine ratings of 10-20MW [14].

UPWIND requires many enabling technologies:

- Aerodynamic blade control.
- Sectioned/modular blades.
- Use of LIDAR for upwind wind measurement and rotor adaptation.
- Embedded/distributed load sensors, such as Bragg gratings in the blades.
- The ability to dual pitch blades (pitching in two parts) for refined control.
- Advanced modelling and control algorithms.
- Real-time condition monitoring of blades as maintenance tool.
- Use of permanent magnet transversal flux generator.
- New types of thermoplastics blade materials and fibre composition to reduce weight.
- New methods of installing massive tower tops at height.
- New manufacturing techniques to enable blade walls of up to 30cm thickness.

This list is not all inclusive but does give a flavour of the scale of the project and the challenges that lie ahead for any 20MW designer. In addition, many of these technologies are relatively new in the wind industry and have certainly not been tested on wind turbines of this magnitude before. Other technologies are still at the research stage and will take many years to fully develop into a commercial product.

It is more likely that any near/mid-term development of a 20MW single rotor will only be able to utilise some of these technologies and as such will suffer from higher loads which in turn will shift the design parameters. This begs the question as to whether a 20MW wind energy conversion device is feasible at-all within the next 20 years.

This begs the question then

"are there are any systems that can provide for individual site ratings of upwards of 20MW but without an associated technological shift?"

This thesis will attempt to answer this research question. A starting hypothesis is that a wind energy device based on a rotating set of blades will be optimal, but that a single rotor device may not work scale well above 20MW. The thesis develops one potential avenue of research, which is based on the concept of multiple rotors on a single turbine structure.

This so-called *multi rotor* concept consists of a single structure containing multiple rotors of a more manageable size which when combined achieve the same total electrical power output as a larger single rotor. In theory such a structure need not necessarily be of any larger scale than the single rotor but has several major advantages over its single rotor compatriot. The main thing from an energy capture point of view is that the system utilises the proven advantages of rotor systems in increasing the energy density transmitted from the wind to a rotating shaft with as little fuss as possible. At the same time the multi rotor system can benefit from much reduced total mass (as a result of the square cubed power law) and therefore can maintain a very good energy/mass and cost advantage when compared to all the other alternatives.

The multi rotor (in a horizontal configuration) shows the largest amount of promise when considering systems on a scale of 20MW and above. Given that only ground level work has previously been done on this concept it is the objective of the next chapters of this thesis to thoroughly investigate and develop this concept further to

identify whether the system is truly a viable successor to the conventional horizontal wind axis turbine (HAWT) at large scale. The study will have the advantage of being able to be compared to the notional UPWIND design and proposals for 10MW single rotor systems to provide a valid comparison and succinct conclusions as to whether the multi rotor system is an economic and technologically viable solution.

2.6 PhD SCOPE

The development cycle of wind turbine design is not yet complete. Indeed, there have been many important and necessary improvements in manufacturing methods, controller design, power electronics and aerodynamic modelling over the last decade that have enabled modern wind turbines to breach the 5MW mark. However, there is reason to suggest that the Danish concept is beginning to suffer the effects of the square cubed law [12] and that significant increases in size will be prohibitively expensive without substantial changes in design. The focus of this work is to examine this suggestion in detail and to explore what alternatives the wind industry has available to it - the main objective being to discover if any alternative design could offer a route to cheaper cost of energy.

CHAPTER III - A CRITICAL EVAULATION OF THE WIND ENERGY DESIGN SPACE

3.1 EVALUATING THE WIND ENERGY DESIGN SPACE

3.1.1 Hypothesis

Wind extraction devices have been developed over millennium to arrive at the designs of today. Designs have remained relatively unchanged over the last 400 years or so since wind-mill yawed towers were first envisioned - with only incremental changes in the intervening centuries. The reasons for this are multi-fold and not least are due to the rate at which enabling technologies such as power electronics, control and materials have developed. It is apparent from even a very quick search that comparatively little research has been carried out on the design of new types of multi-MW systems this decade outside of UPWIND [14]. Primary research and development has been concerned with short-term economic benefits associated with improving the logistics of moving offshore, adapting the electrical grid and addressing reliability issues.

It is hypothesised that there may have been some technological advancement over previous years which may have made previously unviable wind energy converter concepts viable. It is also hypothesised that some of these concepts may in fact be well suited to multi-MW power ratings and with sufficient technology capable of achieving similar or better power/cost ratios than the conventional HAWT.

To address this hypothesis requires an investigation into the wind energy design space broadly in order to identify those WECS toward further research should be directed. The most promising alternative technology will then be presented and discussed so as to pave the way for further into multi-MW machines. If such a statement cannot yet be proved, or if no new technology currently exists which is ready to step-up to the challenge, then this project will act as proof that current designs are optimum (not just historically convenient) and help illuminate the possible paths that the future wind industry could branch down.

3.1.2 Methodology

The wind energy design space contains a broad spectrum of different engineering concepts, some of which are very traditional in their approach to engineering and others which are not. This makes a concerted evaluation difficult if the goal is a comparison of devices. However, by their nature, every device has some common metrics by which it can be compared. For example; every machine is designed to extract energy from the wind and will do so at various levels of efficiency (C_P), they all have some mass (kg), an occupied volume (m^3), an effective area (m^2) and they all cost considerable amounts of money. It is therefore possible to evaluate devices individually based on their unique parameters but also comparatively based on these metrics and their inter-relationships. This 'parametric' study of the wind energy design space is paramount to the discussion of exactly what constitutes a good wind energy conversion system and also allows for the identification of the concepts which are the most effective wind energy converters.

3.1.3 Key Questions/Points

At the beginning of this research project a small list of questions was posed, which if answered would form the wind energy design space review and ultimately arrive at a single concept which merited further in-depth study. The questions were:

1. Exactly what type of Wind Energy Conversion (WEC) systems have been conceived or postulated and where do they fit into the overall wind energy design space?
2. What are the benefits that each of these alternative technologies provide in the context of the standard turbines of today?
3. Where are each of the technologies currently: patent, prototype, design, market?
4. Is there a limit to the size of the 3-bladed HAWT where it begins to fail to offer any advantage over alternative WECS?
5. If a designer with no knowledge of existing conventions were to build a 20MW wind turbine, what should it look like (i.e. what type of system should it be?).

Would this device scale into other power ratings such as 100kW, 5MW, 10MW and so on.

6. Which novel technologies have been examined in the past and which now merit re-evaluation given the significant advances in the wind energy field in the last decade.
7. What limits exist for each technology and where could problems be foreseen.

3.1.4 Sources

The scope of these questions include all existing wind energy converter systems for which information is publicly available - with the focus shifted away from standard HAWT's to more novel designs. The information was drawn from the usual avenues: websites, journals, conference proceedings, patents, presentations and project reports. The total allocated time for this part of the investigation was 12 months and was concluded with a literature review paper titled "A Parametric Study of Wind Energy Conversion Systems" an abridged version of which is included in this thesis.

3.2 WEC DESIGN

Wind energy conversion systems have more or less developed around a few keys principles and historically convenient designs. These designs were formulated at the lower end of the power spectrum (sub kW scale) and incrementally increased in size over the years through gradual improvements in technology to reach the multi-MW turbines of today. Yet there is some reason to believe that current designs may not actually be optimised for wind energy extraction beyond certain scales. Indeed, there are several commonly used metrics which can be used to show that in theory, current designs should only be scaled so far. Yet despite this fact there is very little concise evidence that shows exactly where this ceiling lies and indeed whether industry is close to reaching it. At present the wind industry is making significant inroads into the development of wind energy conversion systems (WECS) in order to drive the cost of energy down such that it might compete with fossil fuels and hydro. There are many ways in which this may be achieved to one degree or another. A reduction in capital costs and maintenance costs would make significant inroads in the savings

at one end of the spectrum, while better utilisation of the land space and a higher capacity factor per turbine would yield more MW per km^2 and therefore greater revenue at the other.

At the heart of all these optimisation problems lie some very simple relationships.

NOTE: The data set provided in this chapter and from which the graphs are derived is commercially sensitive data provided by GL Garrad Hassan and as such is not referenced.

3.2.1.1 The Power in the Wind

The first and most important relationships are the equations which describes the amount of power in the wind. This first relationship (3.1) is termed the power equation and is accepted as giving the amount of power crossing a thin disc lying incident to the wind [15]

$$P = \frac{1}{2} \cdot \rho \cdot A \cdot U^3 \tag{3.1}$$

where P is the power in the wind (MW), ρ is the density of the wind (kg m^3), A is the swept area of the device (m) and U is the incident wind velocity (m/s) through the disc.

From this relationship, it is clear that the most overriding factor in determining the power available is that of the wind speed (being a cubic term). Thus a wind speed increase by a factor of two would yield eight times the original power. Of course, the wind has both probabilistic and stochastic elements, making it very difficult to predict what speed it will be at any location at any given time. Significant work has been done over the past few decades to map the yearly average wind speeds across the world - such as those given by the Wind Energy Atlas [16]. It is now possible to site a wind turbine in a location where the mean wind speed can be predicted with reasonable confidence over a significant period.

The other critical design consideration is the power which is proportional to the swept area. Consider a rotor which sweeps out a disc shape, the area is proportional to the

square of the radius ($A = \pi \cdot R^2$). Assuming C_P is unchanged, a turbine with radius $5 \times R$ would extract $25 \times R$ power. This is succinctly shown in Figure 3.1, which depicts the power to diameter ratio for a range of existing commercial wind turbines as compiled by GL Garrad Hassan and which confirms that the relationship between rating and diameter in reality is approximately square, with each turbines offset from the trend line a result of variation in C_P.

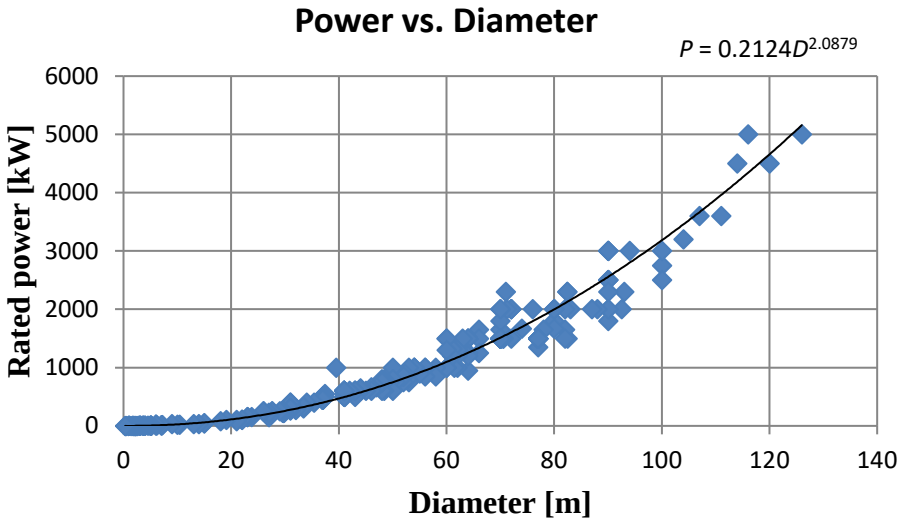

Figure 3.1 - Scaling of Rated Power vs. Diameter

The significance of this concept is that when considering designs which seek to maximise only power, without consideration of other parameters, then larger rotors are favourable. Of course, there are considerably more factors that come into play than just power maximisation when optimising wind turbine designs.

3.2.1.2 Wind Shear

In additional to geographic variations, the wind also has significant variations in the vertical z-axis. Wind shear, as it is known, results in a logarithmic increase in wind speed (with less turbulence) as you move up the z-axis into the atmosphere. Given a specific wind speed a few metres above the ground, the wind speed at some point higher than this can be largely described by the empirical wind shear equation (3.2) [15]:

$$U(Z) = U_{ref} \cdot \frac{ln\left(\frac{Z}{Z_0}\right)}{ln\left(\frac{Z_{ref}}{Z_0}\right)} \tag{3.2}$$

where U is the wind speed (m/s) at the target height Z (m), U_{ref} (m/s) is the reference wind speed at the reference height Z_{ref} (m) and Z_0 is the surface roughness length (m).

In short, using these wind speed relationships, it becomes clear that WECS placed or reaching higher into the sky will experience higher average wind speeds which will help maximise the total available energy. To highlight this, consider the typical wind speed on a windy day at 100m height (measured from the ground) which might be in the region of 10-15m/s gusting to 20m/s on occasion. Around 10km above in the 'Jet Stream', the wind speed might be a constant 35-40m/s. In other words, there is around eight times as much power in the wind at that height [17].

3.2.1.3 Power Coefficient

The third critical relationship, which is dependent on the WEC design, is the power coefficient. The power coefficient (C_p) is a non-dimensionalised ratio which is used as a measure of a wind energy systems ability to extract energy from the wind. It takes the form:

$$C_p = \frac{Power\ Extracted}{Power\ in\ the\ wind} \tag{3.3}$$

This for a standard horizontal axis wind turbine applying actuator disc theory, becomes:

$$C_p = \frac{Power\ Extracted}{\frac{1}{2}\cdot\rho\cdot\pi\cdot R^2\cdot {U_u}^3} \tag{3.4}$$

where: P is the power developed by the rotor (W) and C_p is a dimensionless ratio

For a HAWT, the maximum power coefficient occurs at a tip speed ratio (the ratio of the relative wind speed at blade tip compared to average incident wind sped) for which the axial flow induction factor closely approximates the Betz limit of $\frac{16}{27}$, this corresponds to a maximum C_p of around 0.59 at optimum tip speed ratios [12]. Thus

even the best designed wind turbine can never extract more than 59% of the energy in the wind. Modern turbines are more likely to have a modest C_p value in the 0.35-0.45 region [14].

Non-rotor designs on the other hand can be less succinctly evaluated using this coefficient as normal actuator disc theory is not immediately applicable. This is particularly true for devices which translate over a wide area and which strictly speaking do not occupy the whole area at once. However, it is still possible to apply the same rules to a kite for example, with the area taken to be the frontal cross section that the device passes through.

3.2.1.4 Cut-in, Cut-out and Rated Wind Speeds

The cut-in speed of a wind turbine is the minimum wind speed at which electricity generation can occur and is typically in the region of 3 m/s, although it can be as low as 2 m/s for a very small wind turbine. This lower limit is a result of the minimum aerodynamic torque that must be present on the rotor disc for it to overcome the stiction and friction of the shaft against the bearings and the electrical generator itself.

The cut-out wind speed is the maximum wind speed in which the wind turbine is designed to continue generation. A typical multi-MW HAWT will have a cut-out speed in the 25m/s region, although smaller turbines may be cut-out at speeds much lower than this. The cut-out speed is determined as the wind speed at which the maximum acceptable blade loading under normal operation is reached. Increased blade loading leads to increased out-of-plane bending moments which could cause a blade tip to deflect into the turbine structure or result in blade failure. To avoid blade failure and unnecessary design requirements, at speeds past cut-out the turbine blades are 'feathered' out of the wind (where possible) and 'parked' through the use of both mechanical and/or electro-magnetic brakes.

The rated wind speed is the wind speed at which a WEC achieves rated power. A typical HAWT wind turbine will achieve rated power at around 10-14m/s, although this will vary widely depending on the design and system set-up. When choosing a

wind turbine for a site, a designer will typically try to match the rated wind speed with the peak of the probability density function [18].

3.2.1.5 Rotor Solidity

Comparing different types of WEC solely on C_P does not accurately compare the cost of energy. The power coefficient based on swept area can be particularly misleading when it is applied to devices such as an oscillating element, where the swept area is proportional to the allowed motion as well as to the size of the structure.

The power obtained is dependent on the swept area, yet the cost is only dependent on the size of the structure regardless of its swept area.

The primary power extraction methods can be either lift or drag. As drag is associated with relatively low speeds, large forces and large active areas, it often results in high energy costs therefore it is preferable to focus primarily on lift-based devices.

With aerodynamic lift, power is extracted by lifting elements moving cross-wind. Generally, a lifting element requires a specific solidity (the ratio of active aerofoil / swept area) for a specific C_P and that solidity is tied to relative speed. That is; an element that is travelling at twice the wind speed needs less solidity for the same energy capture as that moving with a relative speed ratio of 1. In-fact, for low solidities and high speed ratios, the required solidity σ is approximately equal to the inverse square speed ratio (3.6):

$$\sigma \propto \frac{1}{\left(\frac{U}{V}\right)^2} \tag{3.6}$$

There is a choice then between a high solidity device with low speed aerofoils that will be less complex and therefore relatively cheap or a low solidity device with high speed aerofoils which requires a more sophisticated design and is relatively costlier.

The cost of conversion to electrical power usually increases with torque and on large machines can account for a significant fraction of the costs. As high solidity machines often result in high torques, it can act to penalise such devices more than an equivalent low solidity device.

3.2.2 The Square Cubed Power Law

The square cubed law (attributed to Galileo) states that scaling an object by a factor, s, in every dimension will increase its volume by s^3 but result in only an s^2 increase in cross-sectional area. The practicalities of this effect mean that a scaled increase in one dimension (in this case R) will result in a cubic increase in mass but, assuming that the same materials are used, only a square increase in the ability of the structure to resist tensile and shear stresses. Thus it becomes apparent that the simple scaling up of a structure will either require significantly more structural material (adding cost) or the requirement for stronger (potentially more expensive) materials. It is somewhat inevitable that the square increase in power output that comes from a scaled increase in rotor diameter will eventually be out-done by a greater than square increase in cost [19][1].

The square cubed law will apply when scaling with similarity, that means preserving:

- Aerodynamic-related stresses and deflections.
- Centrifugal stresses along the rotor
- Aero elastic stability characteristics of the rotor
- Normalised (with the rotational frequency) natural frequencies of the wind turbine

Thus scaling with similarity increases proportionally (with turbine size) all stresses related to self-weight loading. It also affects blade-tower clearance non-linearly (due to deflection of the blades under their own weight) [19].

By avoiding scaling with similarity through the use of different materials or more advanced construction techniques it is possible to 'hide' the cubic increase in mass. This effect is quite prominent when comparing wind turbines over a wide range of

[1] This law is integral to the future development of wind turbines and therefore is at the crux of the arguments in this PhD. The reader is directed towards the referenced text for an excellent (simple) explanation of this power law should they require further explanation.

technologies and over a timescale of a few years and is often mistaken as proof that wind turbine mass does not scale cubically with diameter.

3.2.2.1 Volume to Mass and Cost Relationship

The volume of a device is dependent on its 3-dimensional shape. Consider, some material with density ρ, then it is simple to show that mass is directly proportional to volume and (economies of scale aside) as mass is directly proportional to material cost then cost must also be proportional to volume.

Consider the cubic increase in mass associated with a squaring of turbine swept area (as discussed previously) and assume that the cost of material is at-least proportional to the mass (i.e £/m^3 is constant) then at best it could be expected that the cost of the rotor would also increase as the cube of $\sqrt{A}$. At best this will simply nullify the advantage of the square increase in power on W/kg and W/£ scales, though generally it will cause these ratios to degrade until eventually the cost per MW becomes prohibitively expensive. It is expected that this relationship will be the largest limiting factor in the economics of large scale single rotors in the 10-20MW+ range.

3.2.2.2 Area to Volume Relationship

The relationship between swept area and power output has already been identified, so too has the relationship between volume and mass/cost. It is clear to see that an ideal wind turbine would cover an infinite area with zero volume though clearly not achievable. It is possible to design a device that maximises area, while minimizing its volume and thereby potentially minimising its cost. Generally, the limiting factor arises from the self-weight and wind loading forces present on the structural members of the device and which dictate to an extent the minimum amount of material that must be present. In the purest sense of this concept and taking no other factors into account, the ideal WEC would be an infinitely thin sheet rotating to create a large plan form area and enough structural capacity or flexibility to withstand the aerodynamic forces.

3.2.2.3 Power Density Relationship

The power density relationship deals with the concentration or dispersion of power within a volume, thus has units W/m^3. It is a useful tool in dealing with fundamental material limits.

Power can be categorised into electrical or mechanical power. Electrical power is a function of two terms: current and voltage and Mechanical power is a function of two terms, rotational speed and torque or in hydraulics, pressure and volumetric flow rate (which is dependent on cross section area).

For a given mechanical power transmission, a designer can either utilise high-torque low rotational speed, or low-torque high rotational speed.

The trade-off is that to transmit high torques requires more material capable of withstanding increasing shearing forces but ultimately results in a lower speed of rotation which minimises wear on the shaft bearings, minimises high-frequency vibrations and noise. Conversely a high rotational speed will lead to high-frequency vibration and noise but require much less structural capacity to transmit the power.

Electrical power on the other hand is a function of current and the power loss is a function of current squared making the transmission of power at high currents very undesirable. To achieve a high voltage involves costly technology such as transformers and power electronics and therefore this transmission also has a trade off in much the same way as mechanical speed. Ultimately, current is analogous to mechanical force/ torque and the voltage to rotational speed and the concentration of power using such methods requires increasingly advanced technology to avoid a cubic increase in mass every square of cross sectional area. This means that there will always be some limit at which using high current, or high torque, or high flow rate will become prohibitively expensive per W of power and at which point a change in tact will be required.

3.3 EVOLUTION OF THE HAWT

3.3.1 Wind Turbine Scaling

The recent evolution of horizontal axis wind turbines is very much in keeping with the concept of power maximisation with the goal of reducing the ratio of cost / income.

It is of course very difficult to put an accurate figure against the cost of a wind turbine.

Generally speaking, for turbines with ratings of 1-2 MW, the turbine cost per MW of power approximates to around €1,000,000 as shown by the plot of the data set in Figure 3.2.

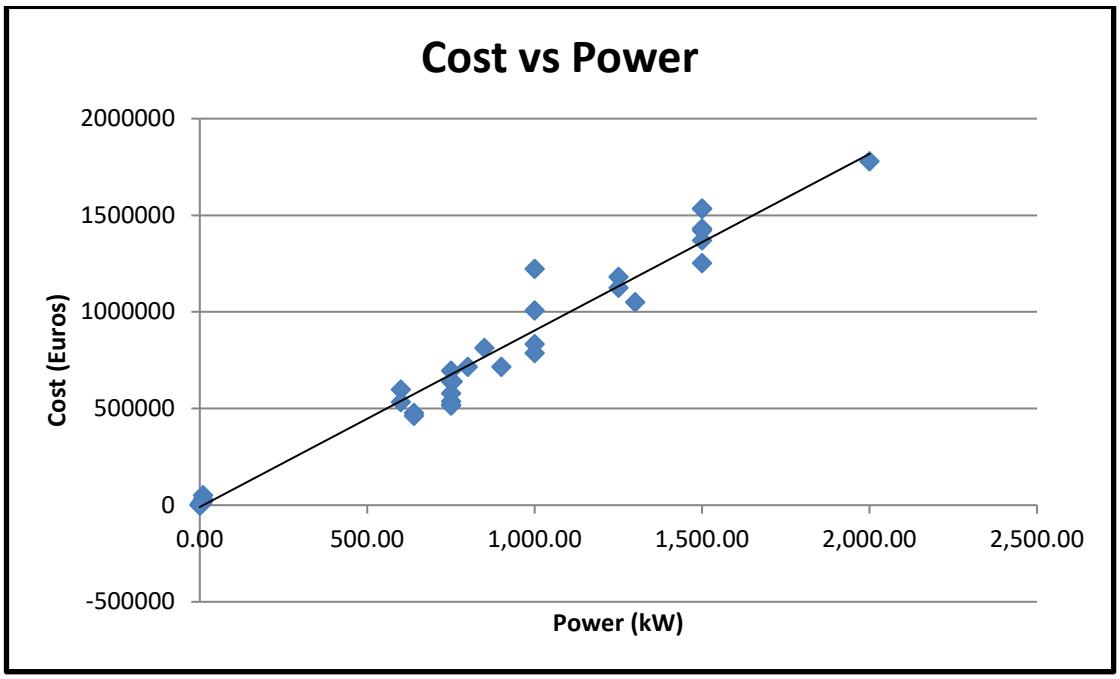

Figure 3.2 - Relationship between turbine cost and power output

The data in Figure 3.2 also highlights the fact that, generally speaking, the cost of a turbine appears to increase linearly with increasing rating with relative accuracy up to around 1.5 MW. This is interesting, as although a small data set, it suggests that the square-cubic law is not entirely capturing the reality of turbine design.

For this linearity to hold, the relationship between cost and rotor radius must be square such that they rise in proportion to the square relationship between power and

radius. In fact, this same data set suggests (Figure 3.3) that the costs of these real turbines do appear to increase as the square of the diameter. It is worth noting that this data set only reaches as far as turbines with diameters of 80m - this is due to the lack of verified data with respect to the actual cost of post 2MW turbine designs. It is entirely possible (and likely.) that the costs of such designs would deform the trend toward a steeper cubic ratio, which would be in line with theoretical expectation. As covered shortly, the use of more advanced manufacturing methods and materials for large blades could potentially be trading off blade mass for cost.

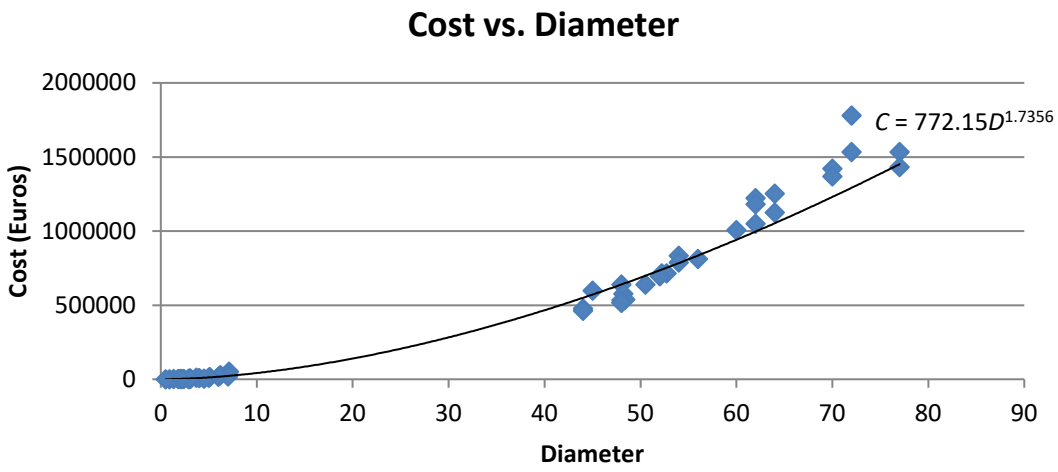

Figure 3.3 - Relationship between Cost and Rotor Diameter

Another simpler, device independent way, of analysing cost is to establish the mass of device and approximate that with the material costs. In this way, it might be expected that the cost of a wind turbine would be proportional to the amount of material used to manufacture it. Indeed, this assumption is confirmed by the data of cost and mass plotted in Figure 3.4 which exhibits a linear relationship.

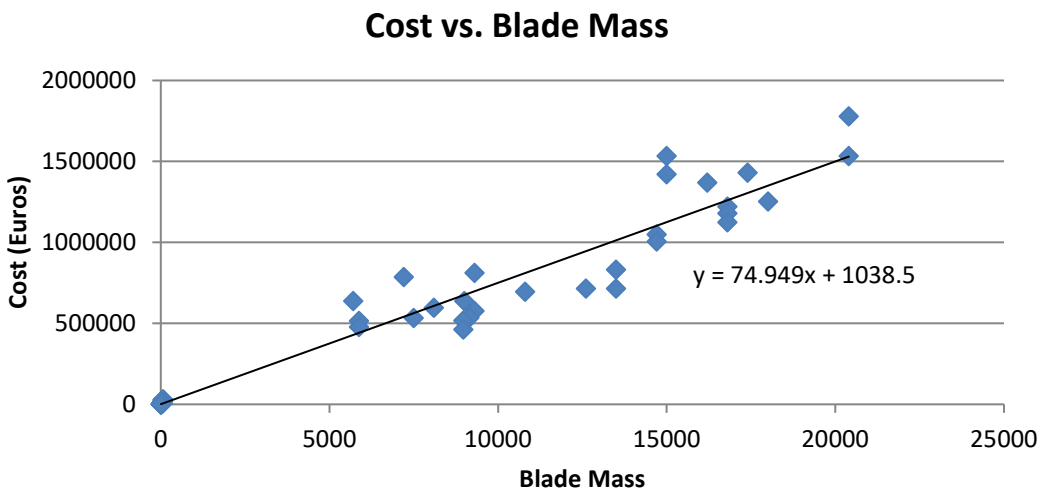

Figure 3.4 - Relationship between Blade Mass and Total Turbine Cost

Assuming that all blades are manufactured using the same material, then as wind turbine blades increase in length, their relative mass should theoretically increase as the cube of the diameter (because of the cubic increase in volume).

Existing examples show that the total wind turbine mass and separate blade mass has only increased as the square of the diameter according to a best fit of available date on turbine mass vs. diameter, Figure 3.5 and blade mass vs. diameter, Figure 3.6.

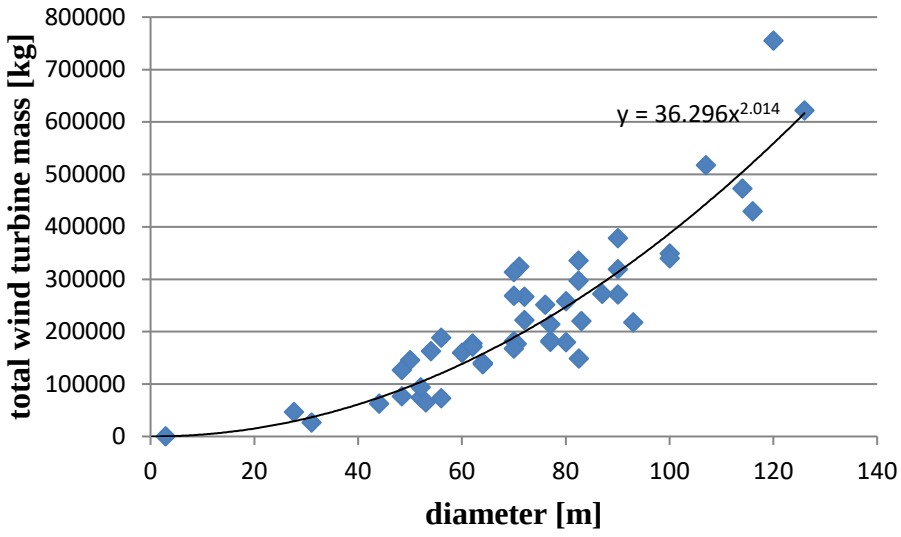

Figure 3.5 - Total Turbine Mass vs. Diameter Relationship

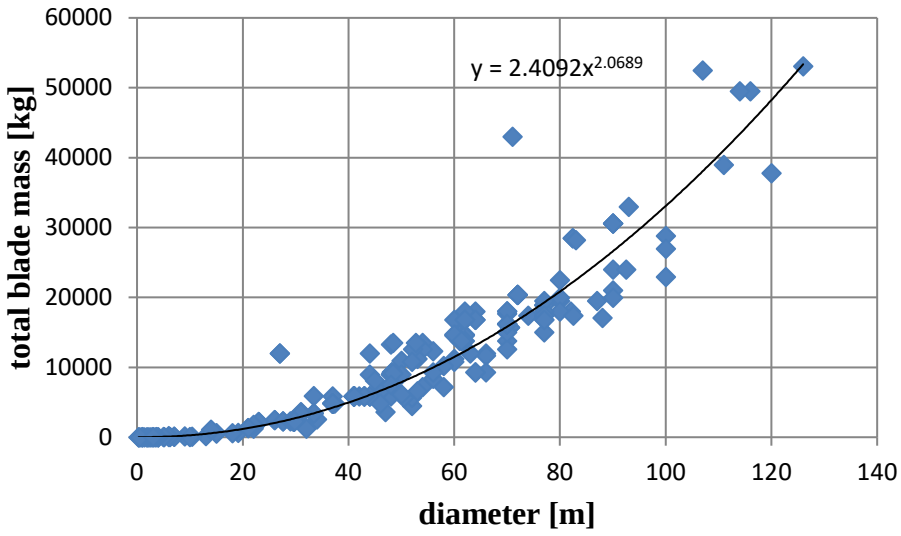

Figure 3.6 - Blade Mass vs. Diameter Relationship

This can be explained by the evolution of blade materials which have gradually moved from wooden laminates to glass epoxy resins and carbon reinforced plastics. Such advanced materials have superior strength to weight ratios, for example; a wood such as Beech has a specific gravity of 0.64 and a tensile strength of 14,900 psi, while a E-glass epoxy composite has a specific gravity of 2 but can support 256,716 psi in tension [20]. Carbon fibre has an even greater strength to weight ratio. This has kept the overall mass of blades proportional to the relative increase in power through the years keeping the relationship between mass and power, as shown in Figure 3.7 linear. The effect has been to delay the onset of the scaling limits that the square cubed power law exists but this effect is now being tempered by plateauing technology advancements in blade materials.

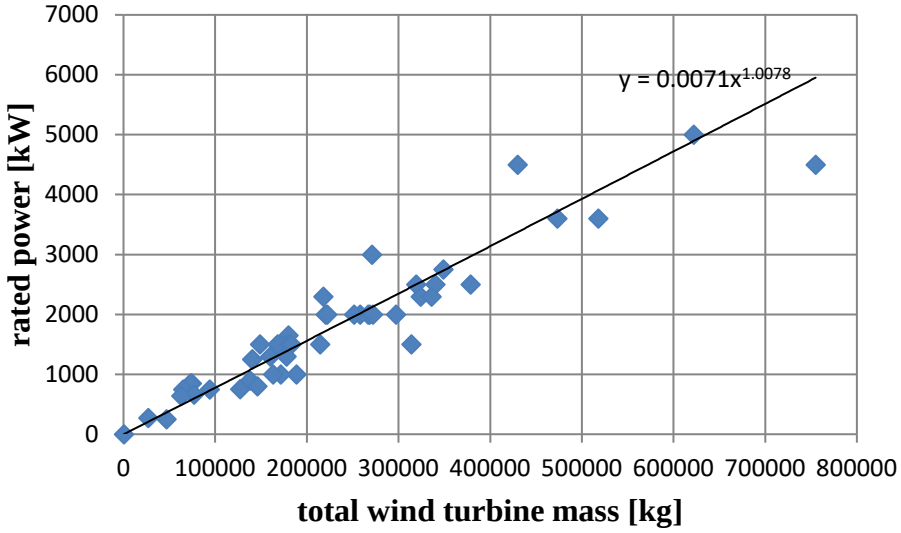

Figure 3.7 - Rated Power vs. Mass Relationship

Plotting the Power/Mass ratio against wind turbine diameter using the same turbine set (Figure 3.8), as turbines have become larger, the power to weight ratio is very marginally improving.

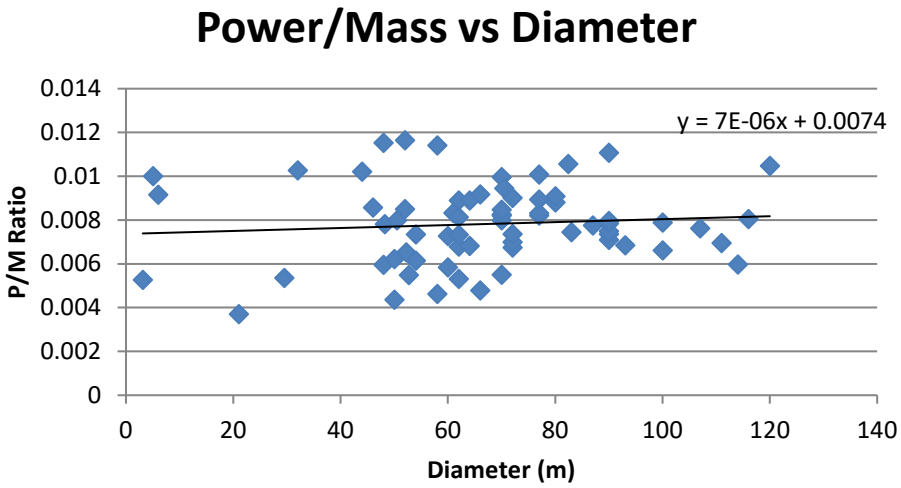

Figure 3.8 - Power/Mass ratio vs. Diameter

As a counterpoint to this, it could be argued that the data set is sufficiently spread that it cannot be completely defined by a linear equation. It could also be said that this graph is based on potentially disputable claims made by manufacturers with regards to rated powers and turbine mass. Regardless, it cannot be disputed that the wind industry is making considerable progress in improving turbine design such that

larger turbines are feasible from an economic point of view. The question is how far this limit can be extended.

Finally, examine how tower height and therefore mass scales with rotor size. Figure 3.9 contains the hub height data points for a series of commercial wind turbine towers plotted against rotor diameter. The relationship is linear as expected for onshore only designs. The outlying lowest data points with lower hub heights and larger diameters are considered to be offshore designs and would achieve a slightly lower and curved trend line if followed.

Given that the ratio of tower height to rotor size is not fixed, it is unclear from mass data alone how tower mass scales with rotor diameter. Thus, the data must be normalised with respect to height to identify the true scaling relationship. Figure 3.10 and Figure 3.11 contains the data points of tower mass with rotor diameter before and after normalizing. The scaling relationship becomes worse than square when normalizing according to tower height.

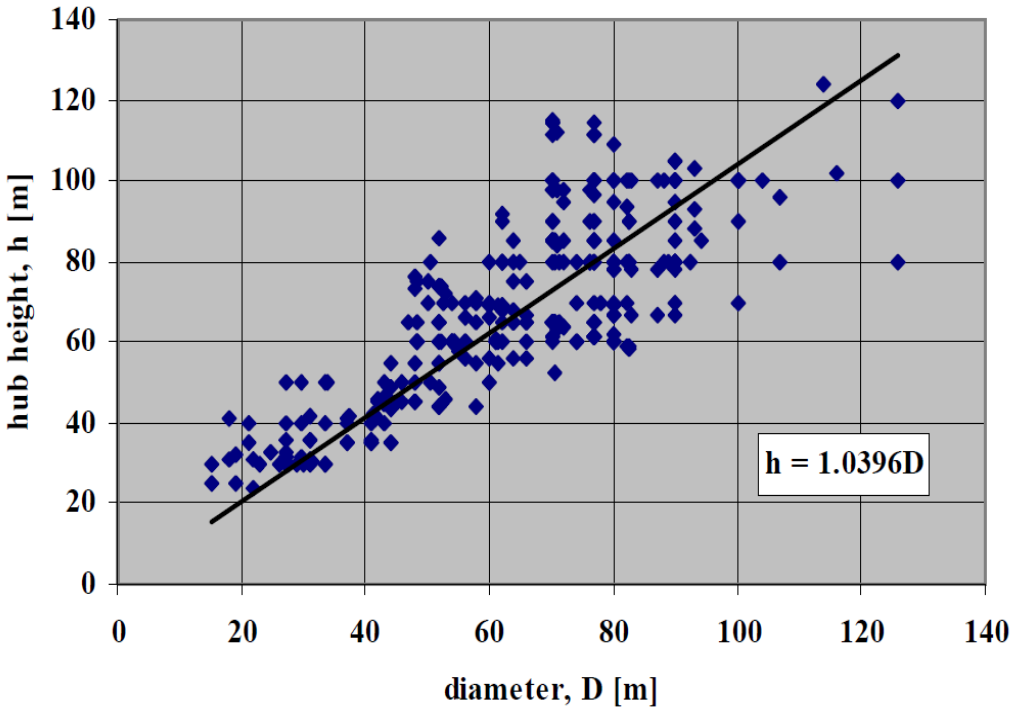

Figure 3.9 - Scaling of Tower Height with Diameter

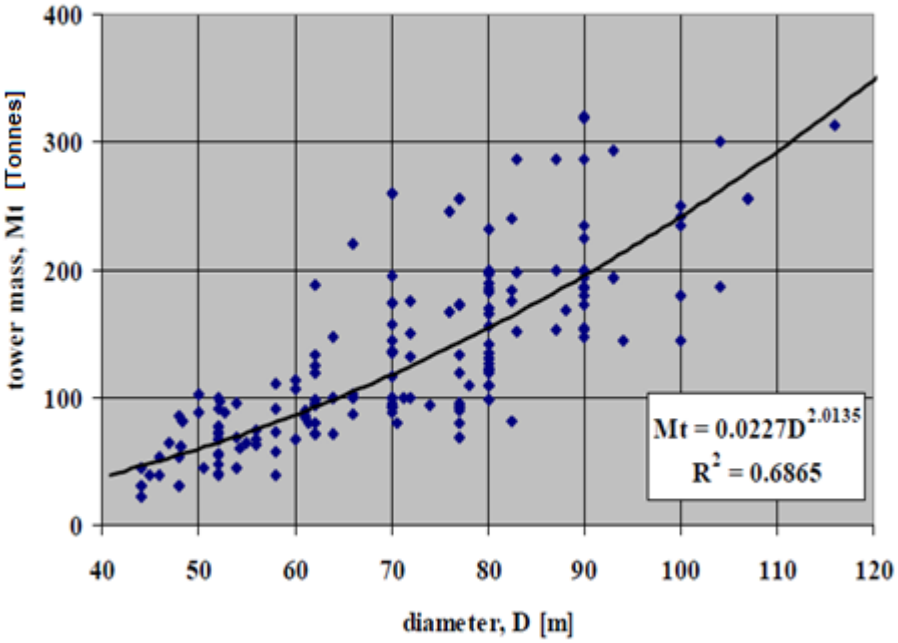

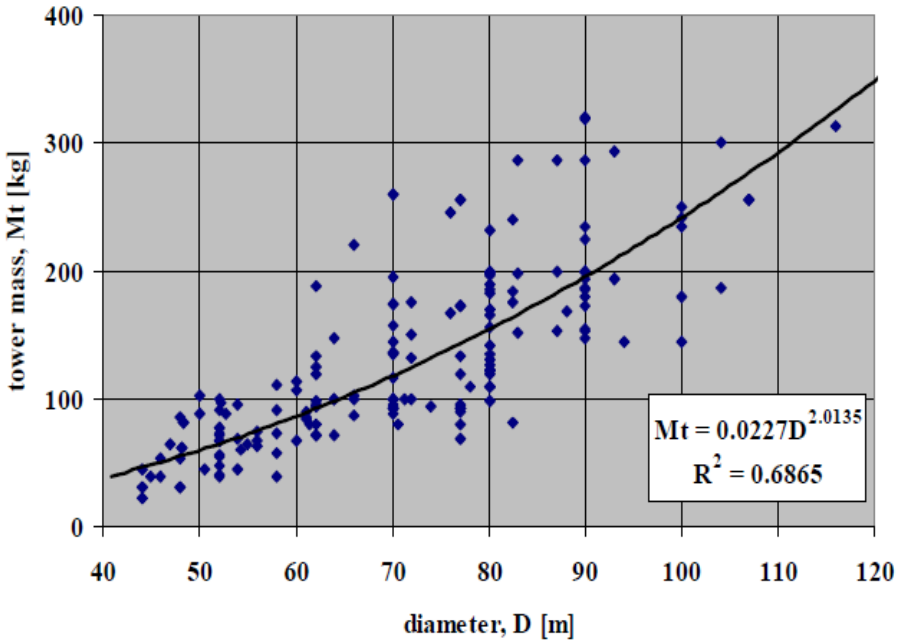

Figure 3.10 - Tower Mass vs. Rotor Diameter,

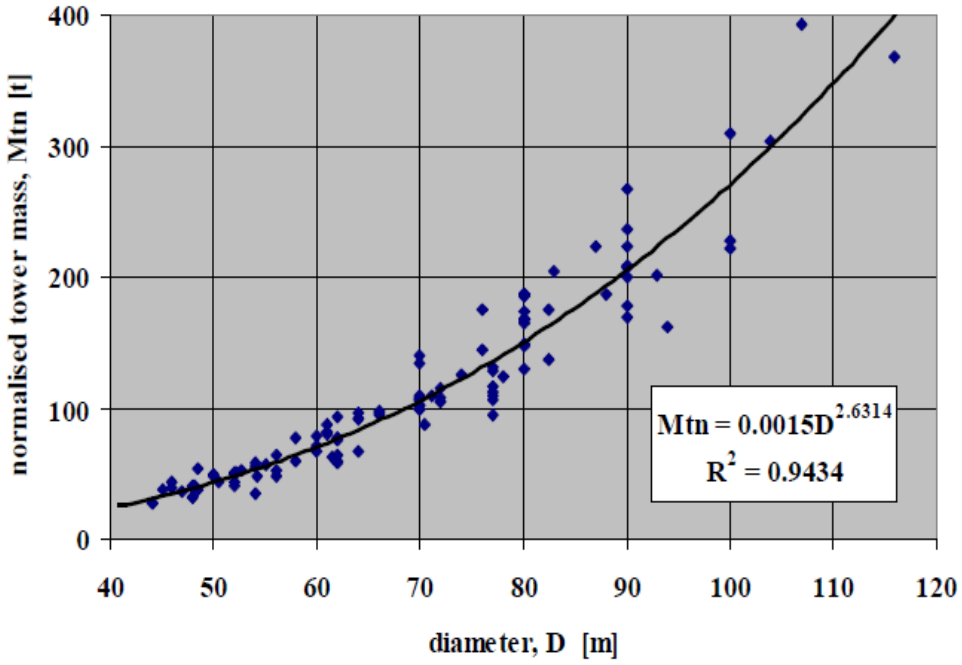

Figure 3.11 - Normalised Tower Mass vs. Rotor Diameter

3.3.2 Transmission of Torque

Another potential factor that may curtail the upward trend of conventional HAWT designs is the relationship of power and torque. Taking the equations for mechanical power (3.6) and the power equation (3.1) arrives at the equation for torque (3.11).

$$T = \frac{\rho \cdot \pi \cdot R^2 \cdot U^3 \cdot C_p \cdot \omega}{2} \tag{3.11}$$

It is apparent that torque increase as the cube of radius given that ω is also a function of R^{-1}. The GL GH data set which has been plotted as a function of torque against diameter in Figure 3.12 suggests the same. Transmission of torque requires material with sufficient shear strength to avoid failure which depends on material strength properties and shaft diameter. It falls to reason that the cost of the shaft increases as R^3.

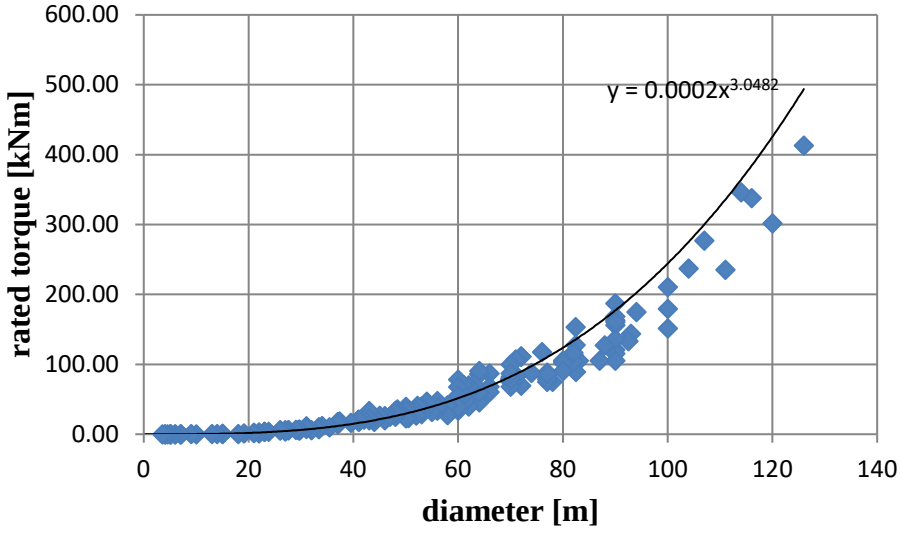

Figure 3.12 - Main Shaft Torque vs. Rotor Diameter Relationship

3.3.3 Energy Density in a Rotating Shaft

One of the primary reasons why the single horizontal rotor (based on the Danish concept) has retained its supremacy as the number one choice of wind energy conversion device is related to the way in which a relatively small shaft (in cross sectional area, using a standard shaft material) of metal aggregates and channels a large amount of power. The use of a gearbox can be used to concentrate this energy into a smaller cross-sectional area by increasing the rotational speed (on the so-called high-speed shaft) achieving an impressive energy density that can be readily converted into electricity using generators based on three phase, polar (circular) configurations. The relative energy density of any alternative wind energy concepts will therefore be an interesting indicator of how efficiently they transport energy.

Figure 3.13 highlights the power density and corrective factors associated with each stage of the typical transmission system in a normal wind turbine. The rotor alone concentrates power by almost 20 times and the gearbox brings the concentration higher several hundred times more above base. Such concentration of power into small manageable sizes makes a very strong case for the use of rotational energy conversion devices. In addition, electrical energy is well suited to being generated by

rotational systems (being cyclical) meaning that rotational energy is converted to electrical without much effort or cost.

It is very hard to see how any other wind energy conversion system can match the rotor in terms of power concentration at minimal cost. However, it is one of the aims of this PhD to explore this concept further and to truly establish whether rotational conversion devices truly are the most cost-effective systems at converting wind energy. To further this study requires an in-depth study of the wind energy design space.

	D [m]	Area [m^2]	Efficiency	Power [kW]	Power Density [kW/m^2]	Concentration Factor	Cumulative Concentration Factor
Wind over swept area	70.5	3903.6	1.00	3636	0.932	1.0	1
Rotor blades input	70.5	204.0	0.44	3636	18	19.1	19
Low speed shaft input	0.564	0.2498	1.00	1611	6449	361.7	6923
Gearbox input	0.564	0.2498	0.98	1611	6449	1.0	6923
Generator input	0.120	0.0113	0.95	1579	139610	21.6	149870
Electrical cables		0.0010	1.00	1500	1500000	10.7	1610244

Figure 3.13 - Power Density at Each Stage of Wind Turbine Transmission

3.4 TAXONOMY

The following taxonomy is intended to provide a broad overview of the wind energy design space and encompass most of the designs for which publicly available data is present. A focus is placed primarily on classifications of machines with the potential to reach multi-MW scale but does not include individual connotations (for which there are many). Throughout the classification of each device five main aspects of the design are characterised these are: rotor type, orientation, aerofoil type, rotor placement and augmentation. This classification system cleanly divides devices by the way in which they capture energy, how they are configured and whether any type

of augmentation is in use (which alters the standard understanding of wind energy capture and conversion to electrical power).

3.4.1 Definition of Terms

Type of System	**A wind energy conversion system is one which utilises wind as the primary energy field.**
Rotor	A rotor is a device which rotates around a single axis.
Oscillating	An oscillating WEC performs cyclic without continuous rotation motion around a point of equilibrium.
Translating	A translating system is one in which the device travels - but does not necessarily describe oscillatory motion.
Electrostatic	A device which uses statically charged particles moving in free space.
Single Rotor	A single rotor rotating around a single axis.
Multi rotor	More than one rotor of identical type arranged in a single structure
Hybrid	A system which contains more than one rotor, each may be a different size/shape and/or rotate around different axis.
Tandem	Rotors, which are aligned one behind another and face in the same direction.
Line	A series of rotors aligned horizontally or stacked vertically.
Horizontal Axis	A rotation around an axis parallel to wind flow.
Vertical Axis	A rotation around an axis perpendicular to wind flow.
Multi Axis	A device which has individual active blade components which rotate around more than one fixed axis.
Grounded	An extraction device that is fixed to the ground through its primary support structure.
Airborne	An extraction device that relies on, or a combination of lift forces and displacement forces (in lighter than air devices) to overcome the effects of gravity.

Suspended	An energy extraction device which is suspended in free space through use of a supporting structure fixed or hinged at two or more points.
Floating	An extraction device which relies on buoyancy/displacement forces in a liquid to de-couple the device from the ground.
Aerofoil	A shape that is designed to generate lift in conjunction with minimum drag – i.e. L/D ratios greater than 1.
Active Aerofoil	One which can have its dimensions or geometry altered in such a way to modify the boundary flow conditions. i.e. through a flap, tab, and so on
Passive Aerofoil	One of invariant sectional geometry.
Non-Aerofoil	A device which has a low maximum lift to drag ratio and therefore cannot be described as an aerofoil in the strictest sense.
Augmented	The use of a device which is meant to increase the local wind speed relative to the surround free-stream.
Non-Augmented	A non-augmented system which has no means of diverting or altering the flow field prior to entering the WECS active area (the use of terrain is not included).
Diffuser	Used to expand and slow the flow of wind to promote mixing with the surrounding fluid and induce increased mass flow through the throat.
Concentrator	Used to control the characteristics of a fluid but in the opposite sense to that of a diffuser. Thus, it is generally used to direct the flow into a smaller cross-section and thereby increase its velocity.
Ducted	A duct is a mechanical device for controlling the path of airflow. Such a system will only alter the speed and direction of airflow.
Delta Wing	A device which is used to generate vortices on the leading or lagging edge of the wing such that the energy extracting device experiences a more turbulent flow than free stream.

3.5 ROTOR WECS

3.5.1 Vertical Axis

Many modern vertical axis wind turbines (VAWTs) still operate in drag mode, exploiting drag in the downwind phase of a cycle while attempting to minimize drag on the upwind side. Attempts to modernise VAWTs to incorporate lift as a primary thrust force have produced a class of machines termed 'Giro mills' and 'Cyclo-turbines'. These machines can be categorised into three sub-categories: fixed-pitch VAWTs includes those having only fixed aerofoils (e.g., the Darrieus machine described in U.S. Pat. No. 1,835,018); self-orienting-pitch VAWTs includes those using reactive elements that orient themselves relative to the wind without a separate control means and mechanically-controlled-pitch VAWTs, are those that utilise variable pitch by mechanical means. Darrieus' patent describes a method of cyclical pitch control of aerofoils using a shifting central rotor post, and then proceeds to demonstrate that mechanical pitch variation can be abandoned if properly shaped aerofoils are accelerated to velocities well above local wind speeds. Doing so creates relative winds of sufficient strength on the aerofoil surfaces, creating lift. The cost of this simplification is the loss of a self-starting capability. Nevertheless, the Darrieus patent and its theoretical approach have formed an important foundation for much of VAWT technology and research that followed.

3.5.1.1 Savonius

Single Rotor, VAWT, Passive Aerofoil/Non-Aerofoil, Grounded, Non-Augmented

The Savonius rotor is based upon some of the oldest designs of wind energy conversion device known to man. A significant branch of work has been devoted to the development of the Savonius rotor such that it can generally now be regarded as the simplest if not cheapest type of WEC available. The basic design is of two semi-circular, half-cylinder blades, set one radian apart around a central shaft and facing opposite directions as depicted in Figure 3.14.

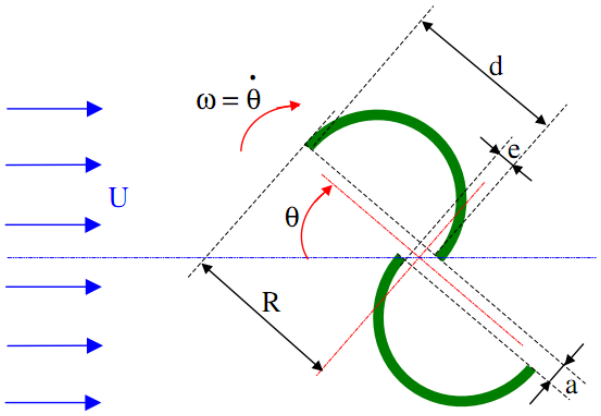

Figure 3.14 - The Savonius D-shaped Rotor

As the Savonius is primarily a drag-type device it is inherently inefficient, meaning that typical C_P values do not exceed 0.2 and tip speed ratios, λ, are unlikely to reach past 1.0. In theory, as the maximum C_P a pure drag device can obtain is 0.15 (and the Savonius can breach this) then it the device should not be classified as exclusively drag.

At the small scale (sub kW) the Savonius has seen widespread commercial success and usage. However, its lower efficiency has proved an obstacle in achieving significant development in the multi-MW range.

There has been some recent interest in the Savonius design with an aim to achieving C_P values closer to 0.3 [21].

3.5.1.2 Darrieus (Troposkien)

Single Rotor, VAWT or HAWT, Passive Aerofoil, Grounded, Non-Augmented

The Darrieus device is a primarily fixed-pitch lift based device. It can be mounted vertically or horizontally. Its attractiveness stems from its indifference to fluctuating wind vectors (no requirement for yaw) and the ability to site heavy generating machinery near the ground making maintenance and access easier. The most famous example of the Darrieus machine are those which utilise the Troposkien, curved blade, though there are also several examples which utilise, V or H-shaped rotors.

One of the issues with the Darrieus device is the complicated highly unsteady flow phenomenon that occurs during its working cycle. On some designs, this can lead to dynamic stall and consequent flow detachment and vortex shedding which results in high drag and lower efficiency. Another issue is the inability of the device to self-start in low wind speeds due to the fixed-nature of the blades, though this can be combated with a Savonius style drag based device somewhere on the rotor.

The Troposkien design of the blades is based on an ideal geometric shape. The effect is that centrifugal forces present on the blades during rotation removes any blade loading and thus place any section of the blade in pure tension. The Darrieus is able to achieve competitive C_P values in the region of 0.4 utilising Troposkien blades and therefore there are multiple commercial examples of devices capable of generating a few hundred kW's [22].

3.5.1.3 Giro-mill (H-Rotor)

Single Rotor, VAWT, Passive Aerofoil, Grounded, Non-Augmented

In 1975, P.J Musgrove at the University of Reading led research to take the Darrieus design and straighten out the blades, forming a simply constructed 2-bladed H-rotor which allows for pitching and feathering of the blades. Such complicated measures were not strictly necessary due to the blades tendency to stall (and thus self-regulate) at high wind speeds [23].

It has been found that 4-bladed designs, although having higher manufacturing costs can reduce the cyclic variation experience by each blade. The simpler design suffers from relatively low C_P values like the Savonius turbine (<0.25) and currently exists only in the sub 100kW region. The design also suffers from the same wake induced flow vibrations that plague other VAWT designs and one recent study showed a variation of 4000 N of thrust on a single blade (3-bladed, 5kW machine) – which for such a small machine is significant enough to cause damaging blade fatigue over time [23].

3.5.1.4 V-Rotor (Aero-generator)

Single Rotor, VAWT, Passive Aerofoil, Grounded, Non-Augmented

The V-rotor is a class of turbine that is not unlike the H-rotor vertical axis machines but has sufficiently different parameters that merit an individual examination and potential classification. This concept is also one of the most recent VAWT designs to have undergone detailed study during the UK EPSRC funded Project Novel Offshore Vertical Axis demonstrator (NOVA).

As the rotor blades experience variation in local wind speed with increasing radius each blade must be tapered towards the tip. Twist is not required and there is the potential to manufacture V rotor blades in sections with considerable cost reductions. The pitching ability provided by the V-rotor provides a host of benefits enjoyed by conventional HAWTS including: higher energy capture, power regulation in high winds, protection from extreme forces in very high winds, blade protection by damping out vibrations.

In addition to the common shortcomings experience by VAWTs, the V rotor design compromises further on aerodynamic performance compared to other Darrieus concepts. The lack of a tower leads to a large proportion of the swept area being near the surface where winds are low due to surface roughness. Also, much of the blade length is close to the axis of rotation where aerodynamic forces contribute least towards the total rotor torque.

Ultimately the vision for the V rotor is that the advantage of scaling up to 10MW+ power outputs while keeping reasonable OM will outweigh the aerodynamic inefficiencies and expensive power train. The design lends itself to the offshore environment with potential cost reduction in terms of manufacture, installation and O&M reduction.

The NOVA project group concluded that the drive train at the base provides a low centre of gravity and transverse spoilers along the blade cancel a portion of the OM. Both of these reduced the support structure size and floating platform cost. However,

while increasing the weight of the turbine, these struts provided no aerodynamic improvement to the blade. The final design also included cables connecting the blades to provide support. The huge pre-tension of the cable and sourcing a material that could provide this function while still allowing the blades some flexibility in the wind would provide a significant engineering challenge [24][25].

3.5.1.5 Hybrid Helical/Spiral

Single Rotor, VAWT, Passive Aerofoil or Non-Aerofoil, Grounded, Non-Augmented

Helical rotors (Figure 3.15) are generally adapted from either Savonius or Darrieus designs. The advantage of this configuration, though harder to manufacture, is that the torque is more evenly spread across the whole revolution which removes some of the damaging cyclical loading. A version based on the Savonius rotor (Helix Wind – S322) has the paddles twisted and moulded like a concertina, with each blade twisting through 180 degrees from base to tip achieving an increase operating envelope 4 m/s and 45m/s of wind, with only 4.45kN of shearing forces at cut-out. A prototype rated at 2kW with a swept area of 3.2m^2 is the only known example and is extremely uneconomical at an estimated $5000 per kW of installed power [26].

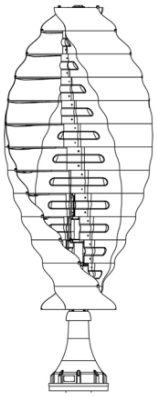

Figure 3.15 - Helix/Spiral Rotor

3.5.1.6 Vortex Enhanced

Single Rotor, VAWT, Passive or Active Aerofoil, Grounded, (Non) Augmented

This passive vortex turbine is a variation on the Darrieus device and in one adaptation utilizes cavities in the blades (Figure 3.16) to capture the vortex as it is shed and aid

reattachment of the flow (also known as 'vortex trapping'. In addition, the cavities can be arranged non-symmetrically such that the angle of incidence that the wing makes to the blade is more favourable throughout the cycle. These adaptations are used to combat the effect of unsteady aerodynamics which often plague VAWT machines, help remove the wake induced vibrations associated with vortex shedding and also may marginally improve the aerodynamic coefficients on the blades making the device more efficient [27].

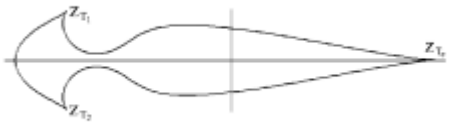

Figure 3.16 - Blade Cross-Section Showing Vortex Generator Geometry

Another variation that utilizes vortexes generates them intentionally (so called vortex generators) using small fins that protrude over the interface of the blade. These fins are mounted opposite each other at a certain angle that causes counter-current eddies in the air flow creating turbulent flow which aids boundary layer attachment. This delays the moment when the blades stall and thus the point at which they lose their capacity to produce power – the lowest part of the blade is thus efficient during a greater part of the turbine's production time. Unfortunately, at low wind speeds, the fins can increase the drag on the blades and thus reduce the lift to drag ratio. None-the-less vortex generators can boost blade performance by up to 4–6% and may even be useful in HAWT's machines of the future [28].

3.5.1.7 Tornado

Secondary Rotor, VAWT, Hybrid, Grounded, Augmented (Vortex)

The Tornado concept has been around since the late 1970s. The interest stems from its apparent ability to maximise the airflow through a rotor of minimum radius without the requirement for a complex structure.

The Tornado VAWT attempts to modify the wind flow in such a way as to promote secondary extraction of the wind energy. It consists of a fixed hollow cylinder with adjustable vertical vanes which are opened on the windward side and close on the leeward (Figure 3.17). The open vanes direct the wind into the tower at an angle tangential to the cylinder which then forces the wind round spirally towards the centre of the device. As it does so, the wind accelerates to conserve angular momentum and rises towards the opening at the tip of the tower. This opening is fitted with a relatively small turbine connected to a generator and this is used to extract energy from the on-rushing air [29].

Independent research suggests that the system is only capable of reaching C_P values in the 0.04-0.1 region, with the latter being achieved experimentally using a system with a turbine to cylinder ratio around 0.6 [30].

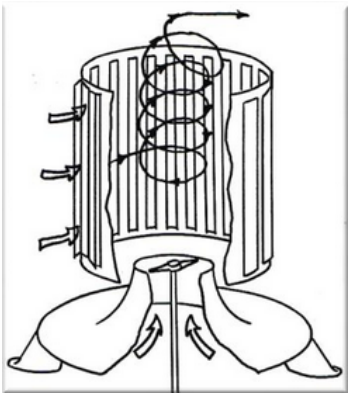

Figure 3.17 - Tornado WECS

3.5.1.8 Kite Rotors

Single Rotor, VAWT, Hybrid, Grounded/Airborne, Non-Augmented

The idea of using cross-wind kites as a method of energy extraction device is a relatively old concept [31]. In recent years, control technologies and power electronics have advanced far enough to accommodate the specialist requirements of unmanned flight.

KiteGen utilises a vertical axis rotor and kite technology from which to extract wind energy in the Earths boundary layer. The concept is to fly a series of kites in a cross-

wind manner, but to transfer the forces present on the kites directly onto a vertical axis rotor through means of individual tethers (Figure 3.18). The kites are controlled in such a way to minimise drag on the upwind side of the cycle and maximize aerodynamic lift on the downwind side of the cycle (in the same way as standard VAWT blades) and in doing so provide net torque to the rotor. The rotor is connected to a generator and this is used to provide the reaction torque for electricity generation and therefore can be scaled up to very large sizes without a large increase in cost [32].

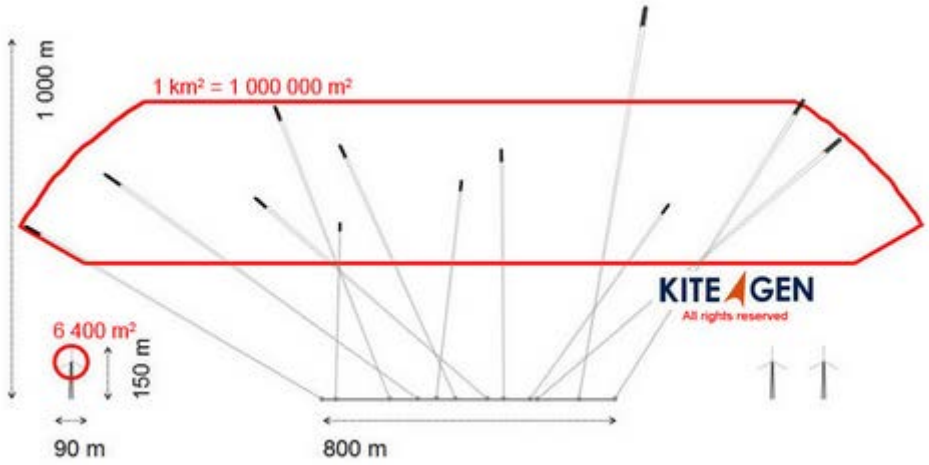

Figure 3.18 - KiteGen Elevation Schematic

3.5.1.9 Boundary Layer Turbines

Multi rotor, VAWT, Passive Aerofoil, Grounded, Augmented (Venturi)

Boundary layer turbines utilise closely spaced discs and boundary layer interactions as opposed to low solidity blades and fluid interactions to generate torque. The first notable example of such a proposed design was made by Nikola Tesla in which he applied a gas to the edge of a series of stacked discs and the boundary layer was used to extract the energy from the gas through friction. To conserve angular momentum, the gas then spiralled towards the centre of the device and was exhausted. For boundary layer interactions, the discs were required to be spaced as close together as 0.4mm and manufactured very smooth to minimise shearing stress [33]. Recent

modified adaptations attempt to extract energy from the wind – the Fuller turbine, Figure 3.19. [34]

Due to the requirement for boundary layer interaction in order to function this device is best suited for use at micro-scale.

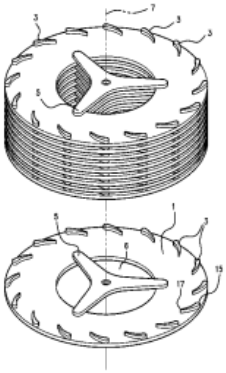

Figure 3.19 - Stacked Boundary Layer Turbine

3.5.2 Horizontal Axis

Horizontal axis machines account for nearly all of today's installed wind capacity. Almost all commercially viable designs are based around the 3-bladed horizontal axis, pitch-regulated, variable speed rotor. Significant research has been invested in horizontal machines since their inception and thus the design space is well populated with different designs and concepts. However, no other design has come close to matching the conventional configuration in terms of commercial success.

3.5.2.1 Vortex Enhanced Delta Wing

Single Rotor, HAWT, Passive Aerofoil, Grounded, Augmented (Vortex)

The delta wing is a passive device that in theory can augment the ability of a conventional wind turbines ability to extract energy, it is a subtle advancement of the vortex generator. The delta wing is useful due to its large angles of attack which help concentrate air vortices (boundary vortices) close to the wings surface. The turbine is then placed within these boundary vortices and according to some sources could allow a power yield increase by a factor of 10 [35].

There are also examples of the use of delta shaped, fixed-pitch, flapped blades in place of conventional aerofoils (Figure 3.20). It is shown that these types of rotors could obtain a maximum torque coefficient at zero *TSR* and maximum power coefficients of around 0.43 at *TSR* of 1.7. Such systems are excellent for applications requiring high-starting torques such as water pumping or in electrical generating applications where operational noise limits are an issue. The delta wing shape is desired in this case due to its ability to maintain attached flow along its surface (due to vortices generated by the edge of the blade aiding re-attachment) over a wide-range of incident angles which pushes off the stall limit and offers the ability for high torque starts. However, the relatively low lift-drag ratios of the device do make it incapable of operating well at high tip-speed ratios as of that of 2-3 bladed devices making it less useful for large multi-MW generation [36].

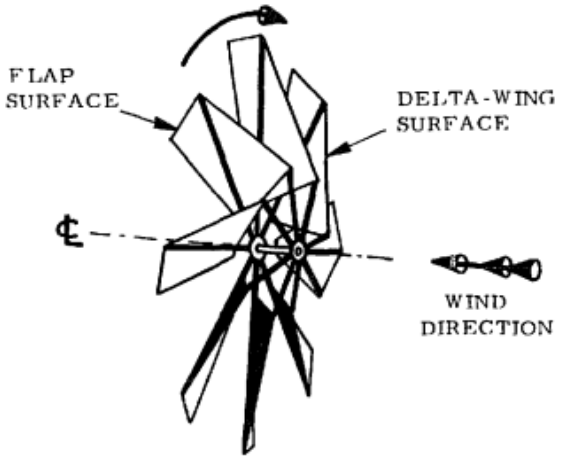

Figure 3.20 - Delta Bladed High Solidity Rotor

3.5.2.2 Vortex Enhanced Tip Vanes

Single Rotor, HAWT, Active Aerofoil, Grounded, Augmented (Vortex)

Tip vanes are small aerofoils that are fitted to the tips of standard wind turbine blades (see Figure 3.21). Research into these devices has been ongoing since the early 1980s. They are designed to create a cone of air which acts like a duct, but in a much simpler and cost-effective manner.

Tip vanes are typically designed for minimum drag, with lift to drag ratios more than 100 desired. The tips are orientated in such a way that they are tangential to the flow field.

Experiments show that the tip-vanes can act to increase wind flow through the rotor by a factor of four and increase power output on conventional machines by a factor of two or more (this factor is smaller than four due to the increased frictional drag created by the vanes) [37][38].

Improvements in field tests yield improvements of around 30% in terms of efficiency with twisted vanes tilted at 20 degrees from the turbine arms were reported in 1983. Further studies have suggested that tip-vanes effectiveness is still an issue in unsteady turbulent wind flows.

There is also the question as to the relative advantage of tip vanes over a simple/cheaper increase in blade length to achieve the same result. A larger rotor can achieve the same result but at the expense of increased noise (high tip speed) or increase torque (low tip speed). Thus, tip vanes may fill niches in onshore locations.

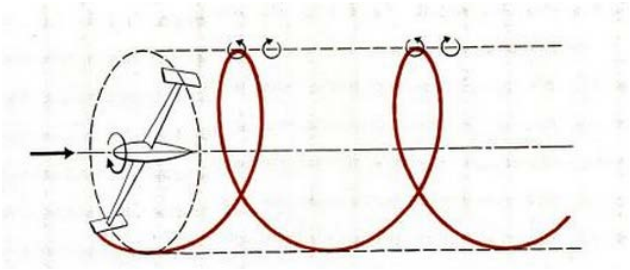

Figure 3.21 - Tip Vanes Propagating Wake Interactions

3.5.2.3 Venturi Effect

Single Rotor, HAWT, Hybrid, Passive Aerofoil, 3D-Augmented

One novel type of wind turbine utilizes the Venturi effect (that of a drop in pressure at a location, such as that seen in a narrowing of a pipe) to increase the efficiency of energy extraction [39].

Wind tunnel experiments in at the Technical University of Delft suggest that a 3-bladed device incorporating this concept can augment the wind flow by a factor of 2

or more from an unmodified wind field. As of date, only small sub kW designs (1.1m diameter) have been developed commercially and above rated speed have C_P coefficients in the range of 0.16 which is well below that of commercially successful Danish designs.

3.5.2.4 Secondary Rotor / Andreau Enfield

Secondary Rotor, HAWT, Passive Aerofoil, Grounded, Non-Augmented, Non-standard drive train

In this design, a two or more bladed HAWT is adapted such that each articulated blade has a hollow core that can vent at both ends (blade tip and tower) Figure 3.22 Initial attempts were characterised by a low overall efficiency of under 22 percent caused by an observed air intake at the rotating joints near the hub shows the airflow path from the point of entry at the base of the tower to the tips of each blade.

The design would perhaps suffer negatively from the fact that it requires two rotors to function but without any reduced complexity in the main rotor and that would therefore negatively impact on the reliability in offshore environments and to date has never been attempted commercially.

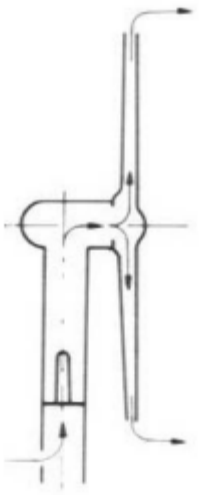

Figure 3.22 - Andreau Enfield Design Showing Airflow

3.5.2.5 Gravity Compression Turbine

Secondary Rotor, HAWT, Passive Aerofoil, Non-Augmented

The gravity compression turbine is a design that has been recently proposed as an alternative energy conversion method for use at large scales. In this device, large reciprocating pistons placed within each hollow blade are used to counter-act the aerodynamic torque present on the standard rotor under normal wind conditions. As the piston moves through the top half of the rotational cycle it falls under gravity towards the root, then once past one radian the piston again falls under gravity back towards the blade tip. These blades describe an asymmetric circle during one full revolution and so generate a net torque that opposes the direction of rotation from which useful work can be extracted. It is proposed that the pistons are used to compress gas which is then used to drive secondary rotors and generators in each blade (thereby negating the need for a centrally mounted drive-train). This would lend itself towards large machines in excess of 10MW. Unfortunately, due to the requirements for stability of the masses (to avoid them from being accelerated outwards indefinitely) the turbine must be rotated at speeds of below 0.6 rad/s and the mass requirement is such that it could contribute an extra 33% or more to the overall rotor weight [40].

3.5.2.6 Shrouded Rotor

Single Rotor, HAWT, Passive Aerofoil, Grounded, Augmented (Concentrator)

This concept does not relate to a specific design, rather a school of thought that aims to direct the wind through some mechanical means towards the rotor swept area. For example, a shroud twice the diameter of the rotor might be used to direct the wind onto the blades, thus augmenting its operation. Theoretically, this could increase the gain of a turbine by up to a factor of four for a given swept area. Of course, the issue lies in the factors that must be considered when placing a potentially very heavy structure at hub height and allowing it to yaw into and out of the wind. One attempt to build a working proto-type resulted in an increase in power extracted of 2.2 which was not considered economical considering the large overturning moment that the

structure had to be capable of withstanding which doubled the cost of the tower and structure thereby negating any income from energy gains. This meant that the only company pursuing the concept (Vortec) closed their doors in 2001 [41].

3.5.2.7 Diffuser

Single Rotor, HAWT, Passive Aerofoil, Grounded, Augmented (Diffuser)

The Diffuser augmented turbine saw most of its development in the early 1970s with Grumman Aerospace Corporation in the USA. In this concept, a squat shroud made from fibre glass is placed around the rotor with the narrow opening around the blades and a larger opening downwind of the device.

Researchers found that the ratio between both openings of the shroud was the crucial factor in determining turbine performance. A small narrow end opening out quickly boosted airflow but was steeper and therefore more difficult to manufacture. Conversely, a large shroud made the device cheaper and more stable but resulted in less airflow and therefore less power. Thus, Grumman finally settled on a ratio between shroud openings of 2.75 and a shroud angle of 60 degrees.

Researchers also found that the use of bell-shaped shrouds causes the airflow to stall in the region behind the blades and it was found that this effect could be eliminated if the shroud was made from concentric rings, stepped in size. This stepped shroud used opening between rings to aid mixing from the outside air and in doing so create turbulence which would delay the onset of stall.

Wind tunnel experiments concluded that the design can improve turbine performance by a factor of 4 [42].

3.5.2.8 Spiral Rotor

Single Rotor, HAWT, Passive Aerofoil, Non-Augmented

This device is of similar set-up to the vertical axis helical rotors, the main difference being the presence of aerofoil blades utilising lift as a primary means of torque generation. Generally, most adaptation of this device use twisted and cambered blades which project downwind from the rotor in a spiral. The aim of the device is to

extend the rotor disc in such a way as to extract more energy from the wind. Although many claim such devices to can achieve C_P values close to or past the Betz limit, these claims are not strictly true as the Betz limit applies only for conserved stream-tube actuator disc theory assuming a thin actuator disc.

3.5.2.9 Tandem-rotor ('Super-Turbines')

Multi Rotor, HAWT, Airborne/Suspended, Passive-Aerofoil, Non-Augmented

Some radical wind turbine concepts utilise tandem-rotors - that is multiple rotors of similar size and configuration operating in one behind the other on a single structure - in an attempt to maximise energy extraction for a given area.

One example of this concept created by the company Selsam attempts to use a several rotors connected to a kite line held aloft by a balloon/blimp (self-supporting) such that a stream of the devices flows downwind of the tether point (Figure 3.23).

A recent prototype (2008) of the design could produce 6kW in 32.5 mph winds, proving that the concept is feasible.

Another variation uses a series of multi rotor connected along a single shaft which is suspended in the sky. To overcome the effects of bending moments due to self-weight, each rotor would be flown in autorotation to minimise gravitational forces on the structure [43].

Such a device would be very difficult to control and arguably is not preferable to a standard multi rotor device or a translating kite design at multi-MW scale.

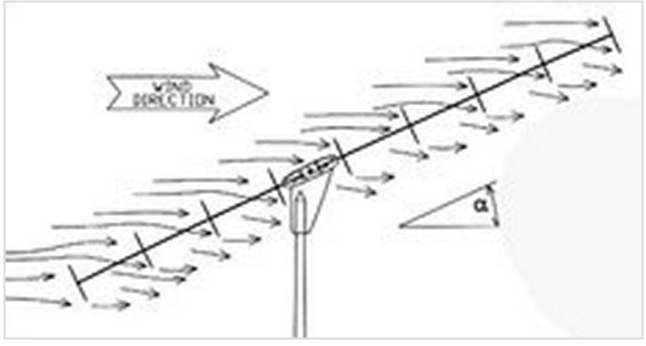

Figure 3.23 - 'Selsam' Tandem Rotor Concept

3.5.2.10 Coning Rotor

Single-rotor, HAWT, Grounded, Passive Aerofoil, Non-Augmented

Significant research was put into the concept of a coning rotor during the mid-90s [44]. The concept focuses around the use of a conventional HAWT rotor but with the added ability of being able to cone out-of-plane into the wind. The effect of this coning is that the cross-section the rotor presented to the oncoming flow is greatly reduced and so too the aerodynamic forces. Such a rotor would not need to be designed for the 50-year storm and therefore could utilise longer blades than would otherwise be possible. This gives the design a greater energy capture at lower wind speeds when compared to normal pitch regulated machines. Primary work has been carried out on stall-regulated coning rotors with a rating of 450kW, but the focus has now moved to pitch-regulated 1.5MW machines.

Regardless of the configuration, the use of both flap and pitch hinges presents problems in itself, due to the large moments that would be required to cone the rotor – particularly if the rotor is still under the effects of centrifugal loading [45] and have an associate cost and reliability penalty that may limit their use in large-offshore.

3.5.3 Multi-Axis

3.5.3.1 Passive Aerofoils

Passive aerofoils are ones in which no dynamic alteration of the blade profile or geometric shape is made during operation. Thus, it includes such techniques as: geometric shaping, the addition of trailing-edge flaps, the use of fixed vortex generators and the use of riblets or grooves to reduce drag. However, a passive aerofoil can still have an active control system, such as pitch-control which acts to change the profile of the blade against the incoming flow.

3.5.3.2 Active Aerofoils

Active aerofoils are those which can be dynamically and actively altered while in operation. Generally, they must consist of both actuators and sensors with some sort of active control loop. Such activity can be used to improve or decrease the blades

performance under specific conditions and therefore can significantly impact on blade efficiency, its response to changing loads, life-span and can be useful in the damping of potentially harmful vibrations.

3.5.3.3 Micro tabs

Micro tabs are small rapidly actuated devices designed to quickly change the lift and drag generated by a section of a wing or a wind turbine blade. They can reduce stresses, dampen vibrations and increase efficiencies by dynamically adapting to unsteady flow conditions. Their development on wind energy systems can be attributed to an evolutionary development of the Gurney flap.

Micro tabs are created using micro electro-mechanical (MEM) devices which can be actively operated locally or remotely in response to changing conditions and control inputs. These tabs are typically extremely small devices that operate on the scale of the boundary layer to disrupt the flow field in such a way as to impact on the whole rotor at the macro scale.

In one application, the tabs are placed along the trailing edge of the turbine blades such that when operated they change the camber of the blade and modify trailing edge wake development, also known as the Kutta condition [46].

Unfortunately, micro tabs suffer from poor phase-lag response dynamics, making their effective control difficult and any subsequent increase in power output almost inconsequential.

3.5.3.4 Circulating Aerofoils

It has been found that by controlling the circulation of an aerofoil, its performance characteristics can be actively modified [46]. The effect, also known as the Coanda effect, is formed by blowing air tangential to the surface of the aerofoil. The effect experienced is an increase of circulation around the aerofoil due to the continued attachment of the boundary layer around the trailing edge. In isolation, this causes air stagnation on the lower side of the aerofoil which then leads to separation of the

flow and thus a decrease in pressure. The effect sees an increase in lift and therefore is applicable for generation of high-lift aerofoils.

3.5.3.5 Jet-Flap

The jet flap is the creation of a plane of jet air at an angle to the free flow so that an asymmetric flow pattern and circulation is generated - analogous to a large trailing edge flap. The jet-flap is created by blowing air through the trailing edge. The MOD began investigating such boundary-layer-control (BLC) in the early 1960s as ways of controlling aircraft performance at low speeds. The jet of air artificially creates a relative increase in the cord length seen by the flow field and thus can dramatically increase lift. By doing this, the vertical force offered by the jet flow is magnified by several times by pressure lift along the surface of the wing [47].

More recent CFD studies (a typical simulation result is show in Figure 3.24) have found that at an angle of attack of $\alpha = 5^{\circ}$ the increase in power per blade section was 10% and for $\alpha = 10^{\circ}$ around 5%. Even greater efficiencies are predicted when less power is expelled through the air jet [48]. In general, it was also found that the inclusion of the Coanda jet in conjunction with the jet flap and so lead to higher lift coefficients and hence higher efficiency.

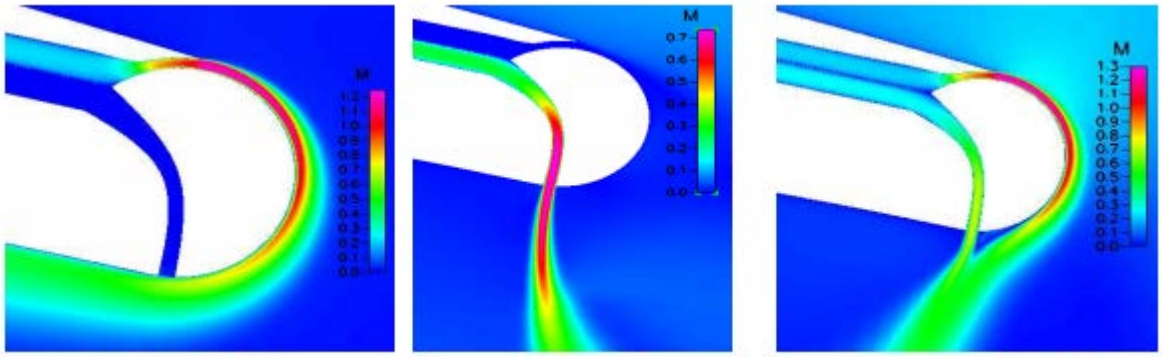

Figure 3.24 - CFD Modelling of Circulating Flow Effects

3.5.3.6 Magnus Effect

The Magnus effect is the process of converting the flow of air over a rotating cylinder into a thrust. To achieve this effect, a cylinder is rotated inside a moving wind field, creating an area of low and high pressure at either side of the sphere from which a

net lift force develops perpendicular to the flow field. The effect (depicted in Figure 3.25) can lead to much greater lift forces than would otherwise be present from a conventional passive aerofoil. The Magnus effect is not very useful at large scale due to low C_p values.

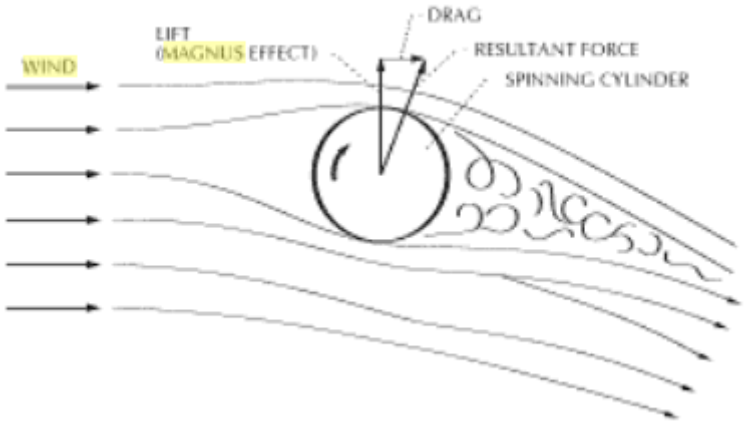

Figure 3.25 - Wind Induced Forces around a Rotating Cylinder

3.5.3.7 Flettner Rotor

Single Rotor, HAWT, Grounded, Active-Aerofoil, Non-Augmented

In the mid-1920s, collaborative work by Prandtl and Anton Flettner led to the suggestion that the Magnus effect could be used to provide an efficient means for propelling ships. The effect that the Flettner rotor (Figure 3.26) achieved was something of interest to the wind industry, and there have been several prototype examples. The idea is that cylinders are much easier to manufacture than complex aerofoils and that their active nature would negative the need for pitch control.

One of the current disadvantages associated with the Flettner rotor is the creation of unsteady fluctuations in the flow-field and subsequent pulsation of the lift force. This is most pronounced through certain regions of velocity ratios (3.5 – 5.5) depending on the Reynolds number of the device. This effect can be removed or at the very least shifted out-with operating regions through the addition of some simple discs to the rotor.

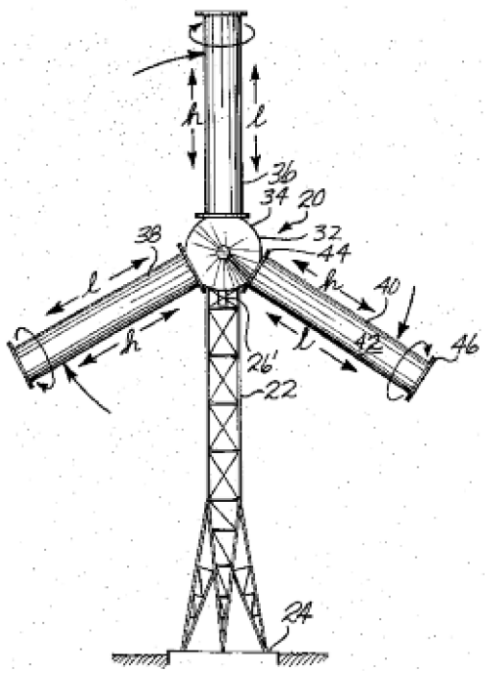

Figure 3.26 - Example of a Flettner Rotor

3.5.3.8 Thom Rotor

Single Rotor, HAWT, Grounded, Active-Aerofoil, Augmented Flettner

The Thom rotor is a variation of the Flettner device (which in turn utilises the Magnus effect) and has discs placed strategically along the cylinder tangential to the surface. These discs can help increase the lift and sometimes cause even negative drag, though the effect is most pronounced at rotor velocity ratios, Ω (U_{rotor}/U_{wind}) of 4 or greater. For example, recent research performed detailed CFD modelling to predict that with $\Omega = 8$, the lift coefficient C_L is found to be 8% higher and the drag coefficient C_D 50% lower than the unmodified Flettner rotor, though these a significantly smaller effect than those found by Thom. The discs can also help alleviate the load fluctuations experienced on the modified rotor, for certain operating regions [49].

3.5.3.9 Spiral Magnus

Single Rotor, HAWT, Grounded, Active-Aerofoil, Augmented Flettner

This is a variation of the Thom rotor disc concept, with the flat perpendicular discs replaced with spiralling projections down the length of each Flettner rotor. The company responsible for this device claim lift ratios of four times greater than

conventional machines and the ability to operate at any wind speed. A patent is currently pending on the concept and is required to shed light on exactly what the benefits of the spiralled groove is over standard Thom discs as a factor of 4 seems overly optimistic.

3.5.3.10 Blade Tip Power System/Rim Generator

HAWT, Non-standard Drive Train

This turbine uses magnets placed on the end of the blades and a ring surrounding the rotor, which forms the stator. The relative movement of the magnets in the blade to that of a rotor create a rotating magnetic field. Such a concept does away with the requirement for a traditional drive-train, gearbox and generator which lends itself well to large-scale multi-MW designs. The major engineering challenge is to ensure that the air gap between rotor and stator is small enough to allow significant magnetic flux to travel but with such tolerance that the two do not touch even under extreme wind loading.

One example of this type of concept is currently under development by *Honeywell* using their patented 'blade-tip power system' (BTPS).

3.5.3.11 Single Axis Secondary Rotors

Secondary Rotor, VAWT – HAWT, Grounded, Passive Aerofoil, Non-Augmented

Typically, the multi rotor design consists of a large rotor rotating around an axis and smaller rotors which rotate around individual axis. The small rotors experience a relative increase in wind speed velocity dependant on the radius from the centre of the large rotor and the rotational speed. The large rotor converts the kinetic energy in the wind into rotational energy which is then extracted using the smaller rotors. Primary work has been focused on the concept of a large V-shaped vertical axis rotor with smaller secondary horizontal axis rotors placed on each blade and facing into the wind.

3.5.3.12 Contra-rotating Rotors

Multi rotor, HAWT, Grounded, Passive-Aerofoil, Non-Augmented

The contra-rotating rotor is a concept that tries to take advantage of the wake vorticity and attempts to extract more energy from the same volume of wind than that from just one rotor disc. Theoretically, the amount of energy extracted by the two rotor discs can be increased from 59% for a single disc (as defined by Betz) to 64% overall for a given volume of air. The rotors are placed sufficiently far apart and offset by an angle, driving a rotor and stator in opposite direction. Studies in the early 00s suggest that the use of contra-rotating rotors can increase energy capture for a given installation by around 40%. Other experimental outcomes also found that the buffeting of the second rotor by the first was not considered a problem and that when both rotors were operating with similar torque, that the total bending stress of the tower was greatly reduced. The best conversion efficiencies appeared to be at low operating speeds, 0.5-0.66 rad/s suggesting that the concept would be better utilised at large scale [50]. Another study performed at the Danish Technical University and in association the wind research laboratory at Risø also confirms an increase of around 43% in terms of efficiencies, with the best C_P values being offered around 20rpm – when both rotors achieve individual C_P values that match at around 0.3 (i.e. total 0.6). Of course, the disadvantage of the system is the relative complexity of both device setup and operation, with dynamic matching of rotor speed being cited as a significant challenge. There is also the issue of cost, and whether it is not just as well building two separate machines with individually lower C_P values [51].

3.5.3.13 Flying Electric Generator

Multi rotor, HAWT, Airborne, Active-Aerofoil, Non-Augmented

The first understanding of auto-rotation in the form of the auto-gyro and its application in wind systems was made by Glauert in 1926 [52]. In the early 1990s, an Oxford bases inventor Colin Jack patented several WEC concepts revolving around the principles of auto-gyration which aim to have a device support its own weight through passive generation of lift [53].

In an energy generation configuration an auto-rotation rotor would convert excess rotational torque beyond that required to maintain flight into electrical energy.

A critical parameter of such a system is the minimum wind speed in which auto-rotation can occur after which it can no longer support itself. The minimum speed for auto rotation may be as high as 10m/s for a multi-MW device meaning that operation is only feasible in areas with long periods of predictable high winds.

One recent peer-reviewed paper gives some parameters for a potential 3.4MW, 4 rotors with a power/weight ratio of 358W/kg and costs of around $700k per MW of device suggesting that the concept has potential. One of the challenges for the concept is designing a tether with both the structural capacity and electrical conduction necessary to achieve operation at such heights with minimum power loss (estimates put the conduction loss at 20% + for a 10km cable.) [54].

3.5.3.14 Cross-wind Kite (Rotor Configuration)

In this configuration, the kite describes a circular figure of eight orbit, constantly changing its aerodynamic properties to maximize its relative speed compared to the flow field. On-board rotors can then be used to extract the energy from the wind, having the advantage of seeing a wind speed many times greater than that of the free-stream. The advantage of this design is that the on-board rotors can also be used as propellers to provide additional lift when required and to allow for powered flight either for landing or in cases when the mean wind speed is not significant enough to generate enough lift to support the devices weight.

The rotors would have similar properties to conventional horizontal axis machines, but be of much lower rating – with an emphasis on lots of smaller lighter rotors as opposed to fewer large ones [55].

3.6 NON-ROTOR

3.6.1 Oscillatory

An oscillatory WEC system is one in which the primary extraction device is encouraged to perform oscillatory motion during energy extraction. Within this branch, the classification can be broken down into three sub-sections: oscillating vanes/beams, oscillating cables and oscillating aerofoils. These classifications are derived from the shape of the extraction device rather than the specific motion - which can be either translational or dispositional. This branch also encompasses the use of purely piezoelectric materials for the conversion of these wind induced vibrations into electricity.

3.6.1.1 Inductive / Wind Belt

Non-Rotor, Oscillatory, Suspended, Non-Aerofoil, Non-standard drive train

This device consists of a magnet placed on the end of a narrow beam. The beam is made to vibrate in the wind with structural resonance, much like the effect of a violin string. The deflection from the normal for the tip of the beam is greatest and thus this moves the magnet relative to a stationary coil and in doing so induces an E.M.F.

As with all other oscillatory devices that rely on structural resonance, the devices considered are all sub-kW in size. One recent prototype generated only 40mW in a 4.4m/s wind though the cost per Watt appears to be as low as $2 making it a good candidate for mobile device charging, low power lighting and so on. The interested reader can find a substantive study at reference [56].

3.6.1.2 Oscillating Beam

Non-Rotor, Oscillatory, Grounded/Airborne, Passive Aerofoil, Non-standard drive train

This configuration utilises a rocking arm mechanism, hinged around a point and with one end tethered to a delta-wing kite capable of generating lift and therefore the work necessary to raise one end of the arm. The arm is counter-balanced by a weight at the opposite end such that when the lift of the kite is reduced, the arm rotates under this

weight back into its original position. Through successive control of the kite's angle of attack, the system can be made to oscillate and so drive an induction generation. The original concept was proposed by Goela as a method of cheap energy generation or for application in the pumping of water in remote regions. Recent research has focused on systems in the 1-5kW range [55].

3.6.2 Piezo-electrics

Non-Rotor, Oscillatory, Grounded/Suspended, Non-Aerofoil, Non-standard drive-train

3.6.2.1 Overview

Piezoelectricity is defined as the charge which accumulates in certain solid materials in response to applied mechanical strain. It is the result of a realignment of polarised electrons in a material under strain which causes a voltage drop to exist between the surfaces of the material in compression and tension. In other words, it is the combined effect of the electrical behaviour of the material and Hooke's law.

3.6.2.2 Theory

The theory pertaining to the use of piezo-electrics has been included in Appendix A and can also be found at reference [57].

3.6.2.3 The Case

The use of piezoelectric material as a method for converting wind energy to electricity is appealing due to their relatively simple nature. The active "blade" area can be as simple as a cantilever beam and is small enough for mass production. The mass of the blade is also relatively small, meaning that potentially the piezoelectric device could have some significant cost savings on a £/W scale. The nature of the oscillating beam means that the electricity generated is A.C and importantly the device itself is also a type of capacitor and therefore may store energy (note: charge placed on the electrodes will gradually leak away therefore there is a time constant for the retention of voltage on the piezoelectric material after the application of force.)

Of key concern, is the need for individual or collective power electronics, which may have to compensate for numerous beams oscillating out of phase and with different

amplitudes. It is therefore likely that each device will need to have its voltage converted into DC before aggregation with other devices. Another key issue is that while piezoelectric transducers are not inefficient in themselves, they are only useful at high frequencies of oscillation – which means that a typical wind profile will not suffice.

On first appearance, it appears that Piezo-electric generators can produce the highest power output per volume when compared against both electrostatic and electromagnetic devices (Table 3.1) [58].

Type	Energy density (mJ cm^{-3})	Equation	Assumptions
Piezoelectric	35.4	$(1/2)\sigma_y^2 k^2/2c$	PZT 5 H
Electromagnetic	24.8	$(1/2)B^2/\mu_0$	0.25 T
Electrostatic	4	$(1/2)\varepsilon_0 E^2$	3×10^7 V m^{-1}

Table 3.1 - Energy Density of PE, EM, ES

However, it can safely be assumed that these energy densities are only achieved when the mechanical frequency of driving vibrations match the electrical resonance frequency of the system – in the same way that maximum electrical power transfer occurs during electrical resonance. Such a condition must exist in order that maximum power transfer can occur.

Of course, this poses a problem as the mechanical system resonance will vary according to the applied force and therefore to maintain maximum power transfer, the system will have to adapt the electrical resonance dynamically.

Certainly, piezoelectric transducers do appear to compete in terms of power density with even batteries and fuel cells which gives them an avenue in the mobile energy conversion market.

One paper reported energy densities in the 9.2 mW/cm^3 region for a PZT cantilever vibrating at resonance at 100 Hz. This is favourable when compared to some other devices based on vertical or horizontal stalks which see energy densities in the 2 mW/cm^3 region [59].

3.6.2.4 Previous Research

There has been a relatively large amount of research done on the use of oscillating devices as 'wind energy harvesters', most of which is fairly recent. This includes research on: the use of piezo-electrics in place of a standard drive-train for a small scale conventional 'windmill' [58], the utilisation of vortex induced (Aeolian) vibrations [59] and also wake galloping effects for an inductive based device [60] and lastly the use of a purely piezoelectric device [61]. All of this previous research has been focused on the use of the devices on a relatively small sub-watt scale, with an interest in their use for low power applications, remote sensing and so on.

3.6.2.5 Parameters

As stated, most devices that have been under development/research are of very small size and rating. This means that the metrics are not necessarily easily or correctly scaled to larger sizes. Table 3.2 highlights the relatively low ratios that current piezo devices can achieve.

Device	**Dimension**	**P_{max} (mW)**	**mW/kg**	**mW/cm^3**	**W/m^2**	**mW/$**
Small HAWT	60x20x0.6	5	77.2	0.579	0.13	0.021
Galloping	100x38x1.54	1.14	72	0.556		
Wind belt		5			1.28	
Cross-flow	41x16x0.205	0.26	576	1.928	0.046	0.069
Cross-flow	72x16x0.205	0.21	343	0.871	0.013	0.034
VESTAS V52		850kW	27,000		400	300

Table 3.2 - Piezo Device Comparison

Comparing even the best piezo-configurations, it is found that they have 50 times less power to weight ratio and nearly 10,000 times less power to swept area than a sub-MW rated modern HAWT. This problem is exasperated by the fact that current piezo conversion efficiencies are only in the 2-3% region (an order of magnitude smaller than even the smallest HAWTs).

The only way in which piezo-electrics could become competitive is through matching of mechanical and electrical resonance which can make the difference between 19 W/cm^3 and 100 W/cm^3. Theoretical work suggests that the maximum electrical power output density and efficiency of a PVF_2 based generator oscillating at 1kHz would be 90 W/cm^3 and 80% respectively. Clearly this shows that the concept of piezoelectricity

is useful, but that the use becomes lessened when such devices are subjected to low frequency wind distributions [61][62].

3.6.3 Translational

3.6.3.1 Madaras Concept

Multi Rotor, VAWT, Grounded, Active-Aerofoil, Non-Augmented

The Madaras concept is based upon a Flettner rotor placed on a cart which translates along a fixed circular track with the idea of plant capable of generating upwards of 40MW. Ideally, the wind is perpendicular to the track and generates a lift force (due to the Magnus effect) collinear to the track. Induction generators are fitted to each of the wheels of the cart, and convert the carts translational velocity into electrical energy. The concept suffers from several issues due to the mechanical complexity of the design, the requirement for the rotors to reverse every half revolution, poor aerodynamic design and the low TSR [64].

More recent development based on this concept (1970s) included individual carts weighing several hundred thousand tonnes with net generation per cart being in the region of 750kW-1MW suggesting very poor power/weight ratios but vastly superior power/swept area ratios to that of conventional rotors (6.25kW/m^2) though as much as half of this power would be needed to power the heavy rotors. If there were 200 cars on the track, then suggested outputs could be near 200MW.

3.6.3.2 Flying Aerofoil / Ladder Mill

Translational, Multi-Axis, Airborne, Active Aerofoil, Non-Augmented

The ladder-mill is a high-altitude wind energy conversion system first proposed in a patent in 1996. It utilises a series of aerofoils (wings/kites) all connected to a ground tether forming a huge rotating loop (Figure 3.27). Like aeroplane aerofoils, the wings cause an upward lift force and by changing the attitude of the wing (specifically its angle of attack) the lift force can be altered.

For half the cycle, the wings are angled to provide maximum lift and while on the other half of the cycle they are angled to only provide enough lift to cancel out their own self-weight such that the whole loop remains airborne. In this manner, the loop creates a torque differential that is then counter-acted by a generator on the ground. Typical cable speed is predicted to be around 5m/s

So far, no existing prototype or model exists so it is difficult to speculate on parameters [65].

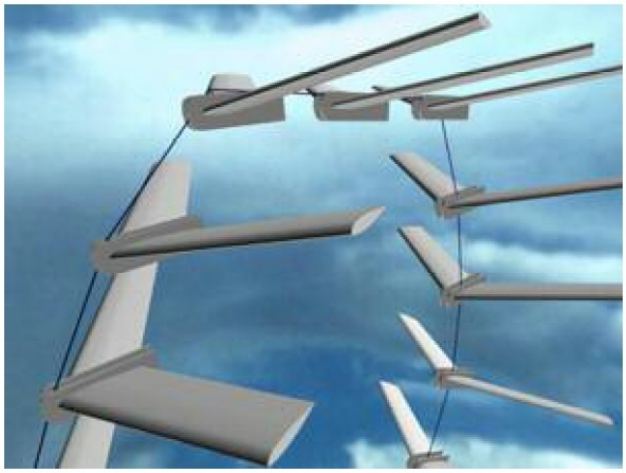

Figure 3.27 - Laddermill Concept

3.6.4 Cross-Wind Kites

3.6.4.1 Introduction

A kite is a kind of tethered aircraft. It utilizes aerodynamic force on what is essentially a simple wing to create buoyancy and lift. It is generally designed to be as light as possible, though for the purposes of this section can be considered heavier-than-air (lighter than air devices are treated separately). Most simple designs simply rely on wind drag forces and are guided by control wires. More advanced designs can be engineered to offer higher lift to drag coefficients and can be flown with minimal input from the user.

3.6.4.2 The Case

Kites are designed to be light enough that they can maintain steady flight at high altitude. This allows them to tap into stronger and less turbulent winds away from

the earths boundary layer. Given that power capture increases as the cube of wind speed this should give kites a significant advantage over HAWT's when considering power/weight ratios. Provided, that the component parts of a kite generation system are equal to or cheaper than that of a similar rated HAWT this should make them serious competitors in the multi-MW range.

Consider that a typical HAWT produces 90% of its total torque using the outer 40% of the blade due to the $T = F \cdot R$ relationship and the fact that the force on the blades is proportional to the square of the local speed relative to that of the air. Tethered aerofoils get rid of the heavier inner support structure and focus on the outer part of the aerofoils that produce the most energy (see Figure 3.28).

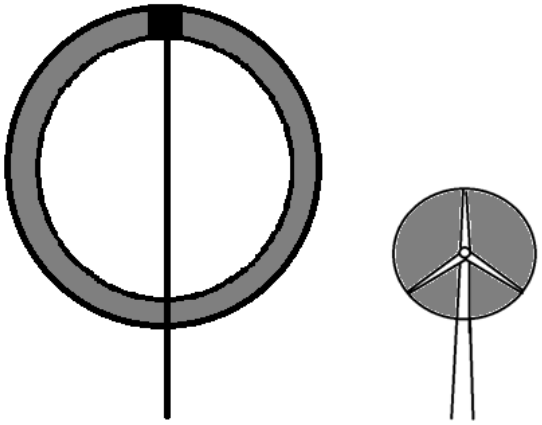

Figure 3.28 - Conceptual Swept Area for a Kite vs Conventional HAWT

A standard rotor blade is designed with strength in mind. It must be capable of surviving the '50 year-storm', must be strong enough to keep forced deflection within specified limits during normal operation and must be capable of supporting its own weight (and that of ice accretions.). A kite does not need to meet these restraints. It can be brought to earth prior to the arrival of heavy winds. It has no tower to which it can strike and because the tether travels at almost the same speed and lags the kite. With these in mind it seems sensible that kites be examined in some depth so that their relative merits can be adequately reviewed.

3.6.4.3 Configurations

Kite energy convertors can be configured either through a tether which transmits energy mechanically to a ground based generator, or by on-board rotors which convert the kinetic energy into electrical energy [66].

Regardless of the type of configuration that the kite is set up for, the fundamental physics that support its operation will be the same.

3.6.4.4 Early Kite Research

Most of the early pioneering research in the use of kites for wind energy conversion was carried out by M. Lloyd in 1979. Using a series of developed equations, he predicted that a kite of cross-section 576m^2 would be capable of producing upwards of 6.7MW of power and a 2000m^2 kite would be capable of producing 22.2MW [66].

Another group of researchers at the University of Sydney led by C. A. J Fletcher also began looking at the possibility of kite powered electricity generation at the end of the 1970s. They investigated four configurations of *kites with secondary rotors* on-board (comparison shown in Table 3.3). These systems were labelled as the: Integrated Diffuser Augmented Turbine Concept (IDAWT), Separated Diffuser Augmented Turbine Concept (SDAWT), Separated un-shrouded wind turbine concept (SUWT), and the Rotary-wing concept (RWC). As part of their research they built scaled models of two of these concepts for testing in wind-tunnel conditions (with a major focus on the IDAWT). These tests suggested that the IDAWT would be capable of C_P around 1.3 for a 1-MW machine suggesting an augmentation factor of around 4 – on par with other research on diffuser designs for conventional HAWTs. But that the power coefficient for the SDAWT concept was also very similar. They also carried out a detailed cost analysis for all four devices that clearly favoured the IDAWT and which suggested capital costs in the region of $659/kW (AUS).

	IDAWT	SDAWT	SUWT	RWC
Rotor Diameter	6.6	9.4	11.4	22.2
Swept Area (rotor)	136.8	138.8	408.3	1548.3
Rated Speed (m/s)	46.4	46.4	46.4	46.4
Rated Power (MW)	2.2	2.2	2.2	2.2
Structure Weight – not inc. Tether	7600	6720	6390	4320
Tether Weight	4180	3710	5630	5900
Total Weight	11780	10430	12020	10220
Delivered Power	1	1	1	1
Capital Cost $K	1658	1568	1764	2162
C_p rated	1.05	0.518	0.088	0.023
Transfer η	0.454	0.454	0.454	0.454
W/kg	186.75	210.93	183.03	215.24
W/m²	7,300	7,200	2,450	645
W/$	0.603	0.637	0.567	0.4625
Operating c$/kWh	4.92	4.94	5.40	16.01

Table 3.3 - Airborne Rotor Comparison

For each of the designs, the need to factor in the costs of replacements weighed heavily on the projected costs of operation and lead to the RWC costs to be 3x more expensive than the other three concepts. The operational wear on kite-rotors would be significant if they were generating for upwards of 7000 h/year which is almost ten times more than a typical aircraft [67].

The first investigation into the use of *lighter-than-air systems* such as a tethered balloon with on-board rotors was suggested in 1981 by G. Riegler *et al.* at the Research Centre Graz. In the proposed system, a zeppelin shaped balloon carries six symmetrical 2-bladed rotors connected to direct-drive generators which transmits the power to a ground station through electrical conductors. Such a high-altitude system would be projected to operate well above the surface boundary layer away from turbulence (4000m for clearance of mountains) and would therefore experience good capacity factors and average wind speeds.

In their analysis, the researchers did not consider rotors of greater than 40m diameter due to weight considerations but discuss a system which theoretically could yield up to 7MW of power [67].

3.6.4.5 Recent Kite Research

In 2005, David D. Lang analysed and graded a host of different kite concepts based on 12 different criteria. His analysis clearly pointing to the simplicity and relative merits of using a kite to reel-out a cable from which useful work could be done [68].

3.6.4.6 Theory

The lift to drag profile is crucial to a kite's performance, its operating height/speed and ability to generate power. This is particularly so for kites and other aerofoil devices for which flight can only be achieved through lift to drag ratios greater than one.

It can be shown that the tan of the lift-drag ratio [$tan\left(\frac{L}{D}\right)$] of a kite will determine the maximum angle it and the kite line can make with respect to the ground. So for example, a lift to drag ratio of 1:1 will create an angle of 45°, *L*/*D* of 3:1 an angle of 72°, a *L*/*D* of 8:1 an angle of 83° and so on. Thus, presuming the maximum lift to drag ratio is known, the maximum height obtainable for a given tether length can also be found.

The force on a kite depends on the kite depends on the aerodynamic efficiency, that is: $\eta_{aero} = \frac{C_L}{C_D}$. Thus, a kite with a *L*/*D* ratio of 8:1 will experience twice as much force as one which has an *L*/*D* ratio of 4:1. The *L*/*D* ratio also suggests is the maximum ratio of cross-wind speed against that of the free-stream wind. I.e. a kite with a *L*/*D* of 8:1 can travel at 80m/s in a 10m/s wind, whereas a kite with *L*/*D* of 4:1 can only achieve 40m/s. Therefore as $P = F \cdot v$ then the power generated must be a function of the square of aerodynamic efficiency. Thus, devices with high lift to drag ratios will be the most optimum for energy generation.

3.6.4.7 Types of Kite

Classifying kite types in any structured format is difficult due to the varied and sporadic evolution of the designs over many centuries many of which do not follow directly from one another. A good summary of each of these classifications is presented by Hobbs in his PhD thesis [69]. The type of kite used will depend on the desired characteristics, for example: box kites are considered very stable but require stronger winds in which to fly and are also less manoeuvrable; on the other hand, a structured-plane-surface such as the Delta kite is much more controllable, suitable for low wind speeds but fairs much worse in turbulence.

A good structured-plane-surface kite design will spread the load evenly across the supporting struts. If the loads are well distributed, then not only are the struts less likely to break but it also means lighter ones with less structural capacity can be used. The kite will also deform less at higher speeds which could be critical for stability. With wind pressure, p, a kite of size L will develop forces of the order $p \cdot L^2$ and moments of the order $p \cdot L^3$. Thus, clearly the overturning moments are increased with the structures size much more than the force which will provide the cable tension needed for generation. This means that the structure will also suffer from scaling effects which require more material as the length of the kite increases. Generally, struts can be kept short, with flexible joints so that no long lever arms are present to generate large couples.

3.6.4.8 The Kite Line

The kite line (the 'tether' that provides a reaction force against the wind) has an important role to play in the kite system dynamics. The most comprehensive study of kite lines was conducted by Goela, his study developed a series of equations which can be used to describe the motion of a kite tether in a cross-wind configuration [70].

His analysis of tethers suggests the ratio of $\Delta L/_D$ (ΔL the difference between the lift and weight force) must not be much less than one otherwise the tether will snap under its own weight. This contrasts with the findings from Fletcher which suggested that $\Delta L/_D$ should be around unity for economic operation [67].

3.6.4.9 Parameters

To conduct a parametric study of kite systems using variables such as power/weight or power/swept area requires an understanding of what constitutes swept area for a kite.

Consider the case of a kite being flown downwind and tethered, it is theoretically capable of occupying a volume that can approximately be described by a cone, with the tip of the cone originating at the tether point. However, under the assumption that the wind can also change direction and that the kite will continue to be flown downwind then this volume becomes something akin to part sphere/part cone.

By considering only the cross-section of this shape that intersects the wind perpendicular then this shape becomes a fan (see Figure 3.29). The area of a fan is simply a proportion of the area of half a circle, dependent upon the angle to the normal thus:

$$A_{half-circle} = \frac{1}{2} \cdot \pi \cdot r^2 \tag{3.21}$$

$$A_{fan} = \frac{\varphi}{2} \cdot r^2 \tag{3.22}$$

where: φ - the internal angle (rad), r – the maximum length of the tether (m)

Of course, the kite can also move downstream but is limited in its range due to tether which in turn limits its overall cross-section height. Thus, the cross-sectional area that the kites orbit describe will always be less than A_{fan}.

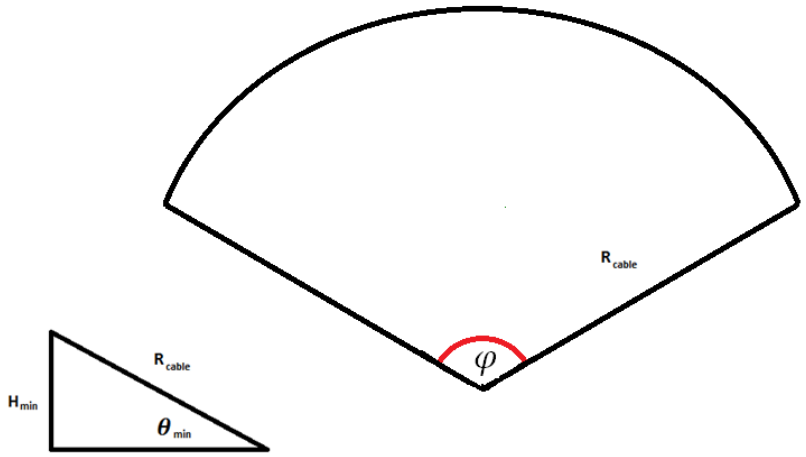

Figure 3.29 - Fan Shaped Cross Section of Tethered Kite

Assume now that the minimum angle, θ_{min}, the kite tether makes to the ground is fixed, then the minimum height can also be calculated for a given cable length: $H_{min} = cos(\theta_{min}) \cdot R_{cable}$

In addition, the fan-shape internal angle of motion, φ, will be equal to: $\varphi = 180 - 2 \cdot \theta_{min}$

A reasonable assumption would be to set the minimum angle to 30-45 degrees (*L*/*D* ratio of 0.57:1 - 1:1) or the minimum height at full extension to 100m – but this will obviously be dependent upon safety distances or the calculated optimum orbit for maximum energy capture. For this study, it will be assumed that the minimum angle that the device makes to the ground is 30 degrees and therefore the maximum cross-section area will be:

$$A_{cross-wind} = 1.047 \cdot {r_{max}}^2 \tag{3.23}$$

This method of calculation is only valid for a single tethered device which can rotate around a fixed hinge point as opposed to a rotation around a disc such as in a carousel configuration (Figure 3.30).

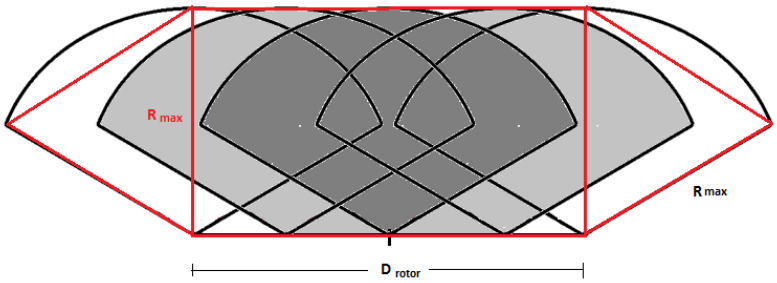

Figure 3.30 - Approximate Swept Area of Kite in Carousel Configuration

Yielding a total swept area of:

$$A_{carousel} = {R_{max}}^2 + D_{rotor} \cdot R_{max} = R_{max}(R_{max} + D_{rotor}) \tag{3.24}$$

3.6.4.10 KiteGen

KiteGen is one of the few companies focused on the development of kite wind energy systems in the multi-MW scale.

Small scale versions include two kite lines wound around a drum and linked to two electric drives. The flight of the kite is controlled by regulating the pulling force on each line. Energy is extracted when the kite does work pulling out approximately 300m of tether for half its cycle. On the other half of the cycle, the tether needs wound and in this expends around 12% of the energy captured during the working phase.

In the carousel configuration, the working part of the cycle could be as much as 300 degrees (5/6) of the cycle using 'tacking'. Only 1% of the energy of the rotor is used to drag the kite against the wind for the remaining 60 degrees.

Some of the information that KiteGen have made available from both hardware tests and simulations show some interesting results (Table 3.4):

Kite Gen	Prototype (Tethered)	Simulated (Carousel)	Predicted (Carousel)
Wing Area (m^2)	10	50	
Number of blades	1	1	
Rotor Diameter	0	300	
Line Length	800	300	
Active Area (eqn. 3.24)	670,080 est.	180,000 est.	280,000
Power Output (kW)	40	200	84,000
Wing Mass	5		
System mass ex. cable		8,000	2,000,000
Cost ($)		1,200,000	
W/kg		25	42
W/$		6	
W/m^2 (swept)	0.06	1.11	300
W/m^2 (occupied)	4,000	4,000	

Table 3.4 - KiteGen Metrics

Based on these figures, it is clear that the prototypes of the design are still of limited scale and potential. This situation is improved by utilising a greater wing area simply because an increase in the solidity of the cross-section allows for greater energy capture. Additional wing area is most easily achieved by arranging multiple individual kite units on a carousel system.

Considering the typical power to weight ratio of a 2MW HAWT is 6.67 W/kg, then a single device (simulated) could have up to 12,000 kg of mass before its power/weight ratio became worse. Even a single 800m cable of cross section $1cm^2$ could weigh less than 60kg, and therefore even with 4 control lines this would represent only 240kg (<2% of this capacity). In essence, the parafoil material could weigh up to 234 kg/m^2 - which give it considerable scope from a power/mass perspective.

3.6.5 Lighter Than Air (LTA)

3.6.5.1 Introduction

The use of lighter than air gases to achieve buoyant lift into the earth's atmosphere has been practiced for over a century. While the use of LTA devices has declined in

recent decades, they are still in use for high-altitude weather observations at the kinds of heights that proposed wind energy generators would operate.

3.6.5.2 The Case

LTA systems are relatively simple – literally lifting a conventional wind turbine rotor into the sky and replacing the tower with a tethered balloon. As Tower mass for a conventional HAWT rises almost linearly with rated power [40] a 2MW machine might have a tower weighing in the region of 120 tonnes while a 5MW machine this might be closer to 260 tonnes. That an LTA system could do away with a tower (and have savings of several hundred tonnes - Figure 3.31) at the same time as tapping into high altitude wind speeds gives it enormous cost reduction and revenue capturing potential [71].

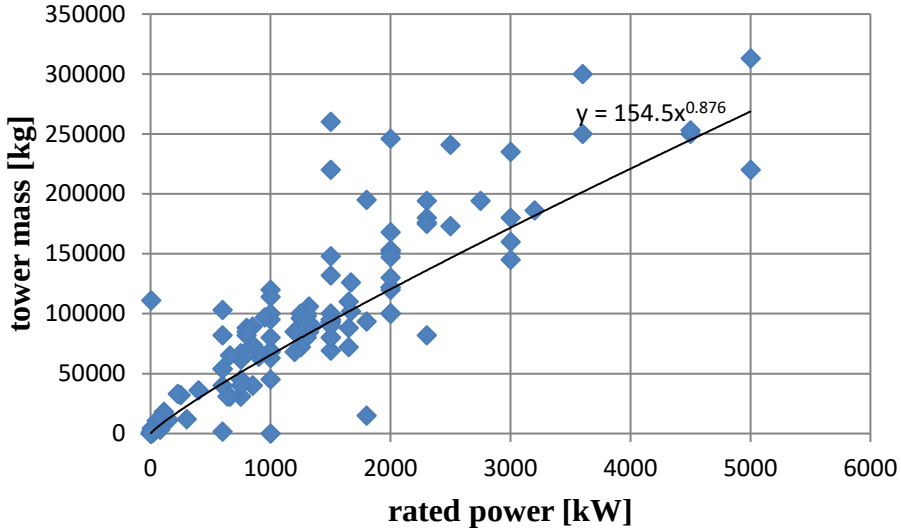

Figure 3.31 - Tower Mass Plotted Against Rated Power

3.6.5.3 Previous Research

High altitude air systems utilising LTA devices have not been studied extensively in comparison to other airborne devices. The majority of concepts exist in only patent form, for example, US Patent: 4,073,516 [72], US Patent: 4,165,468 [73], US Patent 4,450,364 and US Patent: 4,450,364 [74].

Magenn the only known company to be pursuing LTA technology and has performed work on a commercially available 100kW system that has a Helium filled skin of 5663m^3 and weighs in at just under 5897kg.

3.6.5.4 Theory

At a basic level, an airship consists of an outer sheath filled with a lighter than air gas such as: hydrogen, helium or hot air. Other gases have less lifting capacity and a series of other problematic factors such as being flammable, corrosive, toxic and so on.

The objective of an airship is to displace as much air as is necessary to create a force which will overcome its own weight and allow it to become airborne.

While hydrogen is much more abundant than Helium (and is therefore cheaper), has a greater lift capacity and can be easily produced through the electrolysis of water, it suffers from being highly flammable. Helium is only found in natural gas wells and is therefore relatively scarce, but has similar lifting capacity and has the advantage of being inert [75].

Consider a typical the weight of a 40m diameter 3-bladed rotor to be around 8000kg then 76,200m^3 of Hydrogen would be required to lift it into the sky. To put that into perspective, the Hindenburg (the largest airship to ever fly) contained 200,000m^3 and was 245m long, so this device might be around 1/3 this size. This would suggest that such a device would be almost as large as the same power rated HAWT. Clearly, were such a device to exist, there would be an over-riding requirement to bring the rotor weight down [76].

Considering only static lift, there is a limit to how high a non-rigid or semi-rigid LTA system could fly before stasis occurs (when the pressure on the outside of the skin becomes greater than the inside and the structure collapses). Another significant challenge is that the atmosphere at high altitude is also much less dense than at sea-level. This means that a given volume of displaced air actually generates less lift force and therefore limits most systems to specific heights. Modern rigid-airships are

capable of heights of around 30,000ft which would be more than enough to enable such devices to reach the energy rich jet-stream [77].

3.6.5.5 Parameters

This parametric study will only focus on the reported results of the Magenn system due to a lack of other data and the projected size of system that would be required to generate 10MW. A comparison is shown in Table 3.5.

	Magenn	**LTA 10MW (predicted)**
Effective Area (m^2)	830	41500
Number of blades	4	2x3
Power Output (kW)	100	10,000
System mass ex. cable	5897	275,000
W/kg	16.96	36.36
W/m^2	120.48	120.48
Cost $	500,000	2,308,000
$/W	5	0.2308
Volume (m^3)	5663	279,000
W/m^3	17.66	35.84

Table 3.5 - LTA Metrics

The total mass of the Magenn system is 5897kg excluding the mass of the tether. To put this into perspective, a conventional 100kW rotor weighs about 5,000 kg, while the combination of nacelle, rotor and hub can combine to around 8-9,000 kg. Although the tether mass in this case is unknown, it is certainly the case that it would much less than the mass of a conventional 100kW tower. Indeed, if the diameter of the balloon is taken to be something in the region of 60m then it would have a cross-sectional area facing into the wind of 2826 m^2. At an extreme wind speed of 50m/s, this would result in a drag force (using equation 2.27) of 4.3 MN (assuming an absolute worst-case C_D of 1.0). It can also be assumed that at this height the static lift provided by the lifting gas will almost be in balance with gravity and therefore the lift force will not be significant. If the steel cable was designed with a safety factor of two then at worst, this would mean that the cross section of the cable should support

8.4MN. If this cable was made of steel then the cross-section would need to be: $8.4x10^6/_{500x10^6} = 0.0168m^2$ and therefore a 10km steel cable would weigh 1318 tonnes. However, if the cable was made from carbon fibre nano-tubes then this value would drop down to around 41.8 tonnes, but which is still around four times more than the tower and hub weight for a 100kW HAWT. These values suggest that putting a low rated rotor up on an LTA system at 10km would be unfeasible but that at around 1km height the overall weight would be acceptable.

In terms of cost, a 100kW rotor made from solid carbon steel might cost around $4000, crude helium sold at $28 per 1000m^3 for 5663 cubic metres would cost $158.56. This makes the cost of lifting gas less than 4% of the total cost of a normal rotor and if it is assumed to be a perfect sphere then the total area of material required to contain this gas would be 1536m^2. There are dozens of materials that would be suitable for well under 1 $/m^2 taking this total to less than $1750 (around 44% of a conventional rotor). Of course, this does not yet take into account the cost of the active blade area on-board the LTA system which might be equally as expensive as a conventional rotor but then neither does it account for the savings offered by the use of a tether instead of a tower and nacelle which might see the relative cost drop further.

To arrive at the 10MW scaled version of the system, assume that the system must utilise two 5MW rotors and that the only cost/weight savings are made on the tower and nacelle.

The weight of two 5MW rotors is predicted to be 220 tonnes. This weight alone requires 210,000m^3 of helium but it is assumed that the actual requirement is a further 1/3 to account for the rest of the systems mass, i.e. 279,000m^3. In terms of helium, this would cost $7812 and the cost of sheath material around $510 which pales in comparison to the cost of a conventional HAWT (at 1 million USD per installed MW). Assuming that the rotor accounts for around 20% of this cost then the cost would be around $2 million for the active conversion system.

To hold this volume of helium would require a spherical balloon of radius 40.5m which would present a cross-section to the wind of 5150m^2. This would require a tether capable of supporting at least 7.88 MN and if made of carbon nano-tubes would result in a tether (10km) weighing 54.7 tonnes. Unfortunately, the cost of carbon nano-tubes are currently prohibitively expensive at around $50 per gram ($21 billion for a 10km cable.) and therefore it is unlikely they would be used at any point in the near future. Some suggestions of suitable materials for the tether include nylon infused with Kevlar and also dynamee rope – in which case the cost of the cable could come down to as low as $200,000-$300,000.

Thus it would appear that the technology does have some merit at the larger scale. Unfortunately, because the technology appears quite uncompetitive at the lower end of the power spectrum it makes it difficult for any manufacturer to build up the expertise necessary to embark on 5-10MW designs.

3.6.6 Hydrodynamic Systems (HDS)

3.6.6.1 Introduction

Conventional HAWT's achieve rated power at 8-10 m/s after which they pitch their blades to maintain constant power output. In addition, to avoid extreme loading design constraints they are shut-down at wind speeds above 25m/s. Both of these controls result in a loss of potential energy capture at higher wind speeds (generally a turbine spends about 1/3 of its time at wind speeds above rated).

A wind energy convertor which can do away with a rotor and associated drive train could in theory benefit from capturing more of the available wind energy and secondly avoid the reliability issues associated with many moving parts [78].

3.6.6.2 The Case

The fundamental aims of a WEC device is to: 1) extract energy from the wind by applying a reaction force against the wind and 2) create a voltage potential.

Electro-hydrodynamic devices (EHD) utilise the force generated by the wind to move electro-statically charged particles downstream in order to create a potential

difference against which useful work can be done. As solid-state devices with no rotating machinery or moving mechanical parts they can take advantage of high wind speeds without the need to shutdown. There are no intermediate stages whereby energy can be lost and there is no force transfer which means that reliability should in theory be high.

3.6.6.3 Early Research

Research into the use of electro-fluidic wind energy conversion system was carried out as early as the late 1970s in the USA [79]. A more detailed study was carried out in 1984 at the University of Dayton by the same lead researcher [80]. This system comprised of both emitter and collector configuration. The main conclusion from the study were that EHD systems (with correct optimisation) can fully realise a cubic increase in W/m^2 output with increasing wind speed. This lead to researchers predicting energy outputs of up to 700 W/m^2 in 20m/s winds which would lead to a C_P value of 0.14 (not bad considering HAWTs around that time were achieving C_P values around 0.2).

Although the work focused on the optimum horizontal/vertical spacing between adjacent emitters as-well as the effect of collector/emitter voltage potential, the research also identified a conceptual design from which some useful parameters can be found. These parameters are listed in Table 3.6 along-side the findings of more recent studies in the design. The main barrier at the time was the feasibility of charging droplets efficiently in large numbers and in a minimum volume. Technology has now advanced to a point where the concept merits revisiting.

3.6.6.4 Recent Research: EWICON

A significant branch of research and development has been carried out on the EFD/EHD concept, primarily at the University of Delft in the Netherlands. This EWICON system has even made it as far as the prototype stage.

From initial tests, conversion efficiency was found to be low at 7%, a range of improvements were suggested that might help bring this efficiency up to 30%.

This EWICON device tested was capable of producing 50mW per nozzle in wind speeds of 10m/s, utilising 15 um droplets, 70% charge and a flow rate of 20ml/hour. At 12 m/s, a wind surface area of 10cm^2 gives an output of 70mW for an overall area output of 7 mW/cm^2, or 70 W/ m^2. While this value is not exceptional, it is not a far cry from a modern HAWTs 400 W/ m^2 and does so without any moving parts.

However, the investigation did not make conclusive statements about the projected weight or cost of the device making a true comparison difficult. One of the most significant challenges is the engineering of such a large number of nozzles in a small area for use in this device. EWICON suggested the use of a High Pressure Monodisperse System for droplet formation - more details of which can be found in their report [81].

3.6.6.5 Configurations

There are generally two configurations (Figure 3.32) in which a EHD/EFD system can be set up; the first consists of both collector and spraying apparatus and the second requires only spraying apparatus.

In the isolated charging system, wind extracts the charged particles for the system, the earth acts as a collector and the potential of the system rises. Polarity of the system is opposite to the polarity of the particles. The advantage of device two is that it is much simpler and needs only a single structure. The disadvantage is that it can only create a positive or negative potential with respect to ground (essentially halving its efficiency).

The double configuration has the ability to generate much higher potentials, with one part of the device taking up positive polarity and the other negative. The disadvantage is that it requires a potentially very heavy/bulky collector structure to collect the majority of the released charges. It would also need to be yawed with the device such that it was always downstream. Any charges not collected by the collector would suffer from the same differential charge penalty as the single configuration.

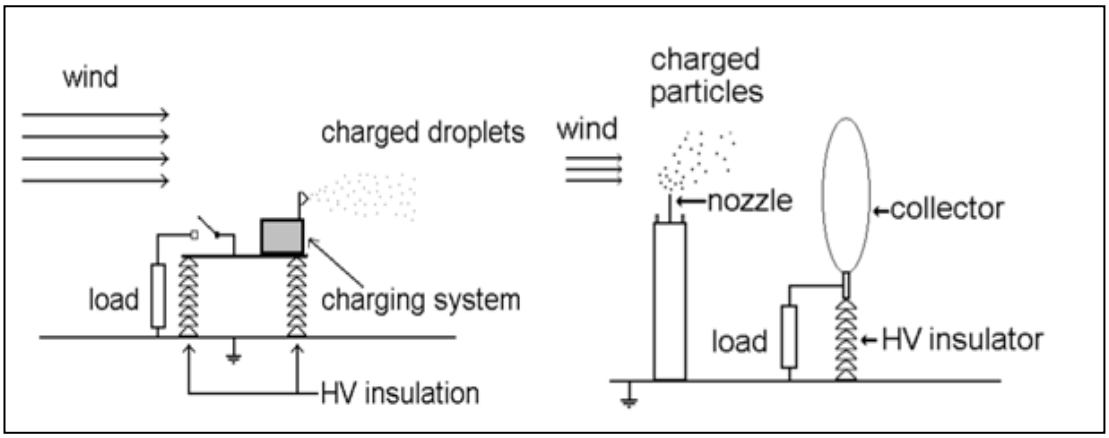

Figure 3.32 - Two EHD Configurations

3.6.6.6 Theory

Further theory for the interested reader is presented in Appendix B

3.6.6.7 Parameters

The following Table (Table 3.6) lists the predicted/conceptual parameters of a 5.7 MW design postulated during the 1980s and also the results from the more recent EWICON prototype. It also includes the predicted scaling parameters that the EWICON researchers think is feasible.

EHD Parameter	EFD 1983	EHD Prototype	EHD2007 (scaled)
Effective Area (m^2)	24000	0.1	400
Number of nozzles		3	1,000,000
Power Output @ 10m/s	5,760	0.00007	100
System mass (kg)	1,721,000	N/A	N/A
W/kg	3.35	N/A	N/A
W/m^2	240	0.7	250
Cost $	23,000,000	N/A	N/A
$/W	4	N/A	N/A

Table 3.6 - EFD Metrics

Clearly, the most over-riding factor in these designs is the overall weight of the system which is necessarily large. In addition to the single/double supporting structure(s), the system must also include pumps, high voltage insulation, power electronics and a fluid reservoir. The result is that for a given power output, the power to weight ratio is comparatively small. It can also be seen that when the design was first proposed, the technology also imposed a significant cost factor on the device

which would have made any commercial opportunity completely unfavourable (the price is still about 3-4 times more expensive per MW than today's multi-MW HAWTs. The actual EFD/EHD method of generating power itself appears to be capable of competing on a W/m^2 scale, suggesting that perhaps the device would have some merit if it could be scaled up into the 20MW range. This scaling would only be feasible if the sunk costs of the structure were relatively independent of the size of the system. It is certainly the case that both the droplets ability to retain charge and also the density of droplet emitters would play a key factor in determining the success of any commercial device.

3.7 NOVEL-ROTOR EVALUATION

3.7.1 Gravity Compression Turbine (GCT)

3.7.1.1 GCT Introduction

The concept of using gravity as a means of generating energy is not a new one, indeed many ideas for perpetual motion machines including the 'Bessler wheel' [82] centred around the use of the Earth's gravitational field. The concept is concerned with the turning of rotational kinetic energy provided by the wind into lateral kinetic energy working with and against gravity.

The concept in its simplest form is described as follows: The wind provides a torque on the rotor which rotates, accelerating from zero. Within each blade is a hollow chamber running from some minimum near the root to a maximum near the tip and inside each chamber is a mass. At rest, the mass is balanced by a component of weight and a spring and this balance point moves as the rotor begins to speed up and the mass experiences a positive outwards centrifugal force. At the bottom of the cycle, both the centrifugal and gravity forces are acting positively outwards and the spring inwards (in a rotating reference frame) and at the top of the cycle both gravity and spring are pulling the mass inwards while centrifugal force acts outwards. Thus through each cycle of rotation and with appropriate parameters the mass can be seen to move through the full length of the chamber twice. The kinetic energy associated

with this movement over time will be approximately equal to the amount of power input by the wind and can then be extracted by some means. With appropriate choices of parameters the path described by each piston can be made asymmetric such that the gravity restoring torque is equal to that of the aerodynamic torque, stabilising the rotor at some speed. One of the key parameters in making such a system work is the rotor speed, which must be kept relatively low in order to ensure that gravitational forces experienced by masses within the blades are proportionally significant compared to centrifugal forces.

3.7.1.2 Theory

In order to better understand such a system, a mathematical formulation of the problem in terms of the dynamics of the system can be established. This is most conveniently done using a Lagrangian for the rotor and sliding mass, modelled as a spring mass damper system. The Lagrangian defines the dynamics of the system as the kinetic energy, T, minus the potential energy, V. [83] (3.57) Thus:

$$L = T - V \tag{3.57}$$

The system will contain kinetic energy in both the rotor and in masses within each blade therefore the total kinetic energy will be a linear sum of terms.

For the rotor, the kinetic energy can be described by the equation for rotor angular momentum,

$$L = \frac{1}{2} \cdot I_R \cdot \omega^2 \tag{3.58}$$

And in a polar co-ordinate system, the mass has kinetic energy both radially from the centre and tangentially thus:

$$E_r = \frac{1}{2} \cdot m \cdot v^2 \tag{3.59}$$

$$E_T = \frac{1}{2} \cdot m \cdot (r \cdot \omega)^2 \tag{3.60}$$

Combining all three arrives at a new equation for the kinetic energy of the system, T minus a damping coefficient, k_d which can be used to represent energy extraction.

$$T = \frac{1}{2} \cdot I_R \cdot \omega^2 + \sum_{i=1}^{b} \frac{1}{2} \cdot m(v_i{}^2 + (r_i \cdot \omega)^2) \tag{3.61}$$

In terms of potential energy, only the free masses are able to convert potential into kinetic energy therefore the Lagrangian potential term consists of gravitational potential energy and the energy stored by the spring.

$$-E_p = m \cdot g \cdot \sum_{i=1}^{b} \left(r_i \cdot \sin\left(\theta + \frac{(i-1)\cdot 2\pi}{b}\right)\right) \tag{3.62}$$

$$E_s = \sum_{i=1}^{b} \frac{k_s}{2} \cdot (r_i - r_0) \tag{3.63}$$

Summing the two terms (3.58)(3.59) arrive at a new equation that describes the potential energy held by the system.

$$V = \sum_{i=1}^{b} \left(m \cdot g \cdot r_i \cdot \sin\left(\theta + \frac{(i-1)\cdot 2\pi}{b}\right)\right) + \left(\frac{k_s}{2} \cdot (r_i - r_0)\right) \tag{3.64}$$

The Lagrangian equation of the complete system can then be formed by substituting (3.61) and (3.64) into (3.57).

$$L = \left(\frac{1}{2} \cdot I_R \cdot \omega^2\right) + k_d + \sum_{i=1}^{b} \left(\frac{1}{2} \cdot m \cdot v_i{}^2 + (r_i \cdot \omega)^2\right) - \left(m \cdot g \cdot r_i \cdot \sin\left(\theta + \frac{(i-1)\cdot 2\pi}{b}\right)\right) + \left(\frac{k_s}{2} \cdot (r_i - r_0)^2\right) \tag{3.65}$$

Using the Lagrangian in (3.65) the equations of motion can be formed for all moving masses within the system, in this case the rotor and piston.

The equation of motion for the rotor is found by differentiating kinetic energy with respect to rotor speed and potential energy with respect to blade angle.

$$\frac{d}{dt}\left(\frac{\delta}{\delta\omega} \cdot T\right) - \frac{\delta}{\delta\theta} \cdot V = Q \tag{3.66}$$

Replacing T and V with equations (3.61) and (3.64) respectively and differentiating, becomes

$$I_R \cdot \alpha + \sum_{i=1}^{b} (2 \cdot m \cdot \omega \cdot r_i \cdot v_i) + (m \cdot \alpha \cdot r_i{}^2) - \left(m \cdot g \cdot r_i \cdot \cos\left(\theta + \frac{(i-1)\cdot 2\pi}{b}\right)\right) = Q \tag{3.67}$$

This equation of motion now encapsulates all the forces and dynamics present in the idealised case of a rotor with moving masses. Of course, this analysis is minus any actual way of extracting energy other than through a damping term. It is expected that this term would be replaced with an appropriate equation to represent energy extraction. Further to this, the dynamics of any liquid or gas used as the working fluid would need to be modelled in the equations of motion as in the case of liquid, this would likely represent a significant added mass.

From this equation of motion, can be identified the terms for the rotor torque, net coriolis torque, piston torque and gravitational torque. These are the forces expected to act on the rotor and therefore act as a check against the differentiation of the Lagrangian.

In similar fashion, the equation of motion for a sliding piston is derived by differentiating the Lagrangian with respect to mass radial velocity and mass radial position.

$$\frac{d}{dt}\left(\frac{\delta}{\delta v}\cdot T\right)-\frac{\delta}{\delta r}\cdot V=Q \tag{3.68}$$

Inserting (3.57) and (3.60) into (3.62) and differentiating once again, derives the equation for the dynamics of a mass inside a blade.

$$(m\cdot\omega^2\cdot r)-k_s\cdot(r-r_0)-m\cdot g\cdot sin(\theta)+k_d \tag{3.69}$$

In this equation of motion, the terms for centrifugal force, spring reaction force, gravitational force and a damping term (which will represent the energy extraction) can be seen. There will be one equation of motion for each of the blades connected to the rotor that contain a piston.

In total, the system will have n+1 equations of motion, with n being the number of blades.

3.7.1.3 Energy Balance

When a constant torque is applied, the rotor will accelerate until the gravity torque is equal to the aerodynamic torque (assuming that a balance can be achieved) whereby

the rotor will attain some near steady state speed. The speed that the rotor attains will depend on the torque applied, the mass of the pistons, the size of the rotor and the cyclical path described by the pistons but for stability must always be satisfy equation (3.70)

$$m \cdot \omega^2 \cdot r_{max} \ll m \cdot g + k_s(r_{max} - r_{min}) \tag{3.70}$$

If a speed that satisfies equation 3.70 is not achieved, then the forces on the pistons will never move the piston towards the centre of the rotor and the pistons will no longer be providing work. In addition, the path described by the pistons will become symmetric and therefore the net gravity torque will become zero and no longer balance out aero torque resulting in rapid rotor acceleration further compounding the problem.

Using this speed and the aerodynamic torque it is trivial to calculate the actual energy extracted from the wind over the simulation time:

$$E = P \cdot t \tag{3.71}$$

In order to satisfy conservation of energy, this energy must be apparent either as rotational kinetic energy or lateral kinetic energy of the pistons. Thus the equation of energy balance is:

$$\sum_{t=0}^{t=T} Q \cdot \omega(t) = \sum_{t=0}^{t=T} \frac{1}{2}(I \cdot \omega(t)^2 + m \cdot v(t)^2) + k_{sEp} \tag{3.72}$$

This of course assumes no energy extraction, and also assumes that the pistons are never brought to a premature halt which is wrong on both counts. Without energy extraction, the pistons will crash headlong into the physical ends of the chamber imparting potentially damaging kinetic energy into the structure and coming to rest. As the majority of the kinetic energy in the system is held in the motion of the pistons it becomes clear that extraction of this energy will give a value very close to the energy imparted on the rotor by the wind and simulations show that this is the case.

3.7.1.4 Piston Orbit

The pistons are free to move within the chamber and will do so depending on the relevant forces present at each point in the cycle. Ideally, for maximum energy extraction the piston would move through the root and through the full diameter of the rotor once per rotation. This orbit achieves the maximum gravitational potential energy through the forcing of the piston to R_{max} when the blade is at $\pi/2$, with reference to the lower potential achieved at R_{max} at $3\pi/2$. Such an orbit assumes that the mass can move from maximum to minimum instantaneously and impart all the energy into some form of extraction device. Unfortunately, such a path is not possible due to time taken for the piston to traverse the distance, the rotational speed component of the piston and the fact that it cannot pass through the centre of rotation. This orbit is further deformed by the process of energy extraction itself which is likely to take the form of a function: $k_d \cdot v$.

3.7.1.5 Rotor Stability

For moving masses in a rotating reference frame there is always a Coriolis force present on each of the masses, fortunately in a conservative system, i.e. the piston mass always moves outwards the same distance it moves inwards, the net Coriolis force is zero. Gravitational torque on the other had plays an important part in the stability of this system.

As mentioned previously, the orbit that each piston describes is fundamental in ensuring that the aerodynamic torque is countered by a net gravitational torque. Without an appropriate right skewed asymmetric orbit, the forces present on the rotor would never be balanced and without any form of braking the rotor would run away. The equation for balance is then:

$$Q = \frac{1}{2\pi}\int_0^{2\pi} m \cdot g \cdot r \cdot cos(\theta) \tag{3.73}$$

While the actual net gravitational torque is difficult to calculate, an approximation can be given by the near-idealised case. In this example, when the mass is on the left hand of the cycle it adds its weight to the aero torque and while on the right hand side of the orbit reacts against Q.

$$Q + \frac{1}{\pi}\int_{\frac{-\pi}{2}}^{\frac{\pi}{2}} m \cdot g \cdot r_0 \cdot cos(\theta) = \frac{1}{\pi}\int_{\frac{-\pi}{2}}^{\frac{\pi}{2}} m \cdot g \cdot r_{max} \cdot cos(\theta) \quad (3.74)$$

Solving and rearranging:

$$\frac{Q \cdot \pi}{2 \cdot g} = (r_{max} - r_0) \cdot m \quad (3.75)$$

Therefore values for r_{max}, r_0 and m for any given value of aerodynamic torque could be calculated for the idealised case. For example, in the case of a three bladed, 20MW turbine with a piston run of 110m and an operating speed of 0.25 rad/s the piston weights combined would need to be larger than 108 tonnes (36 tonnes each). As the orbit of the piston is unlikely to be ideal, this value can be seen as the minimum mass required for stability. Of course, the optimum value of mass is much harder to predict unless the exact orbit is known. In essence, if the orbit can be completely circumscribed then it is easy to calculate the amount of minimum piston mass required.

The choice of piston mass requires careful consideration as it plays a key part in determining the piston orbit, the speed of rotation and therefore stability. Once the turbine is in operation the total mass of the piston must remain unchanged therefore a suitable mass should be chosen for a designed operating speed. An interesting play on this fact might be possible should a liquid be used as the working object rather than gas. In such a system, liquid could be pumped or drained from a central location in order that the effective mass in the chamber might be controlled. There will also be structural considerations which will impact on the maximum amount of mass that can be safely placed within each blade without jeopardising structural integrity.

3.7.1.6 Structural Constraints

The dynamics of the system are impacted on by physical constraints. The size of the rotor is limited by technological and material limits in the same way that current conventional rotors are and many of these points are covered in other sources. Therefore only the unique physical constraints of this system are discussed.

Ideally, the piston would be allowed to move between the full length of the rotor blade, from root to tip. This would allow the piston to obtain the maximum potential energy with each rotation for a specific rotor diameter. This is not practical due to the need for some space at the root of the blade to contain the blades pitch actuators and any energy extraction device that would be required in such a system. At the blade tip, structural and physical constraints would limit the ability for a large mass to move without compromising structural integrity. Of course, it would also be highly undesirable for a relatively massive piston to crash headlong into a thin fibre-glass epoxy resin chamber wall. Fortunately, the process of energy extraction acts as a braking system that can be tuned to extract maximum kinetic energy from each mass prior to reaching these limits.

In terms of the actual mass of the piston the designer is limited by the overall relative blade/piston ratio. It would be unwise to have a piston that weighed similar or more than the blade itself as then the rotor inertia would be highly dependent on the position of the pistons and as a result the rotor speed would fluctuate wildly around some mean. Secondly, presuming that the piston run length is to remain at maximum there arises a structural limit whereby at some value of mass severe bending or fatigue will occur in the blade – particularly at the traditionally thinner tips.

Some suggestions to overcome these problems include: using large masses but limiting the maximum run such that the mass movement is focused in the stronger wider root of the blade, adding bracing supports between blades, which in the case of a 6-8 blade turbine would be achievable, [40] alternatively, stronger blade materials may need to be employed.

3.7.1.7 Blade Mass

Modelling of accurate blade mass and therefore rotor inertia is a difficult prospect when moving outside the current limits of technology. In an absence of actual physical examples, parallels can only be made with the rate at which blade mass increased with turbine size over the last 30 years. One collection of blade mass data

made by Garrad Hassan plotting blade mass against turbine size (for 3-bladed machines comes up with an (optimistic) empirical equation based on a square law.

$$3m = 2.9547 \cdot D^{2.0275} \tag{3.76}$$

This indicates that for a 20MW rated turbine, each blade would at least comprise of 66 tonnes of material. At worst, the empirical equation may be a cube law, in which case the blade mass would be a staggering 138 tonnes. Therefore the actual mass for a 20MW blade is open to conjecture but for the purposes of this study will be assumed to be around 100 tonnes. In comparison, current 5 MW machines have blade masses in the region of 15-20 tonnes.

3.7.1.8 N-Bladed Rotor

The question arises as to the number of blades that would optimise the amount of energy extraction possible for a specific wind speed and also minimise the mass of the piston required. Ideally the rotor disc would contain an infinite number of pistons of infinitesimal mass spaced around the full circumference such that the electrical output and rotor speed were constant. Naturally this type of rotor would have complete solidity and flow blockage would occur hence it is not realisable.

Unfortunately, as the design is made to work at lower speeds the resultant tip speed ratio, λ will be correspondingly low. Lower tip speeds mean lower power coefficients for rotors of a specific solidity with less solid rotors fairing particularly poorly in the lower tip speed regions. Thus a 3-bladed 240m diameter rotor rotating at 0.22 rad/s with, $\lambda \sim 2$ might only be expected to capture 8.43 MW of wind energy due to a poor power coefficient. These extremely low rotor speeds can be mitigated to some effect through careful choice of turbine parameters.

Gradually, with increasing solidity there comes a point whereby blockage occurs and no wind can flow. It is also the case that for high solidity rotor discs, the λ operating range for optimum C_P values is greatly reduced compared to that of say a 3-bladed machine. Some different configurations are conveniently explored through simulation and will be discussed shortly.

3.7.1.9 Energy Extraction

There are several ways in which energy could be extracted from a turbine that utilises a moving mass within the blade. The first is through the use of a liquid or gas placed within the chamber. For all intents and purposes, liquid is incompressible and therefore no useful work can be stored in liquid. However, by applying a cyclic force to the liquid a change in pressure could be achieved such as to drive a wells-turbine in order to generate electricity. The disadvantage of using liquid is that the latent heat energy stored within the liquid is significant and difficult to store without loss. Alternatively, gas or air could be used as the working fluid. This has the advantage of being readily compressible and therefore is much better suited as a means of storing energy in the form of compressed air or gas. S.D Garvey goes into one technique in which air compression may be utilised [40]. Another alternative could be the use of a solenoid coiled throughout the chamber with the piston acting as a moving magnet inducing current within the coil.

3.7.1.10 Scaling

The purpose of this study is to determine the likely parameters that would be required for such a turbine if it were to be rated at 5MW or scaled up to 20MW and to determine whether the concept scales non-linearly for larger machines.

A conventional 3-bladed 5MW HAWT with rated speed at 11.5m/s and a C_P of approximately 0.5 will typically require a rotor diameter of around 120m. A 20MW turbine on the other hand will require a 240 diameter rotor. Three blades are considered optimum as they give a broad C_P-λ meaning that the turbine can operate effectively at a wide range of wind speeds.

In comparison, a three bladed GCT with the same dimensions and rated at 11.5m/s might only be able to achieve a power coefficient in the region of 0.2-0.4 due to the significantly lower tip speed ratios. This represents a significant loss of potential for energy extraction. However, these lower tip speeds are essential if the GCT is to work and in fact as simulations show, are limited to speeds below around 0.7 rad/s in order to ensure rotor stability.

Ideally, for a 3-bladed 240m rotor rated at 20MW the tip speed ratio should be around 5, which would mean a rotation speed of approximately 0.5 rad/s. In order to increase the maximum speed of rotation once the rotor is designed and in operation some of the turbine parameters must be altered, either through a change in r_{max} or k_s.

The first option would be to run the machine sub-optimally at rated wind speed by limiting r_{max}, leaving some room for adjustment should a change in rotor speed be required. The second would be to increase or decrease k_s depending on the applied torque and the desired rotor speed. Unfortunately, a simple increase in k_s may also cause instability - as it forces the piston to follow an orbit with less net positive gravitational torque - thus careful control of k_s is desired. A convenient estimation of the maximum value of k_s can be found by rearranging equation 2.75 and assuming that gravity in the radial direction is equal to zero for the part of the cycle where the spring is fully extended. This represents a close to ideal orbit for at-least ¼ of the cycle. The minimum value is determined by the centrifugal force minus gravity ensuring that the piston will be returned to the root at the peak of the cycle, thus:

$$\frac{m \cdot \omega^2 \cdot r_{max}}{(r_{max} - r_0)} < k_s < \frac{m(\omega^2 \cdot r_{max} - g)}{(r_{max} - r_0)} \tag{3.77}$$

These limits suggest that perhaps a varying spring coefficient might be optimal in the system; indeed having a term that can be controlled to adjust rotor speed is highly desirable given that all other terms are fixed. To minimize the control aspects of this study, a constant value of k_s was chosen for each level of applied torque.

One of the most interesting aspects of the study was finding that GCTs that are designed for a specific wind speed can actually fair better at wind speeds below rated. This is in direct contrast to conventional machines, which are designed to output optimum power at rated speed.

For example, a 20MW three bladed machine with a piston in each blade of approximately 64 tonnes (a ratio of more than 1:2 against blade mass), a Q value of 50 MNm and a k_s value of 23,000 will rotate at 0.4675 rad/s. Whereas, the same turbine with torque at 30 MNm and a k_s value of 36,000 can rotate stably at 0.55 rad/s thereby

capturing more wind power. This data is graphed in Figure 3.33 and show that higher tip speeds can be achieved at lower values of torque by simple manipulation of the spring strength.

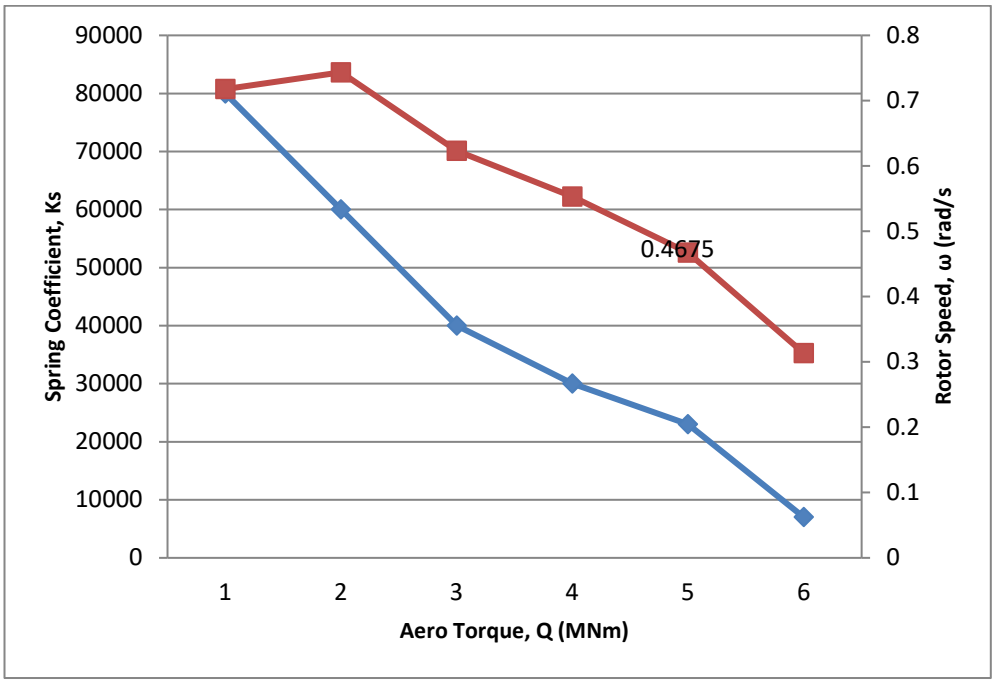

Figure 3.33 - Effect of Spring Stiffness on Rotor Speed

It should be noted that the critical mass (the minimum mass to prevent rotor runaway) was designed with a 60 MNm torque in mind and therefore larger torques cannot be compensated for. This suggests that in order to make the GCT more versatile in terms of the wind/rotor speeds it can operate the piston mass should be set for the maximum value of torque that the rotor is likely to experience.

One empirical method identified through simulation that can be used to determine the critical piston mass for a 240m diameter torque rotor was found by making a rough approximation for the piston orbit shown in Figure 3.34. This rough estimation resulted in an empirical relationship for the critical mass defined as:

$$\frac{Q}{313} = N \cdot m \tag{3.78}$$

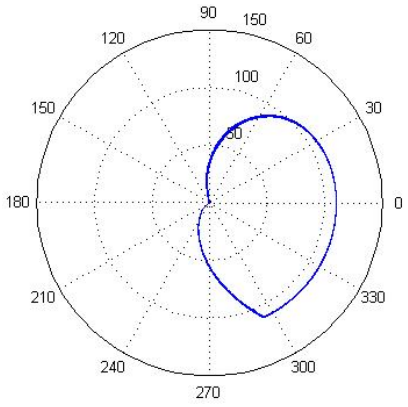

Figure 3.34 - Piston Orbit 20MW Machine

In other words, by plugging a maximum value for torque into equation (3.78) and selecting appropriate mass, then for every value of torque below maximum, the rotor speed can be optimised and the rotor kept stable. The empirical relationship was in good agreement with the minimum mass of all the pistons for stability during simulation.

The simulation was also run with rotors of increasing solidity, namely a 6-blade and 8-blade machine. Increasing the solidity of the rotor would help alleviate the issue of low tip speeds by shifting the maximum C_P value to the lower end of the C_P-λ curve. Another advantage of using more blades is that the rotor speed is much more stable over a cycle and power output is more regular.

Lastly, a simulation was run based on parameters for a 120m diameter rotor in line with current 5 MW machines. For an 8-blade machine, 10 tonne weights would need to be placed in each blade for a 50m chamber run. Unfortunately, due to the requirement for large masses in the blades to ensure stability, the ratio of piston mass to blade mass is over 2:1 which is unlikely to be practical. The situation does not improve when moving to three blades, with the piston requirements increasing to over 25 tonnes per blade. One positive of decreasing rotor size is the increase in rotor speed into the region of 0.6-0.7 rad/s meaning that the tip speed ratio becomes more favourable.

3.8 CLASSIFICATION

The classification of wind energy devices is complex and open to debate. It is possible to allocate a general classification system based on only those basic factors which best define the type of device. For example, it cannot be argued that rotor and non-rotor systems are mutually exclusive, or that a device utilising lift forces is quite different from one using primarily drag. This tree-classification system is depicted below with both branches of system (rotor and non-rotor) is presented, with those branches of the group nearest the top being most common/commercially widespread or have experienced extensive research and development.

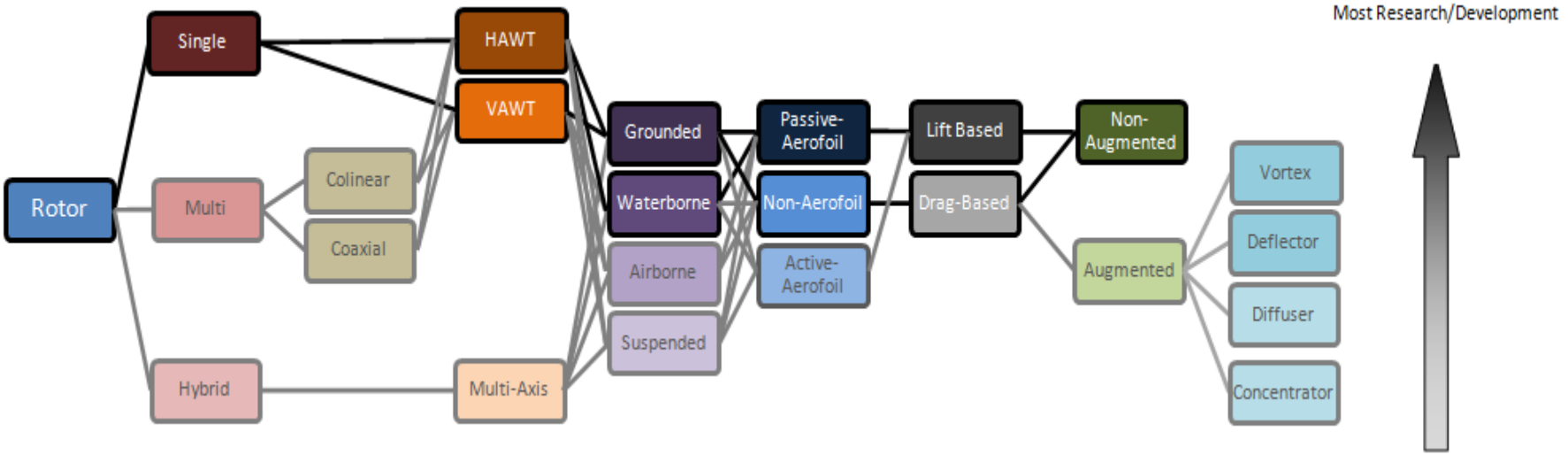
Most Research/Development
Rotor
Single
Multi
Hybrid
Colinear
Coaxial
HAWT
VAWT
Multi-Axis
Grounded
Waterborne
Airborne
Suspended
Passive-Aerofoil
Non-Aerofoil
Active-Aerofoil
Lift Based
Drag-Based
Non-Augmented
Augmented
Vortex
Deflector
Diffuser
Concentrator

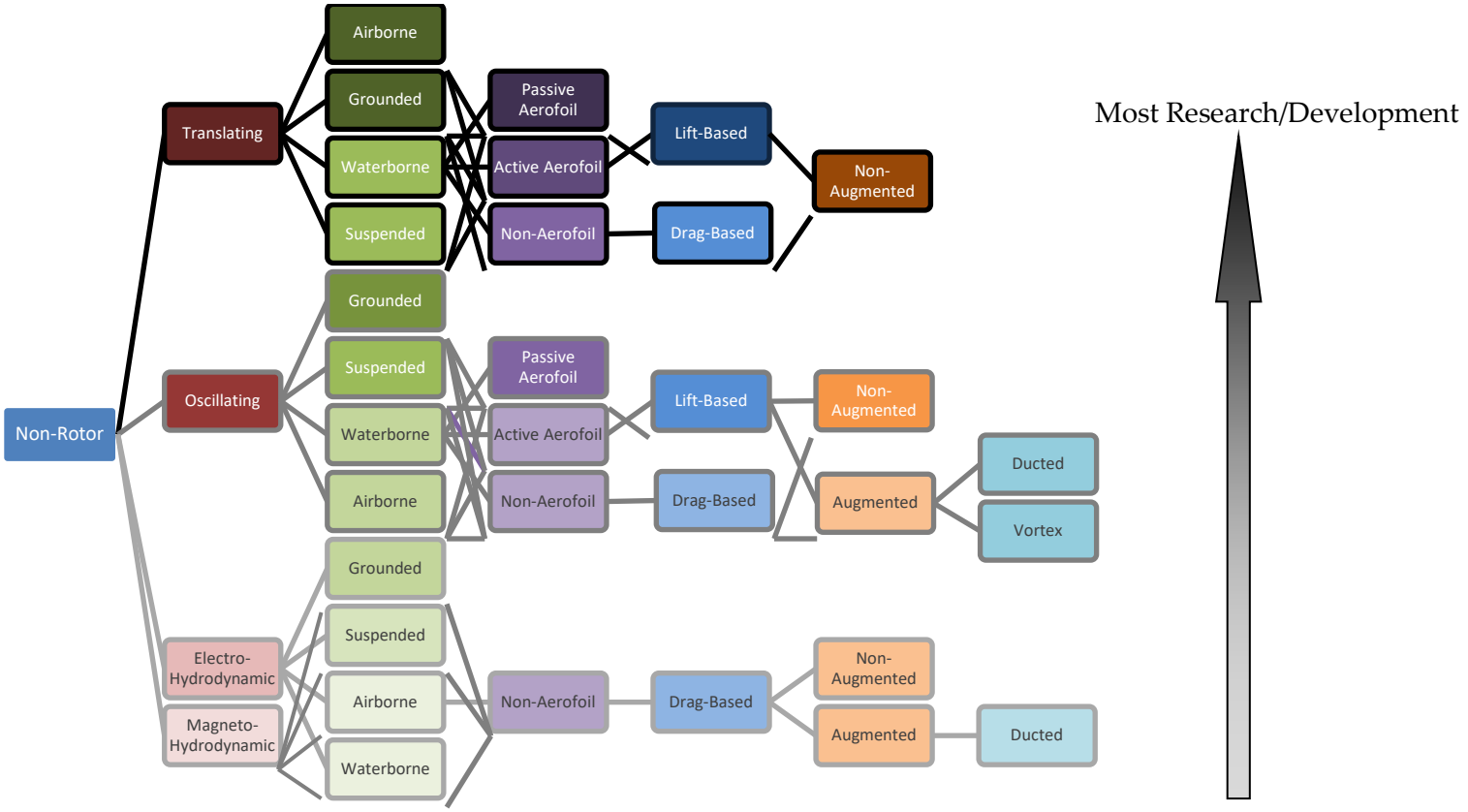
Non-Rotor
Translating
Oscillating
Electro-Hydrodynamic
Magneto-Hydrodynamic
Airborne
Grounded
Waterborne
Suspended
Passive Aerofoil
Active Aerofoil
Non-Aerofoil
Lift-Based
Drag-Based
Non-Augmented
Augmented
Ducted
Vortex
Most Research/Development

3.9 DISCUSSION

3.9.1 The Leading Technologies

An ideal wind energy conversion system would extract all the energy from the wind. The German physicist Betz showed that this is not possible and indeed the theoretical maximum power coefficient for a range of tip speed ratios is determinable. The C_P-λ curve is a reasonably good indicator of which type of device is best suited for a specific location. Figure 3.35 shows a selection of C_P-λ curves for a range of different rotor-based devices (both HAWT and VAWT). They clearly show that no single device can capture the theoretical maximum amount of energy (0.593) for a given tip-speed-ratio. Perhaps the most interesting curve is that of the Smith Putnam machine which shows amazingly good characteristics at high tip speeds and which outperforms even more modern systems [84]. Tellingly, although this device was crafted and designed in the 1940s it was developed by a team headed by the well-respected von Karman and other leading scientists of the day [85]. It could be argued that it has only been in the last few years that the wind industry has again gained the expertise necessary to develop such well performing machines. The graph also indicates the benefit that active blades have on the operating range of a system, that is; the highest C_P values over a wide range of tip-speed ratios. It is likely that their ability to actively modify their characteristics allows for such comparatively good performance (e.g. hybrid Flettner).

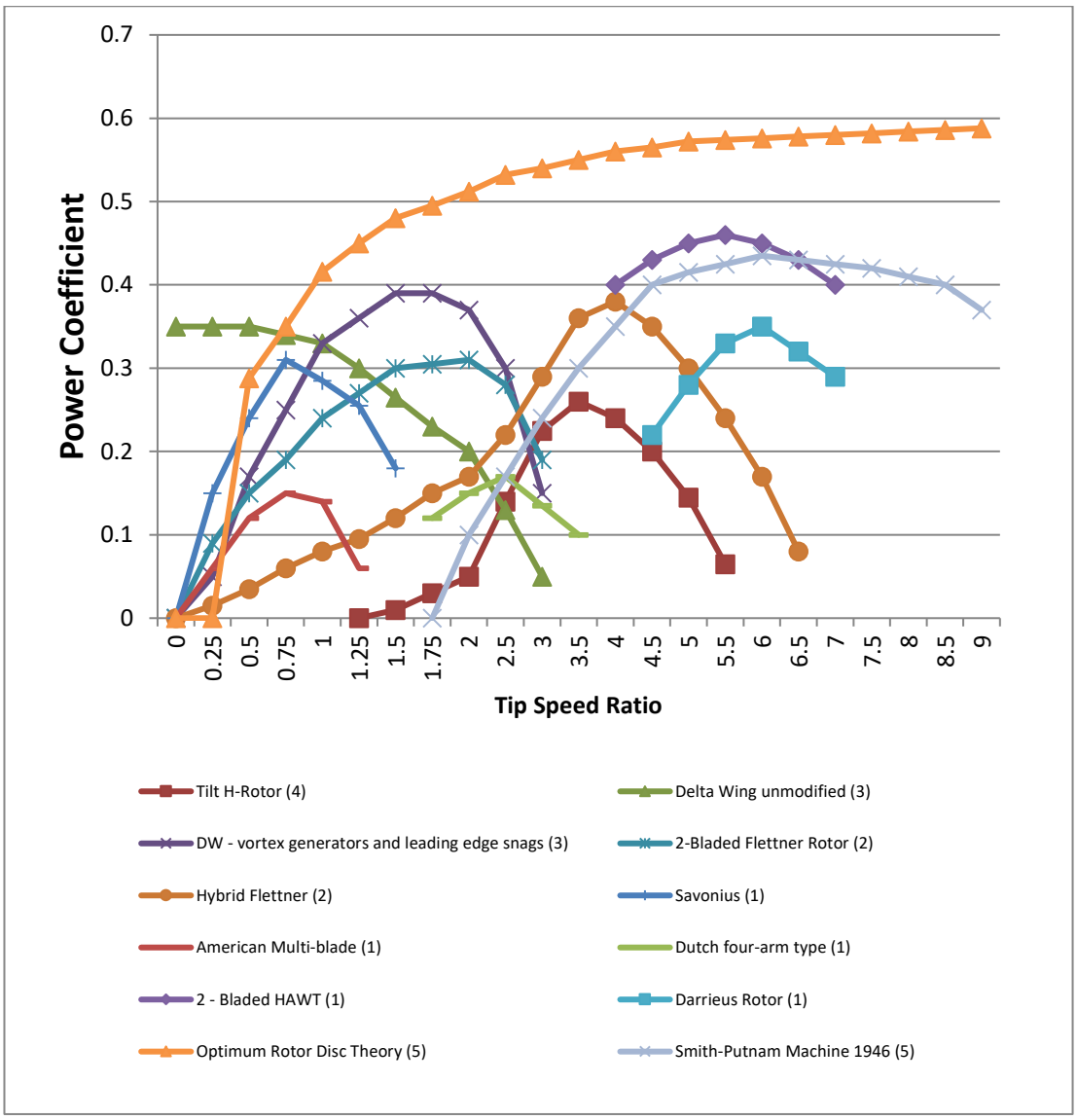

Figure 3.35 - C_p Lambda Curve for Various Rotor Configurations [15] [85]

As part of this study, a concerted effort was made to identify systems that had merit based on theoretical or predicted parameters. For example, kites were examined due to their low mass to power extraction capability and ability to operate at higher wind speeds; LTA system were examined due to their ability to operate up in the jet-stream and also because they could theoretically scale up without incurring tower structural penalties. Table 3.7 shows the results of this parametric study.

It should be noted that airborne rotor systems score highly on the W/m² scale because they have very little active blade area per power output (although the whole devices swept area is considerably greater). It is also uncertain exactly how much area the

original researchers took into account when evaluating each concept and therefore these metrics are included only for reference. Note that active area in this case can be considered the area of the device which captures the wind energy.

Device	Active Area	P_{max}	W/kg	W/cm^3	W/m^2	W/$
Galloping	5832	1.14	0.0720	0.0006		
Wind belt		5			1.2800	
Cross-flow	134.4	0.26	0.5760	0.0019	0.0460	0.069
Cross-flow	236.16	0.21	0.3430	0.0009	0.0130	0.034
VESTAS V52		850	27.0		400	0.300
EFD 1983	24000	5,760	3.4		240	4
EHD 2007	400	100			250	
Magenn	830	100	17.0	17.66 /m3	120	5
LTA 10MW	41500	10,000	36.4	35.84 /m3	120	0.230
Laddermill	24960	130	104.2		26	
KiteGen	50	200	25.0		4,000	6
IDAWT	34	1,000	186.8		7,300	0.603
SDAWT	69	1,000	210.9		7,200	0.637

Table 3.7 - Comparison of Metrics

The range of devices power output is considerable with oscillatory devices occupying the low power density spectrum and traditional systems the upper range. Devices such as: kites, LTA rotors, and flying rotors all fair somewhere in between. This does not suggest that the technology being used is necessarily capable, but rather that used in isolation the power per swept area is not a good indication of a devices capability.

Both airborne rotors fair the best based on the W/kg. This is as expected due to the nature of airborne devices but also the fact that this study was carried out at the relatively large MW scale compared to most systems in early development. In actual fact, although both devices were rated at 2.2MW, a power transfer of only 1MW could be achieved. This is due to the energy required to keep the devices airborne on part of the cycle but also due to losses in the cable which bring the efficiency to below 45%.

A better comparison might be made between Laddermill and KiteGen, both of which are based on rotor/airborne hybrids. Laddermill is clearly favourable from a weight perspective due to its lack of a grounded rotor, however its requirement for such a

large number of blades make it fair poorly in terms of installed area. It is also necessarily more complex that normal tethered kites which inherently raises a whole host of safety issues. KiteGen on the other hand benefits from the use of kites (parafoil) and because of the sunk cost of the vertical axis rotor on the ground, should have its parameters improve with scaling.

The EHD concept stands near the bottom of the power/mass range, with even small devices likely to weigh in at tens of tonnes. While the situation does improve with scaling, the parameters fail to improve on conventional HAWT values and therefore the concept appears non-feasible in its current state of development. It is most notable for being the only concept capable of capturing energy at any wind speed and should a location ever be found where wind speeds were consistently above 25 m/s then this design may become economically feasible – though due to its size and weight it is unlikely this would occur at height.

Lighter than air systems too appear to have some merits, though at small scale the tether properties become prohibitively expensive to the point of economic unfeasibility. This means that the best hope for this system will be above 10MW where the prediction suggests power to weight ratios more than 30W/kg and a cost of installed capacity below $0.3/W (putting it in contention with HAWT machines). Certainly, the current commercial prototype produced by Magenn does not appear to be a strong-contender to replace kW rated devices due to its average performance characteristics.

Lastly, it is almost immediately clear that oscillatory devices have no future (based on current technology and understanding) at the multi-MW level. This is partly due to the low energy content of high frequency wind but also due to the necessity for the system to be dynamically adjusted for both electrical and mechanical resonance. The fact that energy extraction acts as a damper also ensures that oscillations never reach the magnitude that would be required for multi-MW production.

CHAPTER IV - MULTI ROTOR SYSTEMS, INITIAL CONCEPTUAL DESIGN

4.1 INTRODUCTION

Industry effort is presently focussed on very large-scale single wind turbines, with ratings in the 5-10MW range, particularly for use in offshore locations. Recent studies (UPWIND [14] have proposed single rotor machines as large as 20MW in rating, following obvious cost savings associated with minimizing the number of offshore foundations required for a given total power output. A multi rotor wind energy system could offer similar power outputs (or even greater) without escalating structural penalties and at a reduced cost of energy (CoE). Preliminary analysis based on scaling with similarity [84] predicts that the total weight of rotor mass and major drive train components scale as $\frac{1}{\sqrt{N}}$ where N is the number of rotors in a multi rotor system (MRS). Such scaling implies cubic variation of aerodynamic bending moments and the mass of many major components, thus many small rotors may have much less mass and cost than an equivalently rated single rotor. While it is an ongoing challenge to improve technology to avoid cubic up-scaling, it merely requires the application of state of the art capability to downscale cubically.

The concept of a multi rotor wind energy system (two or more rotors on a single support structure) has been in circulation since early in the 20th century [44]. A multi rotor system offered a route to a high rated unit capacity whilst avoiding the difficulty in making very large rotor blades from steel. With the development of modern glass composites, very large rotor blades became feasible and so the concepts of multi rotor systems were largely neglected. However as current generation wind turbines are up-scaled into the multi-megawatt range, the energy benefit from increased rotor size is more than offset by increases in mass and cost. Thus, the conventional single rotor design becomes uneconomic, at least in terms of the turbine cost alone, at very large scale and published price data on wind turbine systems confirms this [87]. Multi rotor systems can offer a solution. They retain the economic advantage of smaller scale systems and yet may achieve a larger overall capacity than any existing single rotor unit.

The underlying logic of multi rotor systems relates to scaling and to the relative costs and productivity of small versus large rotors. The costs of major components, rotor blades, hubs and power trains (rotor bearings, gearbox, brake, generator and so on) account for around 75-80% of the total ex works (i.e. the physical aspects) capital cost of a conventional wind turbine [88]. The cost of multi rotor system rotor and drive train components compared to these components in an equivalent single rotor system is quantified as of the order of $\frac{1}{\sqrt{n}}$ where $\boldsymbol{n}$ is the number of rotors in the multi rotor system. Thus a 36-rotor system will have 1/6th of the cost of these components compared to a single large rotor system of equivalent capacity.

This result follows from an elementary scaling analysis to be presented in adjoining sections but it is not a purely theoretical finding. Market data on the mass and cost of wind turbine systems and wind turbine components, when carefully analysed, endorses the fundamentally cubic scaling of major components. In the offshore context the wind turbine capital cost, typically 70% to 80% of installed cost on land based wind farms may reduce to 30% to 50% of installed cost - depending mostly on water depth and distance from shore. Capital savings in the wind turbine components are less consequential and yet may also be significant. The multi rotor system provides for handling of smaller more manageable components and an integrated system design with power plant, spare parts supply and permanently manned service centre all on a single foundation.

The primary benefits of a multi rotor system are thus related to:

- *Scaling laws* – the total sum of rotors and drive trains of the multi rotor system can have much less weight and cost compared to a single equivalent turbine.
- *Standardisation* – systems larger than 20 MW will be realised with more rotors and not larger rotors. Standardising rotor and drive train components will allow for stable serial/mass production at a size comfortably within industry experience. This in turn will lead to very substantial cost reductions and improvements in reliability.

- *Maintenance* – the multi rotor system will have in effect almost no unscheduled maintenance. Single turbine faults will usually compromise only a few percent of capacity, reducing urgency to find favourable weather windows for remedial action.

A preliminary 20MW multi rotor system has been conceived which places 45, 444kW rotors on a single structure utilising currently available technology. Initial work by Jamieson [84] suggests that the cost advantage of such a multi rotor system can yield CAPEX savings of 11% compared to 4x5MW rotors and 30% compared to a single 20MW machine - if material costs are closely tied to mass.

To validate these values further, this chapter presents one potential structural layout which would meet the energy capture and structural capacity required for a 45 rotor, 20MW multi rotor system in an off-shore environment at reduced mass compared to a single equivalent rotor. From this, more useful comparisons can be made to other alternative options and help solidify the argument for the further research and development of the multi rotor concept.

4.2 IMPACT OF SCALING LAWS

4.2.1 Fundamentals

In up-scaling a wind turbine system, a consistent basis of comparison requires that a representative tip speed is constant. This preserves the flow geometry in terms of the relationship between rotor speed and wind speed at any given operating point. Maintaining a given tip speed at any given wind speed implies that in up-scaling, rotor angular velocity, ω, must vary inversely with diameter, D and hence decrease with increasing turbine size.

The aerodynamic moments of a wind turbine blade about any axes and at any radial station can be shown to scale as cube of diameter. These moments arise as a sum of products of local air pressure on each blade elemental area and associated moment arms about the blade section under consideration. The bending section modulus of a cantilevered structure (blade or tower) at any given section is also found to scale

cubically. Thus up-scaling with similarity will work in preserving constant stress. This does not apply if weight related loads become design drivers as self-weight bending loads will then scale as the fourth power of diameter or more.

There are some subtle effects which prevent scaling with strict similarity being feasible. These include a so-called "size effect" relating to the fracture mechanics of materials [88][89]. For homogenous materials, the larger the sample size, the greater the probability of a critical flaw existing in each sample leading to critical structural weakness. This implies that at some level of up-scaling, it is not adequate to design for constant stress. The allowable stress must then reduce (per structural section) as size increases and mass must scale more than cubically to compensate.

Other violations of scaling similarity relate to fluid boundary layers, the boundary layer around the aerofoil sections of the blade and the earth's boundary layer. In principle, aerodynamic performance increases with up-scaling due to increase in Reynolds number but this is an almost negligible effect for megawatt scale wind turbines. More significant is the effect of the earth's boundary layer where friction between the atmospheric air and the ground leads to a strong gradient in wind speed (wind shear) with wind and therefore local aerodynamic forces on blades increasing significantly with height above ground [90]. Wind shear depends on atmospheric stability and surface roughness being generally less pronounced over sea than over land.

The primary value of a wind turbine, energy relates to swept area (proportional to square of diameter) whereas cost is related to volume (proportional to cube of diameter). This is sometimes referred to as the square-cube law. Wind shear; on account of the wind speed at a given site increasing with height, can effectively augment energy capture as more than as square of diameter mitigating the effects of the square–cube law. However, in accounting net benefits from wind shear it is commonly forgotten that in principle the increase in wind speed with height will also imply some increase in loads which has an associated structural cost.

4.2.2 Area/Volume Relationships

Consider a scenario where n small rotors each of diameter, d, have the same swept area as a single large rotor of diameter, D, and hence to a first approximation, ignoring wind shear, the same power and energy capture in similar wind conditions. It follows that:

$$D^2 = nd^2 \tag{4.1}$$

Since constant blade bending stress with scale is satisfied with geometric similarity, then blade mass must scale cubically. Thus, the mass, M of a set of blades for the single large rotor is given as:

$$M = kD^3 \tag{4.2}$$

Where k is a constant of proportionality. The corresponding mass, m of a set of blades for a small rotor is:

$$m = kd^3 \tag{4.3}$$

Thus, R, the ratio of the mass of the set of small rotors to that of the single large rotor is determined as:

$$R = n\left\{\frac{d}{D}\right\}^3 \tag{4.4}$$

$$R = \frac{nm}{M} = \frac{1}{\sqrt{n}} \tag{4.5}$$

This relationship is of major importance as it shows that by increasing the number of rotors for a fixed swept area, the overall combined rotor mass decreases in comparison to that of a single large rotor of equivalent swept area at the expense of support structure mass and complexity. A similar argument holds for the scaling of the power train. In the conventional arrangement, rotor speed decreases with increasing diameter and the gearbox input torque, (being the resultant of blade in-plane moments at shaft centreline) rises cubically. If the gearbox output speed is held constant then the gear ratio must increase and this, in conjunction with a cubic scaling of input torque, leads to a more than cubic scaling of gearbox mass and cost (to be

offset by a less than cubic scaling of the generator). If the generator input speed is held constant with up-scaling as is usual in conventional wind turbine design, then the generator torque is varying as power leading to generator mass and cost proportional to the square of diameter.

A simpler picture is evident with the direct drive generator where the generator is the whole of the power train and scales cubically (i.e. with input torque). The support structure (tower) of a conventional wind turbine is similar to a blade in respect of being a wind-loaded cantilevered beam and the tower can be expected to scale cubically for the same reasons.

Any given multi rotor system, if up-scaled with geometric similarity, would increase cubically in mass as with any conventional system. The cubic curve representing the up-scaling of for example blade mass, for a 16 rotor multi rotor system, will have a coefficient around ¼ of the value of that for an equivalent single rotor curve. Thus, the multi rotor concept does not defeat the square-cube law and no system that up-scales observing geometric similarity can. However, the multi rotor system can be up-scaled instead by increasing the number of rotors and thereby violating geometric similarity and avoiding the square-cube law penalty.

4.2.3 Scaling and Commercial Data

The development of wind technology has been one of continual up-scaling with genuinely exponential growth in system and component sizes until recently [91]. This means that small blades are almost invariably old ones.

The industry started with fibreglass boat building techniques being employed when blades were manufactured using glass with randomly oriented fibres (chopped strand mat) and polyester resin applied with rollers in a hand lay-up process. Thus the oldest blade designs generally employed designs that were inefficient in use of materials, that used relatively heavy material systems and used labour intensive processes. With passage of time blade manufacture methods have become more sophisticated (now fully automated production has been achieved by Gamesa [89]

and there is ongoing drive to reduce weight and cost in ever larger blades. Thus the scatter of real commercial data appears to cross cubic curves (determined by studies at CRES [91]) to be associated with different material systems and manufacturing processes. An empirical power law fit to the commercial data points in Figure 4.1 suggest a square law dependence of blade mass on rotor diameter but the reality is a progressive development in manufacturing process with intrinsically cubic curves associated with each process type; from the oldest hand lay-up polyester blades to glass carbon hybrids.

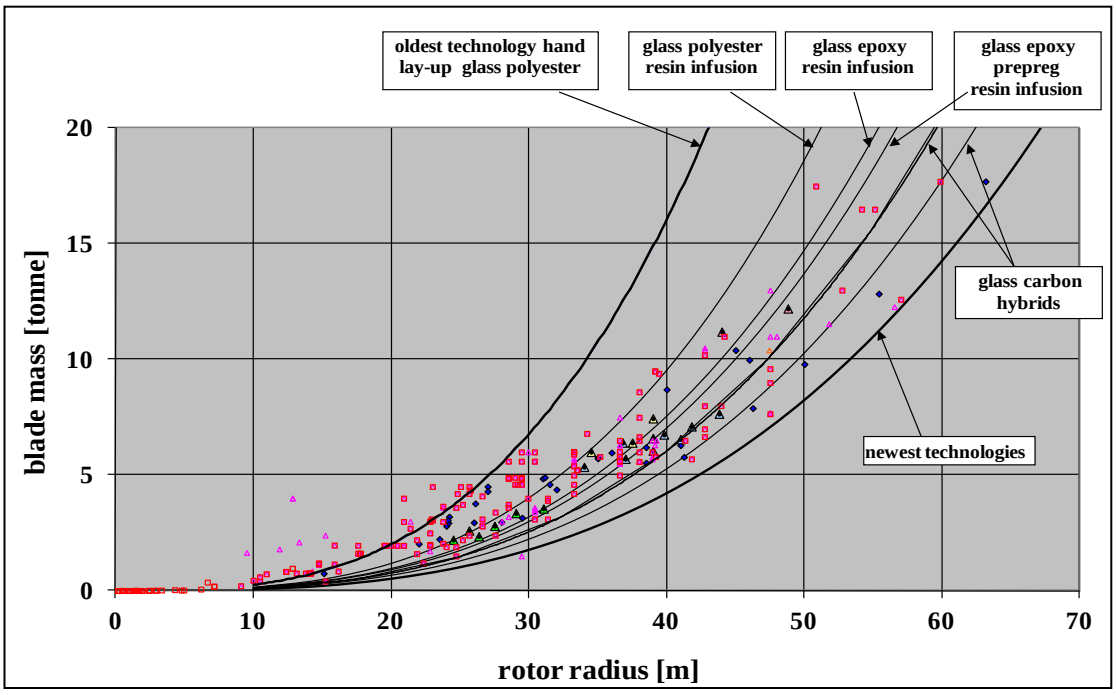

Figure 4.1 - Scaling of Rotor Blades with Technology and Size

Although some smaller wind turbine designs in the hundreds of kW are being revived, there is a tendency to use old ready-made designs with only minimal upgrading so that the full potential for mass and cost reduction in smaller scale designs is not yet much realised. The significance of Figure 4.1 is that, using the latest technology – not necessarily the very lightest, but the most cost effective of the recent technologies with glass and resin infusion – it is possible to *descend* a cubic curve and produce small blades that benefit quite fully from the reduction of $\frac{1}{\sqrt{n}}$ in total mass and cost as compared to a single large rotor.

There is an even clearer picture with respect to drive train components, although the same issues of small being old and large being new could tend to reduce the apparent exponent. There is a clear linear relationship between gearbox mass and rated torque (Figure 4.2) based on commercial data from Winergy, Bosch Rexroth and Eickhoff [92]. Rated torque scales fundamentally as cube of diameter, although this cubic exponent, considering wide ranging commercial data from manufacturer's brochures and other sources may appear slightly reduced by a tendency to design for higher tip speeds in the latest offshore designs.

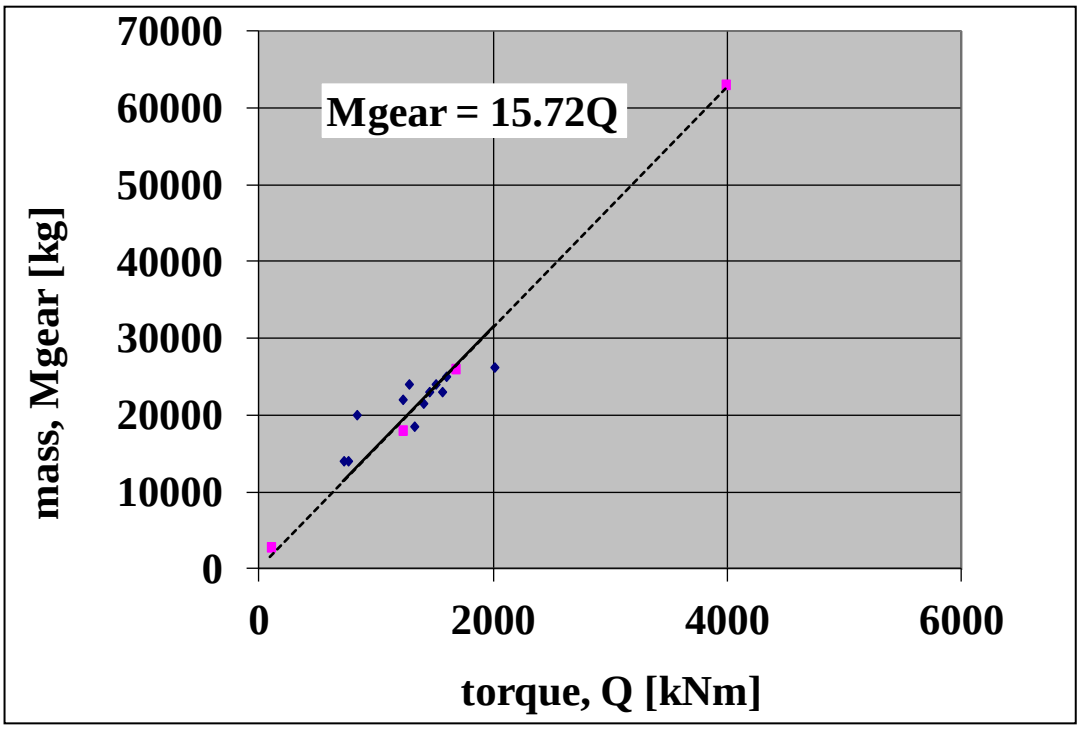

Figure 4.2 - Scaling of Gearbox Mass with Torque

The largest modern wind turbines (5MW+) are eschewing gearboxes in favour of direct-drive systems, where the primary shaft connects directly into the generator (often a permanent magnet generator / PMG). This type of high torque low speed application does increase the relative size of the drive-train when compared to geared systems but is used as a method to counter the tendency for gearbox failure, the chances of which increase with rating [93].

There is insufficient public data on PMG designs to determine corresponding clear trends between mass and rotor diameter. A detailed PMG design model from GL Garrad Hassan, considering PMG designs over a wide range of gearing from direct drive to high speed, indicates a near linear relationship between mass and torque (Figure 4.3) and therefore an essentially cubic relationship between mass and wind turbine rotor diameter. It is well recognised that mass does not directly equate with cost although the correlation is very strong for many engineering components. Nevertheless, it will be obvious that mass savings approximating 5/6 = 83% for 36 rotors or 9/10 = 90% for 100 rotors will imply very large cost savings.

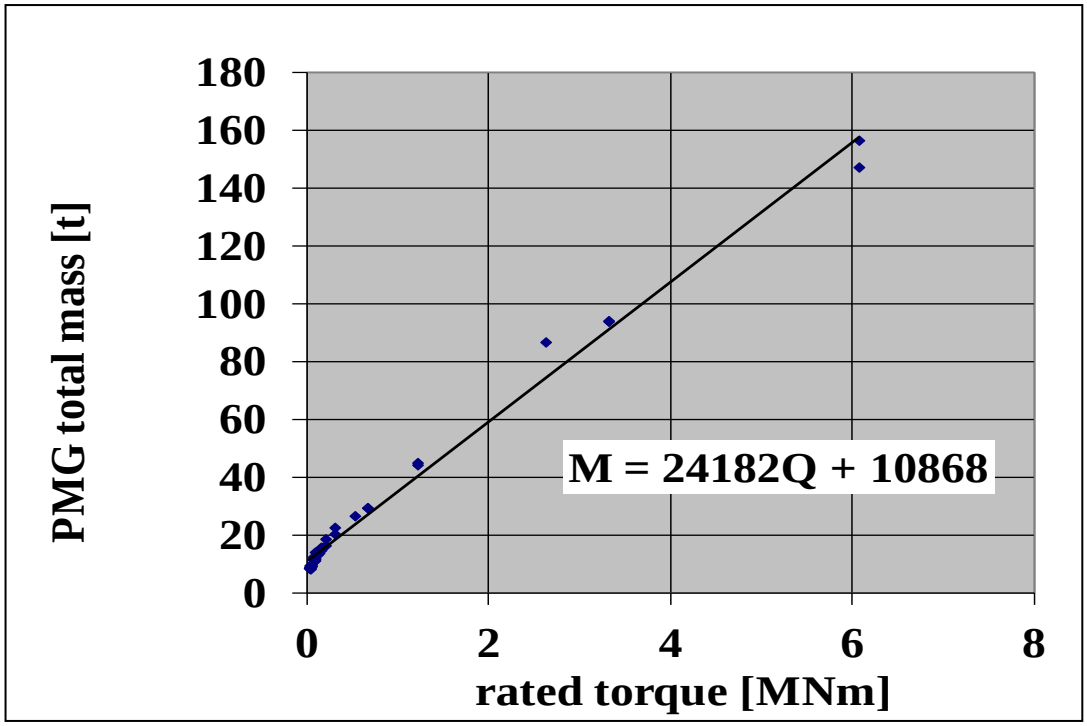

Figure 4.3 - Scaling of Permanent Magnet Generators with Torque

4.3 PREVIOUS STUDIES OF MULTI ROTORS

The study so far has presented a case for the current investigation of multi rotor systems but has not yet made any mention of previous or future design methodology. Previous studies of the multi rotor system are either outdated or of a commercially

sensitive nature. There has been no academic research into the topic in several decades since the death of a multi rotor pioneer, Heronemus.

4.3.1 Aerodynamic Performance

The aerodynamic performance of a group of closely spaced rotors is often questioned when multi rotors are in discussion. In 1985 Smulders [94] conducted wind tunnel tests on a pair of rotors finding no adverse effect on power performance at a lateral spacing as close as 5% of diameter. Much more recently [95], wind tunnel tests on a hexagonal frame carrying a seven rotor array of small wind turbines were conducted in the NASA Langley wind tunnel (see Figure 4.4) in Virginia, USA confirming the same.

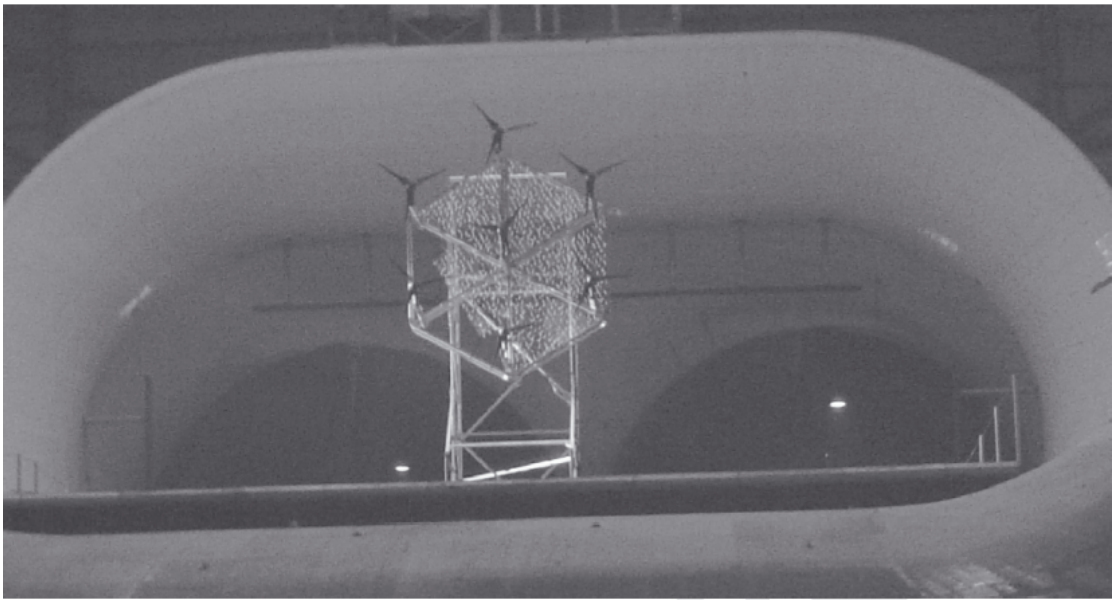

Figure 4.4 - Wind Tunnel Tests on 7-rotor Array [95]

4.3.2 Size and Scale

Previous confidential studies have shown that the critical extreme loads on a 2MW 17-Rotor MRS were generally less than for an equivalent single rotor system. Moreover the weight of a frame to support the rotors plus all the rotors and drive-trains may still be less than the weight of 3 blades of a single rotor. A conceptual solution therefore is to support the frame and multi rotor system on essentially the same tower and yaw ring as the equivalent large single rotor (See Figure 4.5). This

solution may not be optimal. However, it clearly reveals that providing for yawing of a multi rotor system should not be a critical threat to its economic potential benefit.

At present there are no existing commercial examples of horizontal axis multi rotor systems although proto-type sub-MW designs have been constructed in the past. Examples of dual/tandem rotors exist, but these systems look to take advantage of effects other than those considered here and therefore should not be classified under the same category. This leaves all aspects of the multi rotor structure up for debate.

Figure 4.5 - Artists Impression and End Elevation of 17 Rotor Multi Rotor System

4.4 INITIAL CONCEPT

Multi rotor systems (MRS) do not require any technology or engineering practices that are not currently in use today. The full economic potential of the multi rotor system will only be realised by developing optimised designs of wind turbine systems that benefit from the technological progress that is presently being applied to the largest turbines.

The geometric scale of the system will necessarily be similar to that of an equivalently rated single rotor system given that modern designs approach theoretical power capture limits. In addition, there is a strong desire to fully utilise the scaling benefits

of using a large number of small rotors to achieve larger rates capacities. In short the main criteria for the initial concept were as follows:

1. To have a total power rating of 20MW so as to be comparable to the UPWIND single rotor design.
2. To make use of scaling laws to achieve a large mass reduction when compared to a single rotor of equivalent rating. That is, the design should have as many individual turbines as possible while still remaining within a number that is easy for the lay person to envisage, and the industry to manage.
3. To only make use of technologies currently in use today directly or indirectly within the wind industry.
4. To optimise and reduce mass where possible, particularly on the structure.
5. To use a scaled down rotor of a standard design, with similar power density, drive-train, power train and so on.
6. To optimise power flow and energy capture.
7. To take advantage of modularity and thereby reduce maintenance costs - a key concern of offshore wind.

Taking the first three criteria as a starting point it was proposed that the initial concept comprise 45 turbines of 40.5m diameter, each of rated power 444 kW for a total of 20MW. The choice of 45 turbines is somewhat arbitrary, but does give a good balance between rotor numbers and potential weight reductions. In addition, 444kW is a rated value easily within the peak engineering capabilities of the current wind industry allowing for full use of all modern techniques and technologies in each rotors construction. Plotting data points of specific turbine cost with increasing turbine size (Figure 4.6) suggest that the 50m onshore rotor is the most cost effective based on present technology. A rotor in the 40-60m range (41m in this study) rotor should therefore be able to make best advantage of these technologies to achieve a similar level of cost.

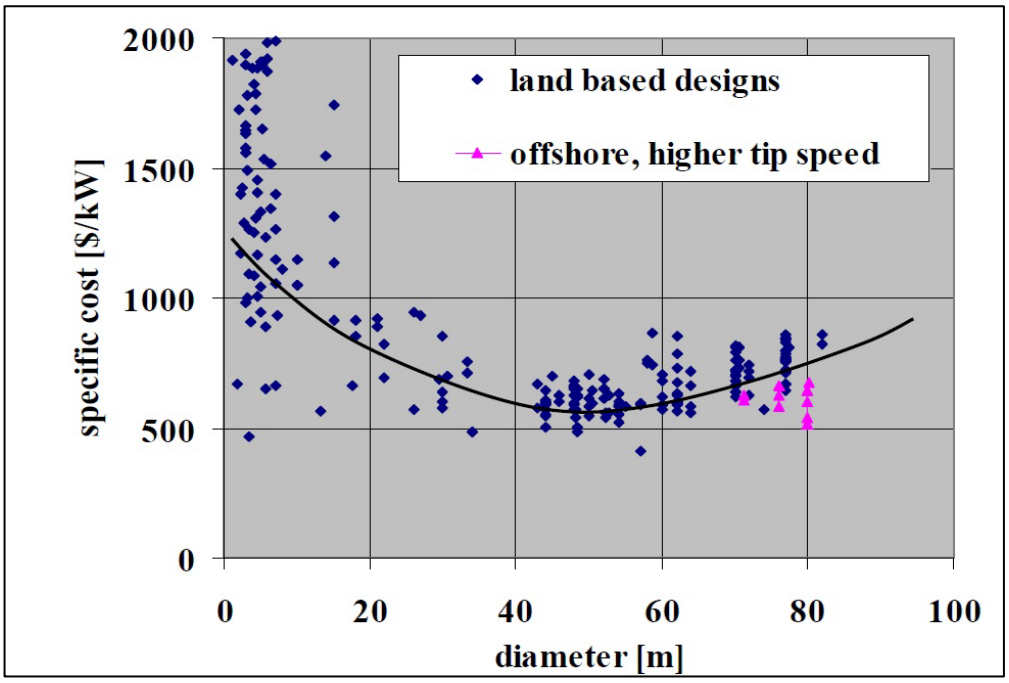

Figure 4.6 - Specific Cost with Increasing Turbine Size [96]

4.4.1 Rotor Spacing

Optimising for structural mass is achieved by balancing structural strength and also the spacing between rotors. It is proposed that although a stepped layout is possible with some turbines a little upstream or downstream of others, the flow interference in yaw of such a system may be disadvantageous compared to planar designs.

To minimise frontal area of the system while making use of the vertical direction, the most efficient packing of the rotors is in a 'honeycomb' shape. In Figure 4.7, rows are offset by $0.866D$ and adjacent rotor centres by $1.05D$. The number of rotors placed on each row is independent of geometric considerations, but it is proposed that a shape approximating a hexagon would provide a good distribution of loads.

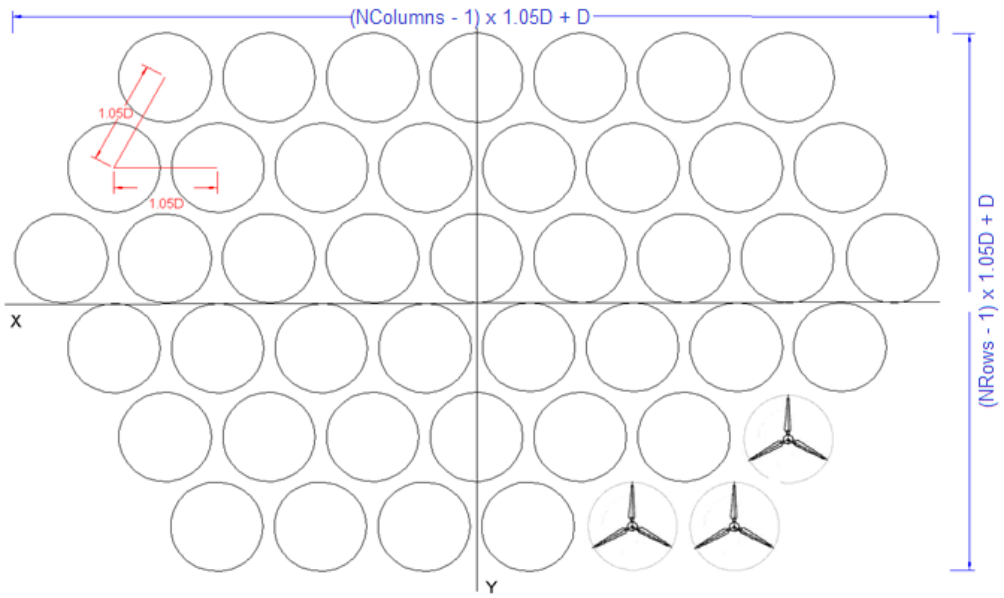

Figure 4.7 - Proposed layout of a 45 rotor multi rotor system.

With the rotors in a hexagonal array, symmetry about the axis of yaw rotation is required to balance yawing moments. Rotors are also arranged to avoid a high centre of thrust. The average member length is 42.5m (1.05*D*) with nacelles placed within modular brackets situated at each node. An absolute minimum clearance of 20.25m is required from the bottom rung of the space frame to the base of the tower/foundations, however in this configuration it is set at 40m - allowing for significant wave height.

The total space frame dimensions are 380.7m (W) and 224.6m (H) not including tower. The total frontal area is approximately 73550m^2 with 57971m^2 active area equivalent to a 271m diameter single rotor assuming equivalent energy density.

It is proposed that this design would only be for use in offshore environments and therefore would make use of a water bearing and differential rotor thrust as one possible option for yawing. It should be noted that the use of a double yaw ring and bearings is within technical boundaries.

4.4.2 Blade and Hub Characteristics

Blade characteristics have been scaled down from a suitable 5MW design using appropriate scaling laws (see Section 1.2). It is proposed that each rotor will have full span pitch control and be variable speed.

Plotting total blade mass vs. diameter for real-world turbine data (Figure 4.8) shows that in 2006, a 20m blade could be produced in the region of 800kg. It is proposed that this could be further reduced using current available technologies and reach 550kg per blade without much increase in cost. Note that the points in the graph represent the total or combined mass of all blades on the rotor, i.e. 1,650kg for the 444kW machine.

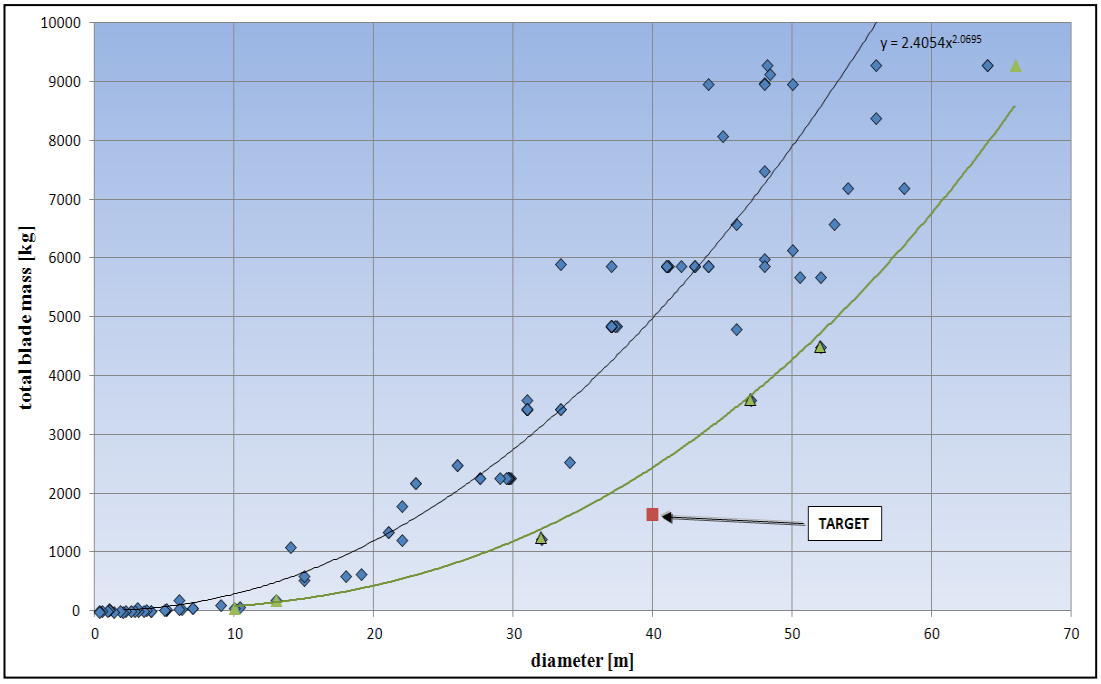

Figure 4.8 - Commercial Data Showing Real-life Blade Mass vs. Diameter Scaling

This data set can be viewed in another manner, with individual blade technology trend-lines added to represent the downwards shift of blade mass with advancing technology (Figure 4.9 presents a more detailed view of Figure 4.1). While newest technologies are only currently seen on multi-MW machines, it is proposed that the same mass savings can be achieved by down-scaling with similarity to the required

rating. The downward shift of mass due to technology in the 20m region is 50% or more, which is a considerable saving.

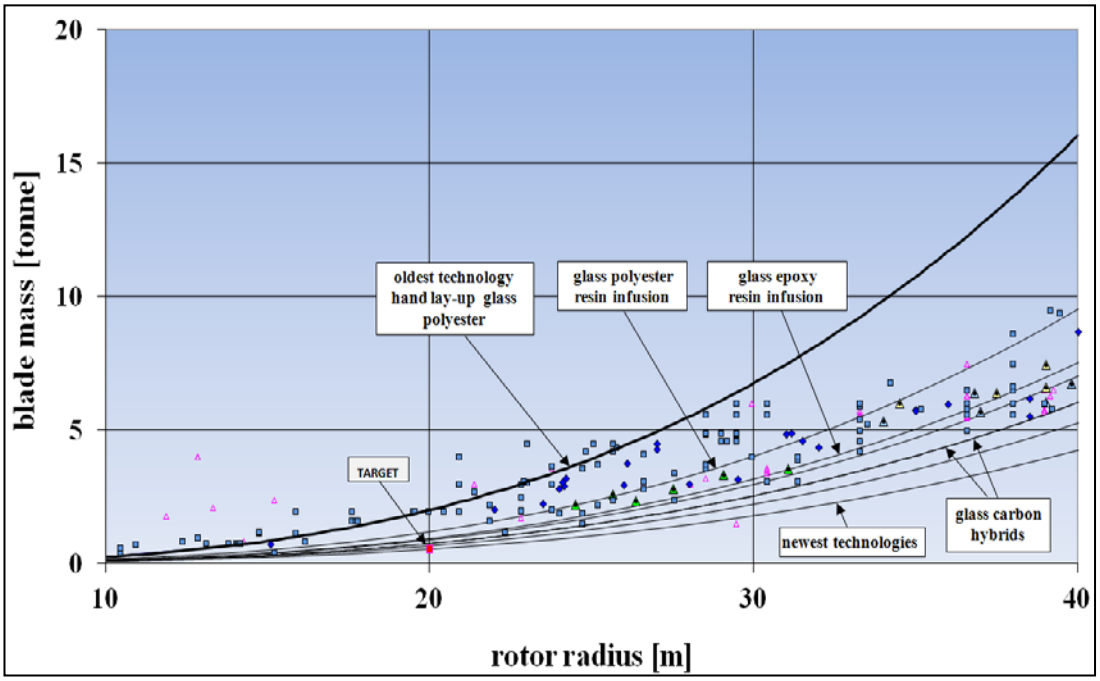

Figure 4.9 - Blade Mass Scaling with Similarity

The same process is carried out for the rotor hub, with newest technology accounting for a downward shift in weight estimates compared to older comparably rated machines. Plotting hub mass against diameter (Figure 4.10), it is seems plausible and perhaps even conservative to use a hub of mass 1500kg.

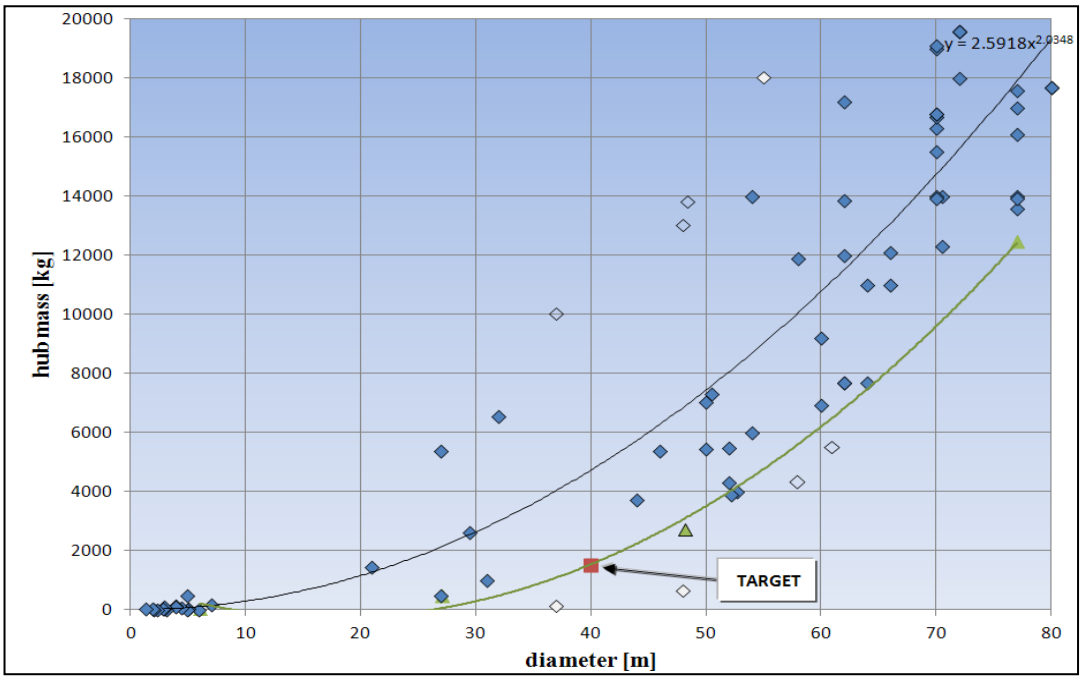

Figure 4.10 - Rotor Hub Mass Scaling with Diameter

4.4.3 Nacelle Housing and Generator Characteristics

Conservative estimates for a PMDD generator in the 444kW region is 1500kg. It would be expected that the amount of space taken up by such a system would be relatively small. The use of a compact generator, lack of requirement for yaw motors/hydraulics and lack of a gearbox allows the nacelle to be 20-30% of the size of other machines in the 500kW region. This neglects the fact that in the multi rotor system could potentially support drive-train and electronics within the fairings of the structure making the actual nacelle weight effectively zero. It is therefore proposed that the nacelle (excluding generator) can comfortably achieve weights of 6500kg. Plotting mass with diameter (Figure 4.11) suggest that a combined mass of generator and nacelle of 8000kg would only need to achieve a 20% reduction in mass in comparison to conventional drive machines, some of which date back 15 years.

Down-scaling rotor and drive train mass of the present lightest 5MW machines cubically suggests the total mass of each nacelle rotor combination may be as low as 11 metric tonnes. For the purposes of this study, it is assumed that this value is achievable.

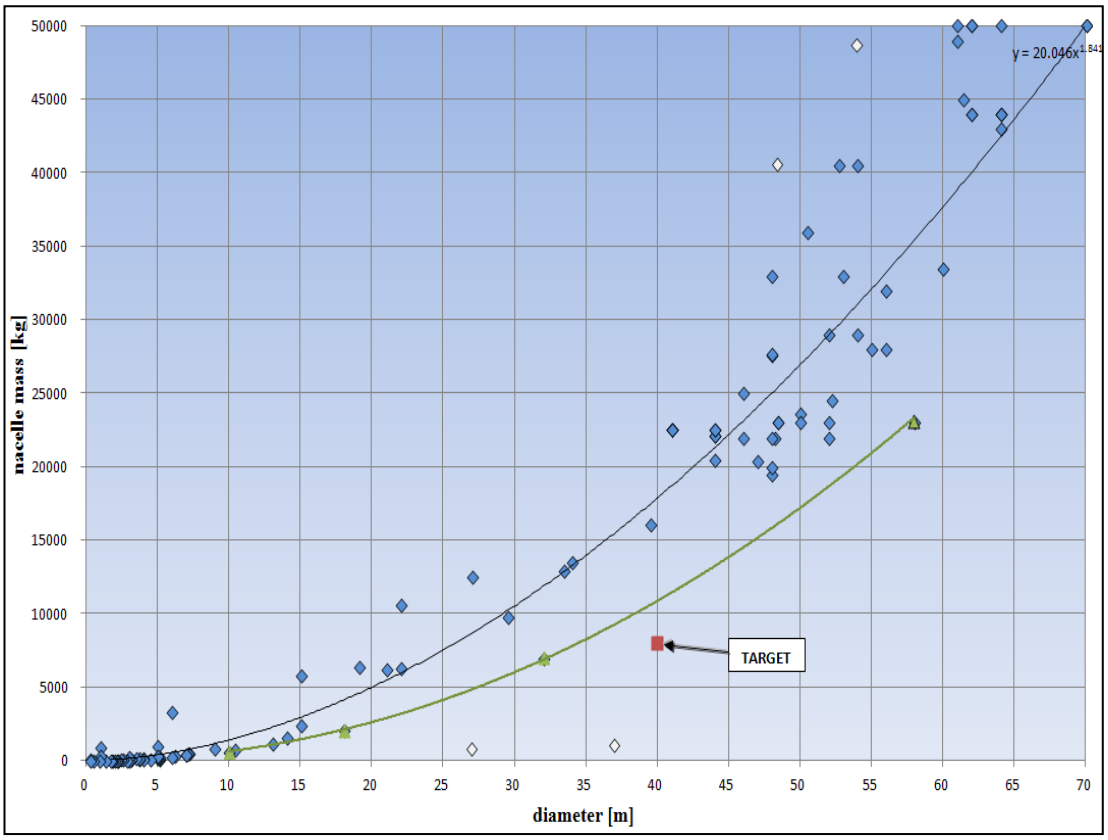

Figure 4.11 - Nacelle Mass Scaling with Diameter

4.4.4 Stall or Pitch Regulated Machines

It is possible to design a multi rotor system using either pitch or stall regulated machines. Stall regulated machines hold some appeal when considering offshore operation due to the reduced number of components (pitch motors and so on) which in turn should result in more reliable machines.

Figure 4.12 is a plot of the power curve taken from one alternative machine that was considered, a 600kW stall regulated machine based on the Nordtank SR600 design [97]. This Figure highlights two important considerations; the first is that the C_P capability of stall-regulated machines is often lower and broader than equivalent pitch regulated machines. The second is that the thrust force on a stall regulated machine increases steadily with increasing tip speed.

Simulations in Bladed showed that this design was more often operating at power outputs of around 540kW due to the inclusion of a less adequate controller.

The inability to pitch in a multi rotor context causes a severe structural penalty that requires the structure to be designed for forces much higher than would normally be expected due to the increased maximum thrust. This over-engineering increases structural weight and therefore also cost. The inability to pitch also removes one layer of control from the multi rotor system*, and it is these additional layers of control for load alleviation and power maximisation that make the multi rotor appealing in the first place. In the end, a standard pitch-regulated 444kW machine which was based on a down-scaled 5MW state of the art (as of 2010) machine was chosen.

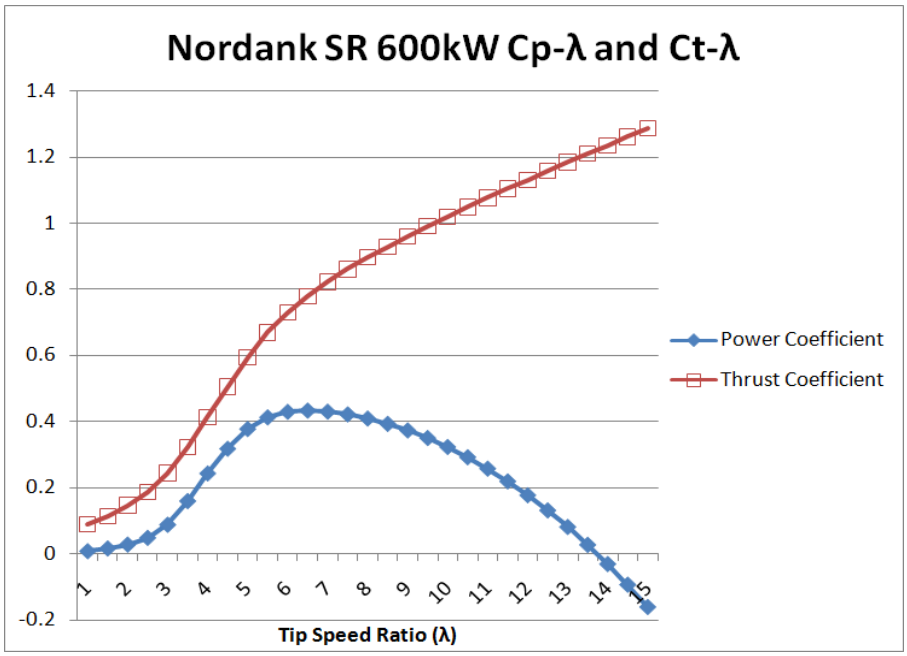

Figure 4.12 - Example 600kW Stall-Regulated Rotor C_p-λ and C_t-λ curves

For the remainder of this project only pitch regulated machines are considered as viable options for multi rotor systems. Data for an unnamed but relatively standard 5MW design is used as a basis for the study. Figure 4.13 which shows the curve characteristic curve plotted for a downscaled 444kW machine against that of an up-scaled 20MW machine in Bladed. The slight differences in the curves are caused by a non-optimised PI controller at both scales. These two systems will be compared against one another throughout the remainder of this project.

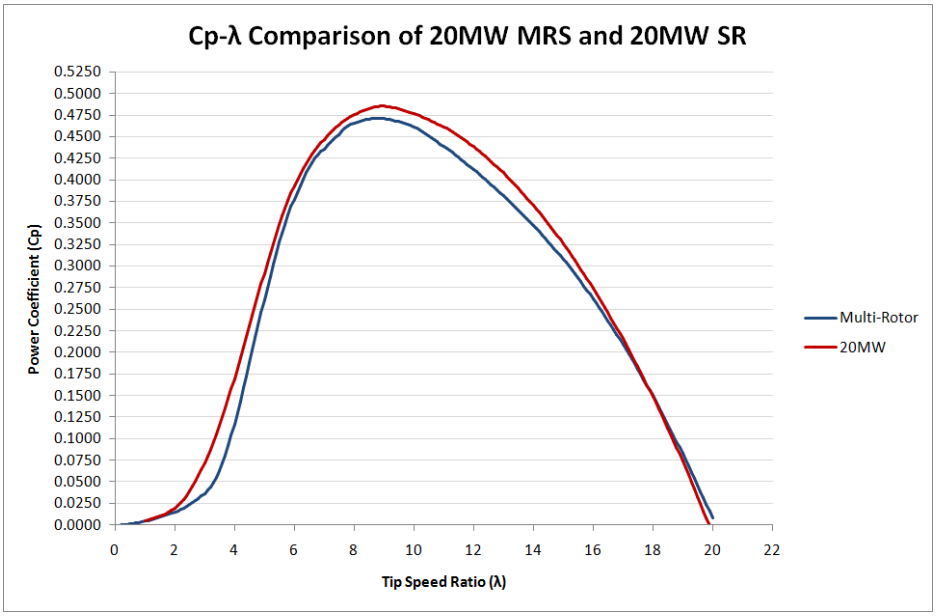

Figure 4.13 - Cp-λ of MRS and Scaled 20MW

4.5 STRUCTURAL OPTIMISATION

4.5.1 Ultimate Loading

At this stage of the multi rotor development it was not yet known what the key load case would be that would define the structural design. In order to design against a perceived maximum, it was believed that this would initially come from an extreme 50-year gust case in a class 1A storm. That is a gusting wind of 70m/s onto the rotors and array.

A very quick and rudimentary calculation can estimate what the hub F_x / thrust loading would be on a single rotor, in this case the calculation is provided by:

$$F = 0.5 \cdot \rho \cdot A \cdot C_T \cdot U^2 \tag{4.9}$$

In this case the coefficient of thrust (rotor drag coefficient, C_D x rotor solidity, σ) was chosen to represent a low value correspondent with a feathered blade in an extreme wind. At 70m/s the representative tip speed ratio for a 40.5m feathered rotor idling at 0.2 rad/s is 0.116. Figure 4.12 shows how the variation of TSR affects both power coefficient and thrust coefficient on a real-world stall-regulated rotor of

approximately similar rating and size. Although the Figure does not show below TSR's of 1, the associated coefficient of thrust will be considerably less than 0.1. In this case the assumption was that the coefficient of thrust could be comfortably controlled in the region of 0.02.

The reference thrust used to make the initial MRS design was therefore in the region of 75kN per rotor before application of the safety factor (S.F) of 1.35 for aerodynamic loadings.

4.5.2 Space-Frame Interconnection

Layout options for the rotors are relatively limited but there are a multitude of possible solutions for linking the rotors structurally and seeking optimum strength to mass ratios. The layout of the supporting frame is not dissimilar to an offshore jacket used on oil rigs and therefore many of the methods employed, e.g. welding techniques, are transferrable. The structural design is affected by self-weight, extreme wind loading and for an offshore environment wave loading, though the latter will not be considered here. Wind loading can quickly become a design limiting factor when considering IEC Class IA 50-year storm conditions and therefore necessitates a careful consideration of the type and thickness of members used to join adjacent nodes.

Numerical optimisation work on member thickness carried out by CRES Athens by varying the outer and inner diameter of these hollow sections in an attempt to minimize mass and maintain mechanical strength under increasing axial loading during an extreme storm case V_e50 = 70m/s.

The findings were that for members with width beyond 1.8m diameter experienced negative effects due to increased drag. Member widths around 0.8m with 8mm thickness allowed for relatively thin sections that ultimately offer the best strength to mass ratios and provide a basis for the initial structural layout [91].

4.5.3 Modularity

The multi rotor system can be designed from the offset to be modular, that is it can be designed such that individual rotors and their housings can be readily replaced should a failure leave them unrepairable. Modularity provides several key advantages to the multi rotor system:

- During the construction and installation phase the rotors/nacelles need not be fitted to the structure prior to transportation. The ability to quickly bracket in each rotor and their relatively light weight means this could be done easily on-site without the need for specialised heavy-duty crane equipment and should reduce overall setup time and cost.
- During any critical failure whereby a component or part of the rotor/turbine has become unrepairable, the entire nacelle and rotor could be removed quickly and replaced with a new one. This aspect constrasts sharply with current practice which would be to decommision and abandon a turbine that had experience a critical failure.

4.5.4 Space Frame Model Setup

The space frame was constructed in the finite element analysis package Abaqus 6.8-3. The space frame consists of a series of steel CHS sections of varying diameter and thickness. All main structural members comprise grade S355 steel. The depth of the frame is tapered from 3.577m (roughly twice the depth of the nacelle) to 17.5m top to bottom.

Nacelles are placed within the bracket at the nodes connecting adjacent members in (see Figure 4.14) There is no requirement to model the blades or hubs other than as point loads at this stage as this would overcomplicate the analysis. An absolute minimum clearance of 18.8m is required from the bottom run of the space frame to the base of the tower, however in this configuration it is set at 40m - allowing for significant water depth. Dynamics due to water or waves is not considered.

Rotors are modelled as a distributed nacelle load of 8t and a F_y point load representing a 3 tonne rotor, bolted into a square bracket of solid steel. A time-varying pressure load is applied to the front face of each nacelle to represent dynamic thrust loading as taken from corresponding Bladed simulations. Time varying moments are applied to each nacelle representing a rotor idling at 0.05 rad/s (for the extreme storm cases), with adjacent rotors rotating in opposite directions. Line loads corresponding to a constant 70m/s extreme wind speed are placed on all structural members. A coefficient of drag for the CHS is taken to be 1.2, though this may be lower in reality.

The starting iteration uses a uniform member width of 0.8m and a uniform member thickness of 0.004m for all members in the space frame.

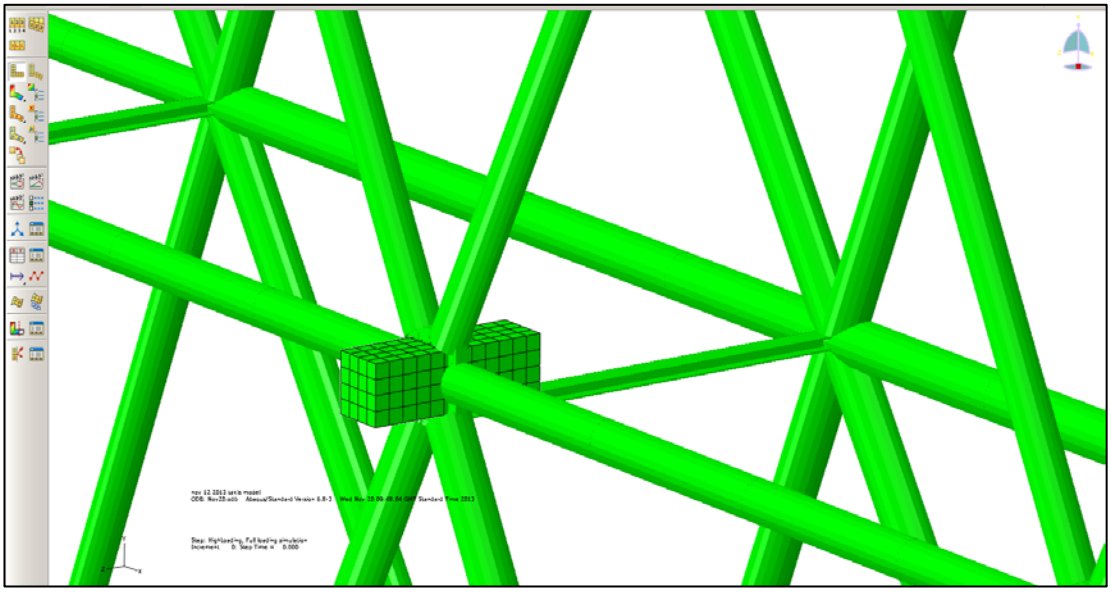

Figure 4.14 - Nacelle with Rendered Frame

4.5.5 Method

Starting with the initial setup the model is run using a constant applied force at each node and on each member. A shear exponent of 0.14 is used to grade the forces at each location according to its relative vertical position with the reference point assumed to be at 115m (i.e. the centre of the array). The simulation is run for 10 seconds so as to allow for any initial transient forces to be resolved.

After 10 seconds the output from the simulation is viewed and those members which have experienced plastic deformation or ultimate yield are identified. These members are highlighted and then have their characteristics updated in successive simulations through increases in member diameter and or thickness until they do not fail under the static forces.

By the same process those members which are seen to have experienced stresses well below their tolerably values are highlighted and have their characteristics reduced through member width decreases and or thickness decreases until the relative stress on those members reaches near critical in successive simulations.

In this manner the structure undergoes a series of iterations, with each iteration experiencing local strengthening or weakening (and associated mass changes) until the whole structure can comfortably survive the statically applied forces. Through this process the structure also undergoes a crude form of optimisation (useful as a first attempt) in order to minimize its mass. Given that this part of the project is only to identify a starting point for the MRS to enable further study it is believed that this optimisation process is sufficient as a first attempt.

4.5.6 Iteration Results

While the iterative process identified a large number of potential member sizes, it would be uneconomic and inefficient to select dozens of different member types for a structure of this magnitude.

To simplify the engineering of a large space frame, a small number of circular cross-sections have been proposed (Table 4.1). The layout of these CHS are presented in Figure 4.15 through Figure 4.21, with each set represented as a darkened outline.

These beams are all between the lengths of 37.6m and 42.5m in length making the summation for the space frame mass approximately 3000 tonnes. The addition of 45 rotor nacelles and expected mass increases due to joint welds, brackets etc brings the total tower head mass to approx. 3450 tonnes. This is equivalent to a cubically up-

scaled (with similarity) ø274m rotor and drive-train. Note that this is neglecting the 'tower' members linking the space frame to the ground.

Beam ID	**Outer Diameter (m)**	**Thickness (m)**	**Mass per Member (tonnes)**	**Number of Members**	**S (I_y/y)**	**M_{yield} (MN/m)**
C4D1	0.4	0.01	3.67	59	0.0012	0.414
C6D1	0.6	0.01	5.55	71	0.0027	0.956
C8D1	0.8	0.01	7.43	40	0.0048	1.721
C11D1	1.1	0.01	10.25	34	0.0093	3.287
C11D4	1.1	0.04	39.89	3	0.0341	12.110
C14D2	1.4	0.02	25.96	15	0.0295	10.485
T20D2	2.0	0.02	37.26	8	0.0611	21.675

Table 4.1 - List of structural members and properties. S is the section modulus and M_{yield} the yield strength under bending.

With the static forces applied, the tower top deflection and maximum member stresses are investigated at 0 degrees flow inclination and -45 degrees (yawed flow).

In axial flow, the space frame deflects by a maximum of 6.42m out-of-plane (Figure 4.22). Torsion caused by rotor overturning moments in the nacelle brackets creates high localised stresses on the order of 10^7 Pa with longitudinal bracing members experiencing both tension and compression). This suggests that an alternative configuration which removes the nacelles and square bracket nodes in favour of an equivalently sized CHS running longitudinally from the front of the frame to the rear (and containing the drive-train) may be preferred.

In yawed flow with fixed boundary conditions at the base nodes, the space frame twists by 0.64 degrees and has a maximum frame top deflection of 6.51m. Stresses are concentrated near the base of the structure and towards the rear bracing members as expected, with a maximum bending moment of 10.8 MNm appearing on a single C14D2 member, suggesting some plastic deformation and subsequent strengthening may still be required.

The use of steel wiring may be a suitable method of improving the overall structural strength particularly when considering that the main contenders for buckling are the bracing members on the bottom run which undergo excessive buckling forces ill-suited to circular hollow cross sections.

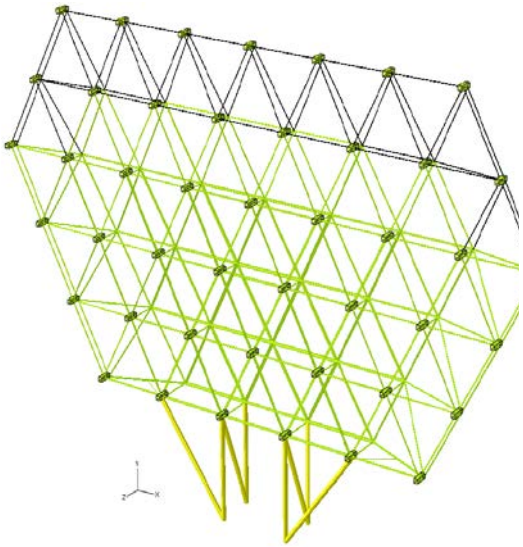

Figure 4.15 - Location of C4D1.

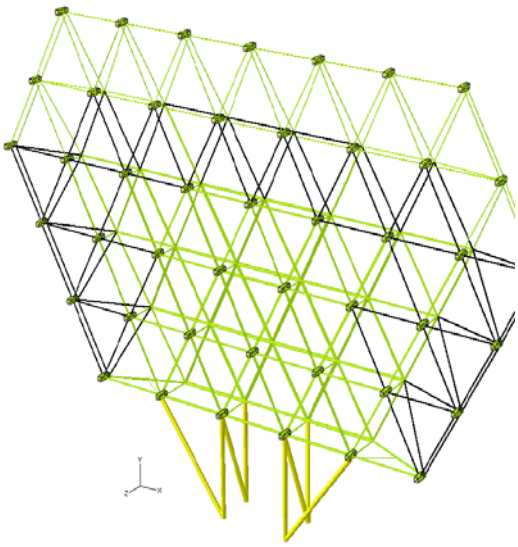

Figure 4.16 - Location of C6D1.

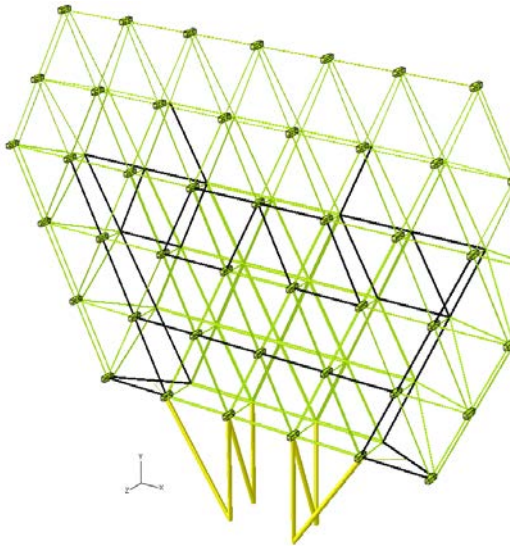

Figure 4.17 - Location of C8D1.

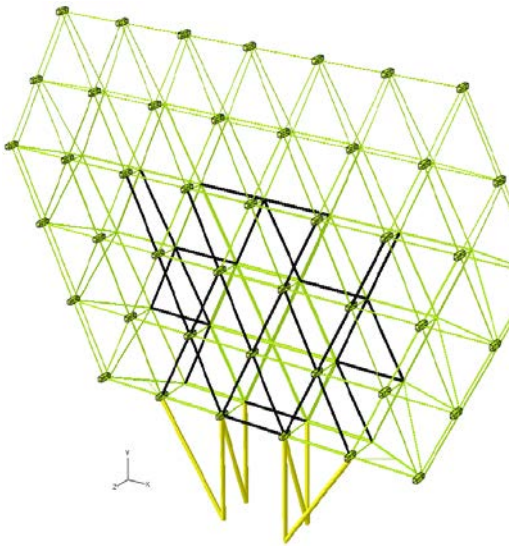

Figure 4.18 - Location of C11D1.

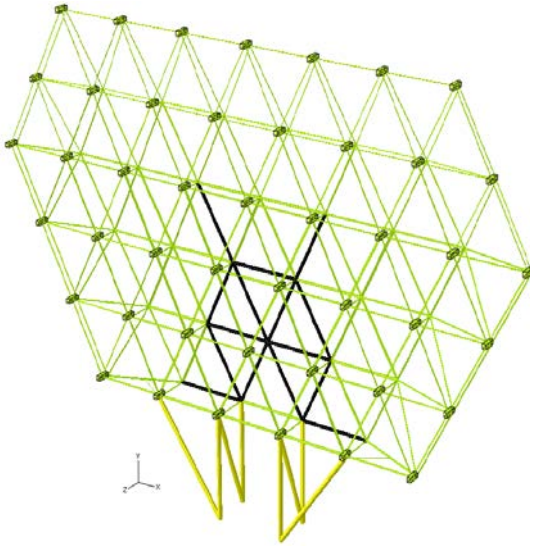

Figure 4.19 - Location of C14D2.

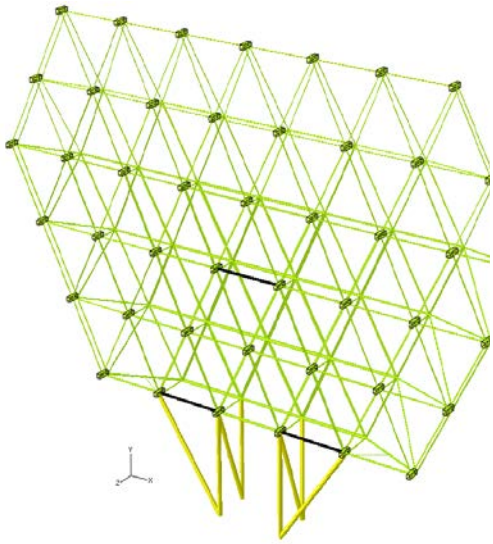

Figure 4.20 - Location of C11D4.

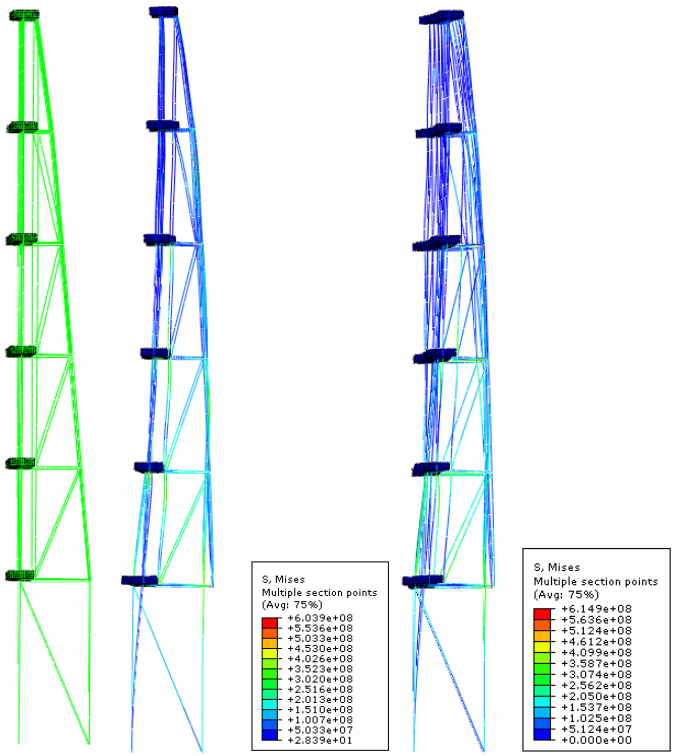

Figure 4.21 - Side view of frame: un-deflected, under axial flow, & yawed flow.

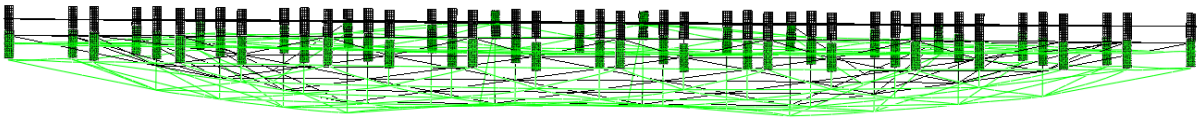

Figure 4.22 - Plan view of deflected space frame superimposed over un-deflected case.

4.5.7 Critical Structure Points

There are several points on the structure that experienced high localised loading under normal operating conditions. The majority of these points were able to be strengthened during the iteration process until structural yield no longer occurred however several locations (above those previously mentioned) remained an issue at the end of the initial design phase.

In the existing design the spar running from the rotor bracket to the bracing members at the rear of the structure are design critical under almost any loading. One of the primary issues with the use of modular brackets/nacelles is that the nacelle undergoes rotation during operation. In a local co-ordinate system the nacelle/rotor tends to pitch forward (around the y-axis) due to the rotor weight while the thrust from the system tends to pitch the rotor up and force it back. On a global co-ordinate system the rotor pitches up around the y-axis due to overall structural flexing. This causes the rear of the nacelle, which is normally sitting on the spar, to dig into and compress the upper skin of the spar. This has the same effect as applying a sharp buckling force at a single point midway down the spar.

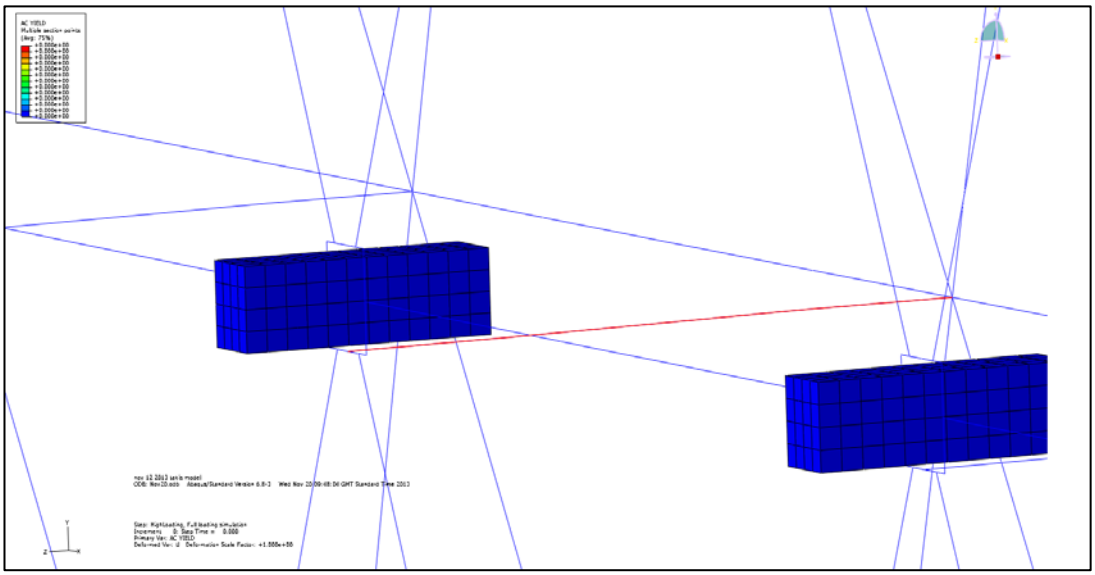

Figure 4.23 - Nacelle, Bracket and Spar Unstressed

Figure 4.23 shows the nacelle housing sitting on top of a single spar under no load. The spar is in plane with the bottom of the bracket housing and the node adjoining

the rear bracing members. Figure 4.24 shows the same location under normal operational loading (DLC1.3) or a localised force of approx. 43.6kN. The nacelle has rotated under the applied forces and is applying a buckling force on the front half of the spar causing it to warp. As the spar is attached at both ends to the larger frame which is comparatively solid it begins to bend near the middle forming a very shallow S. This effect is the same as applying a buckling force to a beam which has fixed boundary conditions at both ends. With some applied force, in this case approx. 68kN the beam ultimately buckles and undergoes plastic deformation and active yield.

It was hoped that by replacing the CHS sections on the spar with I-beams that this buckling would not occur (CHS sections performs relatively poorly under buckling stresses). However, in this design the I-beam was unable to be made strong enough to withstand the additional forces without a complete re-design of the structure. It is expected that with additional strengthening an I-beam approach will be a suitable solution.

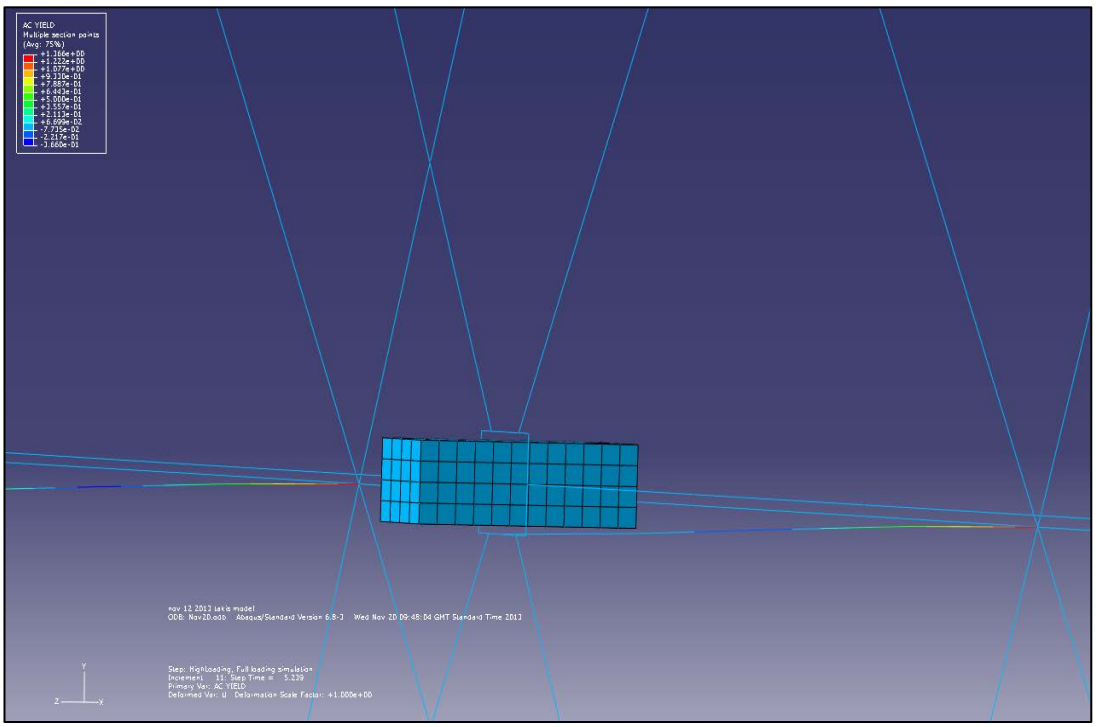

Figure 4.24 - Nacelle Rotation causing Spar Yield

4.5.8 Modes

The complex supporting structure for the 45-rotor array creates many closely spaced structural frequencies. The first 20 modes are shown in Table 4.2 with corresponding Eigen values. Note how all 20 of these modes are present under 1Hz.

All modes from 1 through 16 are present in the operating region of the rotors with 1P at 4.8 rad/s or 0.76Hz. It is therefore likely that these modes will contribute heavily to the overall structural fatigue on the space frame under normal operation, although the extent of this damage is yet to be established.

It is hoped that because of the independent operating nature of each rotor that during operation the forcing frequencies will be spread out over the full range of modes and no specific frequency will dominate in structural fatigue. If fatigue is likely to be a problem then it would be possible and likely advantageous to operate adjacent rotors at slightly different rated speeds to artificially spread the forcing frequencies across multiple modes. Such an operation would only be required if there was a risk that the whole system would be operating in particularly coherent or non-turbulent flow - which the next Chapter will examine in more detail.

0	Increment	0: Base State			
1	Mode	1: Value =	0.41223	Freq = 0.10219	(cycles/time)
2	Mode	2: Value =	1.2001	Freq = 0.17436	(cycles/time)
3	Mode	3: Value =	4.5896	Freq = 0.34096	(cycles/time)
4	Mode	4: Value =	4.7208	Freq = 0.34580	(cycles/time)
5	Mode	5: Value =	5.8166	Freq = 0.38385	(cycles/time)
6	Mode	6: Value =	6.1165	Freq = 0.39361	(cycles/time)
7	Mode	7: Value =	9.6822	Freq = 0.49523	(cycles/time)
8	Mode	8: Value =	9.8408	Freq = 0.49927	(cycles/time)
9	Mode	9: Value =	14.134	Freq = 0.59834	(cycles/time)
10	Mode	10: Value =	15.019	Freq = 0.61680	(cycles/time)
11	Mode	11: Value =	15.418	Freq = 0.62494	(cycles/time)
12	Mode	12: Value =	16.967	Freq = 0.65557	(cycles/time)
13	Mode	13: Value =	19.496	Freq = 0.70274	(cycles/time)
14	Mode	14: Value =	20.832	Freq = 0.72642	(cycles/time)
15	Mode	15: Value =	22.241	Freq = 0.75059	(cycles/time)
16	Mode	16: Value =	23.279	Freq = 0.76790	(cycles/time)
17	Mode	17: Value =	25.585	Freq = 0.80503	(cycles/time)
18	Mode	18: Value =	26.547	Freq = 0.82003	(cycles/time)
19	Mode	19: Value =	27.595	Freq = 0.83605	(cycles/time)
20	Mode	20: Value =	29.337	Freq = 0.86204	(cycles/time)

Table 4.2 - First 20 Modes: Eigen values and Eigen Frequency

The corresponding mode shapes for the first 10 modes (including steady-state) as viewed looking down the z-axis is presented in Figure 4.25. The shapes have been enhanced for visualisation purposes through use of a scale factor of 80.

Clearly the large number of modes which exist well within the operational frequencies of a single rotor pose a complicated problem. It is very difficult to establish how the structure will behave due to the interconnection of so many rotors and this problem will be exacerbated by the addition of additional rotors. It is highly likely that the safest course of option to follow until further examination has been performed to follow strictly to the application of a safety factor of 1.35 for all aerodynamic forces.

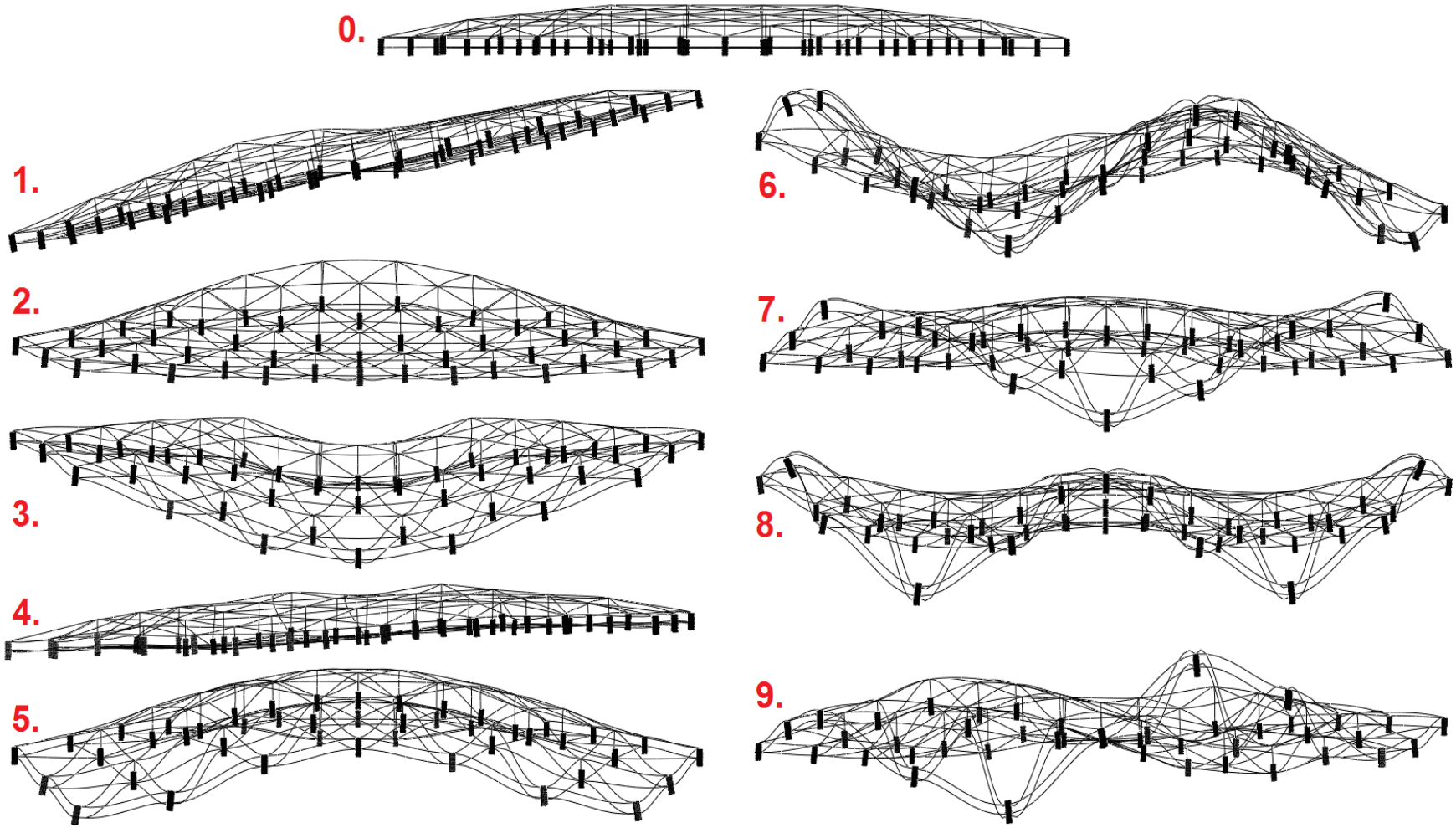

Figure 4.25 - Modes 0-9 of 45 Rotor MRS

4.6 RESULTS

The total space frame mass as calculated approximates 3000 tonnes excluding the "tower". Note that in this example the multi rotor tower is simply the members connecting the space frame to the ground and not a single tubular tower. The addition of 45 rotor nacelles (11t per rotor) and expected mass increases due to joint welds, brackets etc (1t per rotor) brings the total tower head mass to approx. 3540 tonnes. This is equivalent to a cubically up-scaled (with similarity) ø274m single rotor and drive-train. In comparison, the UPWIND design [14] (ø252m rotor) predicts that a tower head mass of 880t and total system mass of 3640t including tower is achievable. To achieve a fair comparison in terms of power density, the UPWIND design would nominally require a 274m rotor. Following scaling laws, this would result in a $(274/252)^3 = 1.3$ increase in tower mass. Thus the MRS system should perhaps be compared to the UPWIND mass estimates inflated by 30%.

A comparison of this data, including the original 5MW mass data is presented in Table 4.3. The 5MW reference is based on current 5MW machines and is multiplied by 4 to achieve 20MW. The 20MW single rotor is scaled up from the 5MW reference with similarity, each 444kW rotor on the MRS is scaled down from the 5MW reference with similarity. The 20MW UPWIND is an advanced conceptual design, scaling down to 444kW with similarity achieves an equivalent MRS system.

Considering the substantial savings in total cost of rotors and drive trains due to downscaling and the reasons cited in Section 4.1,4.22 and 4.3, the CoE of the multi rotor system is unlikely to be penalised by excessive mass or cost in the multi rotor structure.

	5MW Reference x 4	20MW Scaled	20MW MRS Scaled	20MW UPWIND Design [14]	20MW MRS based on UPWIND
Tower Head Mass (t)	1392	2300	3500	880	2850
Tower Mass (t)	2210	3500	400-600	2760	400-600
Total System Mass (t)	3602	5700	3900-4100	3640	3250-3450

Table 4.3 - Mass comparison of three system types.

The results at this stage from a purely structural standpoint suggest that four 5MW rotors will weigh ~ 80% of a single 20MW rotor. A 20MW multi rotor system can weigh ~89% of four 5MW rotors or ~ 70% of a 20 MW single rotor system. If cost is approximately tied to mass, which is not an unreasonable assumption, then these may indicate comparative CoE savings as the structural cost for the multi rotor system does not appear to have a significant disadvantage.

In conclusion the MRS concept can feasibly achieve the aim of 20MW rated power without being adversely limited by design critical loads, particularly extreme turbulent storm cases which often design limit large single rotors. Preliminary calculations suggest that the structure is driven by overall coherent extreme storm loads and not by fatigue loading.

Further loads analysis on the multi rotor structure following approved industry standards is conducted in Chapter 5.

4.7 MRS FLOATER DESIGN

The last thing to discuss as part of the multi rotor proof of concept is the foundation structure. The traditional machine in an offshore environment favours a monopile or jacket foundation (73% and 13% of all offshore installations in 2012 respectively [100]). In 2012 there were only two full scale floating foundation designs, and two downscaled versions. Thus the implementation of floating designs is still relatively novel within the wind industry - however it is not without its merits.

The floating design plays an important role in any multi rotor consideration. Due to the space frame, interconnected structure design, the multi rotor suffers from an inability to yaw in the conventional way (via yaw rings and bearing). By placing the

system on a floating structure it is quite possible to include yaw capability on large multi rotor systems irrespective of their mass, size or construction.

Four hydrostatic floater designs were investigated by CRES Athens as part of work package 1.3.3 within the Innwind Project [101]. The most promising design was the Annular Barge with a 3,000 kg space frame requiring a 12-16,000 kg barge to achieve sufficient fluid displacement to be hydrostatically stable. This concept achieved the best cost/mass ratio ($656 per tonne) at 60m diameter scale and with a total cost in the region of $10-15 million. This equates to $0.5-$0.75 million per MW of installed power.

CHAPTER V – LOADS ANALYSIS OF A 20MW MULTI-ROTOR SYSTEM

5.1 INTRODUCTION

Given the previous research on the multi rotor system at small scale (2MW) has yielded positive results [102], it is with a certain degree of confidence that classical lattice structure proposed in Chapter 4 has been developed for the space frame. The first iterations of this structure were designed using basic theoretical calculations as to the prospective worst-case loading likely to be present on the structural array - in this case extreme 50-year storm thrust loading. These initial forces were used purely as a point of reference with the understanding that the actual design critical ultimate loading would likely be different. Therefore, the second objective of the multi rotor analysis is to establish a full understanding of the loads and designing load cases.

5.2 SCOPE AND OBJECTIVES

The International Electrotechnical Commission (IEC) amongst other standard bodies (such as GL2003 [103]) aim to elicit international co-operation and standardisation in electronic and electrical fields. IEC61400-1 [104] contains 22 design load cases grouped into eight design situations, ranging from normal operation with the introduction of a fault, to rotors idling in a 50-year storm.

This chapter quantifies and compares the design driving loads for two equivalently rated 20MW systems (a single rotor and an 45-rotor MRS) based on these IEC 61400-1 standards [105].

Throughout the analysis a standard Cartesian coordinate system is adopted with the x-direction being positive upwind of the rotor, the y-direction positive right and the z-direction being positive up.

The focus of this loads analysis is to identify which critical loads drive the structural design of the tower and space frame. It is assumed that the individual rotors have already been designed to withstand the environment they are subjected to and therefore there is no consideration of blade bending moments or individual blade forces.

The list of load cases has been condensed to achieve a compromise between computational time and load validity. This reasoning should be valid, provided that the ultimate loading that tends to drive normal wind turbine design is captured in the reduced set of simulations.

Table 5.1 contains an abbreviated list of the design cases taken from the standard and highlights the conditions and types of analysis presented in this paper.

The abbreviations for this table are available in the Nomenclature.

Design Situation	DLC	Wind Condition	Other Conditions	Type of Analysis	Partial Safety Factors
1) Power Production	1.2	NTM		F	*
	1.3	ETM		U	N
	1.4	ECD		U	N
2) Power production plus occurrence of a fault	2.3	EOG	External or internal electrical fault including loss of electrical network	U	A
4) Normal Shutdown	4.1	NWP		F	*
	4.2	EOG		U	N
6) Parked (Standing still or idling)	6.1	EWM		U	N
	6.2	EWM	Loss of electrical network connection	U	A
	6.3	EWM	Extreme yaw misalignment	U	N
	6.4	NTM		F	*

Table 5.1: Abbreviated Load Cases taken from IEC61400-3 [105]

5.3 MODELLING

5.3.1 Bladed Overview

The software GLGH Bladed [106] can model all the key systems that make up a wind energy conversion system, including: the n-blade and n-rotor system, drive-train, power-train and control system. This software is recognised and accredited by the wind industry as a tool to aid in the design and implementation of wind energy systems and therefore can also play a key role in providing a framework for multi rotor design at 20MW scale.

For completeness and to allow for the model to be recreated, a full-list of all model parameters as defined in Bladed are presented in Appendix C.

5.3.2 Model Setup

The structure described in Section 3 is created using Bladed's (v4.4) inbuilt multi-member tower function (Figure 5.1).

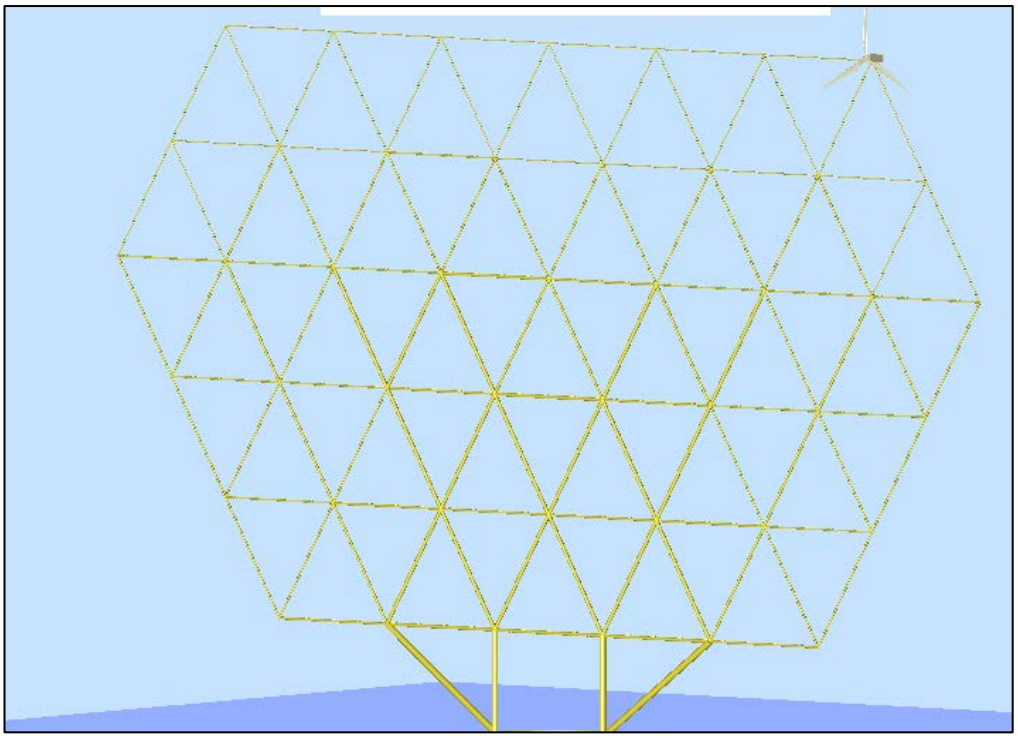

Figure 5.1: Graphical Representation of the 20MW MRS Modelled in Bladed

To simplify the loading analysis at these early stages of the MRS design the following assumptions were made and defined within the model:

- The structure is assumed to be rigidly fixed to the ground by means of four members and therefore both structure and turbines are unable to yaw.
- The rotors are in the upwind position.
- The structure takes the form of the original design created using the iterative process described in Chapter 4 and is not updated further as new loading information becomes available.
- The structure is considered rigid and therefore there is no dynamic interaction between adjacent rotors or the structure and the wind other than that caused by tower shadow.

- The numbering system for the 45 rotor/hubs is as depicted in Figure 5.2, with numbers running from left to right beginning with the bottom row.

Due to software limitations, the only way to establish reasonably accurate results at this stage was to remove all modal frequencies from the array and consider static cases only. These results should be valid when considering the structural design from an ultimate loading standpoint only.

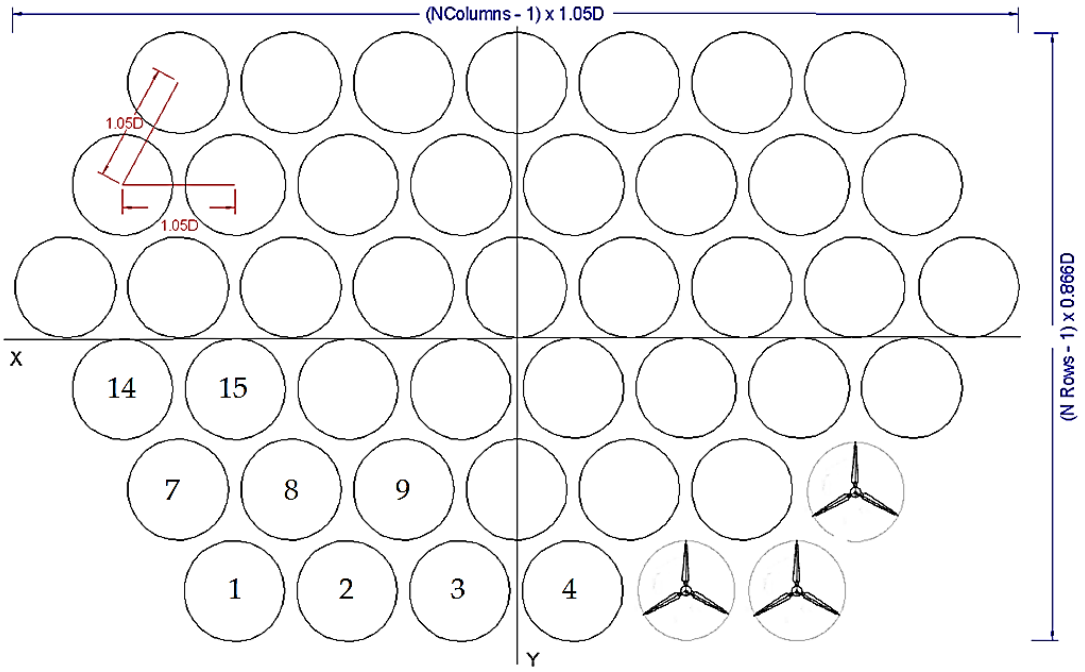

Figure 5.2: Rotor Hub Numbering System

5.3.3 Methodology

To establish the worst-case loading, each load case will be run in accordance with the provisions made in the IEC-61400 standard. After each simulation is run, the multi rotor array will be interrogated by the software at each rotor node on the structure (i.e. 45 times) and the forces and moments recorded as time-series. As a first pass, only hub Fx will be compared as this is the key variable in determining structural requirements under axial flow. Once the ultimate load case has been established, then all six forces and moments for each rotor will be re-evaluated within this single case.

Due to Bladed limitations, the only direct comparison between 45 individual rotor data sets and that of a single rotor is when all 45 individual data sets are combined into a single time-series. This combination is achieved by summing all time-series

together to arrive at the total combined force present on the tower. It is this final combined force which will reflect the ultimate or worst-case loading.

5.4 LOAD CASE ANALYSIS

The parameters used to setup each load case and an overview of the objective of each load case is provided in Appendix E.

5.4.1 DLC-1.2 (NTM) - Fatigue loads

Results:

The Bladed software was unable to provide meaningful results as to the fatigue loading on the complicated structure. The multi rotor array contains 45 rotors (135 blades) in addition to over 130 members.

In addition, there is some uncertainty as to how to accurately reflect the multitude of different load cases that would be present on each of the different rotors throughout each turbines lifetime. This uncertainty will be discussed in more depth in Chapter 7 where reference is made to a wider study of fatigue conducted on multi rotor systems.

Due to the computing time restrictions, both for University of Strathclyde in generating data files and for CRES in employing the data in structural analysis, the fatigue evaluation was quite limited.

A more complete and rigorous evaluation with longer and more extensive simulations and narrower wind speed bins is best done with a fully aero elastic model as may be developed in future work.

5.4.2 DLC-1.3 (ETM) - Ultimate Loads during Power Production

Results:

To establish the equivalent loading of a single rotors hub loading on the multi rotor system, a process of summing all 45 rotors at each moment in time to reach a total force has been adopted. It is proposed that this summing best reflects the total force present on the tower and therefore allows for direct comparison with tubular tower single rotors.

Plotting the aggregated hub F_x from each of the rows (corresponding to a fixed height) in the multi rotor array arrives at Figure 5.3.

The wind turbulence file is defined as having a mean of 11m/s at 115m height (approximately the centre of the array). In theory, under normal wind shear conditions this should mean that rows higher than the centre experience on average higher wind speeds, while rows below centre should experience lower wind speeds. Figure 5.3 shows that this is not the case for the entirety of the simulation window and in fact there is a reversal of wind shear during this 60s window. When turbines are operating around rated there is a large fluctuation in hub F_x with even a change of wind speed of 1m/s. This means that it is quite possible and likely for rows to appear to be operating in reverse shear for short periods of time when the overall wind is turbulent around rated.

If the simulation is run over the full 10 minutes it is shown that individual rows experience on average higher loading at higher rows in the array as expected due to standard positive wind shear. The fact that the loads do vary around the array independent of standard shear does need to be accounted for during the structural design.

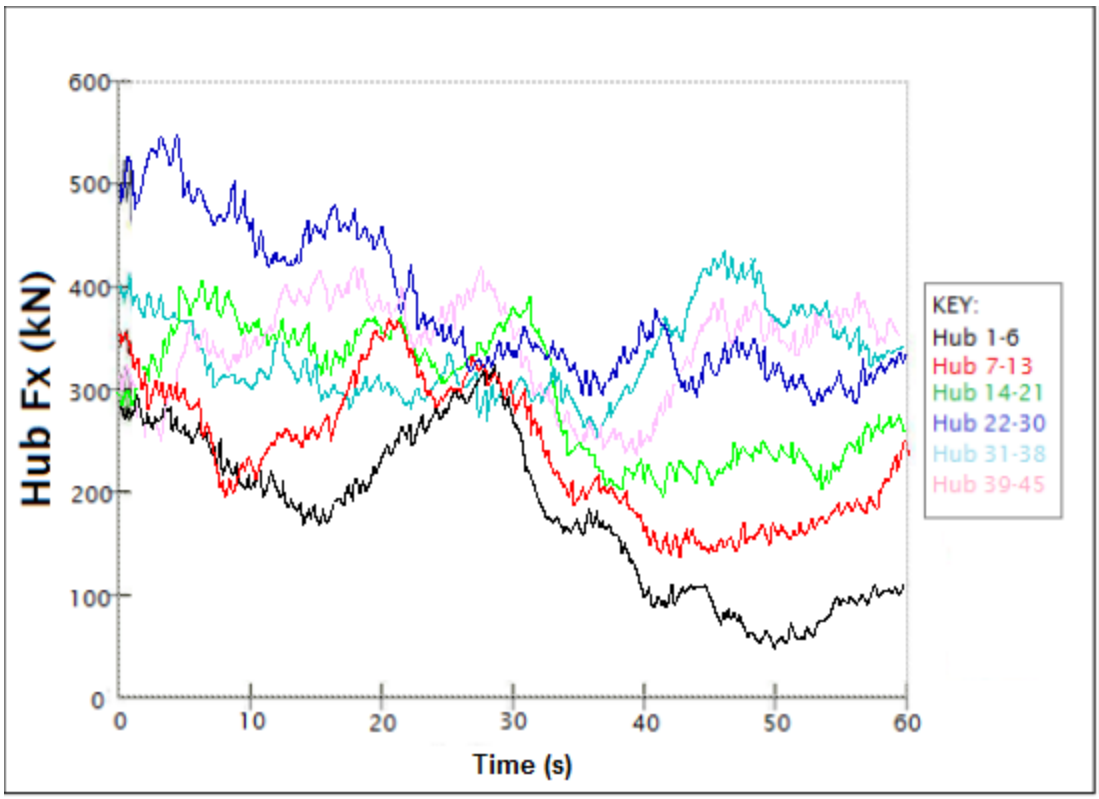

Figure 5.3: DLC1.3a1: Rotor Hub F_x by Row

Aggregating all the hub F_x loads and plotting them over time (Figure 5.4) leads to some interesting observations with respect to the averaging effect of rotors over the whole system.

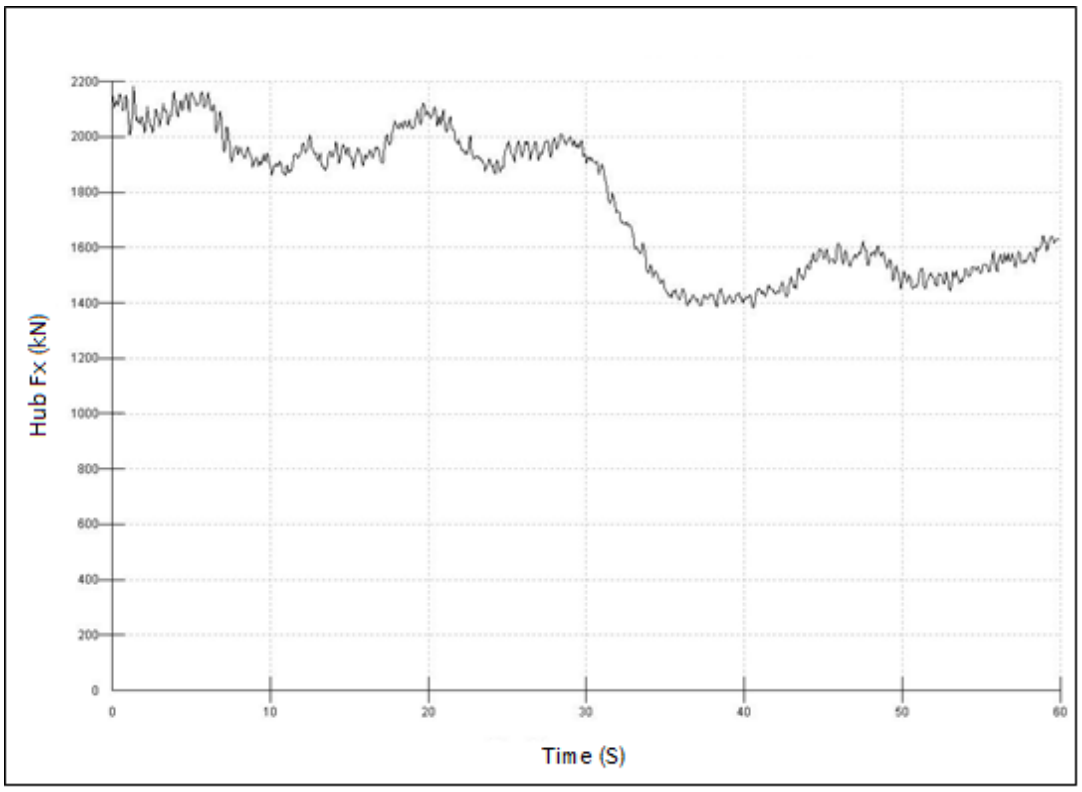

Figure 5.4: DLC1.3a1: Hub F_x Aggregated

In the aggregated data for the first seeded run (a1), representative of the actual MRS, the maximum hub F_x loading is 2182.85kN, with a mean of 1763.68kN and a standard deviation of 247.94kN. Dividing this loading per rotor leads to rotor equivalent loads of 48.5kN, 39.2kN and 5.5kN respectively.

In the same time series, the maximum Hub F_x throughout the whole array is present at rotor 25 and has a value of 102.61kN. This is 25% higher than the average of all the rotor maximums, which is 80.27kN and more than 100% higher than the average maximum per rotor experienced at the time step when whole array was experiencing the worst-combined loading, which is calculated as 48.5kN. These statistics are tabulated in Table 5.2.

Effectively what this shows is that individual hub F_x maximums occur at different times throughout the simulation, prompted by their displacement from each other and a varying turbulent wind. The displacement in time of individual ultimate loads has the effect of averaging and thereby reducing the overall system hub F_x such that

the ultimate loading never reaches close to what it would be if every turbine reached its ultimate loading simultaneously.

Figure 5.5 presents these basic statistics for each individual rotor in bar chart format for easier comparison. Note that rotor 25 sees the maximum loading of any of the wind turbines – due to its proximity to the effective hub height chosen for the simulations.

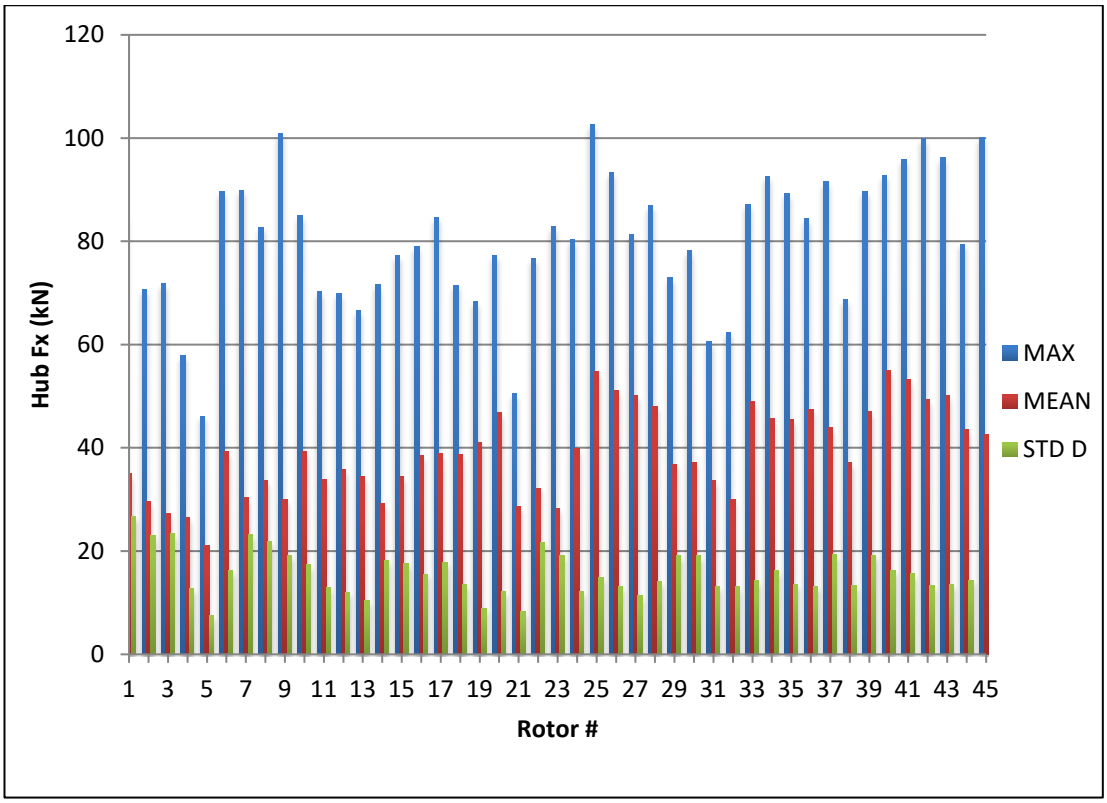

Figure 5.5: DLC1.3a1: Basics Stats All Rotors

Hub F_x	Aggregated Over Array	Avg. per Rotor for 45 Rotor Array	Avg. of Individual Max. Time Series	Stats. of Rotor 25 (worst-case)	45 x Rotor 25 (coherent worst-case)
Mean (kN)	1763.68	39.2	39.2	54.85	54.85
Maximum	2182.85	48.5	80.27	102.61	4617.45
Std. Dev. (kN)	247.94	5.5	15.83	14.93	671.85

Table 5.2: Tabulated Statistics from DLC1.3a1

As evidence that this is not a statistical anomaly, DLC1.3a3 (another run at rated wind speed but with a different seed) is presented in Table 5.3 and the bar chart of Figure 5.6. This shows a higher maximum Hub F_x for the whole array, but individually the rotors overall are experiencing less loading than in DLC1.3a1. This was an effect found in all six seeds run.

The results from this simulation are very promising from a structural standpoint. They show that while one turbine might experience its individual worst-case loading during a single period it does not contribute significantly to the overall loading on the array. As such the worst-case individual rotor loading rarely coincides with the worst-case loading for the whole multi rotor array. This bodes well for instances whereby single rotor faults lead to large localised forces which in a single rotor system would be transferred onto the tower and foundations but in the MRS will have almost negligible effect - a theory which will be tested in later sections.

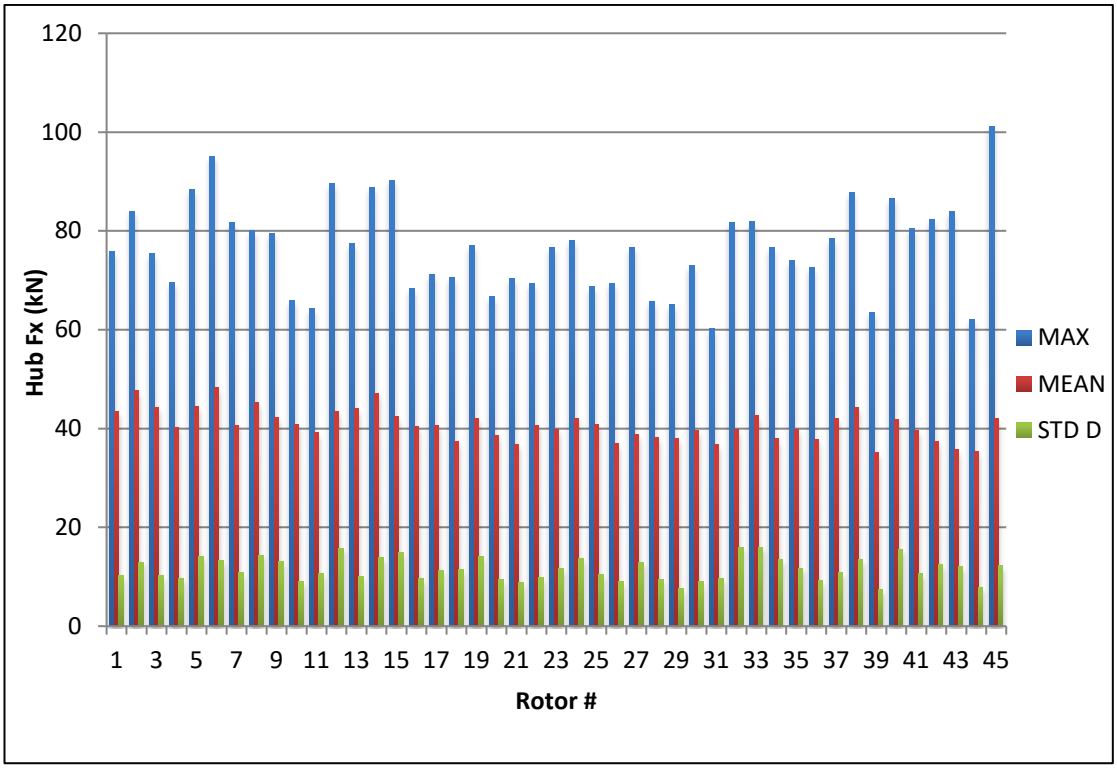

Figure 5.6: DLC1.3a3: Hub F_x by Rotor

Hub F_x	Sum of Whole Array	Avg. per Rotor for 45 Rotor Array	Avg. of Individual Max. Time Series	Stats. of Rotor 25 (worst-case)	45 x Rotor 25 (coherent worst-case)
Mean (kN)	1830	40.67	40.72	42.05	1892.25
Maximum	2460	54.67	76.56	101.22	4554.9
Std. Dev. (kN)	297.1	6.6	11.56	12.223	550

Table 5.3: Statistics of Hub F_x DLC1.3a3

The same DLC1.3 load case is run again at six seeds with an average wind speed based on cut-out speed (25m/s). For the purposes of this study it is assumed that none of the rotors in the array cut-out at any point during the simulation and remain in power production. The results are plotted in bar chart format Figure 5.7 and tabular format Table 5.4 respectively.

It is clear at this stage that operation around cut-out leads to lower ultimate loading across the array irrespective of seed. It can therefore confidently be stated that the worst-case power production loading does occur around rated wind speed.

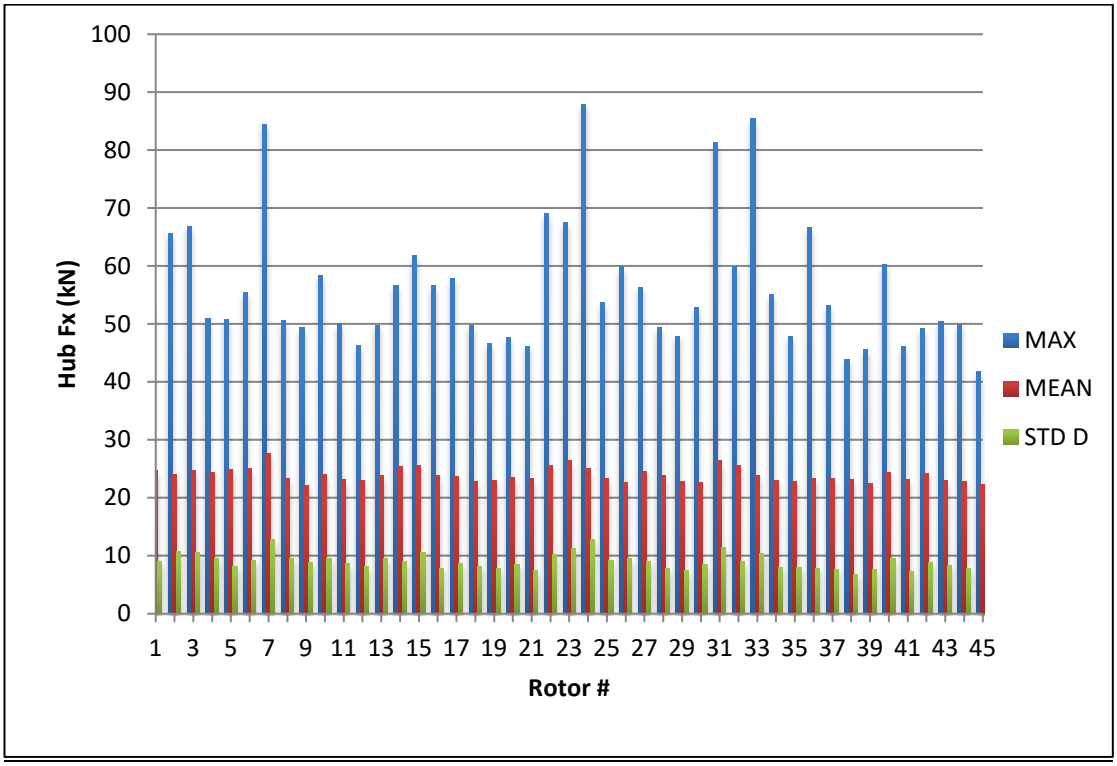

Figure 5.7: DLC1.3b4: Basic Stats for All Rotors

Hub F_x	Sum of Whole Array	Avg. per Rotor for 45 Rotor Array	Avg. of Individual Max. Time Series	Stats. of Rotor 24 (worst-case)	45 x Rotor 24 (coherent worst-case)
Mean (kN)	1077	23.93	23.93	25.13	1130.85
Maximum	1371	30.47	56.35	87.83	3952.35
Std. Dev. (kN)	86.05	1.91	8.96	12.89	580.05

Table 5.4: Statistics of Hub F_x DLC1.3b4

So far there has been some discussion about the positive effect of averaging of loads over the whole array. To better understand this, compare a typical single rotor hub F_x time plot against that of all the rotors average during the same period.

Figure 5.8 is a plot of Hub F_x for a single rotor (rotor 24) from a single run (DLC1.3a1) compared against the rotor averages from the same period. There is a very prominent peak in hub F_x loading for Rotor 24 around 52s into the simulation and generally a much higher average loading overall, as well as a much higher variance. This contrasts starkly with the average loading attributed to each rotor in the array which see lower variance, a lower average and a lower peak loading. This effective averaging effect is very welcome from a structural standpoint as it undoubtedly will lead to lower fatigue loading on the structure during its lifetime and also directly result in a cheaper structure.

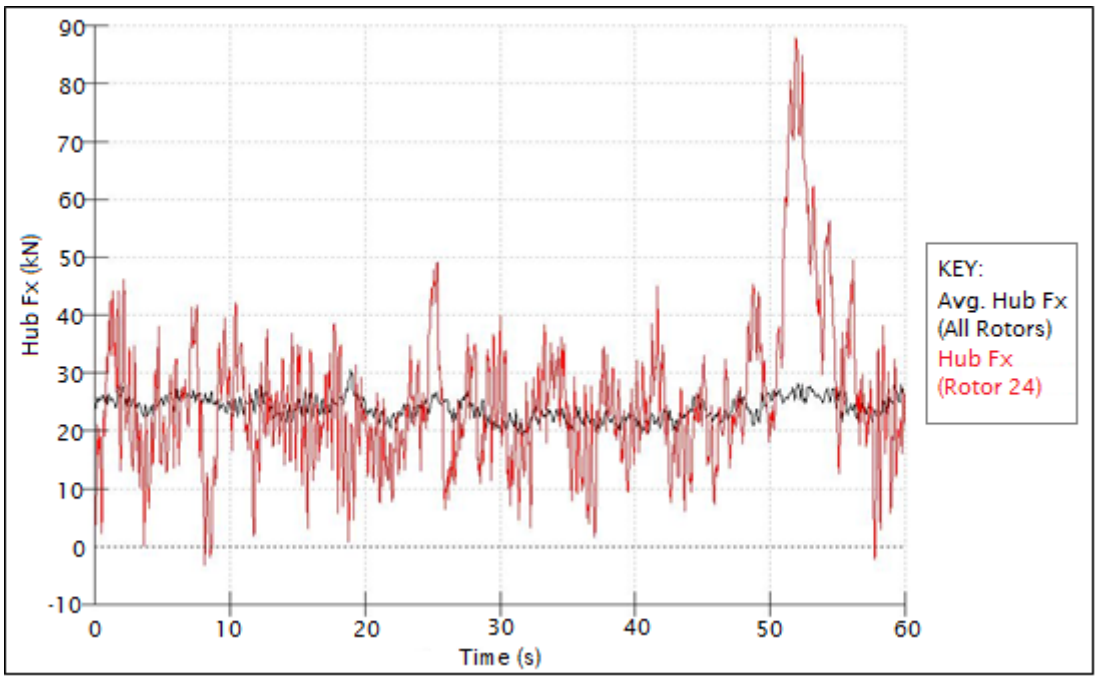

Figure 5.8: DLC1.3a1: MRS Average Hub F_x vs. Rotor 24 Hub F_x

Figure 5.9 depicts the time series of hub M_y for the worst-case rotor (rotor 2) compared to the effective average per rotor seen over the whole array. The effective hub M_y averages and maximums for the array are around 1/8 of the individual worst-case rotors combined mean and maxima.

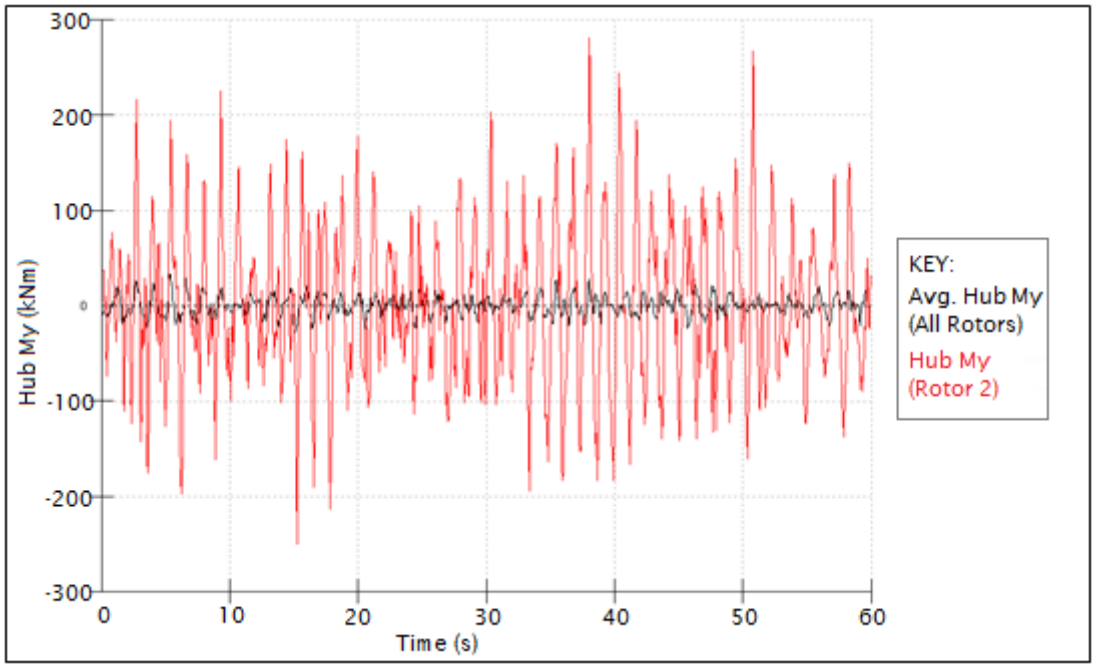

Figure 5.9: DLC1.3a3: MRS Average Hub M_y vs. Rotor 2 Hub M_y

The impressive load reduction effect is also seen in M_z (Figure 5.10) with an effective Hub M_z maximum around 1/5 of that predicted by the average maxima taken from each rotors time series.

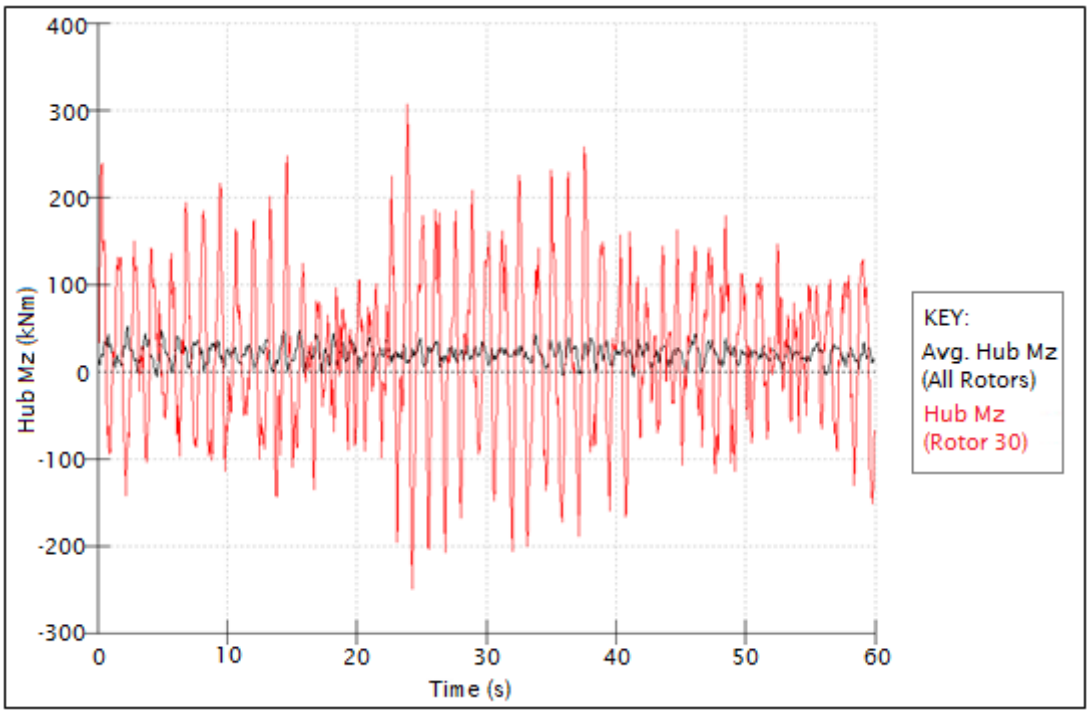

Figure 5.10: DLC1.3a3: MRS Average Hub M_z vs. Rotor 30 Hub M_z

Discussion:

Extreme turbulence normally drives blade bending moment and is close to driving tower base bending moment in a class I storm case for large single rotors. To examine whether a similar observation can be made in the multi rotor system, thrust loading, M_y overturning moment and M_z yawing moments are examined. For the multi rotor system, M_y is taken to be the sum of all the individual hub My overturning moments plus the sum of all the individual moment arms ($Fx \cdot H$) - where H is the height of each rotor centre in metres. Similarly, M_z is taken be the sum of all the individual hub M_z yawing moments plus the sum of all the individual moment arms ($Fx \cdot X$) - where X is the relative position of each rotor centre from the axis of rotation in metres. Figure 5.11, Figure 5.12 and Figure 5.13 present a comparison of these three loads for both the single rotor 20MW system and the 45-rotor 20MW multi rotor system.

As predicted by the scaling-law presented in Chapter 3, the multi rotor system as a whole exhibits reduced total hub F_x loading when compared to the 20MW single rotor system (Figure 5.11). At all points during the 5-minute simulation, the total hub F_x loading experienced by the array is 69% or less of the magnitude of that on the single 20MW rotor. This effect is found to be more pronounced in turbulent wind the reasons for which will be touched on in following sections.

From the My data set in Figure 5.12 it can be seen that the ultimate over-turning moment for the MRS is 350 MNm, when the average hub wind speed is 11 m/s at hub height. Under the same simulation parameters the single rotor 20MW system peaks at 850 MNm at a different period. This effect was seen across all 4 other wind seeds with the ultimate loading varying only slightly for each system within each run.

These results suggest that the multi rotor system has a lower ultimate M_y loading than the single rotor system of equivalent rating. The M_y average is also lower and has much less variance - which may be an advantage when comparing fatigue life. On average the MRS achieves a load ratio in M_y of 350:850 or 41% in comparison to the single 20MW rotor.

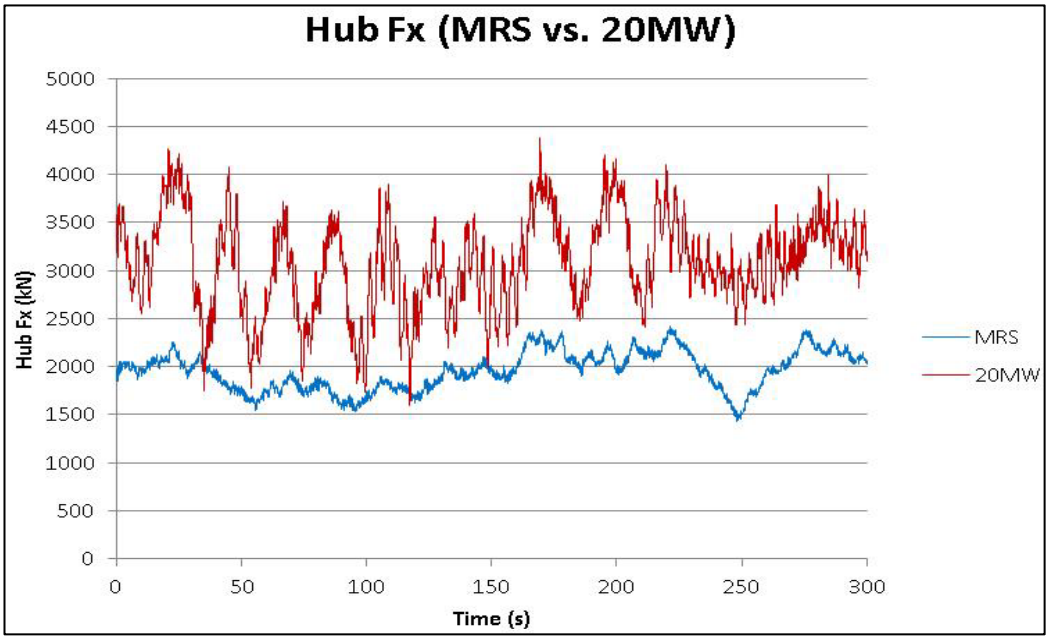

Figure 5.11: DLC1.3a3: Hub F_x Comparison (F_x), 20MW SR + MRS

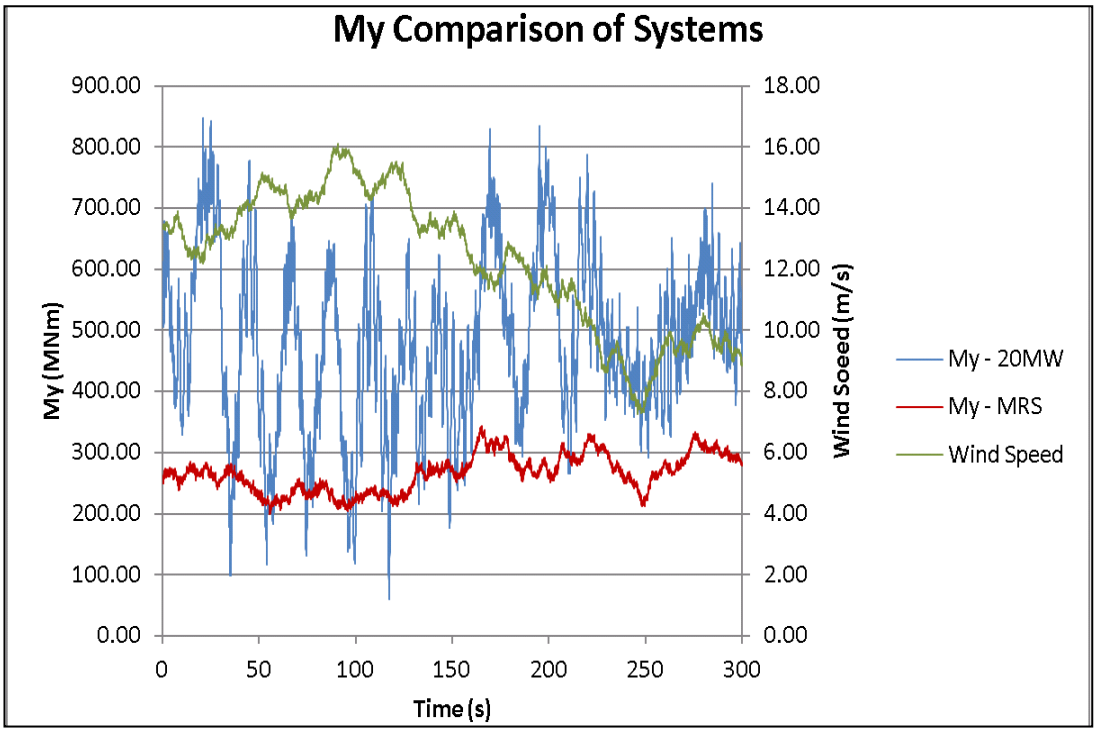

Figure 5.12: DLC1.3a3: Overturning Moment (M_y), 20MW SR + MRS

Figure 5.13 contains a plot of the data for M_z vs. time and suggests that the reduction in ultimate yawing moment for the MRS is even more significant. The M_z moment under the normal wind turbulence model is well balanced around the axis of rotation with the ultimate yawing moment not exceeding 2 MNm. Under the same wind speed conditions the single rotor 20MW system peaks at 47 MNm. This large yawing moment is unavoidable on the single 20MW rotor given the reliance of the moment on the azimuthal position of individual rotor blades (of which there is only 3) and rotor aerodynamic force imbalance under even small yaw errors. In comparison any multi rotor system will have many more rotors and blades and therefore there will be a much greater averaging of aerodynamic yaw moments caused by blade imbalances and wind angles of attack.

On average the MRS yaw moment ratio in M_z is 2:47 or 4.25% of that of the 20MW single rotor under normal operation and without any concerted control strategy aimed at balancing yaw moments.

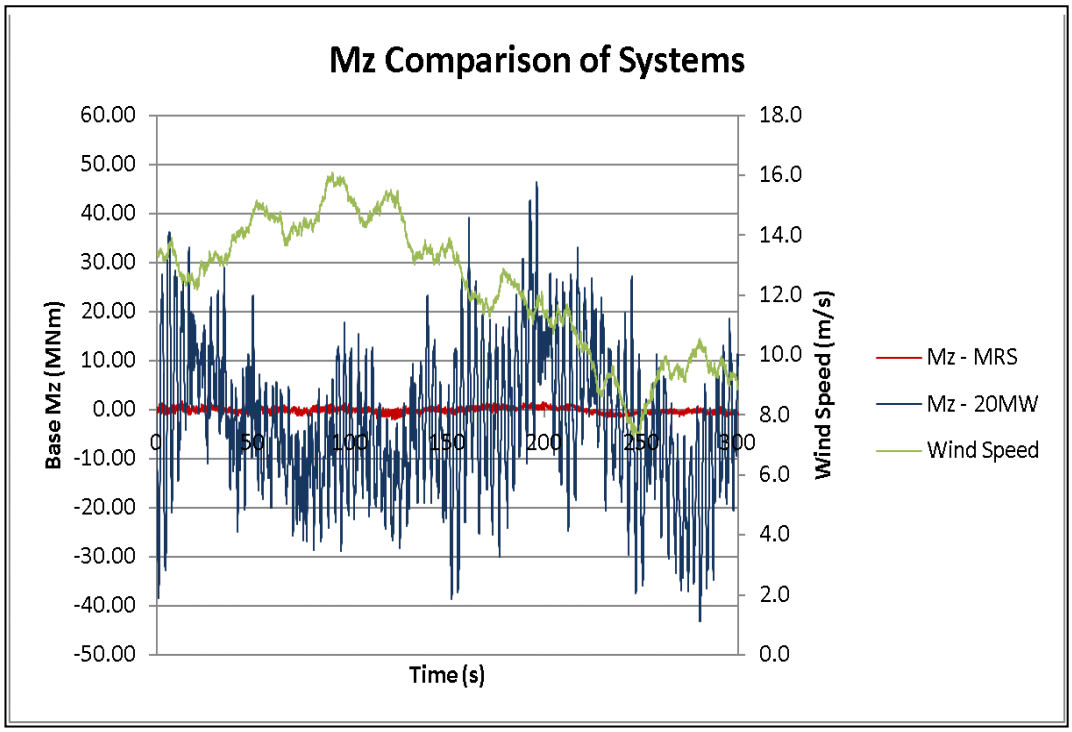

Figure 5.13: DLC1.3a3: Yaw Moment Comparison (M_z), 20MW SR + MRS

5.4.3 DLC-1.4 (ECD) - Ultimate loads during power production

Results:

In this case due to the rapidly gusting wind coinciding with a direction change, the normal shutdown procedure is initiated 6.79 seconds into the event. This shutdown is initiated to avoid potential damage to the rotors and would do on an individual basis. However, in the multi rotor array the effect is to cause a coherent shutdown of every rotor in the array which in turn leads to a large coherent loading in F_x (Figure 5.14). In reality, such increased F_x loading leads to unnecessary ultimate and fatigue loading onto the structure as a whole and should be avoided.

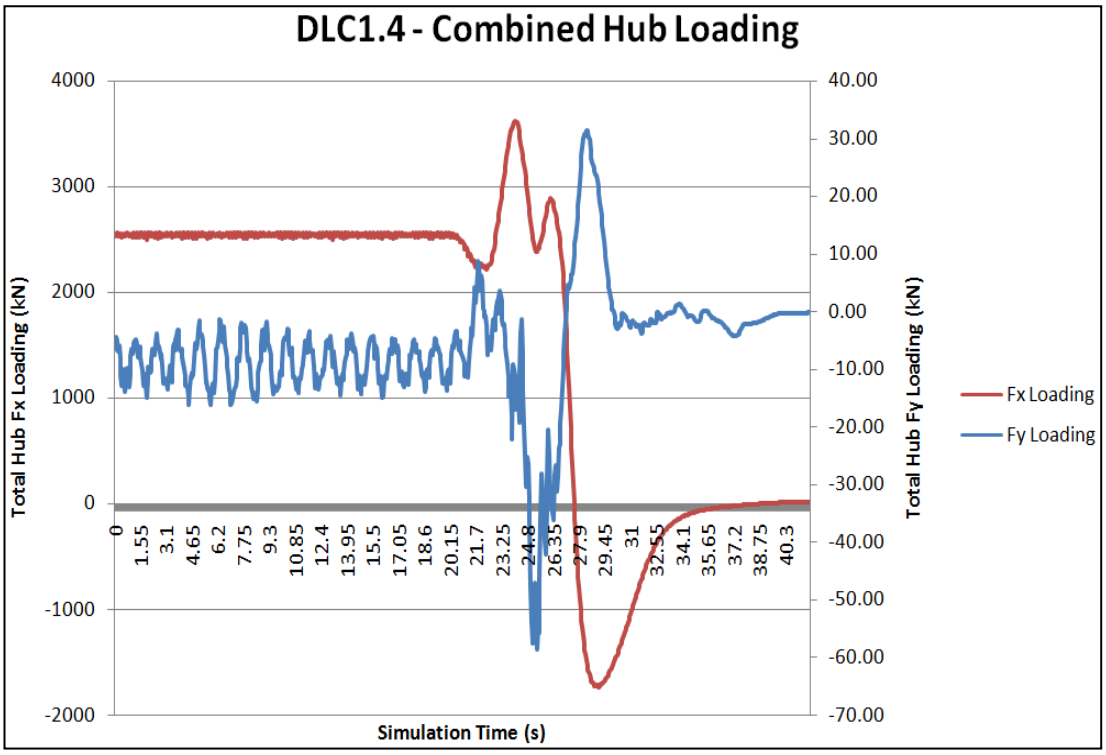

Figure 5.14: DLC1.4: Combined Hub F_x and F_y Loading (+ve)

Hub F_x	Stats. from Total Sum of Rotors	Avg. per Rotor for 45 Rotor Array (sum / 45)	Avg. of Individual Rotor Stats.	Stats. of Rotor 30 (worst-case)	45 x Rotor 30 (coherent worst-case)
Mean (kN)	1,534	34.1	34.1	33.1	1,490
Maximum	3,620	80.4	87.2	97.7	4,397
Std. Dev. (kN)	1,480	32.9	33.5	32.9	1,481

Table 5.5: Statistics of Hub F_x DLC1.4a1 (+ve)

It was initially thought that due to the fact that all rotors are restrained to rotate in a uniform direction that there would be some potentially significant loading differences depending upon whether the wind was changing direction in the positive or negative direction. The same simulation was run and the results show that the loading is not significantly impacted in either hub F_x or F_y, see Table 5.5 for the positive rotation and Table 5.6 for the results of the negative rotation simulation.

Hub F_x	Stats. from Total Sum of Rotors	Avg. per Rotor for 45 Rotor Array (sum / 45)	Avg. of Individual Rotor Stats.	Stats. of Rotor 30 (worst-case)	45 x Rotor 30 (coherent worst-case)
Mean (kN)	1,535	34.11	34.12	33.12	1,490
Maximum	3,611	80.24	87.51	97.63	4,393
Std. Dev. (kN)	1,483	32.96	33.58	32.95	1,482

Table 5.6: Statistics of Hub F_x DLC1.4b1 (-ve)

5.4.4 DLC-2.3 (EOG) - Ultimate Loads during Production with Electrical Fault

Results:

Simultaneous shutdown of all the rotors in the array presents one of the critical ultimate load cases to design against for the MRS system. Such a shutdown would likely be the result of a global event such as grid loss which would trip every rotors safety system and trigger emergency stop procedures. Given that a single rotor F_x is maximum at rated, it follows that the likely worst-case scenario for a emergency stop would be when the array is experiencing an average wind speed of 11m/s (at the effective hub height).

The IEC standard dictates that a check against ultimate load under DLC2.3 conditions be carried out at various gust phases. Figure 5.15 depicts the Hub F_x loading over the event period with the emergency stop occurring at 4 different phases of the gust: 0s, 2.45s, 4s and 5.35s. The ultimate F_x loading is clearly seen to occur when the stop occurs 5.35s into the gust. This gust phasing approximately coincides with the peak of the wind gust.

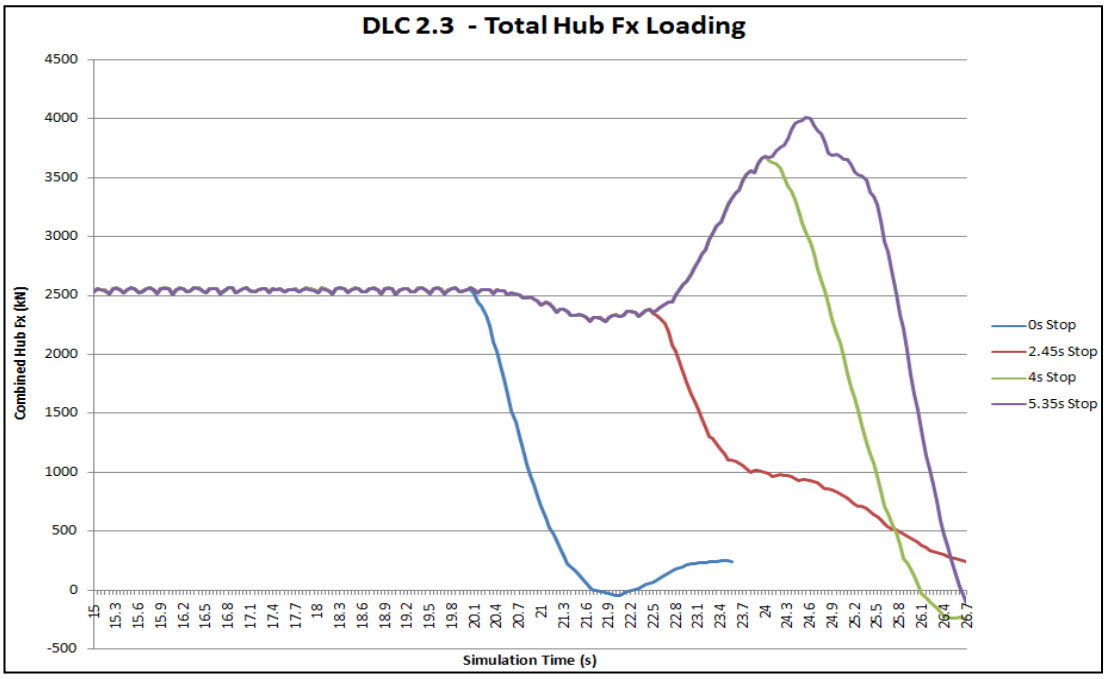

Figure 5.15: DLC2.3: Effect of Gust Phasing on Total Hub F_x

The standard dictates that simulations be carried out at 2m/s above and below rated speed to check that rated speed does indeed equal the worst-case loading. It also acts as a check against the sensitivity of the rotors to small variations in wind speed.

Figure 5.16 contains the results of three different bladed simulations examining the combined hub F_x of the whole MRS array during an emergency shutdown during an extreme operating gust (DLC2.3). The shutdown is chosen to occur 4 seconds into the 10.5 period gust. The runs are labelled a3, c3 and d3 to represent the average hub wind speed of 11m/s, 13m/s and 9m/s respectively. Clearly the shutdown procedure with the average wind speed of 11m/s represents the ultimate loading on the structure.

It is worth repeating that not every rotor in the array will be experiencing a local wind speed equivalent to rated (assuming non-zero shear) and therefore its individual hub F_x may not be at a maximum even when the whole array is at its maximum. It could be suggested that an average of 11m/s over the array would see the most turbines closest to their peak hub F_x when compared to any other average and this lends credence to the practice of defining a single effective hub wind speed.

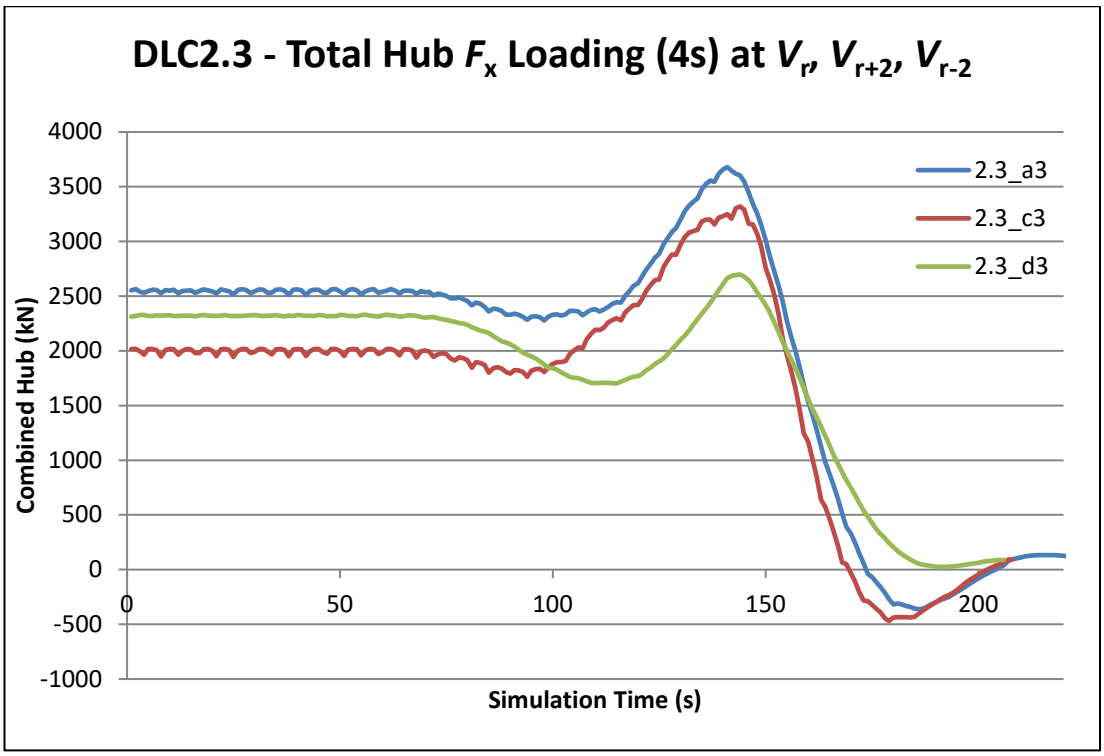

Figure 5.16: DLC2.3: Comparison of Combined Fx during E-Stop around Rated

During the shutdown procedure the main variable controlling the rate at which the turbines shutdown before the application of any mechanical brake is the pitching of the blades. It follows that the faster the emergency pitch rate, the faster individual rotors will come to a halt. During an emergency stop procedure, the control system attempts to pitch all the rotor blades using the maximum available/defined pitch rate. This pitch rate is usually determined during the design phase and is only limited by mechanical considerations.

There was reason to suggest that having a slow pitch rate might adversely affect the multi rotor system – particularly if it caused multiple individual peak F_x's to coincide. The DLC2.3 simulations were run three times at rated wind speed with the emergency stop procedure utilising pitch rates of 9, 12 and 15 deg/s. Figure 5.17 compares the effect on the loading caused by the various pitch rates and it suggests that the problematic assumption is not the case – despite the fact that some individual rotors do experience local differences in loading of 1%.

Pitch rate therefore only determines the rate at which the rotors come to a standstill and can be set independent of overall structural considerations - though considerations of local blade forces may still be an issue.

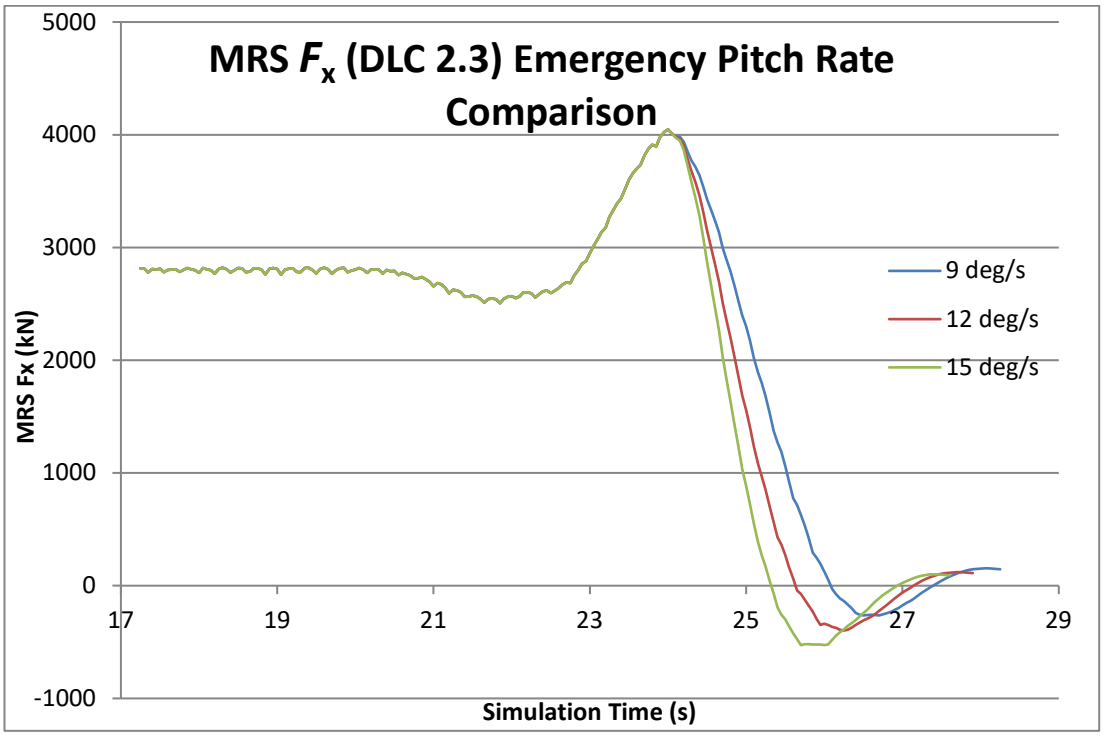

Figure 5.17: DLC2.3: Pitch Rate Comparison during E-stop

Due to initial software limitations in Bladed, rotor azimuths were limited to starting at zero degrees. This meant that each of the 45 rotors began at this same starting angle and as the simulation progressed would work themselves into six groups of azimuthal position due to the non-turbulent nature of the wind in the transient load cases. Given that rotor thrust is dependent on azimuthal position, it was proposed that this shoe-horning of rotors into only 6 groups could potentially cause unrealistic low or high loading.

This limitation was in place during the bulk of the loading simulations due to no other alternative being in place. However, Bladed was later updated by the developers to include the option of setting rotor azimuths to random positions from the offset. This in turn would allow N amounts of rotor azimuths to be possible and potentially average out any abnormal loading previously encountered.

The DLC2.3 simulation was run once with each rotor beginning at 0 degrees azimuthal angle and once again using random azimuthal angles for each of the rotors and a plot of F_x taken (Figure 5.18). While there is potentially 45 different azimuths in play whereas before there were 6, the effect of this is somewhat dampened by the fact that there is effectively only 120 degrees to play with-in a 3-rotor system before symmetry takes hold (in a coherent wind).

The only noticeable action random starting azimuths serves are to smooth out the periodic cyclic variations which are more noticeable in a system utilising only a few groups of azimuthal starting positions. One might expect this given that randomness leads to more averaging than coherence as rule.

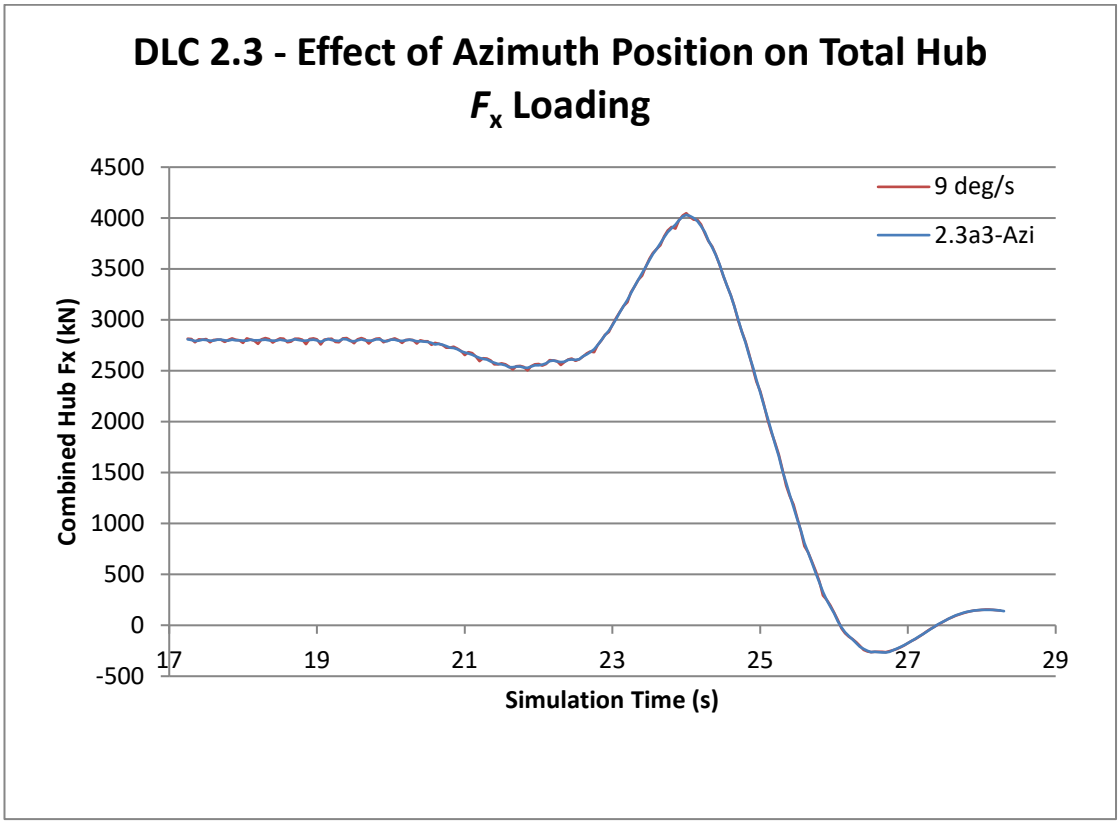

Figure 5.18: DLC2.3: Effect of Random Starting Azimuth Angles

Lastly, this final simulation confirmed that it is safe to assume that all previously run simulations remain valid despite having been subject to restrictions posed by the rotor azimuths.

For comparative purposes with the other run simulations, the statistical values for DLC2.3a3 (worst-case) are presented in Table 5.7.

Hub F_x	**Stats. from Total Sum of Rotors**	**Avg. per Rotor for 45 Rotor Array (sum / 45)**	**Avg. of Individual Rotor Stats.**	**Stats. of Rotor 8 (worst-case)**	**45 x Rotor 16 (coherent worst-case)**
Mean (kN)	2,571	57.13	51.1	60.8	2,736
Maximum	4,010	89.11	96.6	116.1	5,224
Std. Dev. (kN)	462	10.27	21.9	24.0	1,080

Table 5.7: Statistics of Hub Fx DLC2.3a3

5.4.5 DLC-4.1 (NWP) - Fatigue Loads during Shutdown

Self-explanatory fatigue loads during shutdown for three different types of shutdown scenario: cut-in, cut-out and rated. The results are not presented here for the same reason as the fatigue loads in 4.5.1.

5.4.6 DLC-4.2 (EOG) - Ultimate Loads during Shutdown

Results:

The simulations for DLC4.2 are carried out in the same way as DLC2.3 and as such 4-simulations are carried out using stops during 4 different phases of the extreme operating gust (EOG). Figure 5.19 depicts the loading data for the case of the normal stop, both the 4s and 5.35s phases can be attributed to the ultimate load scenarios within this load case. In the same way as in DLC2.3, the normal stop is modelled in bladed as a synchronous shutdown of each of the 444kW rotors and because of the synchronicity of the hub F_x loadings, the shutdown results in maximum hub F_x loading on the array.

The ultimate loading measured as the combined hub F_x is apparent with shutdown phasing 4 seconds into the EOG. The total loading of 4,195kN is marginally higher than the peak loading observed on the array during the 5.35s phased gust of DLC2.3, which was 4,000kN. The IEC standard divides load cases into abnormal and normal load cases and attributes load modification or safety factors to each load case. In this

case aerodynamic loadings taken from DLC2.3 are to be modified by a factor of 1.1 (abnormal) and loadings taken from DLC4.2 be modified by a factor of 1.35 (normal). Multiplying by these factors makes the DLC4.2 normal stop case significantly larger in comparison to the emergency stop case, see Figure 5.20.

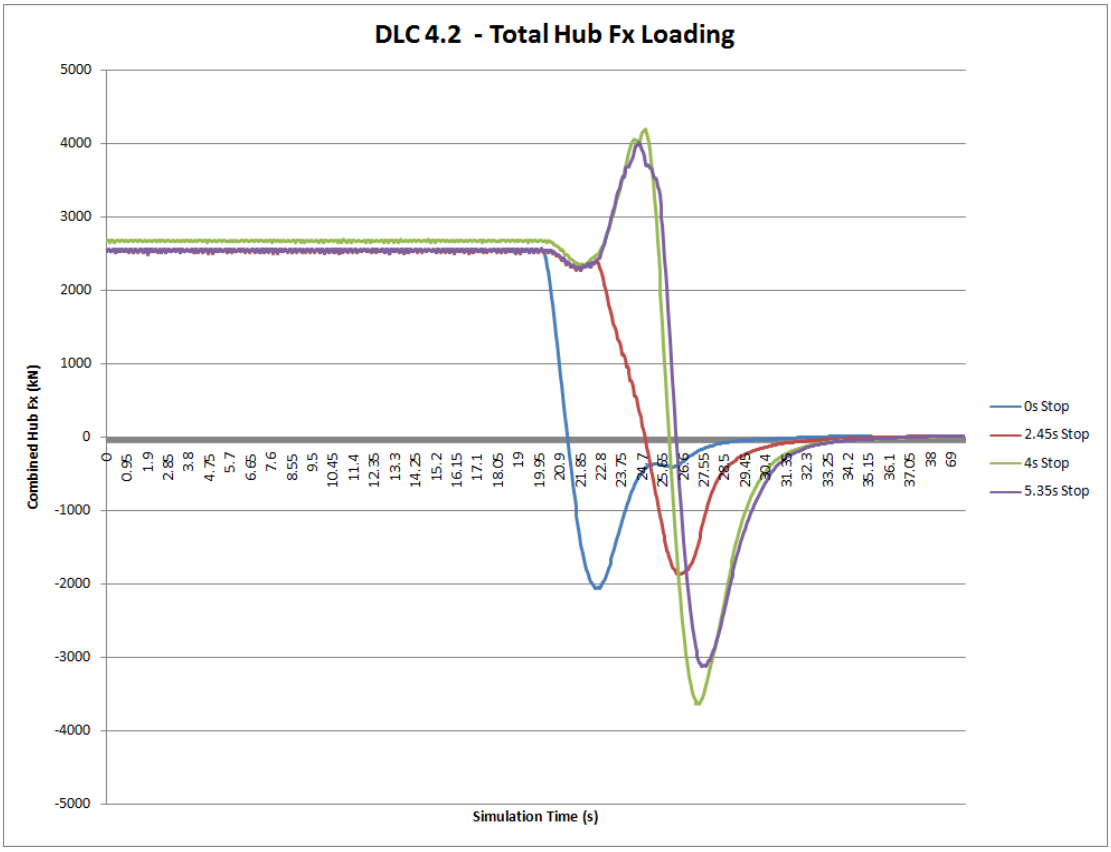

Figure 5.19: DLC4.2: Effect of Gust Phasing on Total Hub F_x

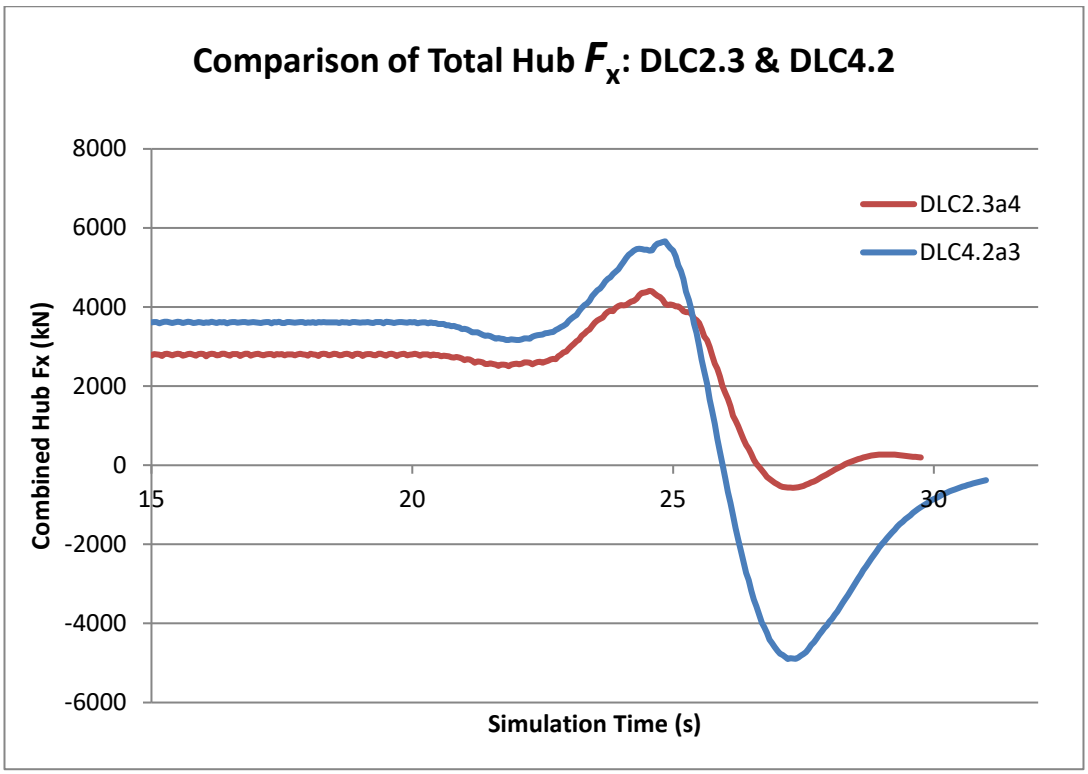

Figure 5.20: Shutdown Cases DLC2.3a3 & DLC4.2a3 (SF Applied)

To complete the load cases, a further set of simulations is run at cut-out wind speed using the 4 different gust phasing's, Figure 5.21. It is once again assumed that single rotors do not independently trip their cut-out conditions prior to the event. Perhaps unsurprisingly, even the worst-case loading at cut-out is considerably less when compared to the runs around rated for the same reasons touched in DLC2.3.

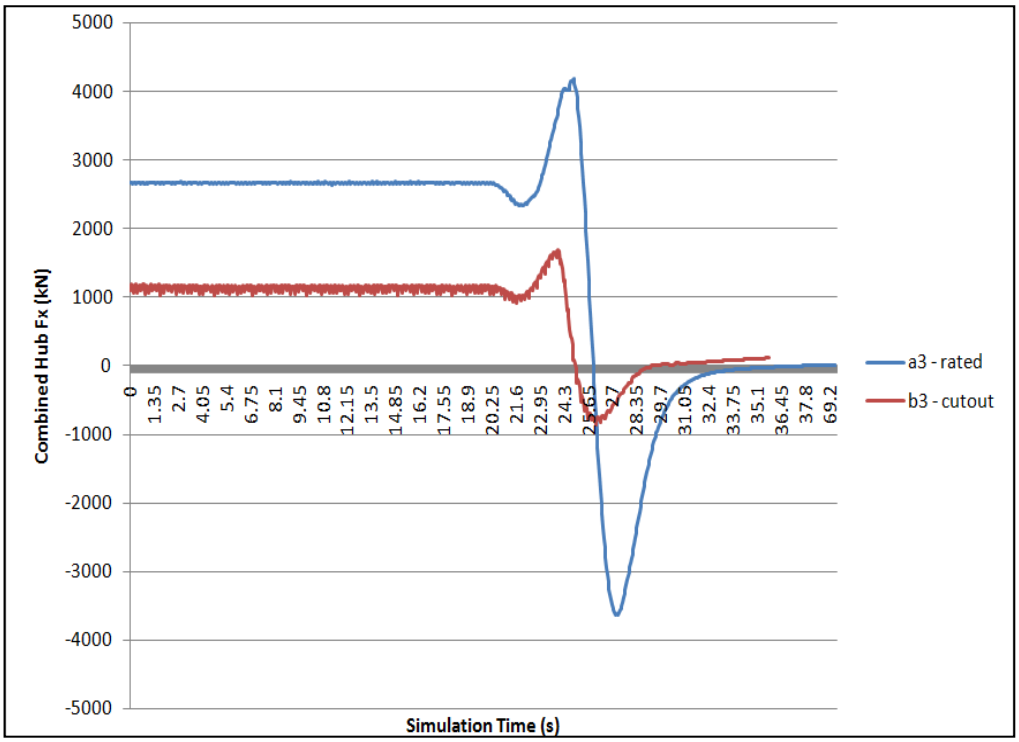

Figure 5.21: Comparison of Hub F_x Loading at Rated and Cut-out Wind Speeds

Discussion:

At this stage it is important to evaluate once again which of the load cases appear to cause the ultimate loading on the array.

Figure 5.22 shows a plot of the worst-case loading for each of the load cases already reviewed: DLC1.3/1.4/2.3 and 4.2. To make a valid comparison, safety factors have been applied in accordance with Table 5.1. At this point, the normal shutdown condition of DLC4.2 appears to be the design limiting case in terms of combined hub F_x by a significant margin.

In fact, all three load cases containing normal or emergency stop procedures and coherent wind out- size the normal power production load case DLC1.3. This raises several key points that need to be addressed in the following sections:

1. Are the effects of coherence and turbulent wind directly opposed in loading terms on the multi rotor array?
2. Can the coherent/synchronous shutdown events be phased in some way to destroy the peak loading present in each of the combined hub F_x time series?

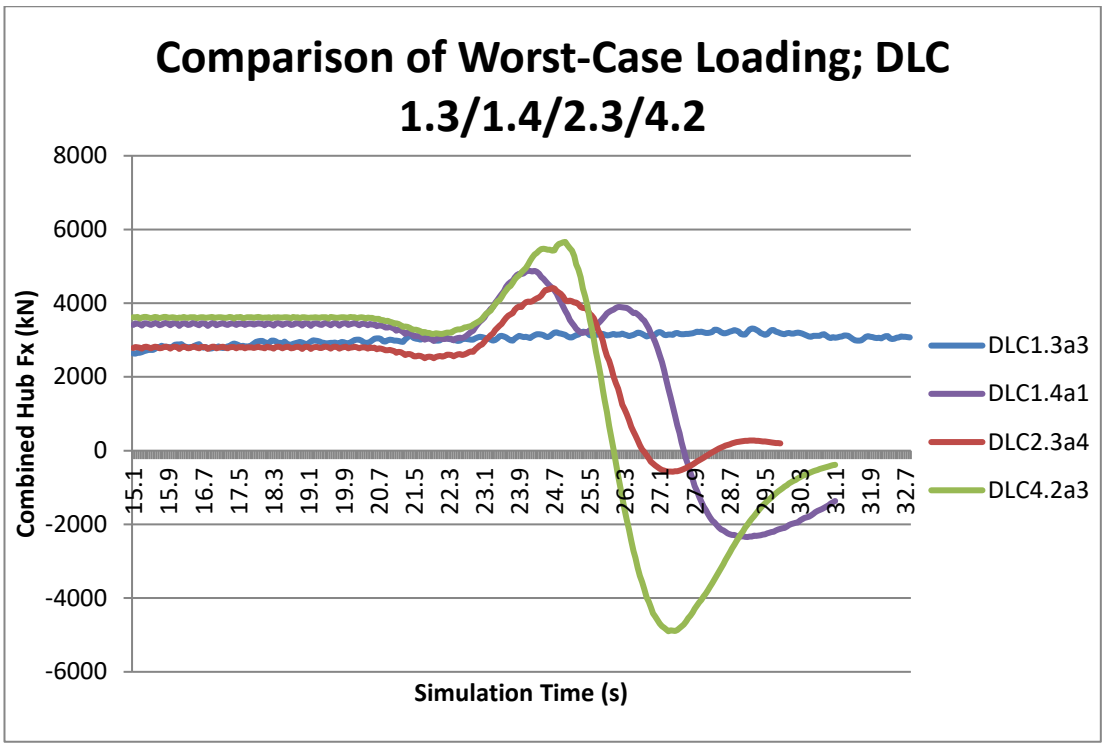

Figure 5.22: Comparison of Total Hub F_x in all Examined Cases (SF Applied)

It is certainly the case that some of these design scenarios are so unfavourable that they should be completely avoided. With some staggering/phasing of the shutdown procedure, which may be possible under certain shutdown conditions, it is feasible that total F_x values may be further reduced.

While load cases such as DLC2.3, which is an emergency stop due to a global event such as grid loss, might be limited in its ability to stagger the shutdown of the rotors. DLC4.2 on the other-hand is a normal shut-down, there is therefore some leeway with regards to the shutdown of the array in the absence of any time critical circumstances, though this is not modelled in Figure 5.19, Figure 5.20 or Figure 5.22. Normal stop conditions therefore have a key advantage when it comes to loading on the array compared to other types of emergency stop.

For completeness, Table 5.8 presents the full statistics for the 4s phased shut down for a direct comparison with the other load cases.

Hub F_x	Stats. from Total Sum of Rotors	Avg. per Rotor for 45 Rotor Array (sum / 45)	Avg. of Individual Rotor Stats.	Stats. of Rotor 16 (worst-case)	45 x Rotor 16 (coherent worst-case)
Mean (kN)	1,536	34.13	34.15	34.35	1,545
Maximum	4,195	93.2	97.2	119.6	5,382
Std. Dev. (kN)	1,780	39.6	40.3	43.6	1,962

Table 5.8: Statistics of Hub F_x DLC4.2

5.4.7 DLC-6.1 (EWM) - Idling Ultimate Loads due to 50 Year Gust

Results:

For a Class 1A site the 50-year gust corresponds to a 70m/s local wind speed gusting for 30s with a change of direction. While the standard dictates that this gust be coherent in nature there has been recent discussion amongst academics and industry that the nature of coherent gusts may not be applicable at the scale that 20MW machines find themselves in (several hundred metres vertically and horizontally). To check against this coherent nature and provide further validation outside the standard, an additional set of simulations were run with a turbulent wind file (of average wind speed 70m/s) as a base. The four sets of data are presented in Figure 5.23, with the turbulent and coherent cases clearly characterised by their respective plots.

The worst-case load case (DLC6.1b2) with turbulent wind represents the worst-case loading in this case and therefore it is from this run that the statistics presented in Figure 5.24 and Table 5.9 are taken from.

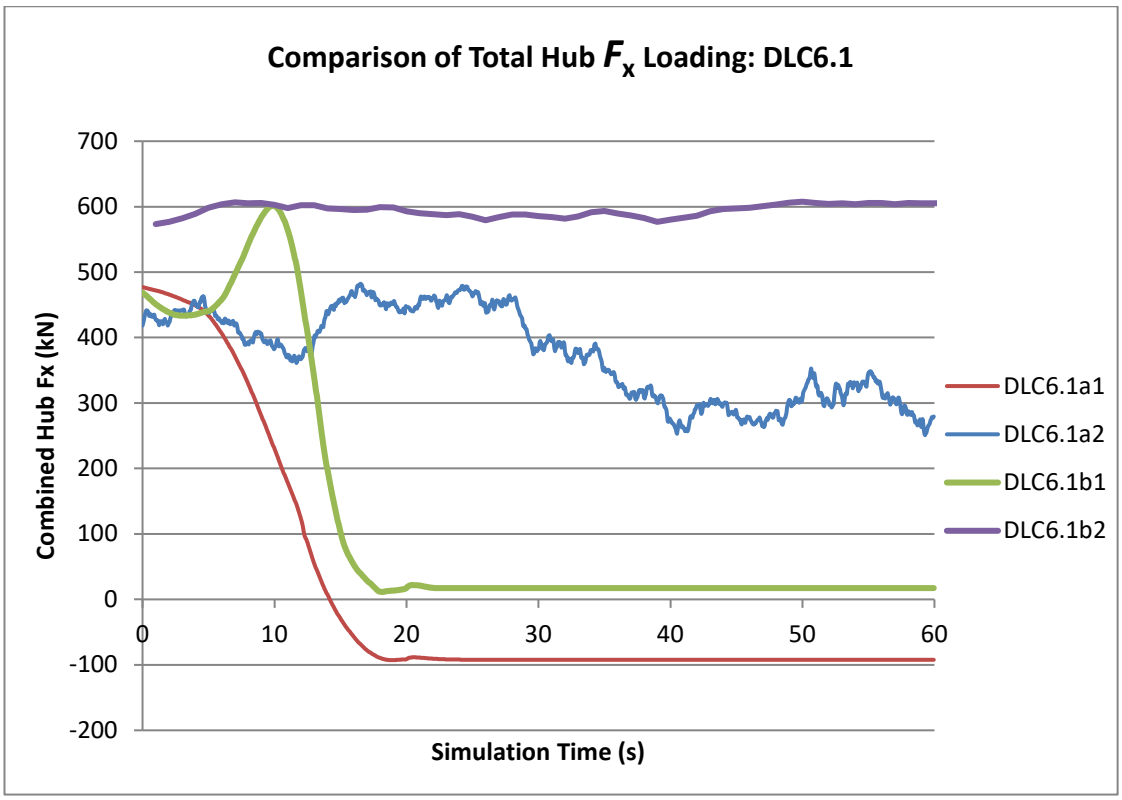

Figure 5.23: DLC6.1a1: Turb. & Coherent Wind in the 50-Year Gust (SF Applied)

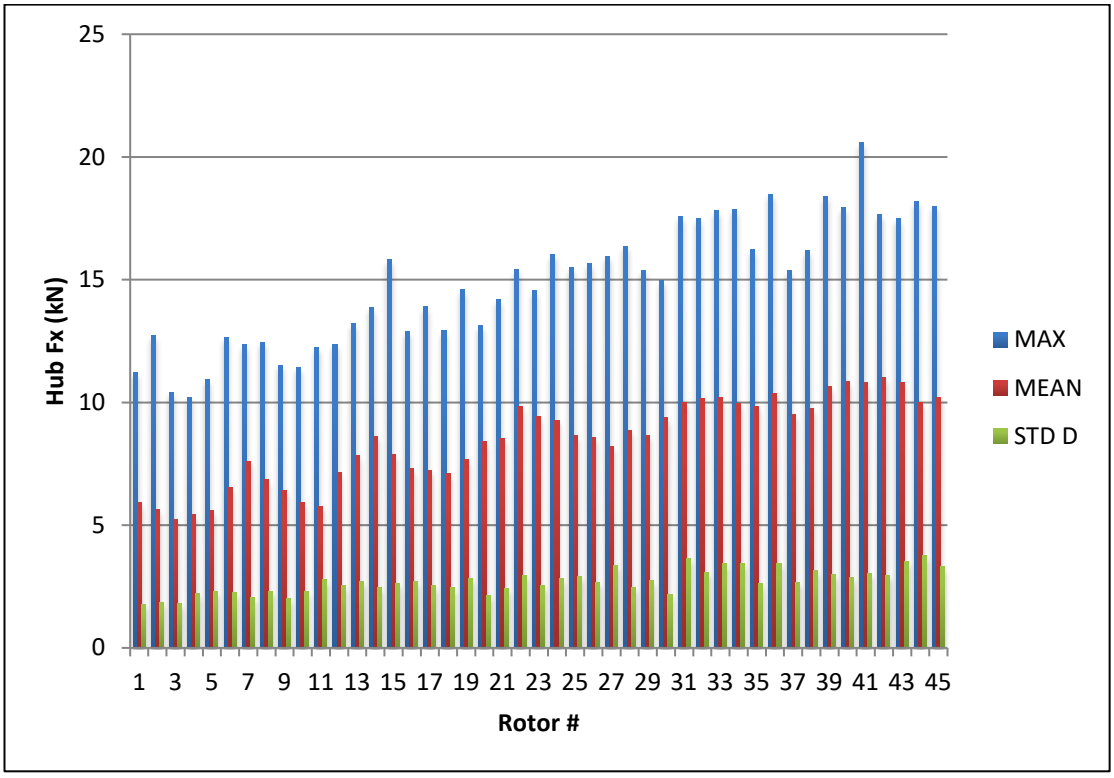

Figure 5.24: DLC6.1b1: Individual Hub F_x Statistics

Hub Fx	Stats. from Total Sum of Rotors	Avg. per Rotor for 45 Rotor Array (sum / 45)	Avg. of Individual Rotor Stats.	Stats. of Rotor 41 (worst-case)	45 x Rotor 41 (coherent worst-case)
Mean (kN)	374	8.31	8.44	10.8	486
Maximum	482.22	10.72	14.89	20.58	926.1
Std. Dev.	69.07	1.535	2.7	3.05	137.25

Table 5.9: Statistics of Hub F_x DLC6.1

Discussion:

These results show that the load case DLC6.1 of a 50-year gust with a positive or negative 15 degree yaw misalignment are no-where near designing load cases in structural terms. The ultimate loading in DLC6.1b2 is only 600kN with safety factors applied whereas the likes of DLC1.3 are dealing with loads in excess of 3000kN.

While in DLC1.4 there was no discernible difference in a positive or negative wind direction change (in essence the same as a yaw error) in this case the wind direction does appear to account for a small difference (around 10%) in terms of Hub F_x loading.

5.4.8 DLC-6.2 (EWM) - Idling Ultimate Loads due to 50 Year Gust and Grid Loss (Effectively Yaw System Non-Operational)

Results:

Figure 5.25 presents the time series of total hub F_x for each of the 5 simulations run. In terms of hub F_x loading, the ultimate loading appears to be at both 0 degrees and 180 degrees as one would intuitively expect. While the first four runs represent a change in wind direction, the 180 degree run represent as full reversal of the wind direction, followed by a return to the original direction. In this respect it is once the wind changes direction fully that the ultimate - F_x loading is experienced and this exceeds that experienced at 0 degrees.

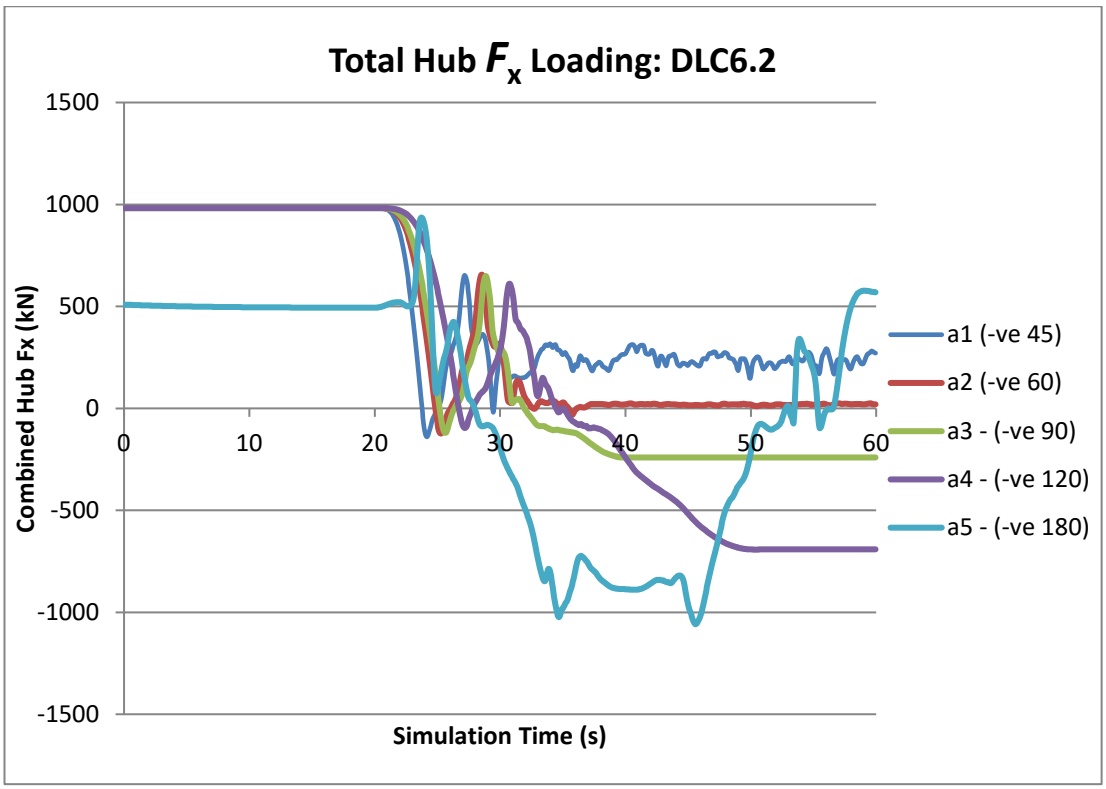

Figure 5.25: DLC6.2: 50 Year Gust and Extreme Yaw Misalignment (SF Applied)

Again the increase in loading even at highly unfavourable yaw angles is not a driving factor in structural design for the purposes of ultimate loads – being significantly less than DLC1.3, with 1,000kN and 3,000kN respectively.

Discussion:

The only notable discussion point in DLC6.2 is as a consequence of the extreme - F_x loading when the wind has been fully reversed. This is not unexpected given that the rear of the proposed multi rotor comprises a multitude of interconnecting members and bracing struts. It is therefore likely that the overall structural blockage is increased when the wind is blowing from the downwind direction which results in the increased loading in comparison to the normal loading from the upwind direction.

It might be proposed that aerodynamic fairings could be used to mitigate the loads on the structure in these extreme wind cases. This was a serious consideration at the start of the project when it was believed that blockage affects and structure thrust

would be the over-riding design case for the multi rotor system. Both DLC6.1 and 6.2 show this to not be the case.

5.4.9 DLC-6.3 (EWM) - Idling Ultimate Loads with 1 Year Gust & Extreme Yaw Misalignment

Results:

The total hub F_x loading in this final load case is presented in Figure 5.26 and shows that a yaw misalignment does indeed lead to less overall hub F_x loading than any of the other considered load cases.

This lower loading is not unexpected and therefore no further discussion will be proposed at this point.

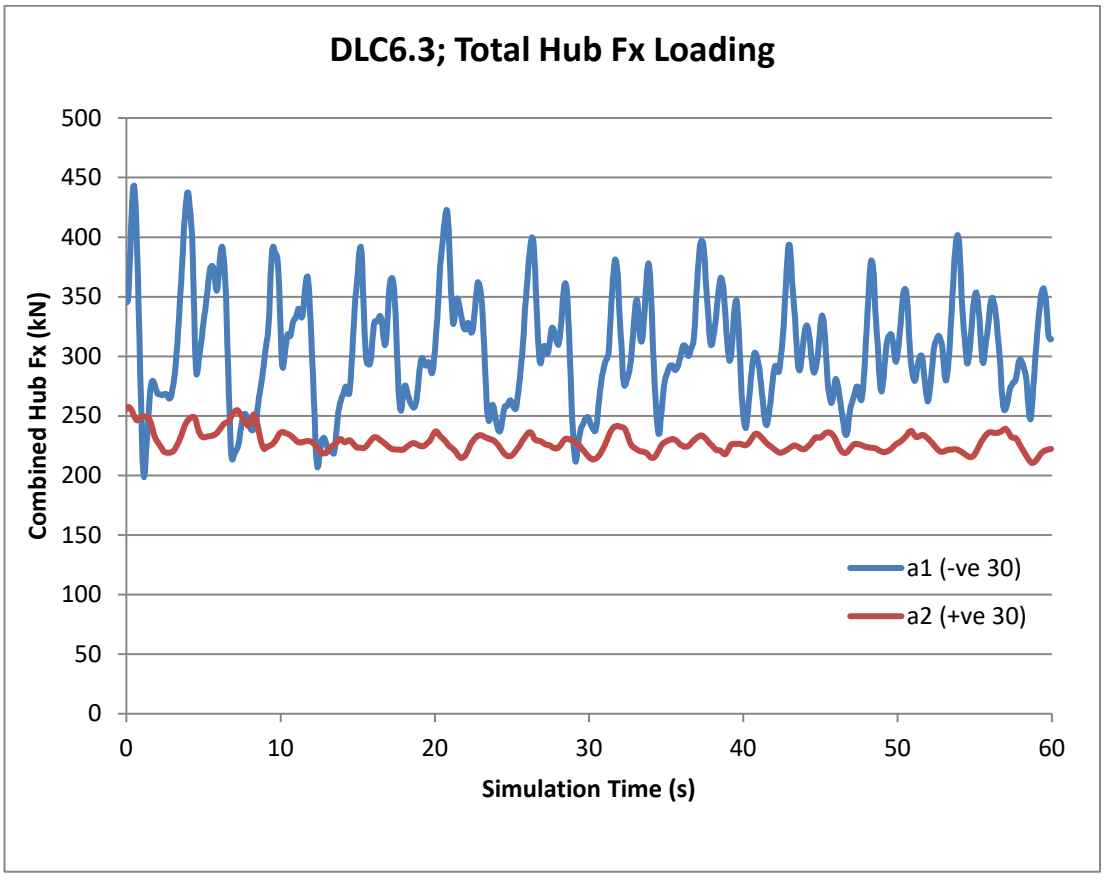

Figure 5.26: DLC6.3: 1 Year Gust and Yaw Misalignment of +-30 (SF Applied)

5.5 LOAD CASE OVERVIEW

In total nine DLC load cases have been fully investigated, with a total of 37 individual simulations encompassing the full spectrum of possible environmental conditions the multi rotor system might be subjected to. In whole these simulations provide the ultimate loads for use in later finite element modelling and structural calculations with a few caveats.

As previously stated, the primary load of interest is F_x loading which drives structural design of both the single rotor and multi rotor. Table 5.10 presents a summary of the combined hub F_x loadings on the multi rotor array for the seven non-fatigue ultimate load simulations. In each case only the ultimate load and corresponding simulation results are recorded, with the other runs being disregarded due to lower overall forces.

Scenario	Maximum Total Hub F_x under Coherent or Constant Wind
DLC 1.3a3	Constant Wind
	4451kN
DLC 1.4b1	Fully Coherent
	4875.5kN
DLC 2.3a4	Fully Coherent
	4411.3kN
DLC 4.2a3	Fully Coherent
	5663.7kN
DLC 6.1	Fully Coherent
	601.2kN
DLC 6.2	Constant Wind
	936kN
DLC 6.3	Constant Wind
	443.4kN

Table 5.10: DLC Comparison Summary: 1st column - load case name, 2nd column – results

The results are presented at this stage as a single column representing the maximum load for each load case in accordance with the standard and also in graphical form (Figure 5.27). They show a clear correspondence between maximum hub F_x loading and shutdown events such as DLC1.4, DLC2.3 and DLC4.2. In fact, comparing the

power production case of DLC1.3 which represents maximum loading under extreme turbulence the force ratio is 4.4:5.6 when compared to the synchronous shutdown event caused by an extreme operating gust and grid loss in DLC4.2. The initial suggestion is therefore that these synchronous shutdowns represent the ultimate loading towards which the structure must be designed. It is very important to note that these scenarios were originally defined in the IEC 61400-1 (edition 3) standard before wind turbines designs routinely exceeded 5MW scale and therefore there is a strong case that these wind conditions may not be readily applicable at 20MW scale. These aspects of the standard are currently being debated amongst industry and academics and there may be arguments for a change in the coming months and years.

To fully understand why these results may no longer be fully applicable towards the multi rotor, or even perhaps the single 20MW rotor requires some additional investigation and inevitable re-simulation as presented in the following discussion.

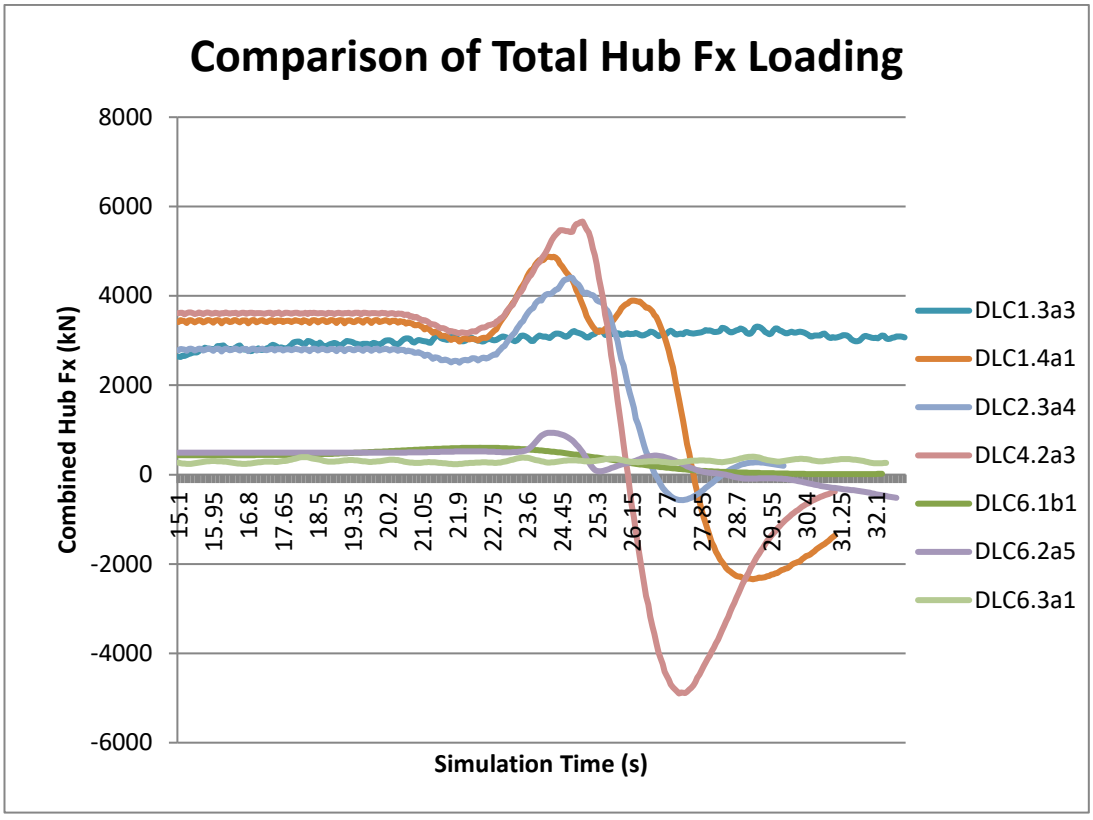

Figure 5.27: Comparison of Total Hub F_x Loading (All Cases)

5.6 STRUCTURAL LOADING

5.6.1 Load Averaging

The first and arguably the most interesting and structurally useful discussion point is that of the load averaging effect provided naturally by the multi rotor system. This load averaging effect results in much lower ultimate loadings than would be expected from the examination of loadings on a single rotor in an array. In other words, the single worst, or even a combination of the worst individual rotor loads does not necessarily equate to the overall worst structural load. To examine this averaging aspect requires an investigation into the 444kW single rotors characteristics.

Figure 5.28 depicts the relationship of thrust to wind speed for the 444kW machine under power production. Configured as a pitch regulated machine, peak loading occurs at rated wind speed. The single 20MW machine by comparison retains the same relationship between thrust and wind speed – being simply an up-scaled version of the same wind turbine.

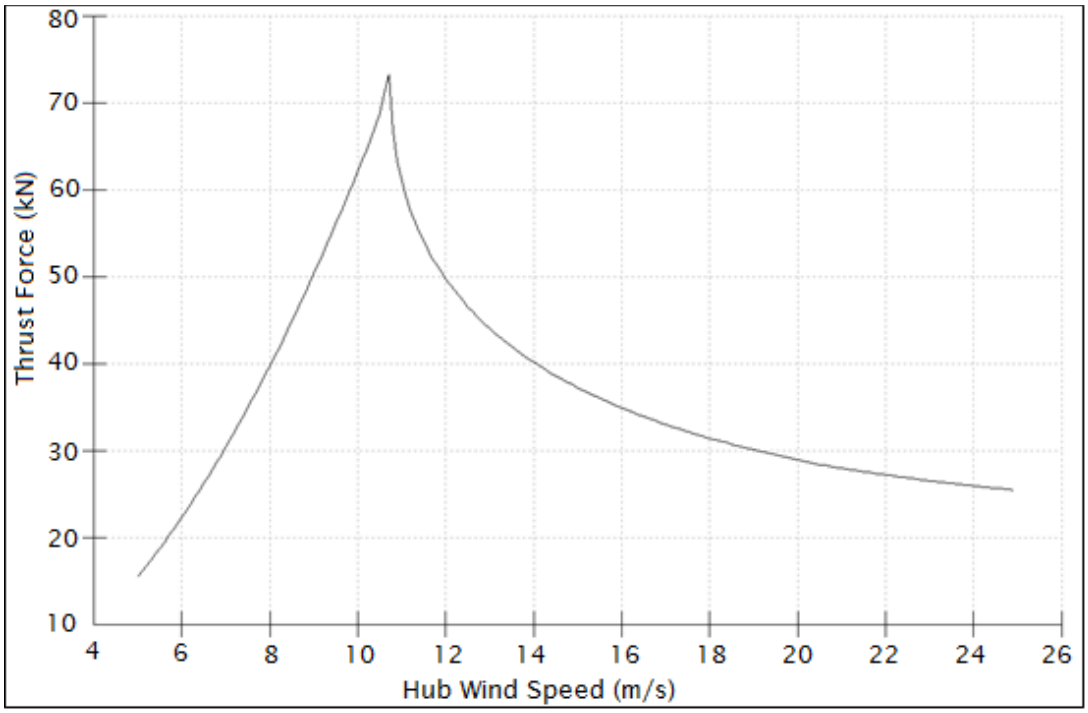

Figure 5.28: Hub F_x Characteristic Curve

For the 444kW machine the maximum hub F_x loading 73.28kN. The theoretical maximum thrust in the multi rotor system would therefore occur if or when every turbine in the array is at rated wind speed. If these conditions were met then the thrust would be the equivalent to a 3297.87kN (45x73.28) force at effective hub height (115m). This maximum is somewhat misleading given that real wind conditions should never be so coherent as to cause this maximum to occur. Any amount of spatial variation in wind strength which causes individual turbines local wind velocity to deviate away from rated wind speed will alter the total thrust and reduce it below this theoretical maximum.

Consider a highly coherent case of an extreme gust coupled with a normal stop, i.e. DLC4.2a3 with 0% turbulence but with a large amount of shear (0.14 exponent). The MRS system is not operating at maximum thrust due to shear across the array even when wind speed at the effective hub height is defined as being at close to rated (11m/s). Table 5.11 contains the total hub F_x loading data for each of the rows in the array, where the shear can clearly be seen in the corresponding average wind speeds.

If each of these rows is weighted according to the number of turbines present then the total effective thrust (hub F_x) on the structure/tower is only 77.24% of the theoretical maximum.

To test that this is not an anomaly, a second run is carried out using a different seed and a slightly different wind speed (10.7m/s). When wind speed at hub height reaches 10.7m/s the maximum power production thrust is found to be 2,683kN or 81.38% of the theoretical maximum.

Row Number	Wind Speed (m/s)	Thrust (% of max)
1	9.59	76.59
2	10.45	92.83
3	11.02	83.29
4	11.45	74.51
5	11.80	70.06
6	12.10	66.98
Weighted		77.24

Table 5.11: Maximum Steady-State Thrust in Coherent Load Case DLC4.2a3

These results suggest that the multi rotor array will never actually achieve its theoretical maximum thrust under normal wind conditions. While this experiment was carried out using a value of shear more consistent with rolling hills rather than a calm sea, they were carried out with 0% turbulence. It is not considered likely that zero turbulence or shear could exist over a 350x300m^2 area as well as an average wind speed around rated.

In normal turbulence conditions, the total thrust across the array becomes less coherent and therefore forces will drop on average. The worst-case power-production load case is considered to be DLC1.3a3, that is, power production around rated with I1, I2, and I3 turbulence intensities set at 39.9%, 24.4% and 17.47% respectively. The combined maximum thrust is determined to be 2421.59kN which represents an equivalent thrust level of 73.42% compared to that of the multi rotor theoretical maximum. However, the average thrust level is considerably lower at 1995.2kN or 60.5% of this same maximum throughout even the worst-case power production scenario. This suggests that up to 17% of maximum thrust loading can be avoided when operating under normal wind turbulence intensity.

Given that the wind speed over the whole array is not fully coherent at any point in time, the combination of rotor thrusts across the array do not necessarily follow the Fx vs. wind speed curve of a typical rotor. Taking the average thrust per rotor at each wind speed and plotting this against the average wind speed at the array centre, i.e. hub height (Figure 5.29) shows that the MRS equivalent curve maintains the same shape as that of Figure 5.28 but with much less definition. Notice that the peak normally seen around 10.8m/s has been completely destroyed by the averaging effect of the rotors. Indeed the total thrust force has been reduced below 55kN for individual rotors and down shifted in wind speed slightly.

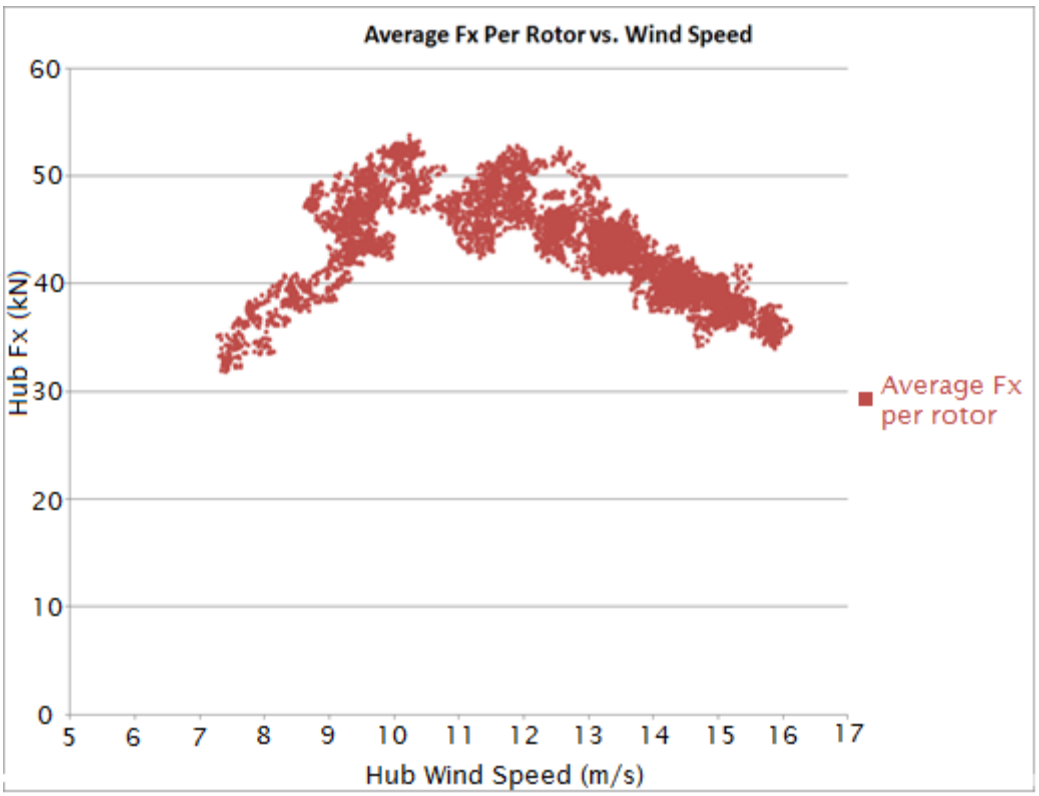

Figure 5.29: Hub F_x vs. Wind Speed for Whole Multi rotor Array

These findings are partly skewed by the limitation that the curved can only be defined with respect to the combined F_x's and wind speed at a single point in space. Even so it does highlight why hub F_x load reduction is possible even when the whole array is operating at rated wind speed. For convenience, the multi rotor hub wind speed is defined as being the average wind speed seen across all the rotors in the array referred to a single point at the centre of the structure (in this example, 115m height). In contrast to the single 444kW machine example of Figure 5.28, Figure 5.29 shows that is not possible to identify a single equivalent or expected F_x hub loading at any particular wind speed, but rather a range of loadings in which the effective total hub F_x will fall. As a result, at normal operation at rated wind speed, the multi rotor system will never experience a case whereby every single individual 444kW rotor is experiencing its theoretical maximum hub F_x loading at the same instant in time.

Taking this into account, the average maximum F_x per 444kW rotor across the multi rotor array is identified as 53.81kN – an average maximum taken from several DLC1.3

runs around rated. This calculated value is within 0.9kN of the singular worst-case hub F_x taken from the worst-case simulation (DLC1.3a3) which was found to be 52.89kN. The closeness of these two values suggests that the method of defining hub height as the geographical centre of the array and the use of effective rotor averaging as a means of identifying likely ultimate loads is reasonable if not erring towards being conservative.

It is therefore highlighted that although it would appear that the theoretical worst-case loading for the multi rotor array is 45x73.28 (3297.6kN), the realisable value is actually much lower (2421.6kN). This is one of the primary benefits of spatially distributing rotors over spans of space that cannot by nature be encapsulated by a single coherent wind speed.

5.6.2 Turbulence Loading

For a single multi-MW rotor the critical design loads nearly always arise as the result of some transient or variation in aerodynamic force across the entire length of a blade. These conditions undoubtedly occur in highly turbulent wind fields, which is why wind turbulence classification plays an important role in turbine design. One of the most unusual aspects of the multi rotor system is that the critical design load is a result of a lack of turbulence as opposed to a high turbulence and that this contrasts sharply with a single rotor machine. This becomes more intuitive after understanding that any move towards coherent wind diminishes the desired averaging effect of loads that the multi rotor system accomplishes.

In Figure 5.30, the total F_x is plotted for various classes of wind turbulence. The total hub F_x loading increases on average in less turbulent classes of wind (Class B and C) at rated wind speed when compared to total hub F_x under turbulence Class A. Apart from a small period where the Class 1A wind with a normal turbulence model peaked, the Class B and C normal turbulence models consistently see overall increased loading when compared to the class A wind extreme and normal turbulence models.

These results further suggest that the multi rotor system reaches its peak load reduction capabilities in extreme wind environments. It also highlights that any form of coherent loading of individual rotors within the array will conspire to ultimately cause extreme design load cases for the whole structure. This latter point is especially critical given that the IEC-61400 standard makes use of several design load cases which base their analysis on extremely coherent wind events. Note that Class B and C represent relatively non-turbulent wind.

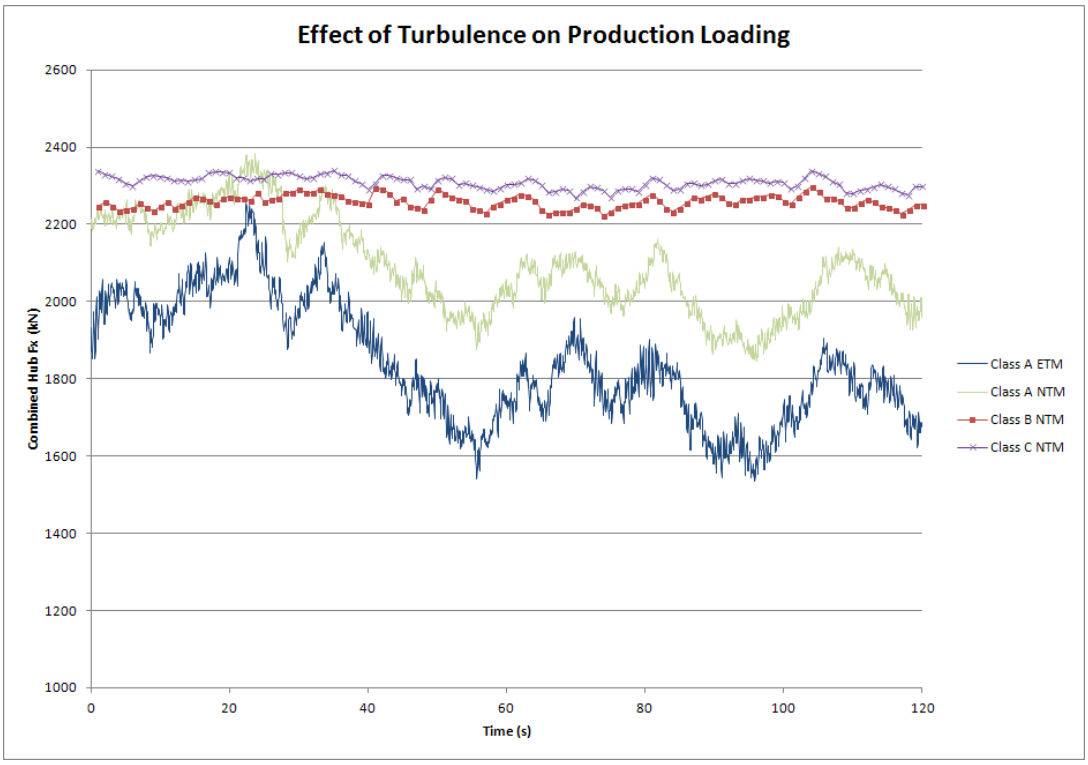

Figure 5.30: Combined Fx Loading on MRS in Various Wind Classes

The multi rotor system therefore finds itself in uncharted territory when considering loads from a design standpoint. Normally designers have to design against extremely turbulent events, some of which would otherwise cause the destruction of a conventional machine. For the multi rotor the opposite effect is felt. It actually has less structural requirement the more the wind coherence is broken down by turbulence. This fact alone gives the multi rotor some interesting advantages when considering potential turbulent sites on land where the wind speed is known to be consistently high but turbulent.

5.6.3 Phased Shutdowns

Consider that with individual turbines it is likely that the general conditions that result in the shutdown of a single turbine do not apply to all 45-rotors on the array at once. Thus it may be that natural wind conditions result in a passive event caused by individual turbines tripping their shutdown conditions individually and therefore providing natural phasing of the total loading on the array. If this natural phasing does not occur, then it is not unreasonable to place limits on the controller to phase the shutdown of rotors, or at the very least to avoid simultaneous shutdown.

Naturally there are dozens of schemes for shutdown of the MRS array. The worst candidate is of course simultaneous shutdown of every rotor which would achieve its peak loadings as shown earlier in Figure 5.20. Regardless of gust speed, simultaneous shutdown results in extreme loading in terms of hub F_x (as all the maximums combine in phase). The optimal choice would therefore be to shutdown the rotors one at a time.

Optimum loading is achieved by spacing the shutdown of each rotor by several seconds to match extreme maximum F_x with the preceding rotors minimum F_x and achieving some cancellation on the combined F_x. The phasing of shutdowns obviously depends on the gust. It is assumed that a gust period of 10.5 seconds is used as defined in the standard. The total shutdown time would therefore become 44x2.35s (103.4s) with a phasing of 2.35s. This has the advantage of reducing the transient F_x to less than that of a single rotors maximum and brings the combined maximum in line with normal production loading as in DLC1.3.

For a relatively quick shutdown, two optional methods are 'pair phasing' and 'quad phasing'. That means shutting down the array 2 or 4 rotors at a time, utilising the symmetry of the arrangement to minimise yawing or overturning moments about the structures axis. A comparison of both these methods is made in Figure 5.31. The objective is to minimize the total maximum hub F_x while minimising the thrust reversal normally seen when shutting down, which can contribute significantly to the fatigue of a wind turbine.

Quad phasing the shutdown results in a peak Hub F_x loading of 2632kN and takes approximately 30 seconds to complete. Pair phasing shutdown yields a lower Hub F_x of 2590kN but takes twice as long. The benefits of shutting down over any longer period than the 60-seconds provided by pair phasing quickly diminishes as the theoretical minimum that could be obtained would be the steady-state average 2545.65kN plus the average standard deviation of a single rotor during shutdown (35.97kN), that is 2581.62kN.

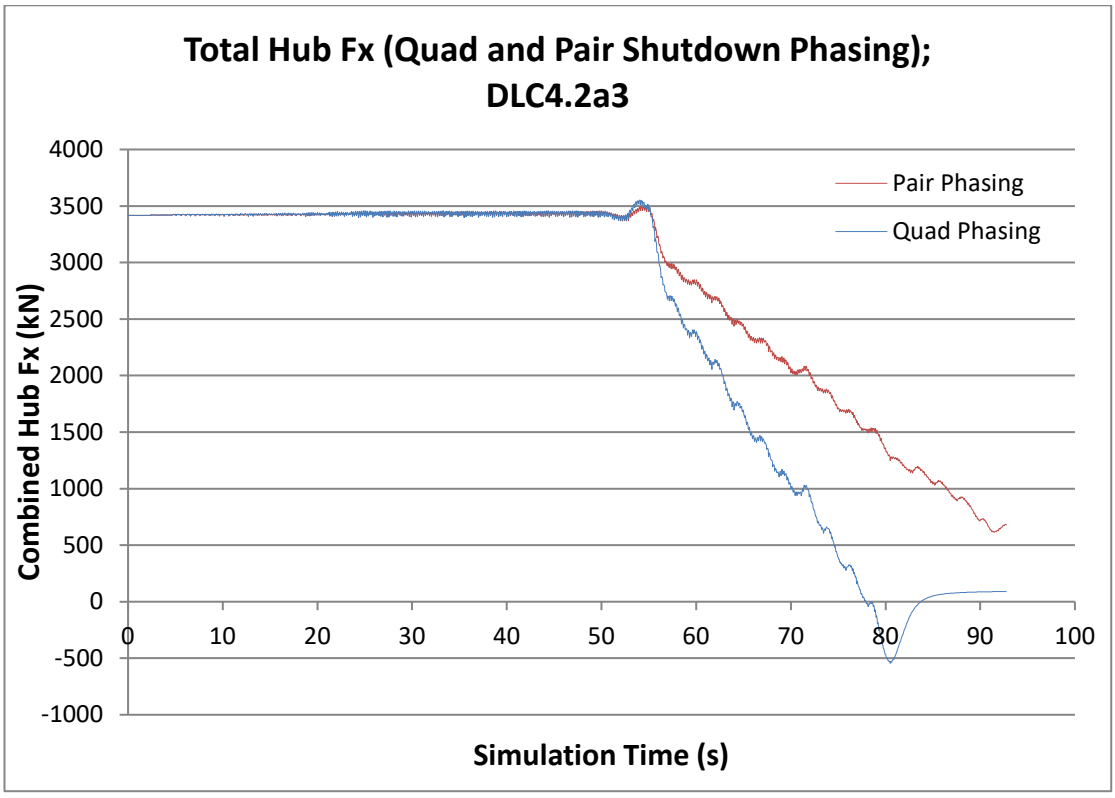

Figure 5.31: DLC4.2: Pair and Quad Phased Normal Shutdown (SF Applied)

In quad phasing of shutdown, the thrust reversal is significantly reduced in comparison to simultaneous shutdown and even in comparison to 5MW machines. In the pair phasing, the thrust reversal is negligible.

Given that the IEC standard creates a scenario whereby the turbine happens to shut down during the unfavourable part of an extreme gust, it can be stated with confidence that any real MRS normal shut-down procedure would never need to have more than a small number of its total rotors shutting down during an unfavourable part of a gust.

Of course emergency stop procedures are likely to require a more rapid response to avoid over speed. As a result of the reduced ability to phase shutdown through control methods, DLC2.3a3 may become the design driving load case for Hub F_x when considering ultimate loads only.

A similar method is employed in DLC2.3. For this load case given that it is caused by an emergency stop it is assumed that there is still a strong requirement to bring the rotors to a halt as quickly as possible. The effect on Hub Fx of the three different shutdown methods is depicted in Figure 5.32: instant shutdown, shutdown in two groups, and shutdown in four groups. In this way, the whole array can be shut down in a matter of seconds while still destroying around 1,000kN from the peak loading. Ultimately, the only thing determining the ultimate load cases involving shutdowns therefore becomes the rate at which total shutdown is required.

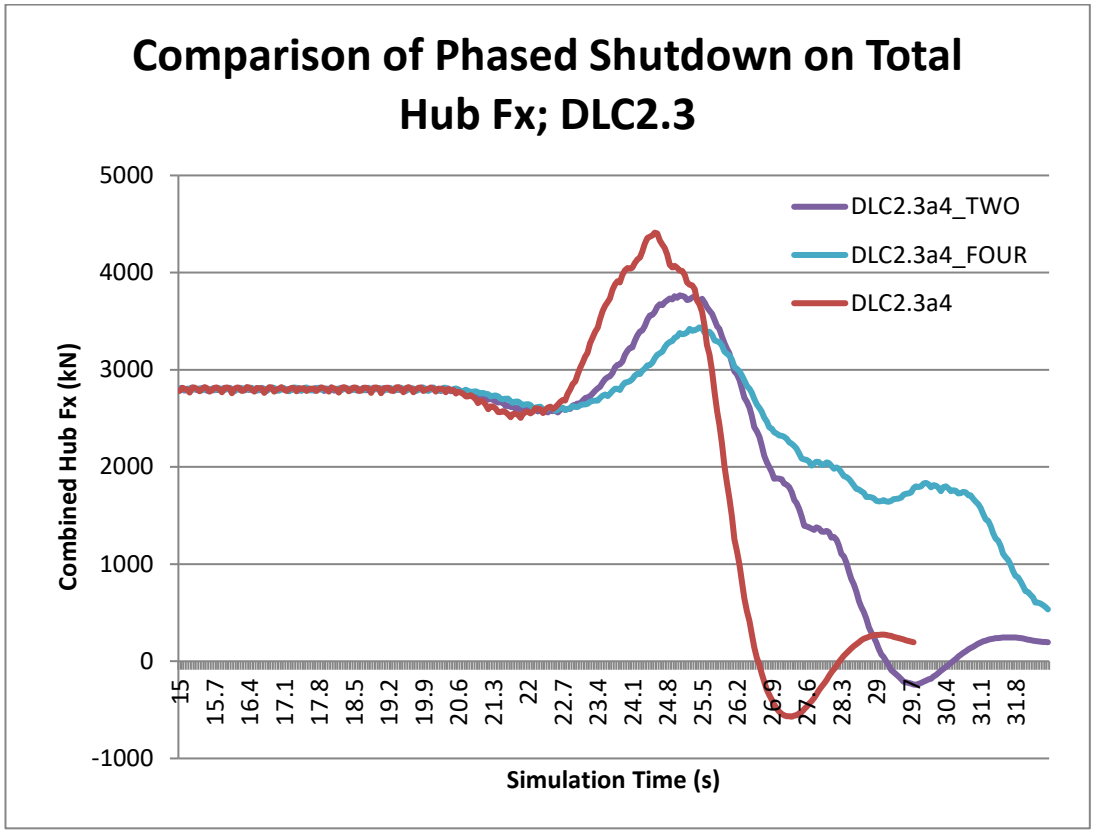

Figure 5.32: DLC2.3: Comparison of Two & Four Group Shutdown (SF Applied)

The effect of phasing shutdowns is important as it allows us to bring the ultimate loads on the structure down to a level comparable with that caused by operation in

extreme turbulence, see Figure 5.33. The advantages of having DLC1.3 represent the critical design loads is that it can represent design critical conditions over a period exceeding those of the shorter transients. The provision of long simulations allows for more data for the purposes of structural design and ultimately leads to higher degrees of confidence.

Of course this still does not address any perceived unfairness or unbalance in the standard that is perhaps unduly affecting the loads comparison. The final discussion will therefore be on the effect of the addition of turbulence on coherent shutdowns.

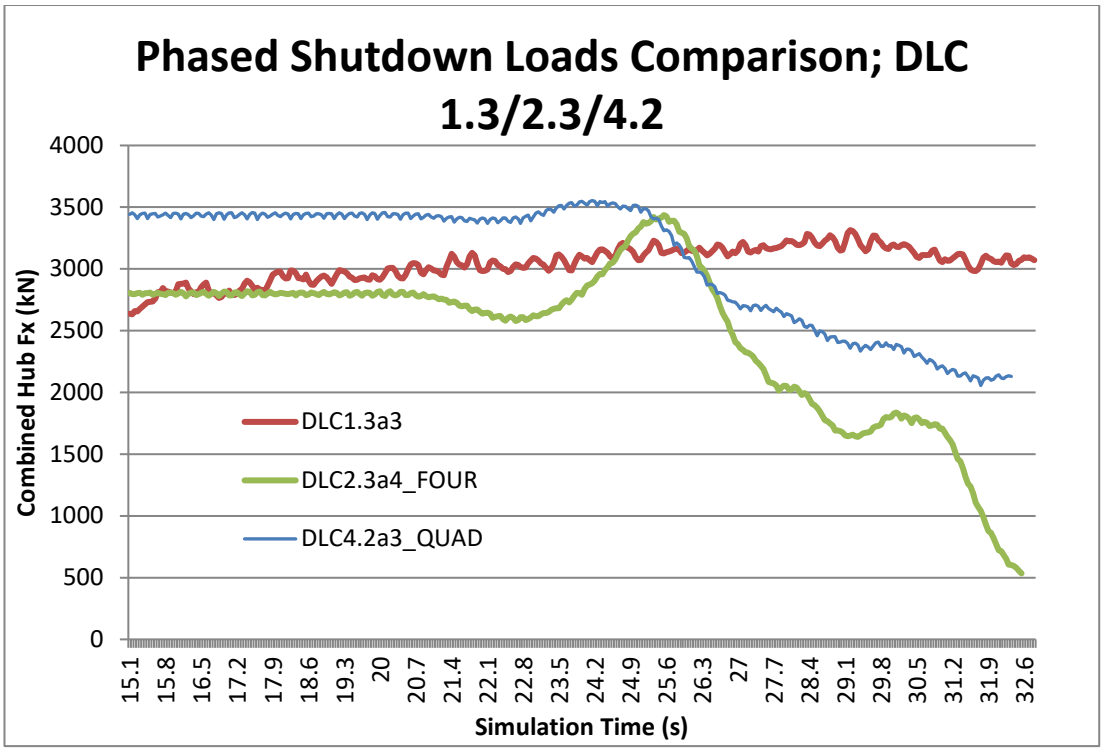

Figure 5.33: Shutdown Loads vs. Power Prod. Loads in Extreme Turb. (SF Applied)

5.6.4 Addition of Turbulence to Coherent Load Cases

In its original form DLC2.3 is skewed by the assumption of extreme coherence across the whole array and simultaneous shutdown. These assumptions are reasonable at 5MW (100m scales) but over 200-300m scale the assumptions are less so. It is expected that this results in an over-estimate of average steady-state loading.

Figure 5.34 shows the effect that adding turbulence to DLC2.3 has on the combined F_x loads when the MRS enters into a shutdown scenario. As the average steady state

loading is typically lower in a turbulent wind field than a coherent one, the total additive effect of individual hub F_x's have less of an impact on the ultimate load. This is illustrated in two ways. The first is a superimposed gust and shutdown on top of a normally turbulent wind field (during both an average and worst-case simulation period), resulting in reduction of 400kN or more on total hub F_x are observed. The second is a normal shutdown event without a gust during a normal turbulent wind field, the shutdown loading is barely noticeable above the average.

The first attempt to establish the ultimate load seems reasonable but even so still requires the following conditions to be met:

1. The coincidence of an undesirable extreme operating gust with a simultaneous emergency shutdown event.
2. The coherence of this gust over an area stretching 350m laterally and 250m vertically both spatially and temporally.
3. Simultaneous shutdown of each individual rotor during the worst phase of the gust.

If any of these conditions are not met then the ultimate loading should by nature or design become less than that of the ultimate loading present under normal power production operation at rated wind speeds (Figure 5.34). It is therefore expected that the multi rotor system need only be designed on the basis of the worst-case power production loading design case DCL1.3.

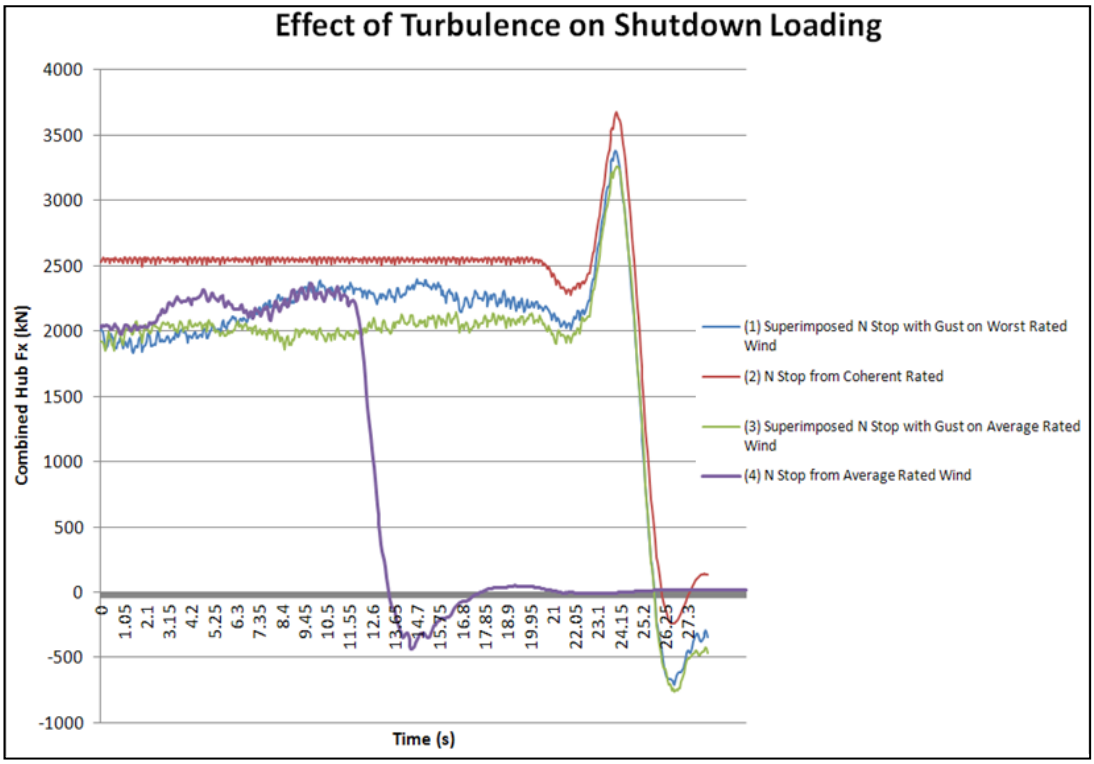

Figure 5.34: Normal Stop Loading Comparisons (No SF)

5.7 LOAD CASE COMPARISON

The final aspect of this chapter calls for the complete load case overview and comparison. Table 5.12 presents the abbreviated results, showing only the maximum total hub F_x for each of the seven load cases investigated.

Scenario	Maximum Total Hub F_x			
DLC 1.3a3	Constant	Turb. Worst-		
	4451kN	3314.3kN		
DLC 1.4b1	Fully	Turb. Worst-	Turb. Average	
	4875.5kN	3309kN	3200kN	
DLC 2.3a4	Fully	Turb. Worst-	Turb. Average	
	4411.3kN	3362.4kN	3216kN	
DLC 4.2a3	Fully	Turb. Worst-	Coh. Phased	Turb. Phased
	5663.7kN	3500kN	3553.6kN	2468kN
DLC 6.1	Fully	Turb. Worst-		
	601.2kN	661.8kN		
DLC 6.2	Constant			
	936kN			
DLC 6.3	Constant			
	443.4kN			

Table 5.12: Full Load Case Comparison

The third and fourth columns represent adjustments (made outside the scope of the standard) to each of the coherent load cases. To adjust for the coherent nature of the wind defined in these three transient cases, the transient event is summed with total hub F_x under normal operation (both in average operation and in operational worst-case). This adjustment better reflects the actual realisable loading across the multi rotor array and ultimately lowers the coherent steady-state loading. These adjustments are also displayed under the Turbulent Worst-Case and Turbulent Average headings in Table 5.12.

Table 5.12 also contains the reduced total hub F_x results caused by staging rotor shutdowns both under coherent and turbulent wind conditions. The results suggest that it is possible to reduce the peak magnitude of the total hub F_x loading during shutdown in both DLC2.3 and DLC4.2 (normal and emergency stop) to a magnitude similar to that experienced during normal power production.

The case is therefore made that the load production case around rated wind speed (DLC1.3) is likely to be the ultimate load case. This load case is examined in more detail in the following chapter for both the 20MW single rotor and 20MW multi rotor for comparative purposes.

5.8 DISCUSSION

The total hub F_x loads combined with a fault are reduced in DLC2.3 and 4.2 compared to DLC1.3 in the multi rotor system due to reduced probability of simultaneous independent faults across the array. Extreme loading due to loss of grid, which would result in worst-case loading, can be designed against using resistor banks which allow for phasing of the rotor shutdown - a method for which will be discussed in Chapter 6. Lateral coherence of gusts are such that individual blade bending moments are not design drivers in the MRS and that overall tower loading is more distributed comparing favourably with single rotor machines of equivalent power rating. A multi rotor system consisting of 45x41m diameter rotors can almost ignore extreme negative wind shear (IEC DLC1.5): normally driving (or close to driving) tip-to-tower closest approach in larger single rotor machines. Extreme coherent gust with direction change (IEC DLC1.4): normally driving bending moments at hub and yaw bearing overturning moment and which is very sensitive to tuning of the supervisory control for a single large rotor is lowered in the MRS with more degrees of freedom and the ability to yaw.

Critically, by comparing the loads from each design driving case it is possible to conclude that the MRS benefits from decreased loads overall compared to other equivalently rated single rotor systems in all examined IEC 61400-1 design load cases. Significant load reductions of 50% or more have been seen in total hub F_x, total hub M_y and total hub M_z on the multi rotor system when compared to a single 20MW rotor.

Reduced loading leads to reduced structural mass and cost, competitive with or less than single rotor systems at large scale. The MRS also benefits from many more

degrees of freedom, inherent redundancy, and increased part commonality compared to single or several single rotors of equivalent rating.

CHAPTER VI - ELECTRICAL INTERCONNECTION AND POWER OPTIMISATION

6.1 INTRODUCTION

The multi rotor system requires an unusual or uncommon electrical layout which merits detailed investigation. The main objective of the investigation is to develop a system for the proposed 20MW system with three priorities in mind:

1) *Minimize cost* - There are two areas of cost associated with electrical systems: initial capital outlay and cost associated with losses.

2) *Optimise mass distribution* - Electrical systems are traditionally heavy. They are most commonly located on the ground and therefore mass is not commonly a design consideration (the exception being overhead lines). However, in the MRS the electrical collection grid and associated power infrastructure will have additional mass that will result in a structural/cost overhead.

3) *Enable rotor independent operation* - Multi rotors have inherent advantages over single rotors of equivalent rating in areas of control for power optimisation and load alleviation. Individual rotors in the array have the capability of operating independently from each other and therefore the system as a whole has many more degrees of freedom than the single rotor. The ability to vary rotational speed is the most important aspect of power maximisation and load alleviation for the MRS and therefore the electrical infrastructure should support this endeavour.

6.2 ELECTRICAL INFRASTRUCTURE

6.2.1 Introduction

The electrical infrastructure of a single wind turbine normally comprises the generator, power electronics, protection systems, transformers and grid connection (see Figure 6.1). The numbers of components in the electrical drive-train (generator and power electronics) are significant and therefore it is a common cause of wind turbine faults. It is commonly cited that 75% of wind turbine faults (which in turn cause 5% of the downtime) are mostly associated with the electrical plant, the converter, electric pitch systems, control equipment and switchgear [119]. To avoid

increase in cost there is little redundancy in many of these systems however this is weighted against the fact that they are usually modular, relatively cheap and quick to replace.

In 2009, EWEA reported that the typical costs of an electric installation for a single rotor is in the region of €18,000 per MW of installed power. The MRS system will therefore be costed using normal electrical conventions for each component typically found [120].

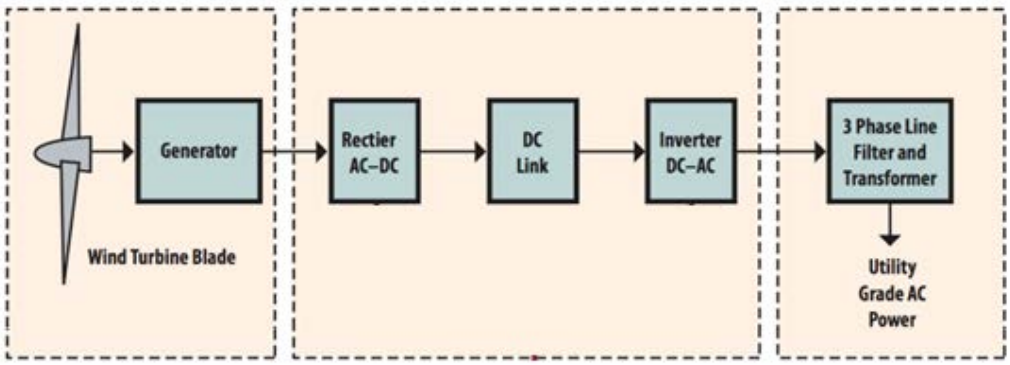

Figure 6.1: Typical High-Level Electrical Layout

6.2.2 Generator

Variable speed generators are the most common wind turbine configurations found within the industry today [121]. The ability to vary rotational speed (i.e. increasing the rotor speed in response to a wind gust) allows the rotor to maintain a constant tip-speed ratio and therefore maximize its power coefficient. On a conventional variable speed machine, the main rotor shaft connects to a gearbox thereby minimizing the generator dimensions for a requisite power output.

There are three main types of generator configuration for consideration in a variable speed multi rotor system: squirrel cage induction machine (which are the most common), the double-fed induction generator (DFIG) and the permanent magnet synchronous machine (PMSG).

DFIG systems require a gearbox to couple the wind turbine to the generator. Although the doubly-fed induction generator (DFIG) is a popular wind turbine generation system due to the balance between cost and performance, as discussed in Chapter 3, a significant disadvantage of the DFIG is its vulnerability to grid disturbances and fluctuations. This is especially true of its mechanically vulnerable gearbox. According to statistics of wind farm operation, 19.4% of wind turbine downtime is due to the gearbox and bearing system which imposes a disproportionate cost on offshore systems [122]. The reliability of the variable-speed wind turbine system can be improved significantly by using a direct-drive PMSG – thereby eliminating the gearbox. Since the development and commercialization of high density magnetic materials, the PMSG has received much attention in wind energy applications because of their ability to be self-excited. The use of permanent magnets in the rotor of the PMSG makes it unnecessary to supply magnetising current. This removes one potential point of failure from the generator and also allows PMSG solutions to be more efficient than other machines due to reduced losses in the windings [123][124].

One of the key advantages from a maintenance perspective would be to run a multi rotor array without any type of unscheduled maintenance. The loss of a single turbine does not significantly impact on the total power output and is therefore not as critical from an economic standpoint. This lends itself well to small, well-made PMSG machines with high reliability which would receive only scheduled maintenance at suitable intervals.

6.2.3 Converter

Wind turbines require a back to back converter to decouple the electrical frequency generated from that of the local collection grid and avoid undesirable and damaging harmonics [125]. This back to back converter is not necessary on fixed speed machines which are designed to operate within with specific frequency tolerances.

In the multi rotor system, where the distances between adjacent machines are not great, there is an additional incentive for equipping each machine with a back to back

converter. When rotors are electrically connected over a low impedance path the path acts like a stiff mechanical spring between the two machines, severely limiting their ability to adjust their speed. Given the lack of gearboxes, this means that individual rotors are not able to track C_{pmax} as effectively and ultimately generate less power. Any artificial or accidental restriction on single rotors abilities to operate independently hurts the power capture potential of the multi rotor system.

Self-commutated inverters (see Figure 6.2) can provide power conversion capabilities in the range of 200kW to 1MW, which should be suitable for most conceivable multi rotor systems and can use pulse-width modulation techniques and quick switching frequencies (several kHz) to filter out troublesome harmonics which otherwise could be let out onto the network.

Although current-source inverters are available, voltage source inverters represent the most common type of inverter in use today. In order to feed power onto the network, the DC capacitor in the link must constantly have a voltage higher than the peak voltage on the network. If the generator is not capable of providing this high voltage to the diode rectifier (at low speeds of operation), then a DC-DC step-up converter must be used [125]. MRS systems have the benefit of using smaller, higher speed rotors they are able to support a higher voltage on the rectifier side and therefore a step up will likely not be required.

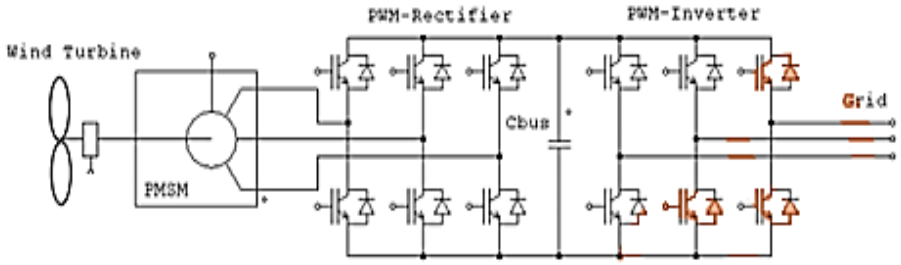

Figure 6.2: PMSG with PWM Converter

6.2.4 Transformer

Offshore electrical collection grids rely on the use of centralised transformers to step up voltages to transmission levels. Any failure of these transformers will cause a cessation in power flow in the same manner as a transmission cable fault.

Typical transformer failure rates can be as low as 0.05% for transformers in their first year and as high as 1.3% after 20 years of continuous operation [126].

Transformer CAPEX cost for a typical small 20MW wind farm would be around €5 million, with repairs and downtime costing an additional €5 million over 40 years. Operation and maintenance would cost in the region of €0.5 million and the value of energy lost in copper and iron losses may total €2 million. The total lifetime cost of a 20MW rated transformer would therefore be €12.5 million over 40 years [122].

Studies have been conducted on the optimisation of transformer placement and redundancy within an offshore wind farm transmission system. Possible redundancy solutions include twin 50% capacity machines, three 33% capacity machines, two 60% capacity machines and three 50% capacity machine.

Research conducted commercially has shown that there is very little advantage in cost (if any) of employing redundancy in transformers. The primary option should usually be a single unit rated at 100% of capacity. Alternatively, under certain discount rates and levels of transformer failure rates two units rated at 60% capacity may be preferable when considering total lifetime costs. A Garrad Hassan study concluded that this two unit option might yield €1.3 million savings (a 10% saving in the example given above) over a 40 year life [122].

6.3 ELECTRICAL CLUSTERING

6.3.1 Electrical Clusters

6.3.1.1 Theory

In the wind energy context, electrical clusters are groups of electrical machines and their components which are connected on a common busbar without any type of electrical decoupling. When two or more synchronous generators are coupled, they are severely limited in their ability to vary voltage and/or frequency. Instead, both systems will settle at an average voltage and frequency - which may not be optimum

- and the electrical network between effectively builds up an 'inertia' resisting change. The inability to vary speed can heavily penalise a wind turbine which relies on variable speed to track C_{p_max} and therefore electrical clustering is rarely practised onshore [126].

Electrical de-coupling is achieved through the use of a DC-link (a short section of cabling carrying DC current) which isolates two adjacent AC links. This decoupling can be provided by simple power electronic circuits such as a thyroid bridge rectifier, however the cost of such electronics scale with electrical rating and as power ratings increase becomes increasingly responsible for a larger portion of overall electrical and grid connection costs. In addition, power electronics are notoriously unreliable in offshore settings and account for a large percentage (75%) of all offshore wind turbine outages [127].

6.3.1.2 Hypothesis

By over-rating individual components in the electrical infrastructure such as transformers or converters and clustering them at common couple points there may be the potential to reduce CAPEX or OPEX costs for multi rotors in off-shore locations. In addition, the nature of MRS turbines close proximity to each other opens the potential for redundancy of components to be used to mitigate the increased O&M costs associated with failures occurring offshore. Redundant components enable less power capacity to be lost due to individual faults and therefore reduce the need for costly unscheduled maintenance.

6.3.1.3 Method

This investigation will look first at the clustering of over-rated power electronics in various configurations.

Each cluster is analysed in bladed under normal wind conditions and electrical output power, C_p and rotor speed information plus hub wind speed are captured from these simulations and post processed into cluster groups (assuming an artificial electrical connection). An average rotor speed is chosen at each time increment and the rotors in that cluster artificially forced into that rotor speed with any associated

loss of C_P due to a change in *TSR*. The new *TSR* and local wind speeds are used to calculate the reduction in power caused by the electrical clustering and this ratio plotted against the power produced if clustering was not in effect. It is acknowledged that this static method is not suitable as a tool for estimating actual power outputs but is used only to present the arguments for/against clustering.

6.3.1.4 Analysis

The first attempted solution is to select a cluster size and shape that appears to (on average) experience the same magnitude of wind speed so that each turbine in the cluster is matched as closely to optimum energy as possible. It is expected that the shape and size of these clusters will probably vary in response to different types of wind variation and strength.

Figure 6.3 displays one such cluster arrangement for the 45 turbine array developed in earlier chapters. The rotors are presented as circles with the dark lines indicating which turbines are linked together electrically for the purposes of this investigation. In this arrangement, there are 15 clusters of between 2 and 4 machines. In this configuration there is the possibility to reduce the number of DC-links, transformers, circuit-breakers and protection equipment by 1/3.

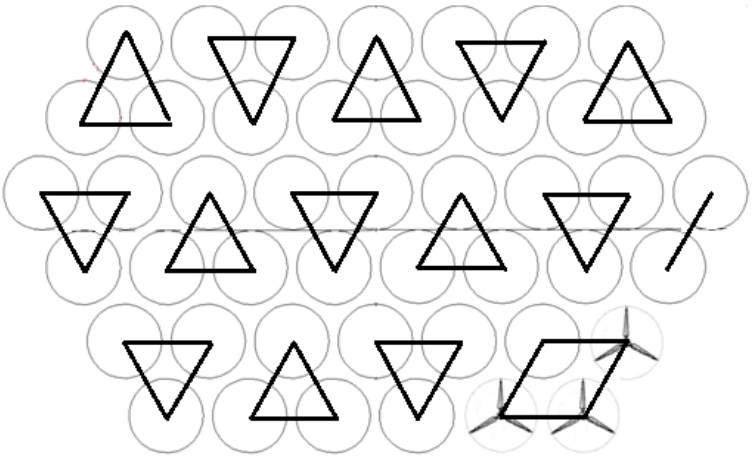

Figure 6.3: Small Clusters of 2, 3, or 4 Machines.

Consider the cluster at the top left of the array. This constitutes turbines 31, 32 and 39 according to a bottom to top, left to right numbering system. Investigating the longitudinal components of the point history wind speed of wind field passing

through this cluster at the three hub points. It is seen that each of the three turbines experience a very similar overall change in wind speed magnitude at the larger along wind (longitudinal) scale but that over the course of several cycles (<5s scale) there can be significant difference. In effect, clustering will act to remove any local variations in power production and average out the effective wind (essentially removing the turbulence).

Combining this wind field information with the known parameters for each of the turbines in the array it is possible to make some observations about the effect of clustering.

At this point it is assumed that the rotor speed is configured to obtain maximum power coefficient for an average wind speed of 11m/s. This corresponds to a tip speed ratio of 8.5 and therefore a rotor speed for a 40.55m rotor of 2.3 rad/s. Assuming that the electrical frequency of the three systems is to remain in phase and assuming that there is no gearbox able to compensate with a fine adjustment, these three rotors will be forced to rotate at the same speed of 2.3 rad/s.

In this wind field, an average wind speed of 11.04 m/s is measured across this cluster at 92.4 seconds. This corresponds to a longitudinal wind speed of 10.94 m/s at turbine 31, 10.59 m/s at turbine 32 and 11.63 m/s at turbine 39. Assuming a constant rotor speed, the tip speed ratios of turbines 31, 32 & 39 are calculated as 8.52, 8.80 and 8.02 respectively.

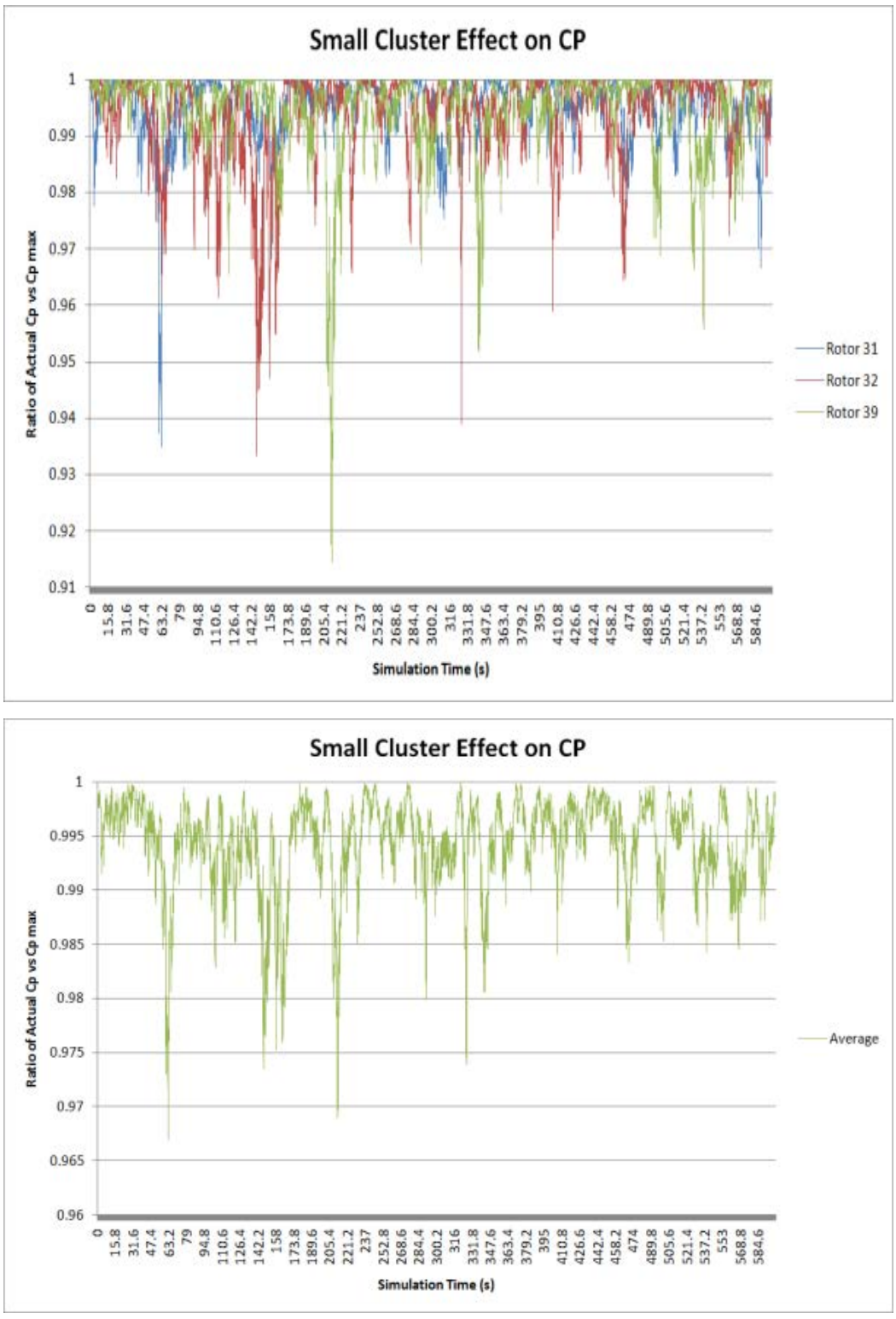

Figure 6.4: Effect of Clustering on C_p (Left: 3 Rotor Overview, Right: Average of 3 Rotors)

Interpolating these values with the C_p-λ for this turbine it is found that all 3 rotors are no longer operating at maximum power coefficient. Rotor 31 remains at $C_{p\ max}$ while rotor 32 experiences a 1.659% decrease in C_p and rotor 39 experiences a 0.945%

decrease in C_P. Total C_P loss for the cluster is therefore averaged at 0.238% for the time point 92.4 seconds. Whether this manifests itself as a power loss is obviously dependent on the rated wind speed of the machine and whether the rotor speed is truly fixed (Figure 6.4).

The same analysis is conducted on a slightly larger cluster using the same wind field and the same time frame. The top left cluster now contains 5 turbines in this instance with the addition of turbines 40 and 33 (see Figure 6.5 left). The pertinent values are shown in Table 6.1.

Wind Speed at Each Hub Node (m/s)					U_{ave}
T40	T39	T33	T32	T31	
11.55	11.63	10.47	10.59	10.94	11.036
Tip Speed Ratio of each Rotor					**Target**
T40	T39	T33	T32	T31	
5.80	5.76	6.40	6.32	6.12	6.1
Associated Power Coefficient					**Target**
T40	T39	T33	T32	T31	
0.422	0.422	0.414	0.415	0.418	0.422

Table 6.1: Clustering Summary

Although only two turbines were added to the cluster the total C_P loss for the cluster in this case is 0.712%, which is nearly three times of a 3 rotor cluster. This suggests that the hypothesis that by increasing the cluster size the spatial coherence of the wind begins to take its toll on each turbine's ability to respond optimally to average control inputs.

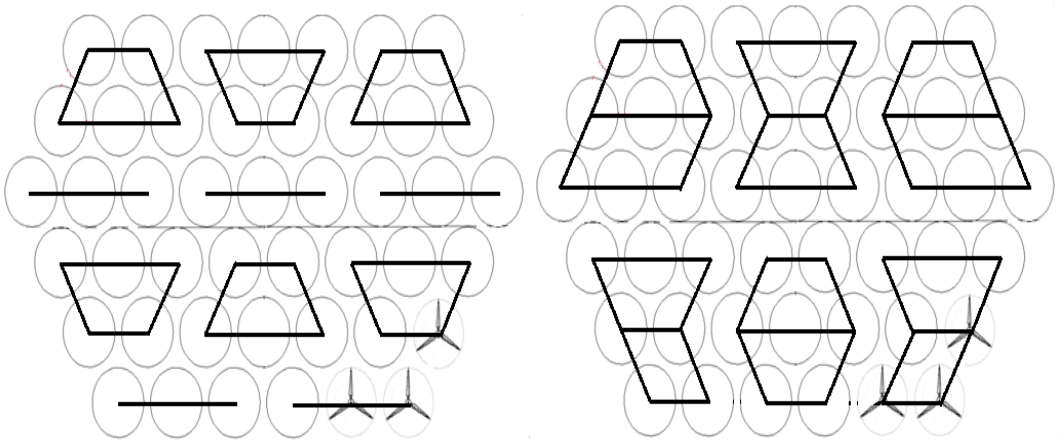

Figure 6.5: Alternative Cluster Options (Left: Medium Clusters, Right: Large Clusters)

The same procedure is carried out on an even larger cluster set. In this case Figure 6.5 (right) presents a cluster containing 8 turbines. Using the same averaging control strategy a total C_P loss of 2% is expected over the cluster, again nearly a three-fold increase in the loss.

This analysis presents an interesting situation for evaluating the total hidden power loss that occurs in single large rotors occupying a widely varying turbulent wind field. The single rotor in essence could be represented by a single cluster utilizing a single averaged measurand used to determine each rotors rotational speed. From this it is possible to work backwards to identify the power gained from the use of localized wind turbines.

These values suggest that the use of even small clusters will result in sub-optimal operation of individual turbines in below rated conditions with class I turbulence as expected. The issue will be further reduced in more uniform wind fields with good spatial coherence both laterally and vertically.

5.1.1.1 Conclusions

Consider that individual turbines will attempt to track C_{p_max} while in the variable speed region, then it's possible to compare the effectiveness with which they do that with the effectiveness with which the cluster groups track C_{p_max}. The ratio of the cluster group average C_P vs. that of the average C_P of each individual turbine then

expresses whether clustering is leading to better C_P tracking (when the ratio is greater than 1) or worse C_P tracking (when the ratio is below 1).

Figure 6.6 contains a comparison of each cluster type's ability to track C_P effectively and it shows, as expected, that clustering has an overall negative effect on the ability to track C_P effectively and this in turn will lead to energy capture loss. The effect is perhaps not as pronounced as one would imagine, being only on the order of 1-2% and it may be that any equipment savings may make up for this.

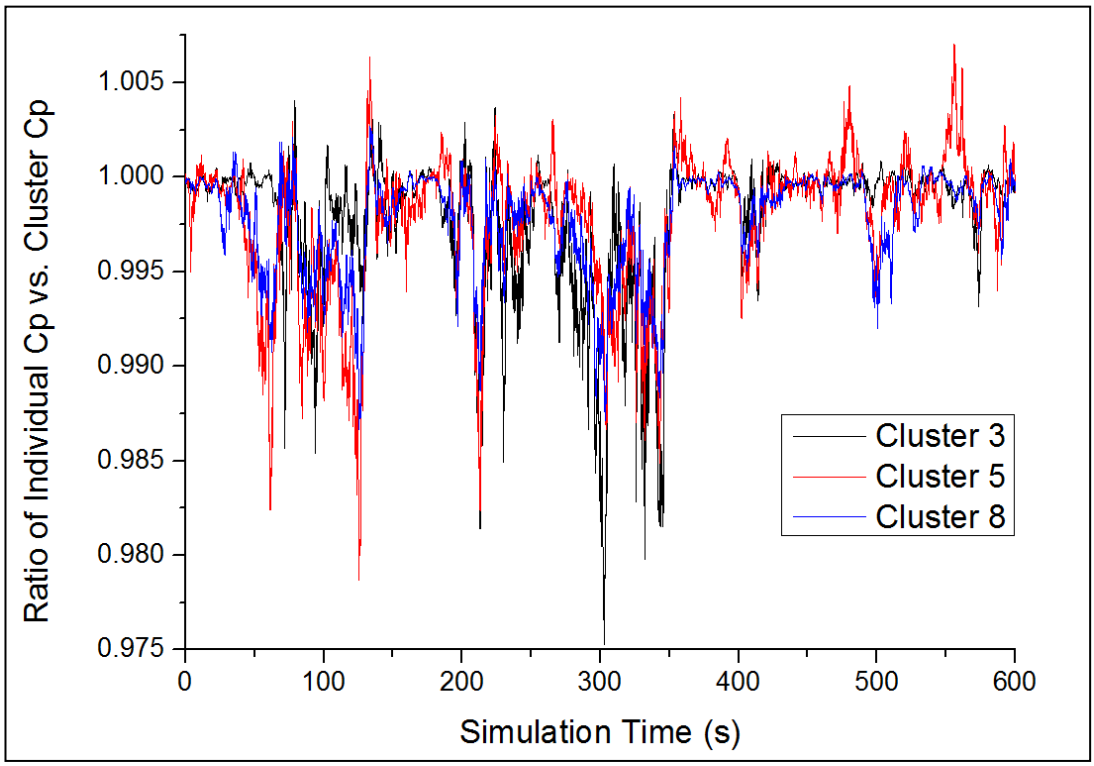

Figure 6.6: Investigation of Cluster Size and Effects on Cp Tracking (No Shear)

Surprisingly, increasing the number of rotors in a cluster from 3 to 8 (in the absence of shear) does not adversely impact on the ability of a cluster to track C_P and in fact in the case of 5 rotors appears to have occasional positive effects above that of individual turbines alone (i.e. there is a greater energy capture over a given period). This suggests that clustering should not be done arbitrarily and that there may be avenues for optimisation in terms of energy capture along lines of wind shear for example.

It is acknowledged that at medium and small cluster sizes any loss in power will only occur at wind speeds below rated. Given that EN regulations permit up to ± 1% change in frequency it is also viable that individual turbines in the cluster are able to adjust their speed in respect to each other by a small amount over short periods. This would allow individual turbines to optimize their speed and therefore power output by a small amount if necessary – in the same way that loading the network has. Such a procedure would have a knock-on effect on other turbines in the cluster and so this control strategy merits further evaluation.

This analysis suggests that further work in optimizing rotor speeds in clusters should be conducted in various wind conditions to maximize the potential benefits of the use of electrical clusters on the MRS. It is likely that some optimal arrangement will be found for a set of wind conditions that the MRS is likely to spend the majority of its time in and this will help offset some of the cost and complexity of the system overall. Clustering is not conclusive in its benefits and will not be considered further at this point given that items such as transformers, circuit breakers and so on can be shared without any impact on C_P tracking.

6.3.2 Collector Grid

6.3.2.1 Introduction

The electrical cabling of a multi rotor system is not dissimilar to that of a standard wind farm with an additional axis. The distance between each rotor on the multi rotor system is 42.5m on the shortest connections.

The shorter cabling distances gives rise to two interesting possibilities for the multi rotor array. The first is that there is less requirement to step up voltages in the collection grid as the distances involved will result in less Ohmic loss than a standard wind farm. The second is that it is less costly to have multiple parallel connections available to individual machines in the array. This contrasts more sharply with a standard wind farm which is likely to feature multiple machines in series connected with one parallel loop acting as redundancy.

6.3.2.2 Cabling Layout and Redundancy

The objective of the electrical cabling configuration is to select a cabling layout which minimizes weight and cost (i.e. makes use of shortest paths) but which also provides a satisfactory level of redundancy within the local collection grid such that single outages (N+1 redundancy) do not wipe out entire swathes of the systems power generating capabilities. Each generator/power train follows the shortest path to the point of common coupling (PCC). This is achieved by cabling downwards and towards the centre of the array at each node, making use of series connections that share cables where possible. In this manner the cabling of the array will appear as per Figure 6.7. Five horizontal cables have been added to the system to provide a level of N-1 redundancy. The location of this redundancy is somewhat arbitrary. The main aim of this redundancy is to connect up groups of rotors at the furthest points from the grid feeders (PCC) which are more susceptible to cabling faults at lower points in the array.

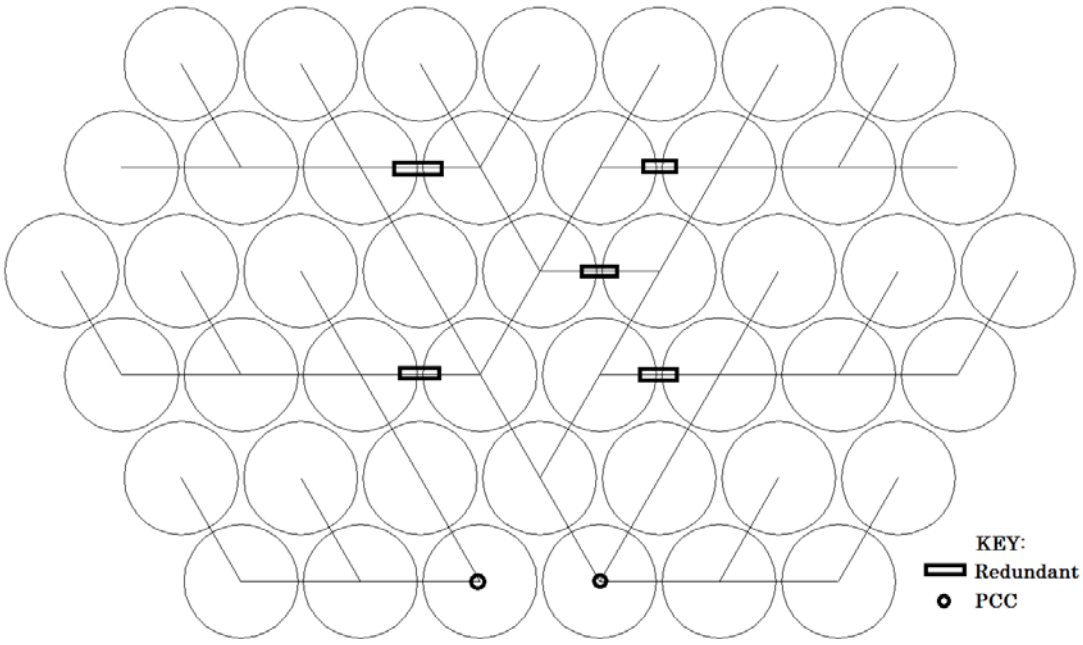

Figure 6.7: Proposed Multi rotor Cabling Diagram

The redundancy provided in the cabling in this example can ensure that no more than 8.88% of the total rated output power from the array can be disrupted as a result of a single cable fault. Figure 6.8 shows the levels of redundancy of each cable, with

percentages marking the percentage power lost as a result of a single cable fault on that individual path. The thick central lines are all N-1 redundant, meaning that a single cable fault at any point within this circuit will result in now output power loss.

The normal standard in electrical fault planning would likely include redundancy up to N-2 (i.e. two independent faults). However, due to the large amount of parallel circuitry in this example, the overhead of calculating and indeed designing for N-2 faults locally is not considered feasible within the confines of this project and likely would be undesirable expensive in any case given the chances of a double independent cable fault.

It is important to note that this circuitry can handle any number of individual machine faults on top of individual cable faults - which is not accurately depicted in the Figures. Each machine is jointed separately to each node (which is essentially a short busbar) and would have its own isolator at a minimum.

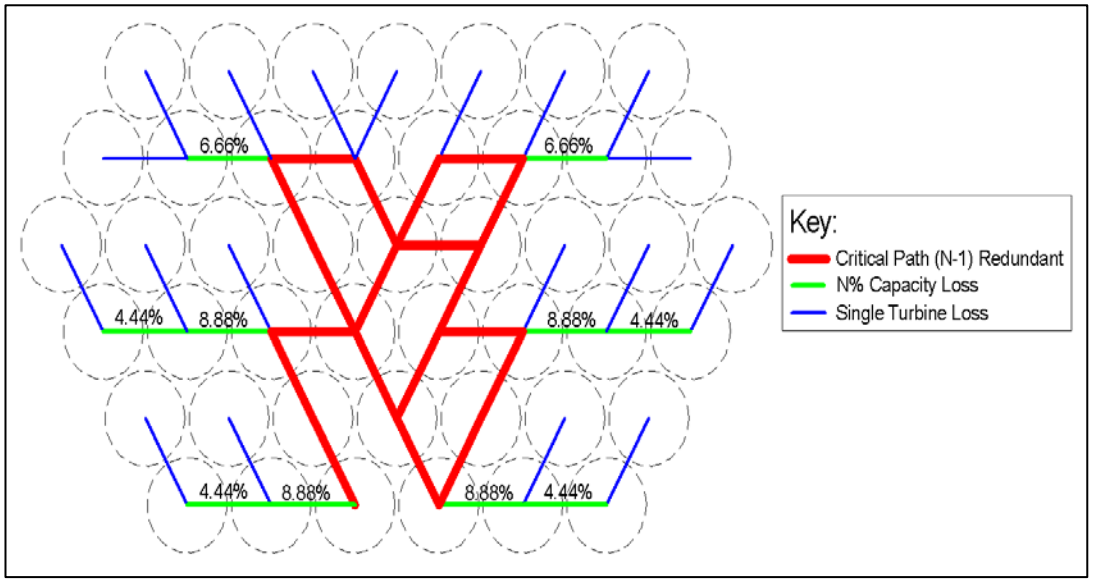

Figure 6.8: Redundancy of Electrical Cabling

6.3.2.3 Steady State Power Flow

In order to conduct an initial power flow study using this wire arrangement the system is modelled within the Power Flow library of Simulink, MATLAB. For the purposes of this power flow study the generators are assumed to act as constant current sources operating at fixed voltage (690V) and rated at 444kW.

In order to size the individual cables in the array the system was simulated 48 times with each simulation representing a different cable outage (open-circuit faults) in the array. Figure 6.9 shows the maxima current flow down each cable under any outage circumstance in the per unit (p.u) frame of reference.

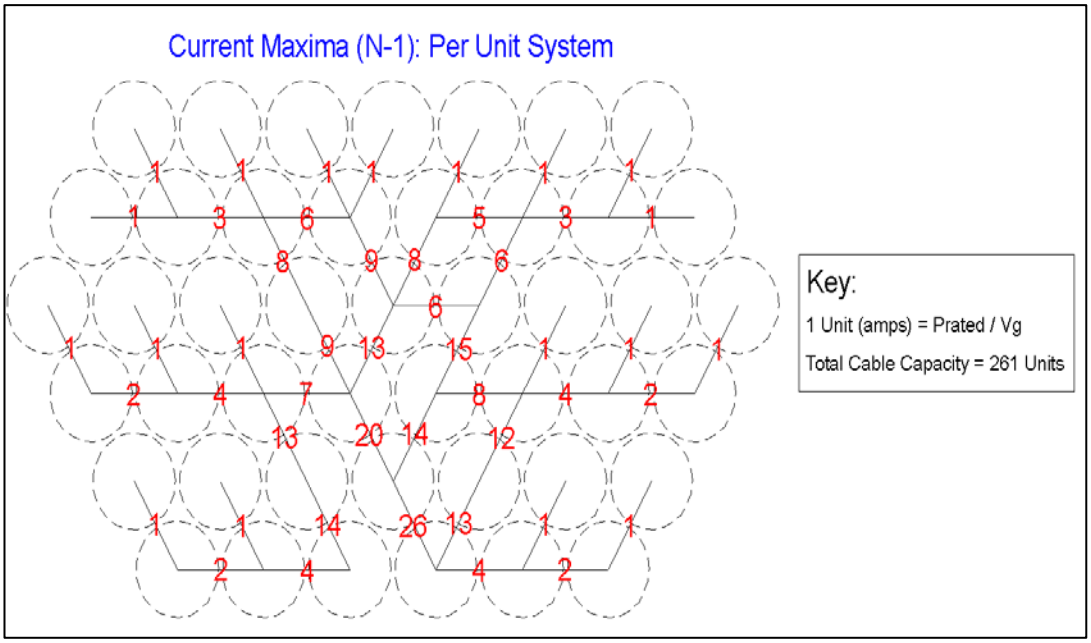

Figure 6.9: Current Maxima for Single O/C Fault

Using this current maxima information each cable can now be sized accordingly. The assumption for maximum cable capacity is taken from the British Standards regarding material resistivity and current carrying capacity. The cables are alternatively modelled as identical copper/aluminium cables with a fixed resistance as a first iteration.

Figure 6.10 shows the steady-state power flow in the per unit (p.u) reference frame using copper cables sized for N+1 maxima. Note how the horizontal redundancy cables highlighted earlier carry very little operational current - this indicates that they do not form part of the optimum path/path of least resistance. This Figure shows a propensity for the current to flow towards the centre of the array and down towards the grid feed.

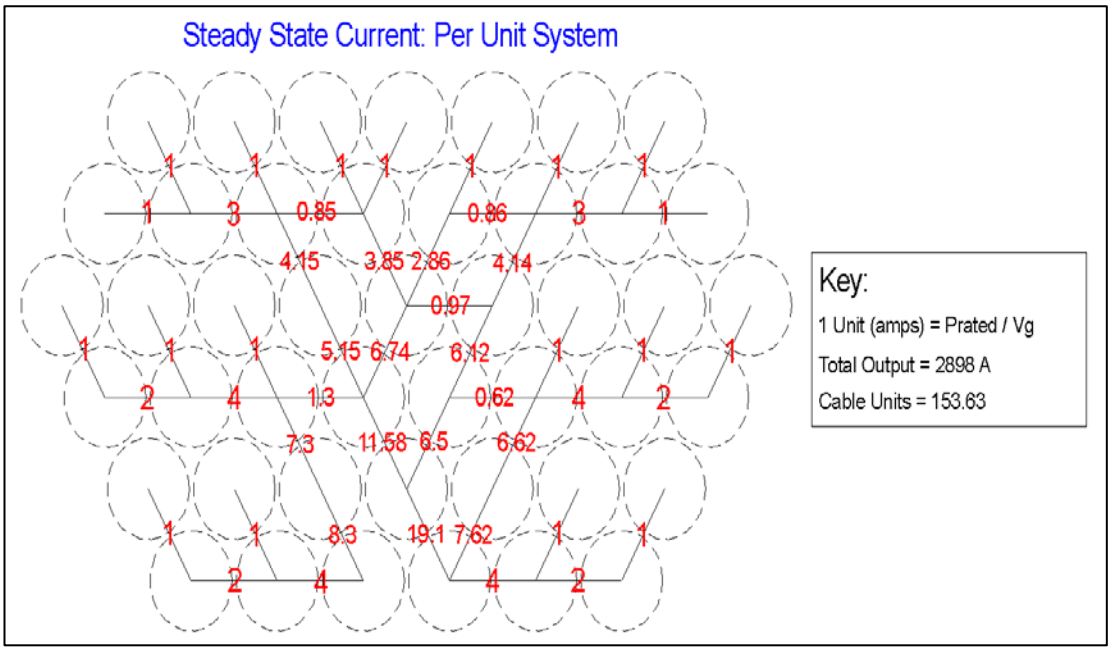

Figure 6.10: Steady State Power Flow

6.3.2.4 Cabling

There are only two realistic materials which can be used to transmit electricity over anything more than a few centimetres; copper and aluminium. The material of choice consists of a consideration of cost. Aluminium is typically 20-30% of the cost of copper depending on the cable current rating, number of cores, and cable type (as of 2015). There is minimum of 42.5m x 261 = 11.1km of cabling within the proposed multi rotor array, not accounting for redundant paths, extra cabling for joints, cable conduit routing and such like. In mid-2015, the international commodity cost of one metric tonne of aluminium was $1,727 USD vs. $7,291 USD for a metric tonne of copper. These prices simply reflect the raw cost of copper and a notional scale factor for wiring, adding shielding, coating, splicing, jointing, transportation and labour costs which would be associated with the actual engineering of the collection grid. A modest scale factor of two can be used to represent these additional cost for copper and a scale factor of four for aluminium (as it is harder to work with)

Table 6.2 presents the minimum cabling costs at a range of different collection voltages (at a rate of 1 USD to 1.6 GBP) and shows that the difference in cost between

materials becomes minimal at higher collection voltages, making ohmic losses a deciding factor.

Collection V.	690V	1100V	3330V	6000V
Aluminium Cost	£251,769	£157,928	£52,643	£28,953
Copper	£299,980	£188,170	£62,723	£34,498
Difference	£48,211	£30,242	£10,080	£5,545

Table 6.2: Minimum Collection Grid Cost

Multi rotor collection grid losses depend on the square of current and there is a strong incentive for the collection voltage to be energised at medium voltage levels (2kV and above). The losses for the array can be quickly calculated given that the final cable ratings and associated resistances are known along with the steady state current at full power.

Aluminium loses 0.022% less energy than copper at 690V, 0.05% less energy at 3300V and 0.03% less energy at 6000kV.

Using these values it is possible to identify a range of possible costs associated with the energy losses in a MRS at different levels using these two different materials, varying collection voltage and different unit feed in prices [129] presents this analysis for a range of MRS capacity factors ranging from 30% which would be considered normal onshore to 60% which is the world record for an individual machine over a single year. It shows that the income lost as a result of energy lost at the collection stage is very insignificant at 6000kV, amounting to around £10,000 over the machines lifetime. At the lower collection voltages, such as the proposed 690V generating voltage the cost is slightly higher, but not punitively so; between £60,000 and £80,000 depending electricity market price over the machines lifetime and assuming a high 52% capacity factor.

In addition to the array losses, the one other area of energy loss comes from the transformers. 2% losses are quite common at around 75kVA rating while the minimum efficiency of a 500kVA transformer might be 98.7% and a 2500kVA transformer might achieve a minimum efficiency of 99%. Transformer losses are also highly dependent on the loading, with load losses increasing as the load on the

transformer increases (due to heating and associated winding resistance increase) [130].

6.3.2.5 Summary

Without considering whether the voltages in the collection grid are as generated or stepped up a decision can be made about its material composition in attempting to balance costs and suitability [131].

Table 6.3 gives a complete overview of how material composition will affect the cost, both in real terms and in terms of potential lost income. The difference is significant at low voltages such as 690V with aluminium appearing to have advantages in excess of £300,000 over 20 years - which is probably enough to justify the use of aluminium despite its corrosive properties in an offshore environment.

However, copper should be the material of choice if the collection grid is energised at 6000V as the difference over the project lifetime of £36,000 is not enough to justify the risk of the use of aluminium.

In comparison, the NREL WindPACT study which estimates cabling costs for a single 1.58MW machine at $17,800 (£11,000). Reviewing this system with its 100m cabling length as per the raw material method used in this project, the cabling cost of a 1.58MW machine would be $18,700 (£11,500). The Figures are close enough to suggest that this method of calculating cabling cost is at-least sensible, with the difference easily explainable by inflation of commodity prices over the intervening 6 years alone [132].

Material	Collector Voltage(V)	Collector Loss (kW)	Collector Loss (%)	Weight (t)	Material Cost ($)	Factored Costs (£)	Lost Inc. (£)
Al	690	23.01	0.115	24.090	41,603	£104,009	£251,769
Cu	690	27.42	0.137	39.972	291,433	£364,291	£299,980
Al	1100	14.44	0.072	15.111	26,097	£65,242	£157,928
Cu	1100	17.20	0.086	25.073	182,808	£228,510	£188,170
Al	2200	7.22	0.036	7.556	13,048	£32,621	£78,964
Cu	2200	8.60	0.043	12.537	91,407	£114,259	£94,084
Al	3300	4.81	0.024	5.037	8,699	£21,747	£52,643
Cu	3300	5.73	0.029	8.358	60,936	£76,170	£62,723
Al	6000	2.65	0.013	2.770	4,784	£11,961	£28,953
Cu	6000	3.15	0.016	4.597	33,515	£41,893	£34,498

Table 6.3: Mass and Losses of the MRS array

6.3.3 Power Systems Equipment

6.3.3.1 Introduction

Transformers are used to step up or step down voltages within a power system. They are a vital requirement for power systems at both collection and grid level as they allow currents to be minimized (reducing losses) while maintaining equivalent power flow. Oil cooled transformers are by far the most common type in use, however these are bulky and heavy and not conducive to a light weight multi rotor structure.

There are three potential cases for transformer placement within a multi rotor array. The first assumes that the entire array is collected at generator voltage and then stepped up to grid/transmission level at base level. The second assumes that there is some amount of collection or grouping of generators prior to voltage step-up and a second step up at grid/transmission level. The third case assumes that each individual generator is stepped up to the requisite collection voltage using its own transformer, cited closely to the generator.

Collection is conducted at medium voltage levels on a wind farm scale before being stepped up again to high voltage levels (30kV and above) at a wind farm central substation before transmission to shore.

6.3.3.2 Power Systems Scaling

Transformers

There are a large number of commercial transformer designs available and therefore an endless number of data sets which could be integrated into this study. The type of transformer chosen in any future multi rotor design would likely be chosen on the merits of weight, cost and compactness. It can be assumed that these transformers would likely be oil cooled based on current conventions, but there is a possibility that water-filled transformers could be investigated.

Table 6.4 contains some publicly available data on a range of transformer ratings and sizes taken from manufacturers spec sheets, without any prejudice or favour for any brand or model. Certain rows have been highlighted to represent the nearest whole number (rounded up) of generators that could be serviced by that transformer.

Figure 6.11 plots the power to mass ratio of this same data set across power ratings up to 20MW. It shows that the smallest machines are capable of power to mass ratios of 0.1kVA per kg and the larger machines up to 0.7kVA per kg. Applying a trend-line to this data suggests that transformer mass scales as $P^{1/4}$. This weight advantage is sensitive to the amount of oil used for cooling, which can account for up to 20% of the total transformer weight at 1MW ratings but which accounts for only 15% at 2.5MW (oil volume scaling cubically). This scaling law appears to give a clear advantage in terms of mass when using single highly rated transformers as opposed to multiple smaller ones of equivalent total rating. In a multi rotor context, this would mean that a few centrally located transformers will be more optimal when considering mass, compared to utilizing individual transformers per machine.

	Secondary Coil Voltage 3.3kV or 6kV					Dimensions				
#	Capacity	Oil	Tot	Oil	kVA	L	W	H	Vol.	kVA
	30	75	295	25.42	0.101	80	46	88	0.32	92.64
	50	85	395	21.52	0.126	85	58	94	0.46	107.8
	63	95	420	22.62	0.150	86	62	96	0.52	122.0
	80	103	480	21.46	0.166	87	66	97	0.56	141.8
	100	115	540	21.30	0.185	88	67	10	0.59	168.7
	125	130	645	20.16	0.193	89	75	10	0.69	180.0
	160	145	740	19.59	0.216	90	82	10	0.78	204.5
	200	175	885	19.77	0.226	91	83	10	0.82	245.1
	250	195	1010	19.31	0.247	12	77	11	1.04	240.5
	315	230	1205	19.09	0.261	12	82	11	1.23	255.7
	400	255	1375	18.55	0.290	12	84	12	1.35	297.0
1.13	500	285	1620	17.59	0.308	14	10	13	2.05	244.5
1.42	630	350	1960	17.86	0.321	16	10	13	2.24	280.9
1.80	800	405	2310	17.53	0.346	16	11	13	2.56	312.7
2.25	1000	490	2690	18.22	0.371	17	11	14	2.75	363.0
2.25	1000	515	2985	17.25	0.335	18	12	15	3.66	273.5
2.82	1250	550	3315	16.59	0.377	18	12	14	3.54	353.4
2.82	1250	630	3460	18.21	0.361	18	13	17	4.16	300.4
3.60	1600	625	3985	15.68	0.401	19	13	15	4.15	385.5
3.60	1600	710	4015	17.68	0.398	19	13	17	4.64	344.8
4.50	2000	745	4520	16.48	0.442	10	14	16	2.38	841.6
4.50	2000	730	4425	16.50	0.452	20	17	20	7.29	274.2
5.63	2500	730	5260	13.88	0.475	20	18	21	7.97	313.4
7.09	3150		7900	15.00	0.398	39	27	28	30.34	103.8
11.26	5000		12424	15.00	0.402	25	22	27	15.82	316.0
14.19	6300		12300	14.00	0.512	35	29	32	33.48	188.1
18.02	8000		15300	14.00	0.522	40	30	35	44.63	179.2
22.52	10000		17858	13.00	0.560	41	27	36	41.94	238.4
28.15	12500		20042	13.00	0.623	45	30	38	52.82	236.6
36.04	16000		23740	12.00	0.674	52	32	46	79.61	200.9
45.05	20000		28186	12.00	0.709	53	34	46	85.30	234.4

Table 6.4: Oil Filled Transformer Scaling with Rating

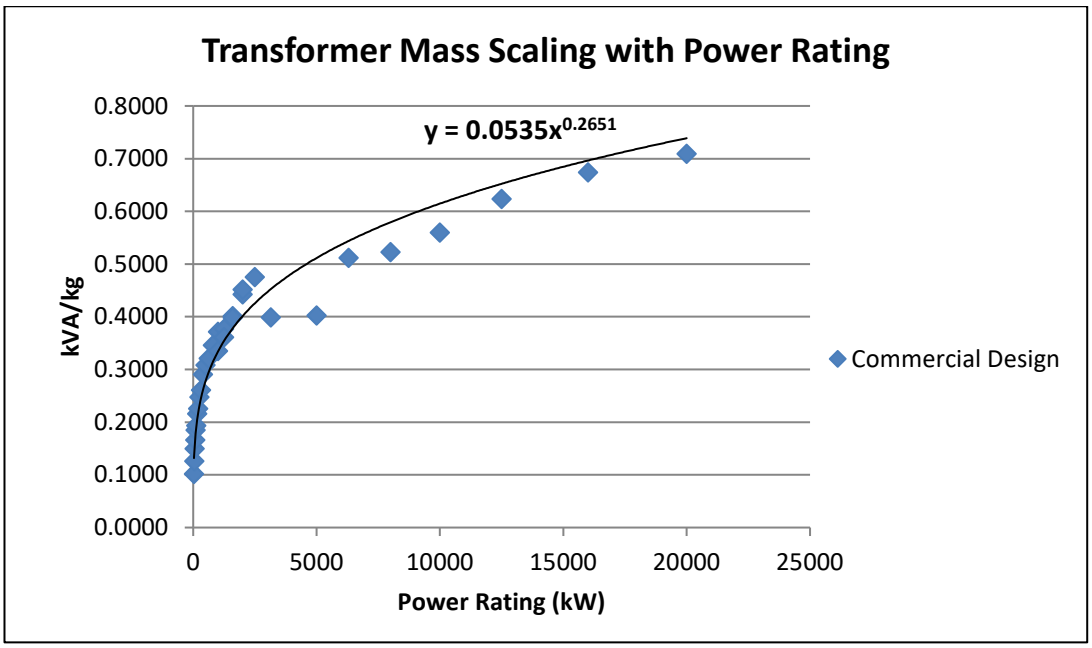

Figure 6.11: Transformer Mass Scaling with Power Rating

Figure 6.12 plots the power to volume ratio of the same sample group of commercial oil cooled transformers. The relationship between size and power rating is approximately linear above 1MW power rating and that no savings in volume can be achieved above this value. However, below 1MW there is a region in which small increases in transformer volume yield increase power rating capacity. In this region, there is significant flexibility in terms of minimizing transformer size for a specific rating. This is interesting in the multi rotor context as a 1MW transformer can provide step-up or step-down voltage transfer to two individual rotors and could do so in potentially a very compact space. In any case it suggests that there may be some ability for such machines to be fitted within the multi rotor super structure rather than bolted on separately which would be highly desirable from an aerodynamic and drag limitation point of view.

Transformer losses are not as straight forward as cabling losses. They are highly dependent on the design of the transformer and it is quite possible to have two machines with the same load rating with a variation of a fraction of a percent. There is a slight tendency for machines to become more efficient the physically larger they become as they tend to operate cooler - see Figure 6.13. The cooling effect scales with

volume (cubically) while the heat increase scales as I^2 thus larger rated machines will tend to be more efficient. A difference of even 0.1% can make a significant impact over system lifetime.

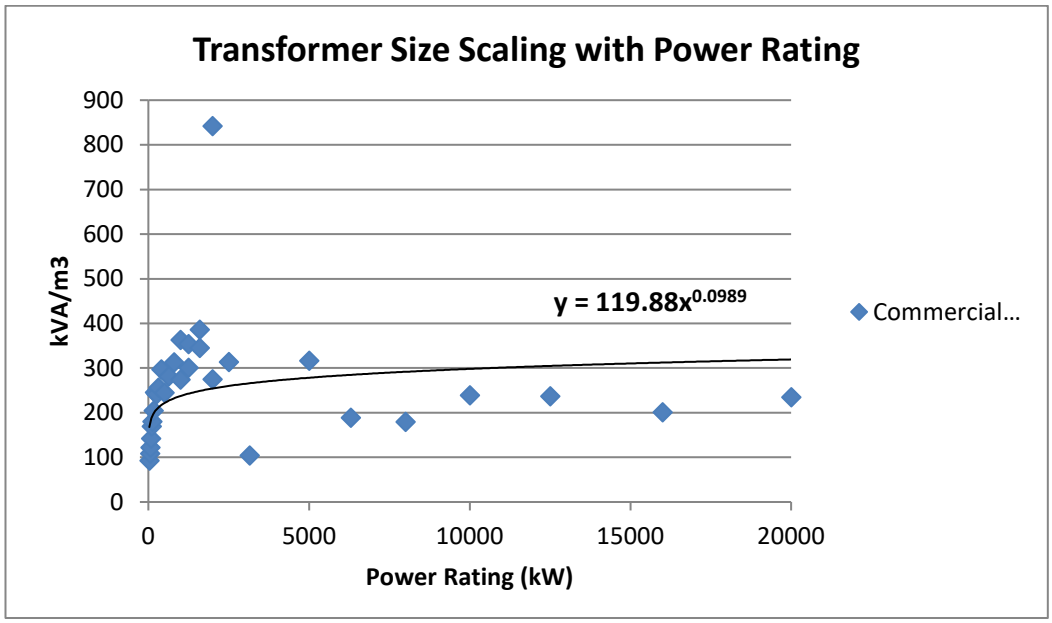

Figure 6.12: Transformer Size Scaling

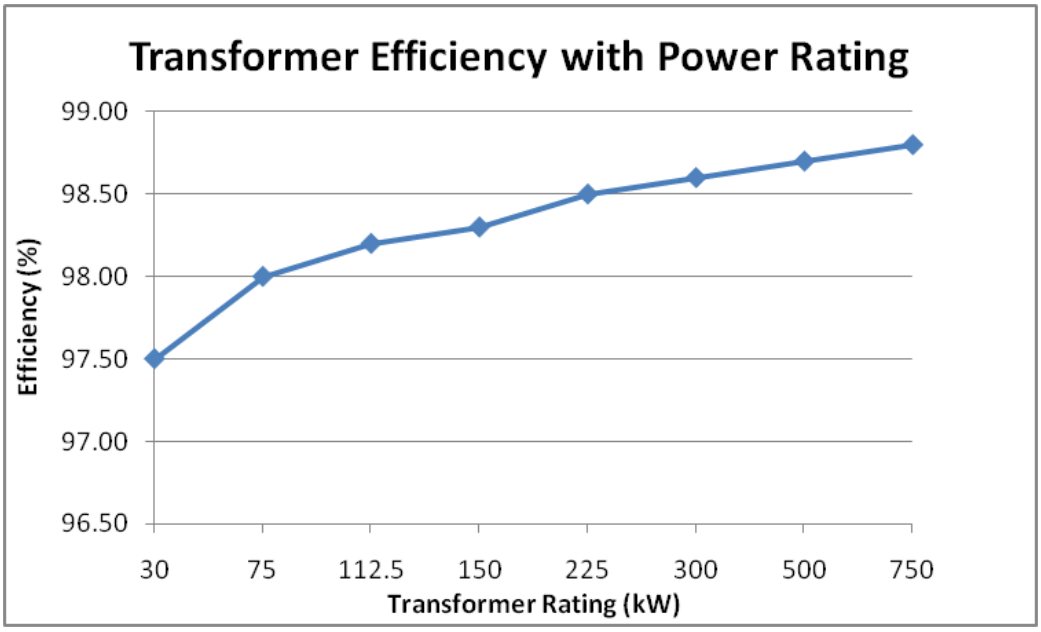

Figure 6.13: Transformer Efficiency with Rating

In addition, transformers also have increased 'load' losses with increased loading which is more than linear (scales as the square of the load) on top of 'no load' losses which are dominated by hysteresis and eddy current losses. A typical transformer

load vs. efficiency curve will look like Figure 6.14 with the peak efficiency occurring around 50-60% of full load typically.

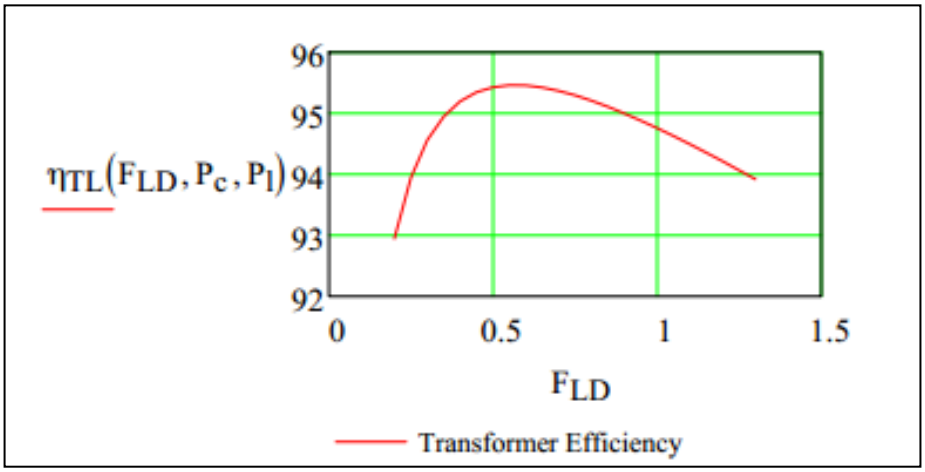

Figure 6.14: Transformer Full Load Efficiency

The capital cost of a transformer can vary depending on manufacturer and it is difficult to put up a definitive Figure. ABB power for example provide a 1500kVA oil-cooled transformer for $30,000. Chinese OEM manufacturers meanwhile provide at slightly reduced costs ($20-24,000 for the same rating). A Figure of $20 per kVA suggests a reasonable first estimate. Using this factor, the total cost for a 500kVA transformer is $10,000 and a 2500kVA transformer is $50,000 and so on.

This confirms well (erring on the side of caution) with the findings of the NREL study on transformers as part of the WindPACT study and which estimated a 1580kVA transformer would cost $22,500 [132].

Switch Gear / Circuit Breakers

Figure 6.15 plots the current to weight ratio of a sample set of commercially available circuit breakers for current breaking capacities equivalent of 3MW up to 18.7MW at 690V. Although single poles HVDC circuit breakers do exist they are not considered here other than to show that they can obtain higher current breaking capacities for a given mass. The nominal choice would be a 3-pole or 4-pole arrangement (if breaking the neutral was considered necessary). The Figure shows that a 300% increase in rating from 9kA to 27kA achieves only a 33% increase in the current/weight ratio. The

relationship between current breaking capacity and mass is not significant enough to not be worth considering as an optimization parameter in the multi rotor system - given that circuit breakers weigh in at only a few hundred kg.

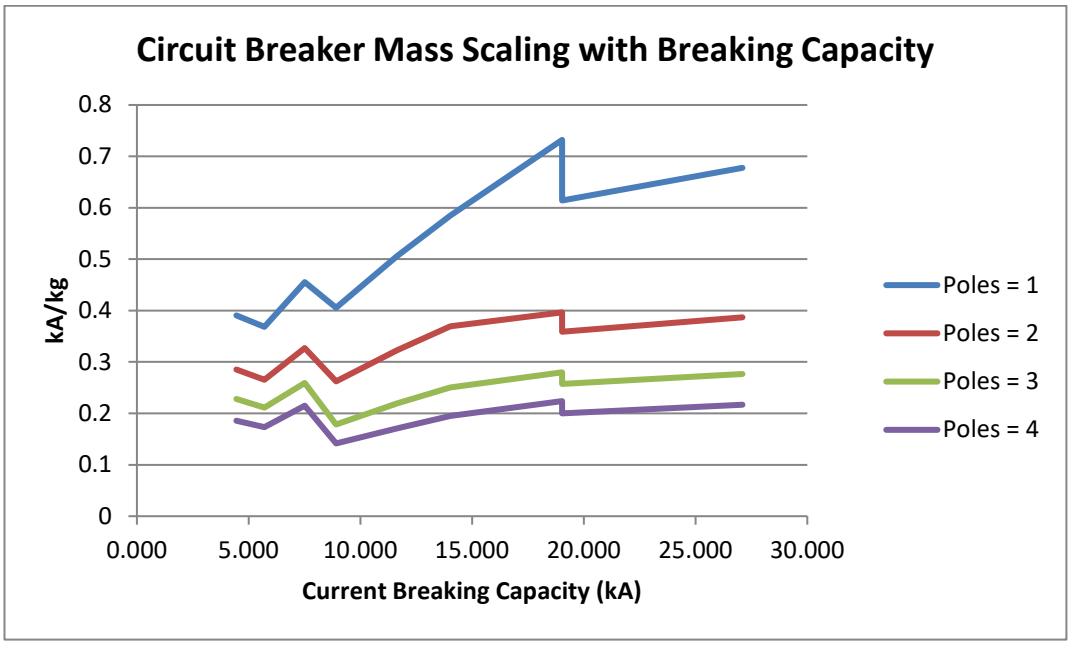

Figure 6.15: Circuit Breaker Scaling with Number of Poles

The circuit breakers need to be sized according to the fault current breaking requirement. It is proposed that the circuit breakers should nominally be located on the secondary (higher voltage side) due to the lower level of fault current. These values are provided below for both a single stage (690V) and two stage collection (3,330kV). Working is provided in Appendix D.

For the case of generated voltages being stepped up to 6kV the fault breaking requirement (per machine) would be 1.37kA. A cluster of 5 machines could be serviced by a circuit breaker rated for a fault current of 6.94kA.

Circuit breaker costs scale linearly with rating and therefore there will be no cost advantage or disadvantage in the multi rotor system - unless serviced by additional circuit breakers over and above 20MW overall capacity. However, cases 2 can make a saving in circuit breakers as it can utilise more than one circuit breaker to limit fault current - whereas both cases 1 and 3 have limited options.

The NREL model uses a value of $7/kW for scaling of switchgear and in the absence of any additional data this is the convention used here. In this case the total cost for the system will be dependent on the collection grid layout.

6.3.3.3 Case 1: Single Stage Collection

Case 1 assumes that individual generators are collected, routed to ground and then stepped up to transmission level or wind farm level voltages

Typical wind farm generation voltages are 460V but it is proposed that it would be worth the cost to generate at slightly higher voltages, 690V and eschew the use of transformers in case 1. Figure 6.16 shows the single line diagram for the 45 generator multi rotor array with two 20MVA transformers placed at the base of the tower. These transformers are weighted on the assumption of transformation to a medium voltage of 6 kV, but other higher values could be selected. The voltages that are ultimately chosen will greatly impact on the power losses and overall weight of the array and this will be considered in more detail in the next section.

The main issue with this type of arrangement would be the large current flow throughout the array which would necessitate higher rated cables. The higher current would lead to high cable losses and would also pose issues with breaking current (requiring large and expensive circuit breakers). The requirement for large circuit breakers may force the circuit breakers to be placed at base of the tower rather than at each node. This would remove any uninterrupted fault clearing capability within the array.

In figurative terms: 27.43kW or around 0.137% of rated capacity would be lost as Ohmic losses in this configuration assuming a copper collection grid and a collector voltage of 690V. The mass of the collector grid in terms of raw material would be 39.97 tonnes with an estimated material cost of £364,291. The combined mass of the two transformers is 56.2 tonnes, however this arrangement has a very key consideration in that the transformers can be placed at ground level where weight and size are not an issue. Note that both transformers would take full load in the event of a fault thereby providing N+1 redundancy.

Individual circuit breakers are shown in this case for each generator each capable of breaking 12.06kA. One circuit breaker could be used to service an entire group and would be rated at N times this value. The weight of the circuit breakers would be on the order of a few hundred kg and inconsequential in the grand scheme of things. The choice of grouped or independent circuit breakers depends on how faults should be cleared within the system. Individual circuit breakers allow for quicker clearing of faults at slightly increased initial capital cost. For example, using the convention \$7/kW the circuit breaker capital costs in case 1 would be \$139,860 (£87,400).

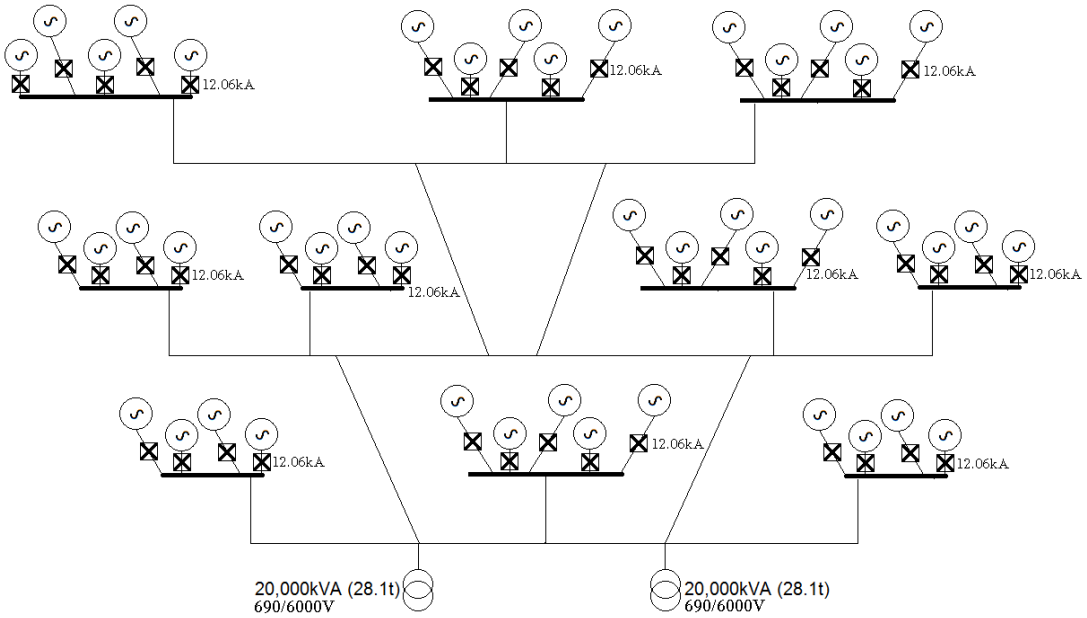

Figure 6.16: Single Line Diagram Case 1

6.3.3.4 Case 2: Two Stage Collection

Figure 6.17 and Figure 6.18 show a single line diagram for a two-stage voltage collection grid. In this case machines are grouped into groups of 4 or 5 generators which are connected to a common busbar, with the generated voltages being stepped up from 690V to 6kV. Each transformer in this case is rated at either 2MVA or 2.5MVA and combined weight (oil filled) would be around 4.5-5.28 metric tonnes. These transformers would necessarily have to be located within the nodes of the array, for structural, electrical and aerodynamic reasons.

Case two has several advantages over case 1: that the circuit breakers can be located after the first step up and as a result they are less in quantity (1/4.5) and need only break just over 1/10th of the current as in case 1. The mass requirements overall are therefore much reduced. The cost of circuit breakers is insensitive to rating so the saving is primarily in mass. As a representative mass, a 3-pole circuit breaker capable of breaking 2500kA of current would weigh only 100kg. Fault current requirements would be considerably higher than this. Having such large electrical components and associated weights located at points in the array which are particularly slender does open a host of mechanical and structural questions. The addition of these substantial weights could adversely impact on the modes of the whole structure for example, and certainly would require additional strengthening above and beyond that already discussed.

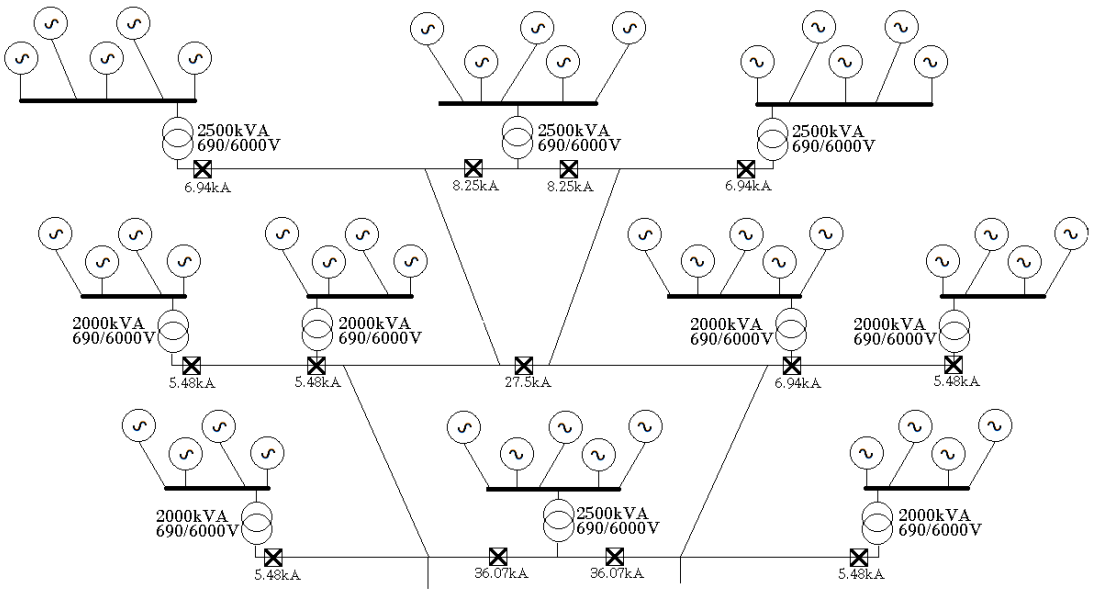

Figure 6.17: Electrical Layout Case 2

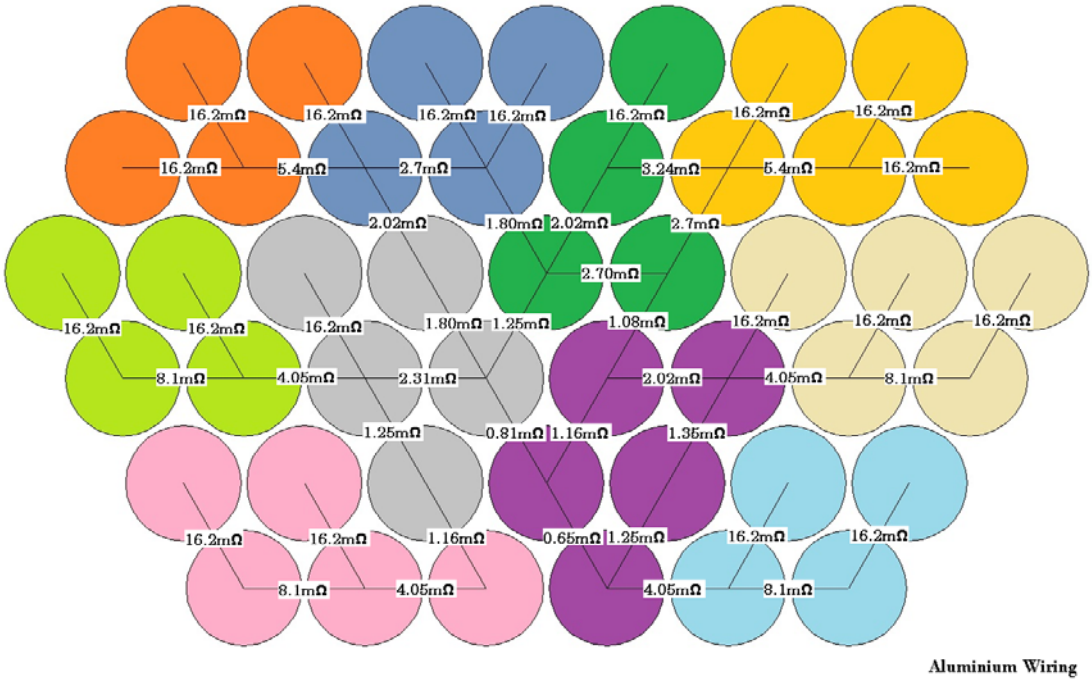

Figure 6.18: Case 2 with Groups Coloured and Cable Resistances Labelled

Case two suffers from several problems:

1. Generators cannot connect onto bus bars or cables at the wrong voltage. This means there is additional wiring overhead as each generator must be wired to a common busbar in its group.

2. The bus bars are additional costs over and above the normal wiring of case 1 and 3 for some of the groups.

3. There will be some conduits where more than one set of cables is required and with power flow in opposite directions.

4. The use of centralised transformers will reduce some of the cabling redundancy, as the likeliest cause for cable fault would be CHS member failure (through fatigue or blade strike) and each rotor would only be wired to one busbar and transformer.

In figurative terms, it is estimated that 3.94kW would be lost on the array side in a copper array with a further, 23x616W turbine side leading to 18.1kW losses total. This represent a power loss saving of 9.33kW on case 1. The total mass addition to the array in case two would be approximately 25 tonnes worth of transformer and 1 tonne

worth of circuit breakers for a total mass addition of 26 tonnes - or less than half of the weight proposed in case 1. However, the key difference would be that this mass would be at height and impose an unknown structural cost. The collection grid from 6kV down to the feed would be 4.59 tonnes and the individual generator feeds to the common busbar of each grid add an additional 3.415t for a total grid weight of 8 tonnes. In terms of collection grid cost, this places case 2 around £72,010 in material cost.

6.3.3.5 Case 3: Individual collection

The final case considered is that of individual step up transformers located as close to each generator as possible and stepping up the generated voltages from 690V to an intermediary 6kV collector voltage (Figure 6.19). Figuratively this would require a total machine weight of around 1.62t per turbine for a total weight of 72.9 tonnes distributed across the array. A Circuit breaker for an individual generator rated at 550kA would weigh in at only 27kg, small enough to be insignificant. The added weight to the array in such an individual collection system would be in the region of 4.597 tonnes in terms of cabling mass and cost in the region of £41,900.

Stepping up to 6kV would reduce losses to 3.15kW for the whole array, which is around 11% of those predicted in case 1. This would lead to substantial cost savings during operational life.

Switch gear / circuit breaker capital costs will be the same as for case 1 (given individual switch gear per turbine) and would be $139,860 (£87,400).

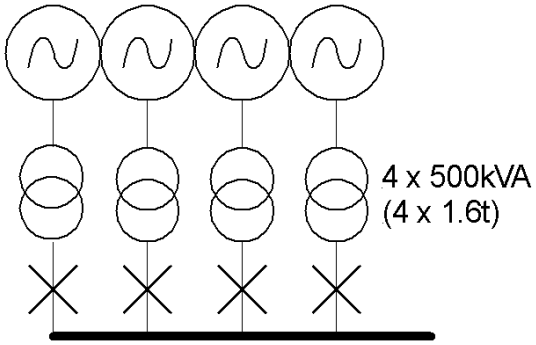

Figure 6.19: Electrical Layout Case 3 (Example of a Single Cluster)

6.3.3.6 Physical Considerations

One of the most difficult aspects of the multi rotor system which marks it differently from a standard wind farm is space constraints on the space-frame. The objective of the space frame design was to minimize mass and it has been designed to be as compact and slender as possible. The addition of bulky power electronics, several tens of metres above the ground does provide a logistical and engineering challenge.

Consider the 2500kVA transformers proposed as per case 2. Typical sizing for such a machine would be in the region of 2.1m height, 1.8 width and 2.1m length. Compare this scale against that of the proposed nacelle, as per Figure 6.20, and note that a conventional transformer cannot fit within the confines of the nacelle. This means that the transformer must necessarily be placed either within, or on the structural frame itself.

The 550kVA transformers proposed in case 3 do not suffer from the same problems as that of case 2. Figure 6.21 shows a typical 550kVA machine placed next to the proposed nacelle. The dimensions are very similar and it is conceivable that a custom transformer design which was adapted to be smaller in height could fit within an elongated nacelle housing. The ability to encapsulate the transformer within the nacelle housing would be a massive boon as it would not impact significantly on the aerodynamics/drag of the super structure. It would also simplify the structural analysis as the mass of the transformer could be lumped with the mass of the rotor and power-train instead of considered separately.

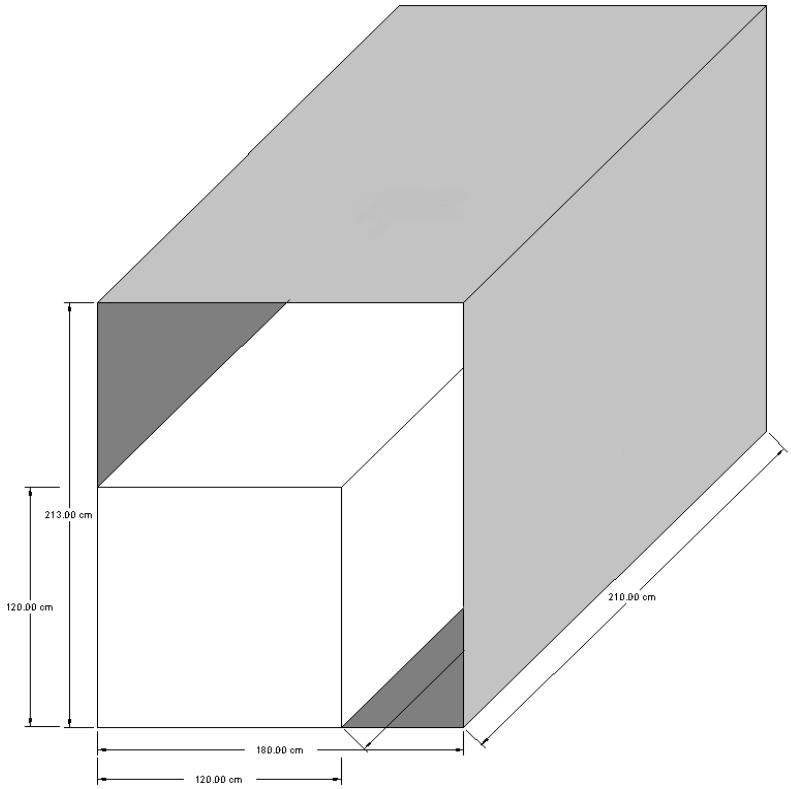

Figure 6.20: Proposed Nacelle (inset) Sized Against 2500kVA Transformer (shaded)

Transformer over-current protection should be 120% of full load current and have a time-delay setting of around 0.1s to enable the device to ignore the initial large magnetisation currents when the system is energised. Over-current protection on the primary side is typically a circuit-breaker sized for the transformer rating of 2000kVA.

A cost of £100 per kVA of fault breaking capability is assumed. This would include the circuit breaker mechanism, plus any isolator switches, voltage and current transformer, magnetic relays and so on.

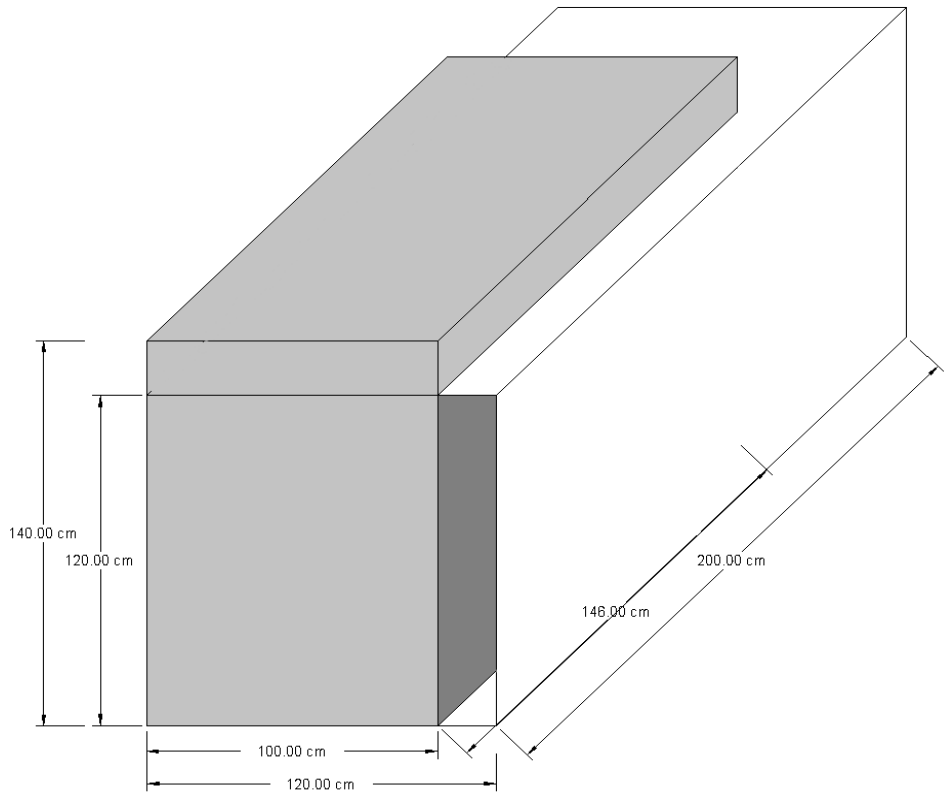

Figure 6.21: Proposed Nacelle Sized Against 550kVA Transformer (shaded)

6.3.3.7 Other Costs

The cost of power electronics is very hard to establish as the final cost per unit will be ruled by a huge number of factors. A ball park figure is all that is required at this stage.

Power Converter

500kVA converters can be found (OEM) for around $3,000. The price increase is relatively linear to power rating.

An NREL study which included the cost of power electronics gives the figure as $79/kW of capacity or £48.75/kW. This would make the full power electronic system for each 444kW machine (requiring a 500kVA converter) cost in the region of £24,375.

Jointing

Joints often represent the weakest points in electrical networks, being a construct of human endeavour. The multi rotor has a requirement for many more electrical joints

than even a typical wind farm - with a minimum of 156 individual cable joints in the electrical collection grid.

Assigning a value of each joint of £500 then the total additional CAPEX cost is £78,000. This cost is not so much a material cost as it is a time cost - as each joint can take more than one hour to complete (shielding stripping, joining, reapplying non-conducting coatings and then re-shielding). This cost could be alleviated by the provision of readymade cable lengths with pre-existing spliced ends that could be quickly jointed and which would make economic sense in a wind farm comprising several dozen multi rotors.

6.3.4 Summary

Electrical systems only account for 1.3% of energy lost over a typical year (Chapter 3). Transformers will make up a suitably small amount of this. Case 1 assumes that each transformer is capable of full load thus there will be no downtime associated with transformers. Case 3 each turbine has its own transformer and the losses as a percentage of system production will be very small. A decision on the best configuration for transformers should be based on the balance of losses versus structural cost.

Lost revenue is based on a capacity factor for the lifetime of the system of 52% (upper limit) and an energy market price of 12p/kWh (conservative) or 16p/kWh (upper limit). It is assumed that the cost of energy rises in line with inflation at a rate of around 3% per year. The actual final figures for lost revenue are not important and therefore this choice of energy price is also not important. The only interest these figures provide is to put a monetary value on the losses associated with each choice and as such give representative figures which reflect actual operating costs (opportunity costs) as an alternative to capital costs only.

The figures suggest that the choice of electrical layout composition gives very little variation in terms of overall life-time cost regardless of energy price.

Case 1 loses slightly less power due to increased transformer efficiency and could save something in the order of a few hundred thousand pounds over a 20-year system lifetime. However, the increase array capital costs bring the total cost slightly higher than case 2 or 3. Thus case 1 appears to be the non-optimum case regardless of revenue lost.

Case 2 and 3 are very closely matched, with case 2 appearing slightly cheaper at lower energy costs. However, as energy prices increase, case 3 becomes more optimum.

Given the fact that case 3 is either equal to or better than both case 1 and 2 - it can be assumed that this is the likely optimum case for electrical interconnection of the multi rotor system. Comparing case three's capital costs with values reported within the wider wind industry allows for some observations.

In 2009 EWEA reported that the typical costs of an electric installation for a single rotor is in the region of €18,000 per MW of installed power. Scaling up, a 20MW single rotor might be expected to have costs in the region of €360,000 or £290,000 which when adjusted for 5 years of inflation (at 3%) arrives at a value of £336,000. This final value is around 62% of the capital costs presented for case 3 of the multi rotor electrical array (£539,000) [133] and which is presented in Table 6.5.

	Grid (£k)	Trans (£k)	Electronics (£k)	Jointing (£k)	Fault Protect. (£k)	CAP Ex. (£k)	plus losses @ £0.12/kWh	plus losses @ £0.16/kWh
Case 1	364.3	500	84.38	78.0	54.2	1,080	3,575,179	4,406,616
Case 2	72.0	275	84.38	78.0	16.4	525.0	3,348,327	4,289,164
Case 3	41.9	281.2	84.38	78.0	54.2	539.0	3,430,058	3,865,468

Table 6.5: Summary of Costs - All Values in GBP

A moderate increase is expected given the electrical complexity of the multi rotor system and in fact at the start of the project it was estimated that electrical integration may have a premium scale factor of 2 on an equivalent single rotor and this has proved to be close to the mark - if not on the conservative side.

Table 6.6 contains a summary of the reported electrical cost data for three different ratings of wind turbine electrical equipment as reported by the Wind Energy

Association. Scaling up the 3MW by a factor of 6.6 arrives at a final figure of $1,545,218 or approximately £1 million. This is roughly equivalent to the estimated value of case 1 in the multi rotor array, or double the estimated cost of case 3 and the EWEA data.

	750 kW		1.5 MW		3 MW		Method
	Cost, $	Cost/ kW	Cost, $	Cost/kW	Cost, $	Cost/ kW	
Power electronics	26,560	35	53,119	35	106,238	35	Power rating
0.95–0.95 substation VAR control	5,779	8	11,557	8	23,114	8	Power rating
Transformer	12,938	17	25,875	17	51,750	17	Power rating
Cable	8,023	11	16,046	11	32,092	11	Power rating
Switchgear	5,233	7.0	10,465	7.0	20,930	7.0	Power rating

Table 6.6: Summary of Electrical Costs for a range of Wind Turbine Ratings [134]

There is significant uncertainty in the electrical cost to justify a more detailed study out-with the scope of this PhD study. However, this limited study has shown that the electrical costs of the MRS array are not likely to be prohibitively expensive when compared to equivalently rated single rotor systems.

Even with a cost premium, the multi rotor can obtain several advantages over the single rotor, namely increased redundancy and less impacts of faults. These advantages should be borne out in future O&M cost evaluation conducted in Chapter 6.

6.4 PROTECTION SYSTEMS

6.4.1 Introduction

The last area of investigation for the multi rotor array is in the protection systems - an important aspect of any wind turbine system. This is particularly true of the multi rotor systems, for which the protection systems have a unique ability to provide load alleviation. The ability to alleviate loads out-with normal aerodynamic pitching methods, is an important ingredient of minimizing the cost of the MRS.

6.4.2 Grid Stability

The stability and reliability of national grids depend strongly on the penetration of wind farms and other highly variable generator systems. The increasing penetration of wind farms around the globe and especially in Europe has led to operators modifying their Grid Codes to allow for larger integration of wind. Wind farms must maintain an uninterrupted supply throughout power system disturbances and in turn support the network voltage and frequency. To do this, they must provide low voltage ride through (LVRT) and reactive or active power capabilities. Low voltage ride through is particularly important to maintain in areas with a high concentration of wind power generation (such as offshore wind farms). If the wind turbines are not designed with such standards in mind then any power systems disturbance may lead to cascading turbine failures which may amplify the disturbance on the grid [135][136].

Voltage dips which require LVRT capabilities are characterised as a drop in voltage of between 10-90% and lasting between 1 cycle and 1 minute. They are typically caused by short-circuits and earth faults throughout the grid.

Operator grid codes specify that wind turbines must support voltage dips at the point of inter-connection with the transmission network without tripping. The amount of dip and the time that it may last are dependent on the operator, but most allow for voltage dips that last a maximum of 0.1-0.5s. Figure 6.22 shows the fault ride through requirements for the largest distributed network operators (DNO's) in the UK/EU.

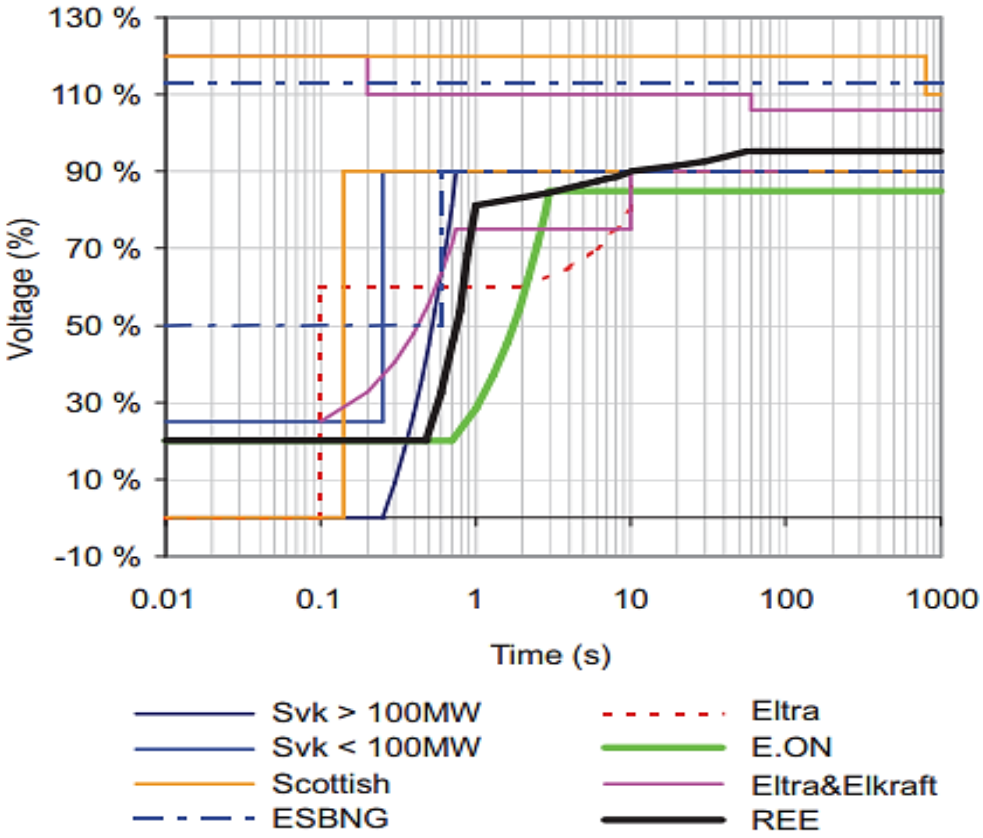

Figure 6.22: Ride Through Requirements for the main DNO's in Europe [137]

6.4.3 Fault Ride Through: Voltage Dip

During a voltage dip, the power injected into the grid is reduced immediately, despite the output power from the PMSG remaining constant. This imbalance of power results in a rise of the DC-link voltage of the back-to-back converters which in turn can damage the power electronics [138].

If the DC voltage is controlled about its reference voltage, the current injected into the grid by the grid-side inverter will increase sharply which may also destroy the converter. An energy discharge circuit is required to dissipate or store the energy that is not able to be injected to the grid during the dip and in turn help limit the DC voltage rise - with the aim of protecting the power electronics - the options for this are discussed in the next section.

To understand this effect in more detail, consider the following equations. The power injected to the grid from the PWM converter, P_e is expressed in the phase reference frame (a,b,c) as the sum of all three phases:

$$P_e = v_a i_a + v_b i_b + v_c i_c \tag{6.1}$$

In a synchronous reference frame (d-q) it can be alternatively expressed as:

$$P_e = v_d i_d + v_q i_q \tag{6.2}$$

When the q-axis is orientated to the direction of the grid voltage vector, the d-axis lags it by 90 degrees and is therefore zero, simplifying the expression to:

$$P_e = v_q i_q \tag{6.3}$$

If the grid-side invertor was working at its upper current limit with unit power factor before the voltage dip. When the voltage dip occurs, the input power from the generator is higher than the power being exported to the grid and must be reduced to avoid an over-voltage in the DC-link.

The power injected into the grid becomes P_f and if the quadrature current is controlled to remain constant, the voltage (v_{qf}) must decrease away from the reference (v_q):

$$P_f = v_{qf} i_q = P_e \frac{v_{qf}}{v_q} \tag{6.4}$$

On a short time-scale and to maintain rotor inertia (on the assumption the fault will last only a few seconds) this can only be achieved by letting the rotor accelerate to a new operating point where C_P is lower than optimum. The increasing rotor speed leads to increased electrical frequency which the stator windings resist and result in a lower e.m.f voltage. It is important at this stage that the controller limits the speed of rotation of the rotor through pitch actions to a safe level until the voltage dip has cleared and the power demands from the grid exceed that now generated by the wind turbine. A fault ride-through capability of a few seconds can thus be achieved.

6.4.4 Power Electronic Arrangements

The protection of wind turbines, particularly their power electronics is initially more important than staying connected to the grid. In offshore locations, this leads to the introduction of power systems protection turbine side.

For large-scale systems based on voltage-source converters, the serious short-circuit fault consequences are an over current along the DC cable due to capacitor discharge and the removal of load torque which results in wind turbine over speed. Thus, a fast DC circuit breaker (CB) / fuse is required along with other electrical over speed limiting methods such as a dump resistor which is used to dissipate excess power during power transmission disruptions.

There are several possibilities for dump loading and these are depicted in Figure 6.23. Note that not all options could be considered in isolation and most would generally be employed in addition to pitch control. Each of these options is considered briefly.

6.4.4.1 DC CB and DC-Chopper

A DC circuit breaker is used to rapidly interrupt the DC over current from the capacitor discharge. However, this will result in DC-link voltage increase which could result in flash over. Inserting a braking resistor into the DC-link between both convertors acts as a dump load to restrain the DC-link voltage. This type of protection system is more useful as an option for enhancing fault ride-through capability of PMSG's and is not suitable for mechanical load alleviation as required from Section 4.

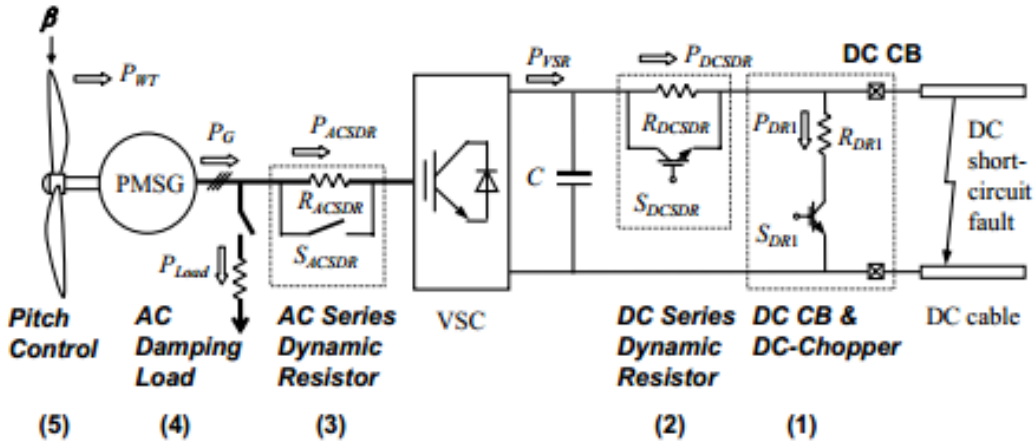

Figure 6.23: Protection Options Turbine Side: 1-5 [139]

6.4.4.2 DC Series Dynamic Resistor

A DC series dynamic resistor can be placed in the DC-link circuit to help reduce a large DC over current and protect the convertor equipment. A fast solid-sate switch is used to bypass or engage the resistor during normal operation and fault conditions.

6.4.4.3 AC Series Dynamic Resistor

On the AC side of the turbine a power-electronic-controlled AC series resistor, which is connected to the stator windings of the generator can be used to limit the rotor acceleration during a fault. This three-phase braking resistor is used to consume the active power being fed from the generator and thereby improve generator stability during a fault. The advantages of a series dynamic braking resistor, when connected to the generation circuit, were studied by Yang [137]. It was used to enhance the fault ride-through of a fixed speed wind turbine.

6.4.4.4 AC Damping Load

A three-phase AC damping load is connected at the generator terminal to help dump the redundant energy generated by the wind turbine. This has an alternative use in traditional turbine-generator systems as an electrical braking system in case of mechanical failure.

6.4.4.5 Wind Turbine Pitch Control

Pitch control is widely used in large-scale wind turbines to cope with the incident wind over speed [139]. Pitch control can also be used as a method to reduce the rotor over speed if power damping is not adequate. If the power recovery is not required to be immediate, the turbine blades can be pitched to reduce the aerodynamic torque. Mechanical braking is usually used to hold the turbine standstill and will be used after and as a backup of the pitch-controller.

The resistance calculation is based on analysis of the redundant energy dissipation. The energy from the wind turbine should be dissipated by the protection scheme. Taking all the normal parameters as 1.0 per unit value, the resistance value should also be 1.0 p.u. in the steady-state operation of the protection circuit. For example, if the rating power of the generator is 5 MW, with a rectifier voltage of 1 kV, the resistance value is 0.8 Ω.

6.4.4.6 Summary

Yang conducted an excellent summary of these five different options each tested in conjunction with the operation of a 2MW DFIG machine and the rotor speed in the per unit system was recorded. Figure 6.24 shows the results of this investigation and which clearly show that the use of AC series damping load is the best over-speed limiting option and thus the only option that can seriously be considered as part of the multi rotor shutdown and load alleviation strategy - and will be expanded on in the next section. The other options shall therefore not be investigated in any further depth as part of this PhD.

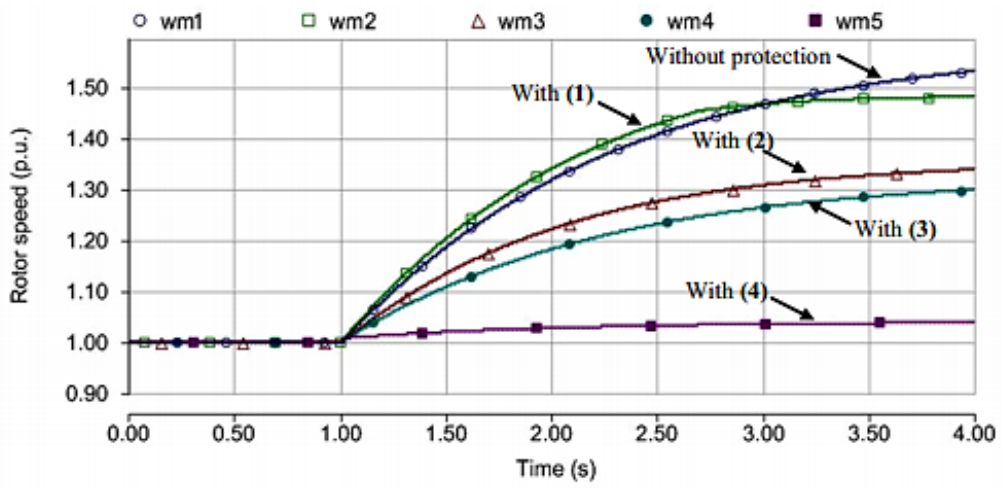

Figure 6.24: Comparison of Over-speed Limiting Protection Options, corresponding to Fig 6.28

6.4.5 Load Alleviation: AC Load Dump

The extreme designing load case for the multi rotor system would occur if all the rotors in the array were simultaneously shutdown - for example, to avoid over-speed after a system wide fault. This corresponds to the IEC design scenarios DLC2.3 and DLC4.2.

The ability to stage the shutdown of rotors in the array - by only a few seconds - is enough to eliminate these scenarios from structural design considerations, which in turn will bring down the cost of the structure.

One method of enabling a staged shutdown is to provide dump load resistors for the MRS such that the loss of the grid does not immediately result in a loss of load and therefore rapidly increasing rotor speeds. The requirements for such a load dump would be that it draw power for a set period while enabling a staged shutdown of all the rotors in the array. The load itself would need to draw the full rated power from the array, though the total power through the load would reduce gradually over this period.

There are two types of load dump that might be contemplated either in isolation or partnership. The first would be an auxiliary battery bank which would be charged - but limited by current input and therefore of limited capability. The second is a set

of simple load dump resistors whose only job is to absorb the power and convert it to heat safely, for dissipation into the surrounding environment. The latter would be limited only by size and weight considerations.

For a 45-rotor array rated at 20MW a potential load dump system has been investigated. This would comprise of 900 individual resistors in the form of 45 parallel paths of 20 resistors formed from a mixture of iron and copper. With individual resistance of 21.5Ω, a specific heat capacity, *C*, of 20 J/kg.K and mass of 5kg. The resistors have been sized according to a requirement of dual-staged (pairs of rotors) shutdown with stages offset by 2.35s each.

Initial Ohmic heating would exceed 222°C/s (assuming no loss), however the system load will be successively reduced such that no individual load resistor will a safe percentage of melting point. With the addition of a fin heat-sink array and potentially (offshore) the use of water cooling will help ensure that the load dump system can safely dissipate the MRS load for the duration of the shutdown.

All this could be achieved using individual resistors with sizes in the region of: 0.1 x 0.075 x 0.075m resistors weighing in at 5kg for a total system weight of only 4.5t - which in comparison to the additional structural requirements to design for DLC2.3 and DLC4.2 (in the region of 200-300t) the weight cost is inconsequential. See Figure 6.25 for the line diagram of the electrical layout.

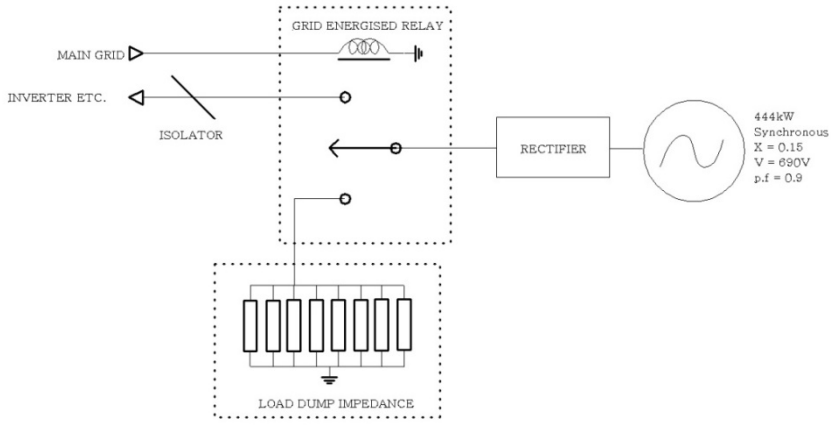

Figure 6.25: Line Diagram of Load Dump Resistor (AC Series Damping) Configuration

6.5 DISCUSSION

The use of variable speed permanent magnet generators has been identified as the best compromise between compactness, cost, efficiency and improved reliability. The absence of any gearbox is a key improvement in terms of system reliability. It is proposed that each power train be serviced by its own power converter based on voltage controlled source inverters to separate frequency. Clustering of machines (fixed frequency) was investigated and found to provide some savings in cost in exchange for a loss of energy capture due to in-optimum C_P tracking. It was inconclusive whether this would be a worthwhile saving to make given it would remove some redundancy from the system and merits more detailed research.

This chapter has developed a rotor layout and electrical interconnection for the multi rotor system based on CAPEX costs, cost of operation and structural penalty (mass) in the array. The priorities of the development have been to identify an arrangement that minimizes these costs while achieving a good level of redundancy and making use of both the multi rotors ability to capture additional energy from turbulence (over and above a large single rotor of equivalent rating) and its load alleviation requirement as discussed in Chapter 4.

The difference in capital costs for the three potential options for power collection, that of:

- Case 1: Individual collection at generated voltage with transmission to base.
- Case 2: Grouped collection with transformation to MV before transmission to base.
- Case 3: Individual transformation to MV before collection and transmission to base.

Analysis of likely material costs has shown that Case 2 and Case 3 have an advantage on the order of half a million pounds in CAPEX when compared to Case 1. However, when considering losses at likely energy sale prices the difference in all three options becomes much reduced. With the difference as low as £140,000 or £400,000 over a twenty year operational lifetime, assuming a 52% capacity factor and £0.12 or

£0.16/kWh respectively. Table 6.7 shows a summary of these costs as developed within this chapter.

	Grid	Transformer	Power Elect.	Joints	Fault Protect.	Total Capital	plus losses £0.12/kWh	plus losses £0.16/kWh
Case	364,291	500,000	84,375	78,000	54,200	1,080,8	3,575,179	4,406,616
Case	72,010	275,000	84,375	78,000	16,430	525,81	3,348,327	4,289,164
Case	41,893	281,250	84,375	78,000	54,200	539,71	3,430,058	3,865,468

Table 6.7: Summary of Collection Grid Costs

Case 3, that of a collector array with each turbine generator stepped up to 6kV through its own independent transformer has a small advantage over the other two options when considering both capital cost and losses associated with collection at different levels of voltage and different size transformers. In addition case 3 has a high level of redundancy with individual transformer, circuit breaker, or cable faults not resulting in more than a small percentage (2.2-8.8%) of actual rated capacity lost. A high level of redundancy will help reduce O&M costs and should reduce total CoE in comparison to systems with lower levels of redundancy.

It is acknowledged that there is some limitations to this analysis. Cost data for power electronics, jointing, fault protection and even the final cabling cost beyond raw material is difficult to quire. Data presented here is based on tentative figures found in the public domain, with scale factors used to ensure that figures err on the side of caution. The main conclusion is that case 3 is the optimum choice of collection grid and this conclusion would not be affected by changes in material costs - given that it would affect all three cases equally.

Lastly, this chapter has investigated likely protection systems requirements for the array and found them to be like that of conventional single rotor machines. The only difference is that the AC series resistor takes on more prominence in the multi rotor array, given that it has an additional load alleviation requirement beyond fault-ride through.

The total cost of the multi rotor system electrical interconnection is around 60% higher than that predicted by EWEA for single rotor machines. However, the EWEA study

does not include the cost of transformers and these can comprise a large component of final CAPEX cost. Following the same conventions as carried out in this chapter for 10MW single rotors (2x10MW) with transformers at base results in estimated electrical costs in the region of £1,000,000. In this case the multi rotor achieves a saving on the order of 46% because due to a use of higher voltages from point of power collection to ground - allowing for less cabling mass. Something which the large single rotors cannot take advantage of due to space constraints in the nacelle.

CHAPTER VII - REVIEW OF THE MULTI ROTOR STRUCTURE UNDER ULTIMATE & FATIGUE LOADING

7.1 INTRODUCTION

The loads analysis carried out in Bladed and presented in this Chapter preceded the final structure design. The layout was predetermined (as described in Chapter 3) without any rigorous investigation of alternatives which would have significantly increased the work of this thesis as the merits could only be established retrospectively after a full loads analysis and costing. The aim for the original layout design was to develop a workable arrangement combining efficient stacking of rotors while limiting the height of the centre of thrust and minimizing the base footprint. The initial loads analysis in Bladed provided aerodynamic loads at each rotor centre without any interaction from structural dynamics [140].

By revisiting this problem, it will be possible to identify whether the original iterative process and load estimates were suitable for ensuring a structurally sound design and at the same time make a case as to whether the structure should be strengthened or weakened as appropriate. With the final structure in place it will be possible to arrive at an estimated capital cost for the entire system using both established and newer cost models.

Before revisiting the structural optimisation problem there required some consideration of the effects of wind resolution on the load simulation results presented in the previous chapter. It was decided that a check of the effect of wind resolution on loading was required to validate the results which had previously been carried out.

7.2 SIMULATION LIMITATIONS

7.2.1 Wind File Resolution

Bladed has a hard coded limitation due to standard computer system memory resources which limits wind files to 50 lateral point and 50 longitudinal points for a 50x50 point grid spanning the X-Y plane. This 50x50 resolution is quite suitable for single rotors as there can be any number of points covering each blade up to a maximum of 25. For a large multi rotor system such as the one proposed with 45

rotors, the lateral and vertical spacing is such that even when using a 50x50 grid there are only 1 or 2 points from the wind field spanning each blade. The low resolution of the wind field over individual rotor scales gave concern that the fatigue loading on the system may not be adequately represented and this was investigated.

To understand this affect in more detail requires examination of the energy auto spectrum for the rotors present in the system. Of interest are Hub F_x and Hub My which dominate the ultimate loading investigation.

The Bladed limitations mean that simulations can only be run using low resolution wind files. Individual simulations can be run for each rotor using a high resolution wind file, but these simulations will show no coherence between them and cannot give an accurate depiction of a wind field's effect on the structure as a whole. It was hoped that by combining simulations for each rotor in the frequency spectrum from both high and low resolution files that a good understanding of the predicted forces could be ascertained while maintaining a representative wind field. To achieve this, the auto spectrum plots of the two key forces: Hub F_x, and Hub M_y were created from the time history data.

7.2.2 Fatigue Calculations

There was a concern that the use of low resolution files (which can be used to accurately reflect coherent wind across the array) in any fatigue calculations would not accurately predict structural fatigue and subsequent failure. If the structural capacity was based on fatigue calculations using these low resolution files (which are much lower resolution than normally practiced in wind turbine design) then there is a chance the structural capacity would be lower than required.

The use of the high resolution files in isolation were not considered sufficient as a method of predicting the mechanical soundness of the current structure given that there is no correlation between the wind speeds on adjacent rotors and therefore it does not accurately reflect real environmental conditions.

Figure 7.1 shows three auto spectrum plots of hub Fx for three different rotors in both high resolution and low resolution wind. At the low end of the frequency scale, below 1P (4.8 rad/s) there is a tendency for the low resolution wind to under-estimate the amount of energy at these frequencies. It does however adequately capture 3P and 6P depending on the simulation in question. The high resolution wind fields on the other hand generate a more consistent view of the energy contained at each frequency, though they fail to capture any additional information above 3P.

It was decided that to create a consistent and as accurate an estimation of the energy at each frequency a file containing a combination of both high a low resolution forces should be created. This combination would contain all the information from the high resolution file above 1P and sum this with the low resolution signal. In this way, the high resolution files would be superimposing a modification to the force on each rotor adding to its accuracy while the underlying low frequency file contained all the data linking adjacent rotors (maintaining the correct coherency between locations) and therefore grounding the results. These combined forces signals would then be used in the fatigue calculations and the results compared with the same fatigue calculations using the low resolution signals only. If there is good agreement between the low resolution fatigue runs and the combined resolution fatigue runs then it can safely be assumed that the low resolution fatigue runs previously run would be sufficient.

The combined auto-spectrums from three of the F_x series (hubs 2, 8 and 17) can be seen in Figure 7.3. The high pass combination filter designed in MATLAB and used to achieve this is depicted in Figure 7.3.

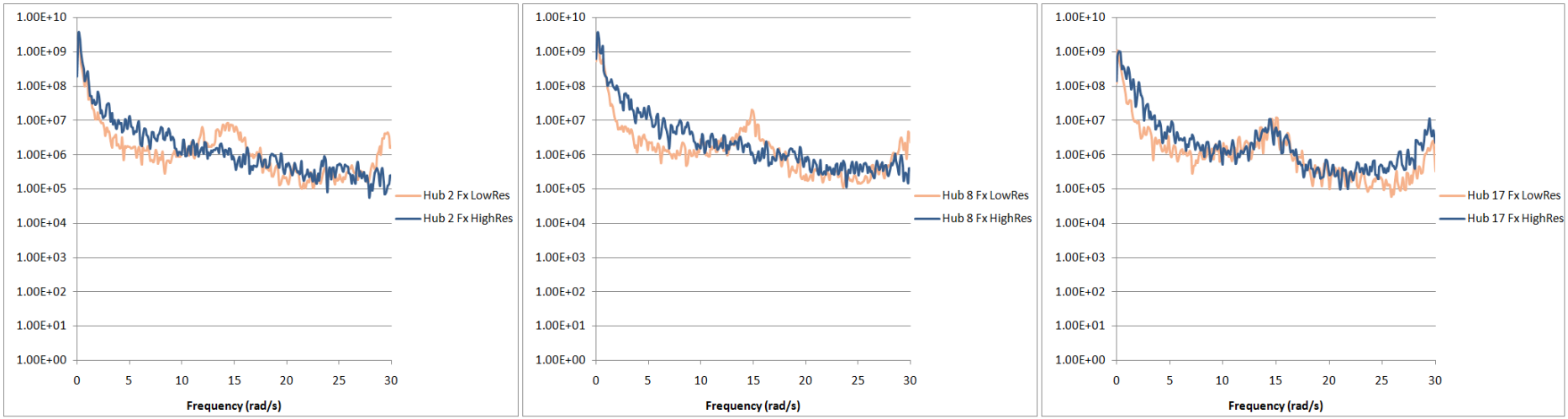

Figure 7.1: Examination of Hub Fx Auto-spectrum in High & Low Res. Wind

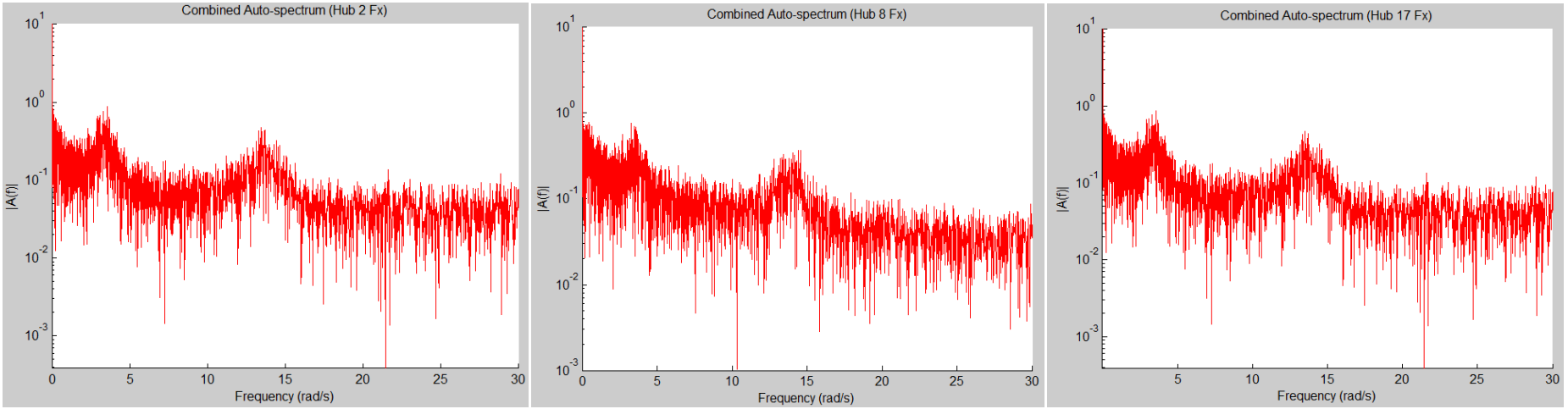

Figure 7.2: Hub F_x Auto-spectrum of Combined High & Low Res. Signals

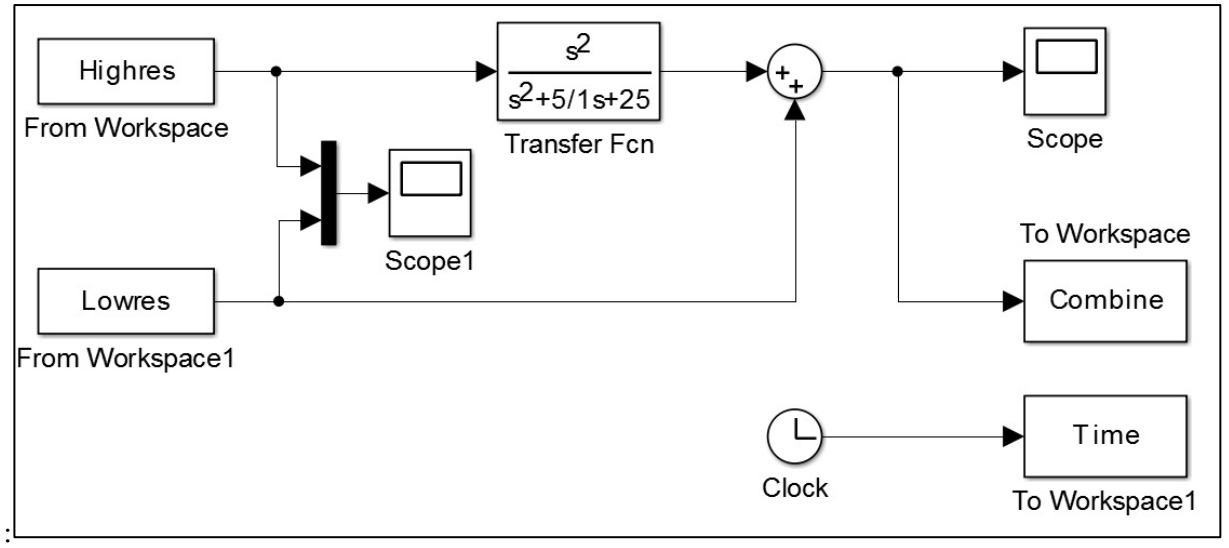

Figure 7.3: Simulink HPF for Combination of Low Res. & High Res. Signals.

From examination of the auto-spectrum plots in Figure 7.3 it is clearly apparent where 1P and 3P are and it is as these frequencies that the highest fatigue will occur. The high frequency component is clearly obvious when compared against the lower resolution Figures.

These results will be used within the fatigue analysis presented in the next section.

7.3 STRUCTURAL RE-OPTIMISATION

7.3.1 Ultimate Loading

The original MRS design was constructed using a theoretical thrust force on the assumption that the design critical loading would arise because of an extreme gust in a 50-year storm. The loads study conducted in this Chapter shows that this assumption was true but for the wrong reasons. The maximum thrust on the individual rotors is found to occur during operation at rated wind speed (DLC1.3). The original reference thrust (extreme storm) used was 75kN per with a safety factor of 1.35 for aerodynamic loadings (i.e. 101.25kN). In DLC1.3 individual rotor maxima can reach as high as 120kN without S.F or 162kN with safety factor applied. Crucially, the averaging effect of summing individual rotor loads (destructive interference) lowers the equivalent loading per rotor to 80kN (with S.F) which is below that of the theoretical value used previously.

It is proposed that on this basis alone, the structure would appear to have been over-designed and as a result not optimised in terms of load bearing capacity and weight. There is now a need to revisit the structural optimisation problem using the new loads data to establish if any weight savings can be made.

7.3.2 Yawed Flow

The IEC61400-3 standard does not require that single rotors be tested in ultimate loading conditions at every flow angle increment from 0 to 360 degrees. Instead the 50 year gust is restricted to +- 30 degree yaw error. It is acknowledged that very severe loading can occur from a rotor stuck in yaw errors of 180 degrees in an extreme

50 year storm however, generally this loading can be adequately captured from the load cases covering annual gusts which is typically tested at all yaw angles.

The multi rotor is in a unique position compared to its contemporaries in that the overall system is not designed based on operational rotor loads but rather is determined by extreme gust structural interference and associated loads. Thus, the optimisation problem becomes an issue of optimising member width and drag forces to arrive at a structure capable of surviving wind conditions at all directions.

7.3.3 Structural Drag

Consider a long cylinder in a fluid flow, in this case standard atmosphere. A generic plot of Reynolds number vs. coefficient of drag (Figure 7.4) shows that at high Reynolds numbers the coefficient of drag (C_D) for a cylinder is generally 1-1.3 through most of its operating range. It is generally accepted that at some values of Reynolds number the C_D on a cylinder will drop to as low as 0.4, as shown by the notch between Re $5x10^5$ and $5x10^6$. This is caused when the laminar boundary layer surrounding the cylinder becomes unstable and turbulent at $Re > 5x10^5$ [141].

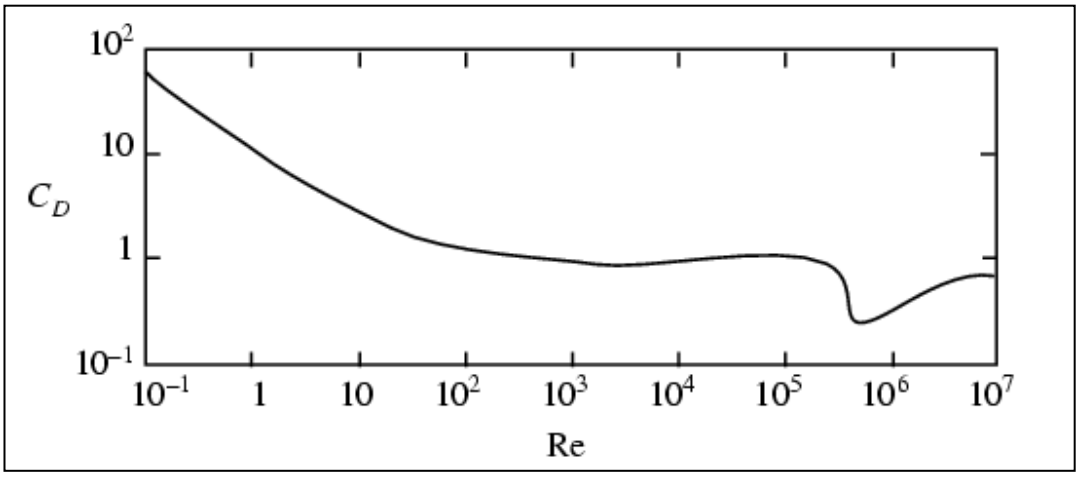

Figure 7.4: Effect of Reynolds Number on Coefficient of Drag (Cylinder)

The range of Reynolds numbers expected for a multi rotor system structure is slightly higher than the average single rotor. This is because individual members are much smaller in diameter (characteristic length) than a standard steel tubular tower due to a distribution of forces. This makes it entirely possible to use CHS members with

characteristic lengths in the minimum C_D region, though they will not stay there throughout the entire operational range of the machine. Figure 7.5 shows a plot of Reynolds numbers for a constant wind speed of 70m/s and 50m/s across all the proposed member diameters. It shows that most of the lighter/smaller diameter members will likely benefit from some reduction in C_D during extreme storm cases where the wind speed exceeds 50m/s given that the Reynolds numbers fall within the notch of Figure 7.4. This will undoubtedly lead to reduced loads across the structure in these design cases and is a benefit that most large rotor towers cannot take advantage of.

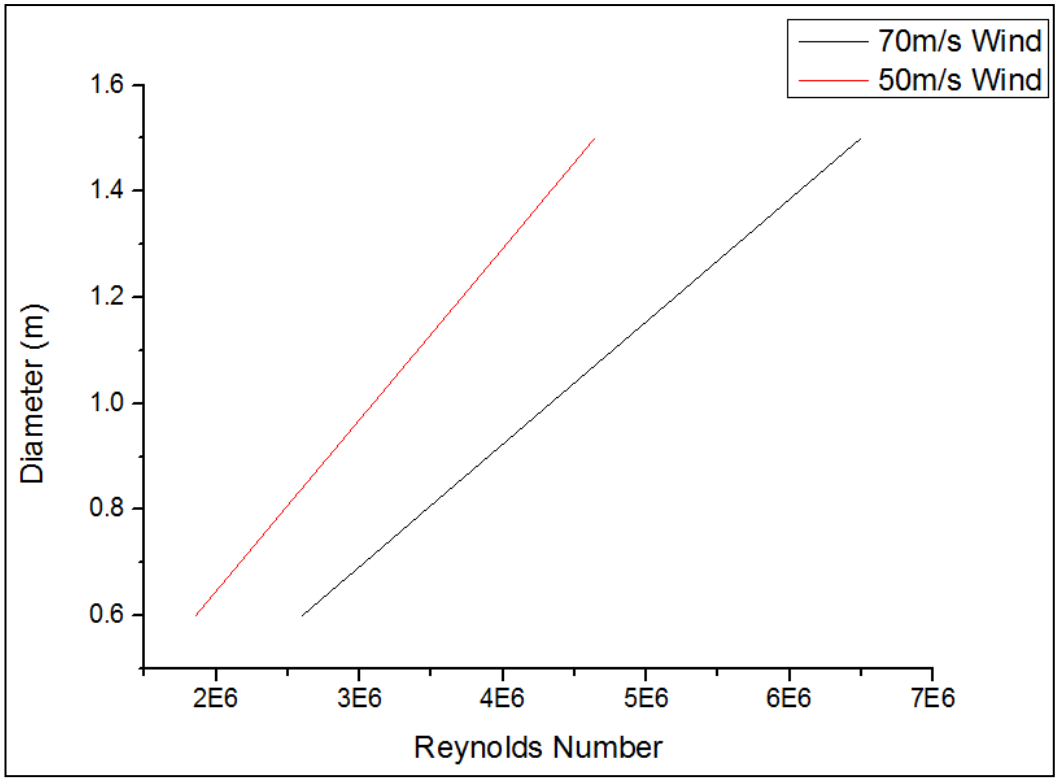

Figure 7.5: Members Reynolds Number for 70m/s Wind

Even without the adjustments for C_D within this range of Reynolds numbers it is clear to see (Figure 7.6) that at extreme wind speeds the actual rotor thrust contributes only a small amount of the total forces on the structure.

Consider a section of node 8 taken from the structure designed earlier. This is a node on the second level and has moderately wider and thicker members than many of the rotors on higher levels. Consider line loadings of 50% of total, given that the other

50% would be attributed to the adjacent rotor if the structure was sectioned off in this manner.

Figure 7.6 shows the force breakdown, with the rotor thrust represented as a single value in the central bracket and the drag forces on each member displayed on each line. In the case of a 70m/s wind speed, the rotor thrust contributes to only 5% of the total equivalent F_x loading. In the case of the 50m/s wind, the rotor thrust contributes only 10% of the total equivalent F_x loading. While each wind turbine will be experiencing locally different loadings, this generic example shows that there is a clear case for designing the structure based on optimising strength vs. drag alone. In other words, drag as caused by an extreme gust in a 1-year or 50-year storm is ultimately the main contribution to the critical design loads. This makes the multi rotor rather unique, in that the rotor design has very little impact on the structural design - in stark contrast to the single rotor.

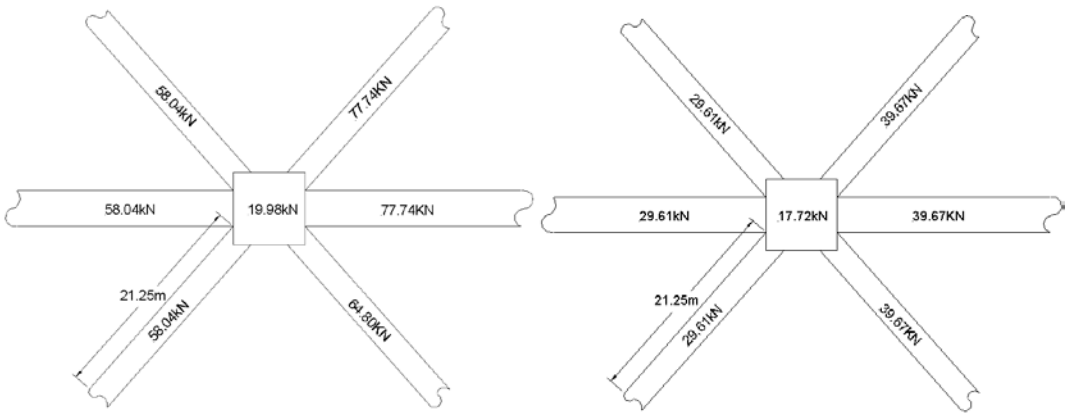

Figure 7.6: Left: Node 8 F_x Static Loadings @ 70m/s, Right: Node 8 F_x Static Loadings @ 50m/s

7.3.4 Space Frame Re-Construction

The space frame required strengthening in several key areas to be capable of surviving extreme drag forces under yawed flow. The new proposed cross-sections are presented in (Table 7.1). The layout of these CHS are presented in Figure 7.7, with each set labelled. The extreme wind case is simulated in 10 degree increments around the entire structure and a safety factor of 1.35 applied to all.

The structure was set up as per the initial concept and using the thickest type of member calculated in Mathematica and using the worst-case F_x loading as taken from Bladed and then iterated with successively decreasing member size until one or more structural failure. In this way, the structural members are optimised for minimum mass and structural integrity in the worst-case loads.

To simplify the engineering of a large space frame, a small number of circular cross-sections are selected from all those determined during optimisation (Table 7.1). The near optimum layout of these CHS are presented in Figure 7.7, with each set labelled.

Beam ID	**Outer Diameter (m)**	**Thickness (m)**	**Mass per Member (tonnes)**	**Number of Members**	**S (I_y/y)**	**M_{yield} (MN/m)**
CHS3	0.6096	0.0064	4.04	8	0.0018	0.642
CHS4	0.7112	0.0064	4.73	24	0.0025	0.878
CHS5	0.8128	0.0071	5.99	26	0.0036	1.273
CHS6	0.9144	0.0079	7.50	32	0.0051	1.794
CHS7	1.016	0.0087	9.18	30	0.0069	2.439
CHS8	1.117	0.0095	11.02	20	0.0091	3.220
CHS9	1.219	0.0111	14.05	36	0.0126	4.472
CHS10	1.320	0.0127	17.39	12	0.0169	5.991
CHS11	1.422	0.0191	28.07	14	0.0291	10.337
CHS12	1.524	0.0254	39.88	8	0.0440	15.636
CHS13	1.625	0.0318	53.07	10	0.0621	22.063

Table 7.1: List of structural members and properties. S is the section modulus and Myield the yield strength under bending.

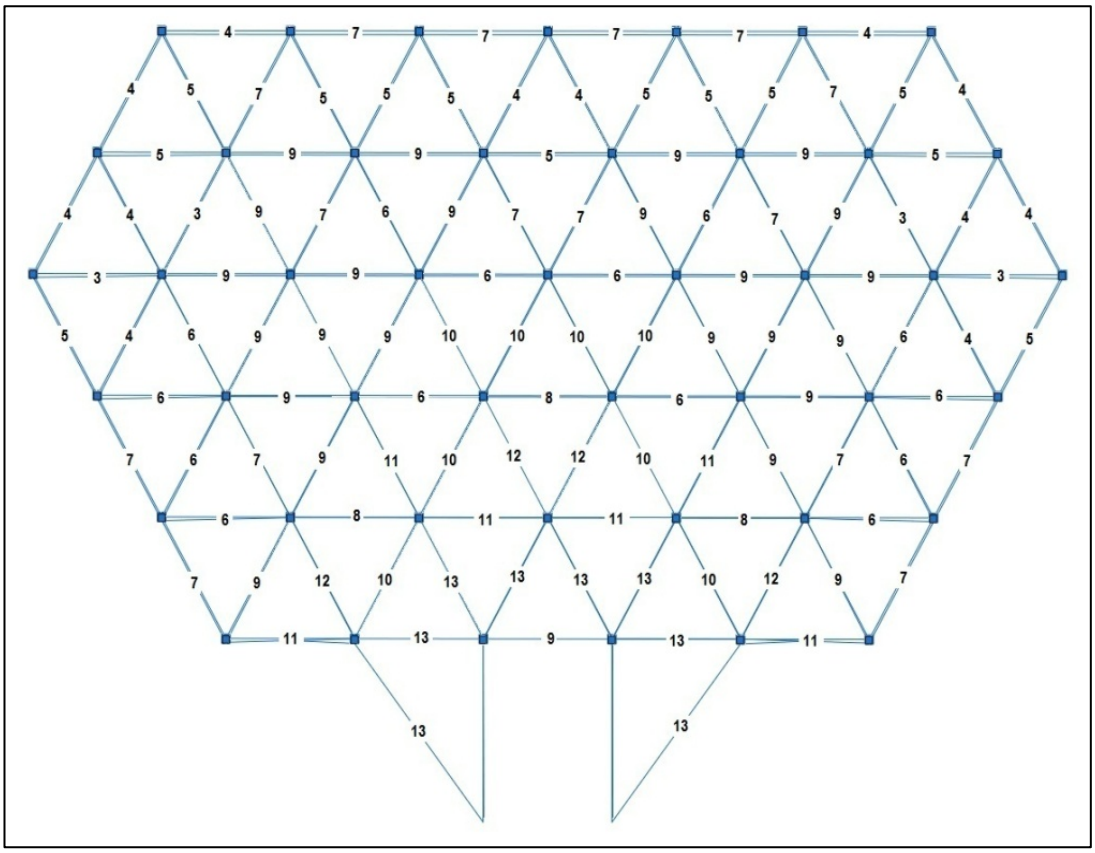

Figure 7.7: Front Elevation of MRS with CHS Members Labelled

7.4 FREQUENCY ANALYSIS

An Eigen value analysis of the multi rotor space frame was carried out by CRES, Athens [101] and the first 200 of these Eigen values are presented in Table 7.2. This analysis forms the basis of future work examining fatigue loading on the structure and is presented only briefly here.

The proposed space frame has a wide range of closely spaced natural frequencies, some of which lie within the main excitation frequency range of the rotors (0.44 Hz to 0.78 Hz). However, the rotor frequency varies randomly and destructive interference of the aggregate input from the rotors to the structure leads to vastly reduced fatigue load ranges compared to a single large rotor. Thus it seems unlikely that undue resonant response and fatigue loading in general will be problematic. Final fatigue load calculations are presently being conducted by CRES and will be published in due course.

N/N	Hz																	
1	0.35	21	1.33	41	2.11	61	3.01	81	3.55	101	4.18	121	4.81	141	5.78	161	6.69	181	7.75
2	0.39	22	1.35	42	2.16	62	3.02	82	3.60	102	4.23	122	4.82	142	5.86	162	6.75	182	7.90
3	**0.49**	23	1.47	43	2.24	63	3.08	83	3.61	103	4.24	123	4.85	143	5.88	163	6.78	183	7.92
4	**0.56**	24	1.50	44	2.27	64	3.09	84	3.65	104	4.28	124	4.91	144	5.92	164	6.82	184	7.92
5	**0.59**	25	1.51	45	2.30	65	3.15	85	3.66	105	4.30	125	4.97	145	5.94	165	6.85	185	7.97
6	**0.66**	26	1.54	46	2.38	66	3.19	86	3.75	106	4.33	126	5.04	146	6.04	166	6.90	186	8.16
7	**0.67**	27	1.68	47	2.45	67	3.20	87	3.76	107	4.35	127	5.06	147	6.06	167	7.01	187	8.23
8	**0.75**	28	1.70	48	2.46	68	3.25	88	3.80	108	4.38	128	5.08	148	6.12	168	7.04	188	8.33
9	**0.78**	29	1.71	49	2.52	69	3.26	89	3.84	109	4.40	129	5.12	149	6.15	169	7.10	189	8.35
10	0.80	30	1.72	50	2.57	70	3.27	90	3.87	110	4.43	130	5.14	150	6.24	170	7.12	190	8.37
11	0.83	31	1.77	51	2.62	71	3.28	91	3.92	111	4.50	131	5.23	151	6.26	171	7.14	191	8.43
12	0.85	32	1.80	52	2.65	72	3.30	92	3.94	112	4.54	132	5.30	152	6.32	172	7.18	192	8.48
13	0.89	33	1.83	53	2.69	73	3.32	93	3.95	113	4.55	133	5.30	153	6.36	173	7.36	193	8.52
14	0.90	34	1.89	54	2.74	74	3.34	94	3.95	114	4.56	134	5.40	154	6.39	174	7.44	194	8.59
15	0.93	35	1.96	55	2.75	75	3.36	95	3.99	115	4.59	135	5.42	155	6.46	175	7.45	195	8.61
16	0.99	36	1.97	56	2.78	76	3.38	96	4.08	116	4.60	136	5.55	156	6.48	176	7.47	196	8.69
17	1.01	37	2.01	57	2.81	77	3.38	97	4.11	117	4.64	137	5.58	157	6.55	177	7.51	197	8.81
18	1.13	38	2.05	58	2.86	78	3.43	98	4.15	118	4.66	138	5.63	158	6.57	178	7.55	198	8.91
19	1.15	39	2.07	59	2.90	79	3.47	99	4.15	119	4.76	139	5.65	159	6.64	179	7.68	199	9.02
20	1.30	40	2.09	60	3.00	80	3.50	100	4.16	120	4.80	140	5.73	160	6.68	180	7.70	200	9.05

Table 7.2: First 200 Eigen values of the proposed multi rotor space frame with Eigen values in the 1P operational range highlighted in bold.

7.5 FATIGUE ANALYSIS

Carrying out an extensive fatigue load study was not possible within the time constraints of this project. However, within the remit of the Innwind project and in conjunction with CRES this data was used as the basis of a detailed study into the fatigue loading on all members in the structure of which a short excerpt of the results is evaluated here. This study comprised of fatigue calculations using both the low resolution and combined resolution files. The low resolution files were found to provide adequate coverage and representation of the correct level of fatigue and therefore are the only ones presented here.

S-N fatigue analysis curves for all members are shown in Figure 7.8. It is generally seen that the maximum stress level is below 0.4-0.5 of the yield stress for most members, indicating that it is possible to design the structure within acceptable fatigue life. In isolated cases (like the group of four members that clearly exceed the horizontal S-N limit line) larger values are seen, indicating that an adjustment of the relevant sections may be needed. Nevertheless, the fatigue analysis performed for the MRS structure in the present framework is not at all exhaustive. A complete analysis is much beyond the scope of Innwind.EU where the focus is the proof of the MRS concept and a first evaluation of the mass and cost of its constituent substructures. To

that extent, the final design presented in this Chapter is considered adequate from a fatigue consideration alone. It is this final design which will be used for the basis of the cost analysis in the final Chapter.

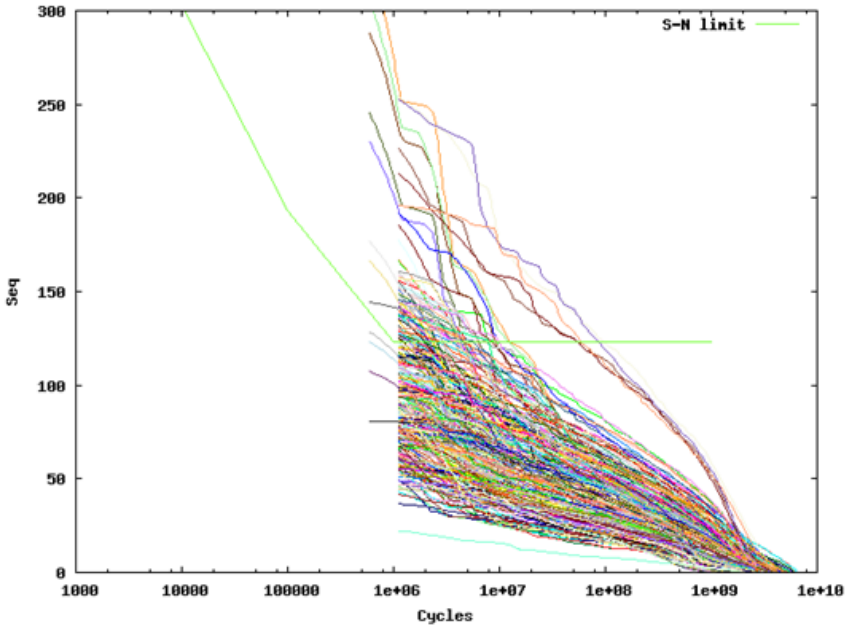

Figure 7.8: S-N curves for all the 275 members of the support structure

CHAPTER VIII – ENERGY CAPTURE IN MULTI-ROTOR SYSTEMS

8.1 Introduction

The energy capture capability of a WEC is usually evaluated over the period of a year. A year period is chosen because it adequately captures both diurnal (daily) and seasonal wind speed variations. The Weibull distribution is the most commonly used distribution due to its close representation of the variation in hourly mean wind speeds of a year at many typical wind turbine sites.

8.1.1 Weibull Definition

Year to year variation of wind speeds are hard to predict and therefore are best characterised in terms of probability distributions.

The distribution takes the form:

$$F(U) = exp\left(-\left(\frac{U}{c}\right)^k\right) \tag{8.2}$$

where: *F(U)* is the fraction of time for which the hourly mean wind speed exceeds U. It is characterised by a scale parameter, c, and a shape parameter, k, which describes the variability around the mean. c is related to the annual mean wind speed $\overline{U}$ by the relationship:

$$\overline{U} = c\Gamma\left(1 + {}^1/_k\right) \tag{8.3}$$

where: Γ is the complete Gamma function. This can be derived by consideration of the probability density function

$$f(U) = -\frac{dF(U)}{dU} = k\frac{U^{k-1}}{c^k}exp\left(-\left(\frac{U}{c}\right)^k\right) \tag{8.4}$$

as the mean wind speed is given by:

$$\overline{U} = \int_0^\infty Uf(U)dU \tag{8.5}$$

The Rayleigh distribution which has a shape factor of 2, is commonly used to represent typical wind profiles. In this case: $\overline{U} = 0.8862c$. Higher values of *k* indicate sites with a smaller hourly variation in the wind around the mean, while a lower value of *k* indicates a larger hourly variation.

A consideration of energy capture using a shape factor of 2 (as opposed to other shape factors) will be considered adequate as the investigation is whether the multi rotor system captures more energy of turbulence which has a time constant on the order of a few seconds. The shape factor on the other hand only describes local wind speed variations on the order of one hour intervals and these variations will be captured by both the MRS and its equivalent single rotor comparisons.

The Rayleigh distribution of the Weibull p.d.f. will be investigated using a range of annual mean wind speeds within the range 7m/s-11m/s. For a wind turbine site, 7m/s represents what would be considered at the fringe of commercial viability for a far offshore location and 10-11m/s represents a very typical average wind speed for moderately deep water locations [142]. The Rayleigh distribution can be used as a tool for establishing whether the multi rotors should be de-rated (i.e. have a lower maximum power which becomes rated at a lower wind speed). De-rating, and having a larger rotor in far offshore locations (where size or noise is not an issue) can have potential benefits.

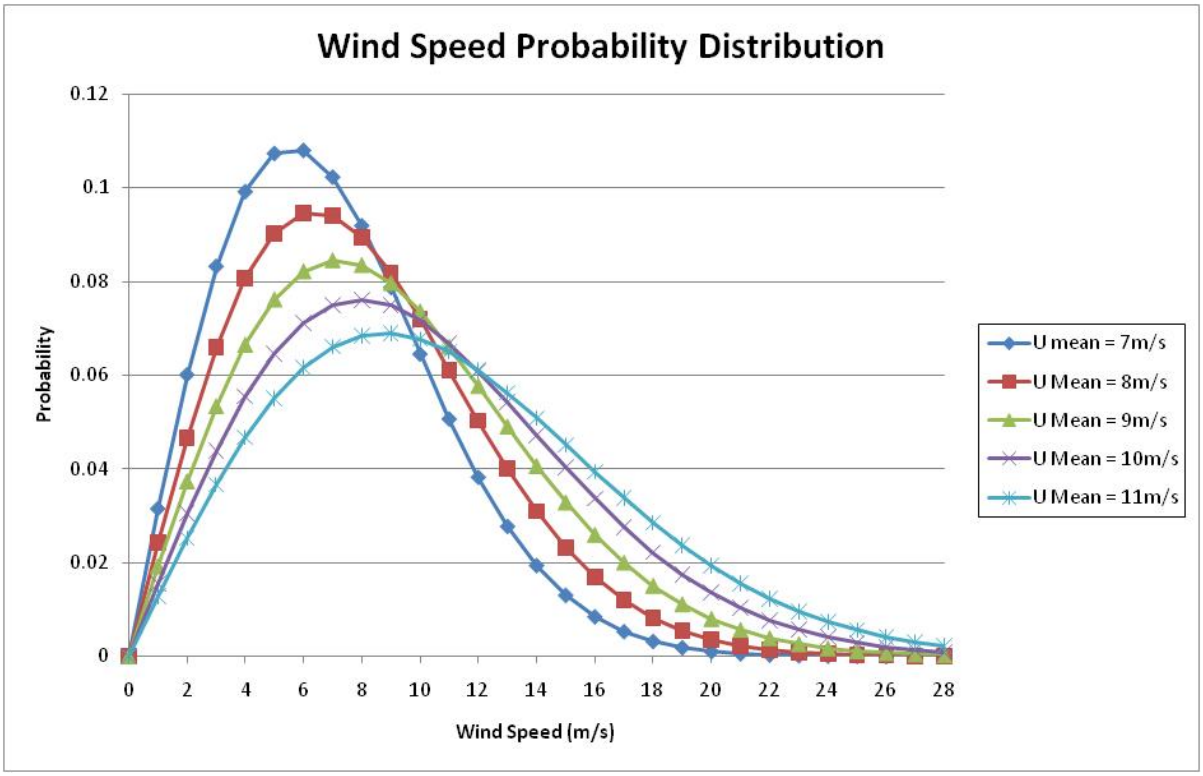

Figure 8.1: Rayleigh Distribution from 7m/s to 11m/s

8.1.2 Standard Energy Capture Model

8.1.2.1 Introduction

As a first attempt at determining the energy capture capability of the MRS in comparison to a single equivalently rated rotor, a combination of power production simulations taken from Bladed and the Weibull distribution described in section 8.1.1.1 was evaluated. The objective was to give indicative energy capture estimates over the machine lifetime to enable equivalent cost of energy calculations a discussion on the economic viability of multi rotors in an offshore environment.

8.1.2.2 Method

The method proposed is the commonly used, tried and tested method of combining simulated data, allocated into wind speed bins and passed through a transfer function which represents the Weibull-Rayleigh characteristic probability distribution [143].

8.1.2.3 Limitations

It is acknowledged that there are some limitations associated with the use of the Weibull curve, particularly in conjunction with a multiplicity of rotors. The spatial-temporal structure of the flow (of which turbulence is arguably the most important part) is not captured using this method. Turbulence levels are usually specified as 95 percentile values for conservatism in load calculations (within the IEC61400 framework) and therefore do not give an accurate representation of the distribution of mean wind speed and turbulence for annual energy estimation and consequent CoE evaluation.

The usual methods define turbulence intensity of a reference level and generate distributions of turbulence over a mean wind speed range and this is the method first attempted in this section. There remains a question as to whether it is valid to combine such distributions with a Weibull distribution of mean wind speeds. The preferred scenario would be the use of real or representative data combining annual joint distributions of mean wind speed and turbulence - however access to this data was not possible within the confines of this project.

A discrepancy of only a few percent is enough to make either the MRS seem appealing in comparison to the single-rotor or conversely particularly unattractive and presentation of this data without acknowledgement and further investigation would be foolhardy.

8.1.2.4 Results

Figure 8.2 shows a standard energy capture model using the Weibull-Rayleigh implementation. In this representation, it was assumed that the scale factor is 10, which approximates to an average annual wind speed of 9m/s. Figure 8.2 is annotated with a series of notes to explain each row of the data.

Weibull calculation :						Amount of Power Produced Per Year (MWh)		
Av wind speed (m/s)	calc type	lower bin	upper bin	hours/year	fraction	MRS	SR	#
2.5	idling	0	5	1562.8	0.18	0	0	1
6.5	powprod	5	8	1900.5	0.22	10341.3	8363.3	
9.5	powprod	8	11	1913.7	0.22	27863.8	23215.4	
13	powprod	11	15	1891.6	0.22	36869.1	35453.0	2
20	powprod	15	25	1432.7	0.16	27860.1	28573.1	
25	idling	25	35	64.7	0.01	0	0	3
AMWS	10		Sum	8766.0	1.0000			
shape factor α	2		Hours/year	8766				
	Original (as per power runs)		Power / Swept A.			TOTALS (MWh)		
Single Rotor (D 251m)	Swept Area (m2)	49750.12	402.01			102934.30	95604.83	4
Multi Rotor (D 40.5m)	Swept Area (m2)	54337.61	368.07			100.00%	92.88%	5
	Scaled with Similarity		Power / Swept A.	P. Reduction Ratio		Scaled TOTALS (MWh)		
Single Rotor (D 263m)	Swept Area (m2)	54337.61	368.07	0.9156		102934.30	87533.32	6
Multi Rotor (D 40.5m)	Swept Area (m2)	54337.61	368.07			100.00%	85.04%	
Power Density Calculations ^						Before Losses (MWh)		
						106386.12	92160.82	7
						100.00%	86.63%	

Figure 8.2: Standard Energy Capture Model

Important notes: 1 & 3: assumes small rotors are not allowed to cut in, 2: power production bins with average speed in column 1, 4: the yearly productions totals as determined by simulation, 5: the percentage of the baseline MRS total produced by each system, 6: the yearly totals scaled to equivalent swept areas, 7: the scaled totals discounting any mechanical or electrical losses.

This analysis shows that for a site with annual mean of 9m/s, the multi rotor appears to have an energy gain which exceeds an equivalently rated 20MW single rotor. This percentage gain is tentatively presented as 7% which is a substantial in a wind energy context. The percentage gain is further increased when the single 20MW rotor is up-scaled to an equivalent energy density to elicit a fairer comparison with the yearly energy gain as much as 13.5% after discounting losses on both systems.

Figure 8.3 continues the analysis further by applying the same method to both systems over a range of wind speeds (7-11m/s) which represent varying annual mean wind speeds at hub height.

A key observation (expanded on in the next section) is that the multi rotor performs better than the single rotor at lower average wind speeds when the majority of time is spent below rated. This point is interesting as it opens the MRS to a niche capability of operating at sites where perhaps a single large rotor would not be as economically viable - this in addition to sites with a high level of turbulent wind.

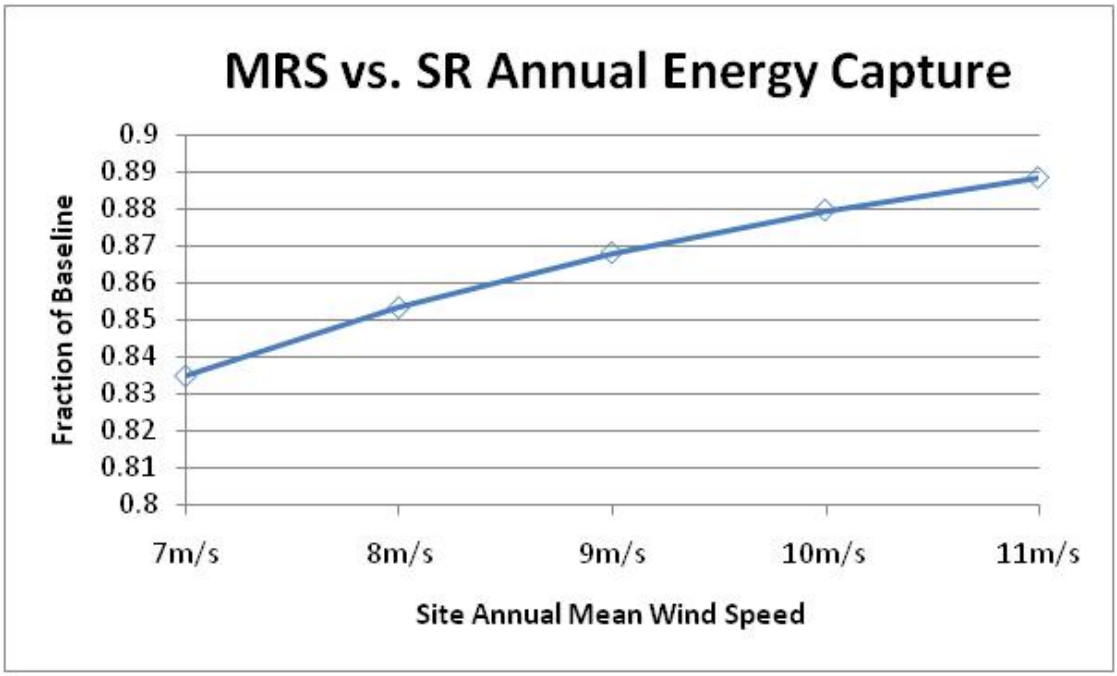

Figure 8.3: Comparison of 20MW SR as a Fraction of Baseline MRS Annual Energy Capture

8.1.2.5 Discussion

Controlling tip speed ratio is difficult in large rotors due to their geometric scale, which encompasses a large area, much larger than typical turbulence length scales.

The control processes for power maximization at sizes up to 5MW are generally very successful and more than capable of managing varying wind conditions. However, it remains to be seen whether this success will be translated into larger machines with ratings exceeding 10MW. Consider for example, that a 20MW rotor's blades must necessarily span several hundred metres and therefore each part of the blade will be operating at varying lift/drag ratios, varying angles of attack and potentially experiencing wind speed variations of more than 2m/s (10% turbulence at 20m/s). Given that parts of the blade are by default operating non-optimally, there will be a subsequent loss of 'potential' power. The UPWIND concept looks to address this using dual pitch systems which allow pitching at the root of the blade and also the tip. The project also considers the use of trailing edge flaps on the blades to enable changing of the aerodynamic profile on the fly. These system trade better blade control at the expensive of higher aerodynamic imbalances on the blades which leads to negative structural considerations.

Rotor inertia and acceleration also plays an important factor, with large rotors being unable to accelerate quickly (in comparison to a smaller rotor) to the optimum tip speed ratio and thereby optimise aerodynamic torque.

8.1.3 Bladed Energy Capture Model

8.1.3.1 Introduction

The first and most obvious strategy applicable to a wind turbine is to maximise or optimise each individual rotor's ability to capture energy contained in wind local to itself (i.e. a local gust). New optimisation abilities are available to the multi-rotor system centred around ensuring that individual rotors respond quickly to local changes in wind speed over short time periods. A difference in energy capture on the order of a single percentage over the course of a year can significantly impact on CoE.

8.1.3.2 Method

The multi rotor system is modelled in Bladed as is a single 20MW rotor of equivalent rating. A power production simulation at wind speeds around rated (10.5m/s) and using the same 3D wind file are run on each system and the power production and local wind speed investigated at various time steps.

Figure 8.4 is a crude graphical representation of the simulation wind field at a single moment in time. While an extreme representation, the smaller rotors which cover dimensions on the same scale as the turbulence length scales clearly experience local averages much different from the overall 10.5m/s average which defines the wind field.

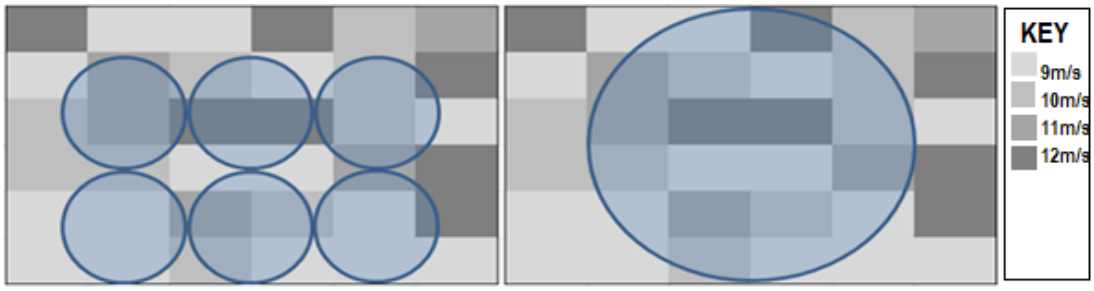

Figure 8.4: Smaller rotors wind sampling vs. a large equivalently rated rotor

8.1.3.3 Results

Consider Figure 8.6 which shows the wind speed at each of the hub centres at a single moment in time for a wind file defined with an average of 9.15m/s. The average wind speed measured at each of the hub centres is 9.53m/s which is 0.38m/s higher than the total wind field average but lower than rated wind speed (10.5m/s). Despite this, during this time step, 14 of the 45 rotors in the array are operating at rated power and the total output power from the array is 13.8MW - which is very close to the total power of 14MW that would be output if every turbine was experiencing a constant local wind speed of 9.53m/s. For comparison, the single 20MW rotor was simulated in the same wind conditions. During this same time step the single rotor experiences different wind conditions. The local hub wind speed is only 9.21 m/s and the subsequent output power at this constant wind speed is only 11.43MW.

In this model the multi-rotor is seen to capture almost 20% additional during this time step as a result of localised control.

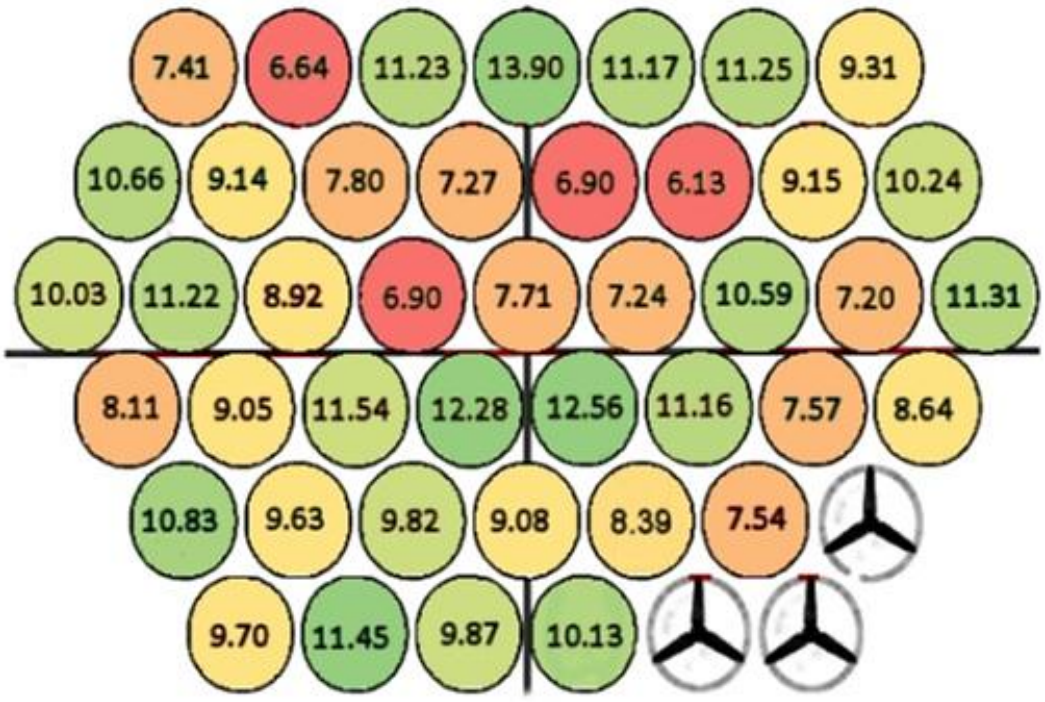

Figure 8.5: Wind Map 2, Single Time Step with 9.15m/s Average Wind Speed

Consider Figure 8.5 which shows the average wind speed at each node during a single simulation time step where the overall field average is 13.8m/s and therefore above rated. Two of the rotors in the multi rotor array (highlighted in red) are both operating at wind speeds below rated. In this example, the total output for the 20MW single rotor is 20MW and only 19.6MW for the multi-rotor which is a 2% loss in potential energy capture.

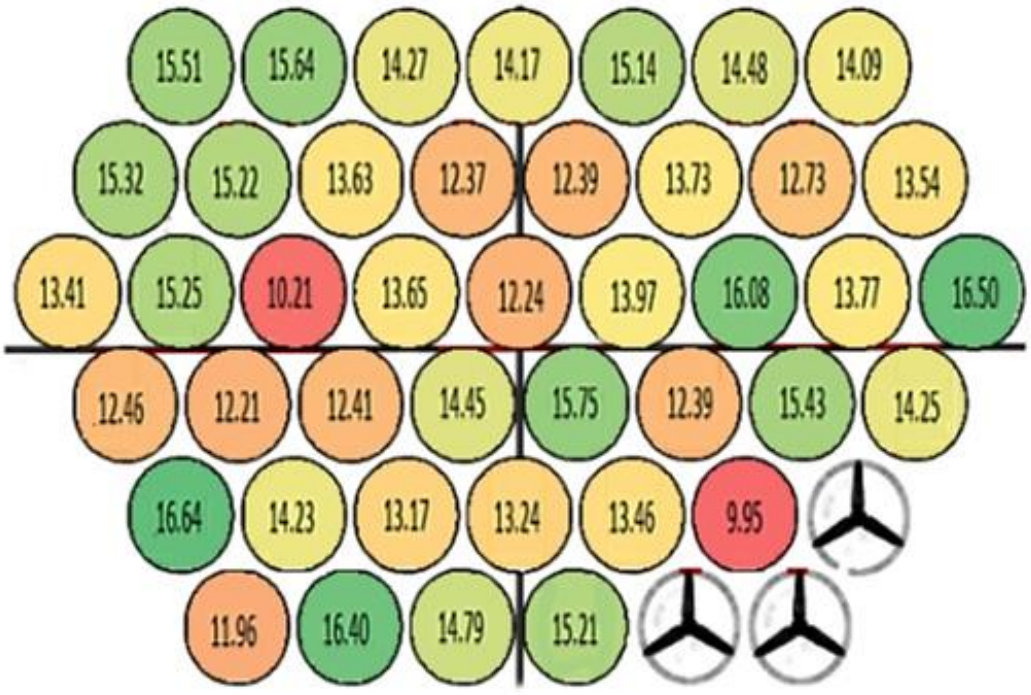

Figure 8.6: Wind Map 1, Single Time Step with 13.8m/s Average Wind Speed at 115m

8.1.4 Turbulence Energy Capture Model

Wind turbulence poses an interesting area of investigation in the context of energy capture for wind turbines in general but even more so when considering multi rotors.

Turbulence contains additional energy over and above that of the mean wind speed which can be extracted from the wind assuming the wind turbine can sample this turbulence. 5MW machines can capture the vast majority of turbulence energy, but it remains to be seen whether 20MW single rotors would be capable of doing so.

Without doubt, the ability to extract energy from localised turbulence increases with the number of rotors present. It is prudent to explore the concept of the energy in turbulence above mean wind speed and how multi rotors might best exploit this.

8.1.4.1 Turbulence Definition

Turbulence primarily derives from the stochastic non-deterministic component of wind. Its influence on the mean wind speed can therefore only be stated in terms of probability. For power production calculations, the turbulence intensity in the longitudinal direction is stated as a percentage of mean wind speed with 50% probability with lateral and vertical turbulence taken as a fraction of longitudinal turbulence.

The longitudinal turbulence is essentially the standard deviation about the mean wind speed, that is:

$$\sigma\left(V_m, I_r\right) := I_r \cdot \left(a \cdot V_m + b\right) \tag{8.6}$$

where: a and b are constants, V_m is the site mean wind speed, and I_r is the reference turbulence intensity taken from real world data.

Substituting 8.6 into the expression for turbulence intensity:

$$I\left(V_m, I_r\right) := \frac{\sigma\left(V_m, I_r\right)}{V_m} \tag{8.7}$$

This equation can be used to find expected turbulence intensities at various wind speeds with 50% probability. If $a << b$ the curve shows that turbulence decreases with increasing wind speeds.

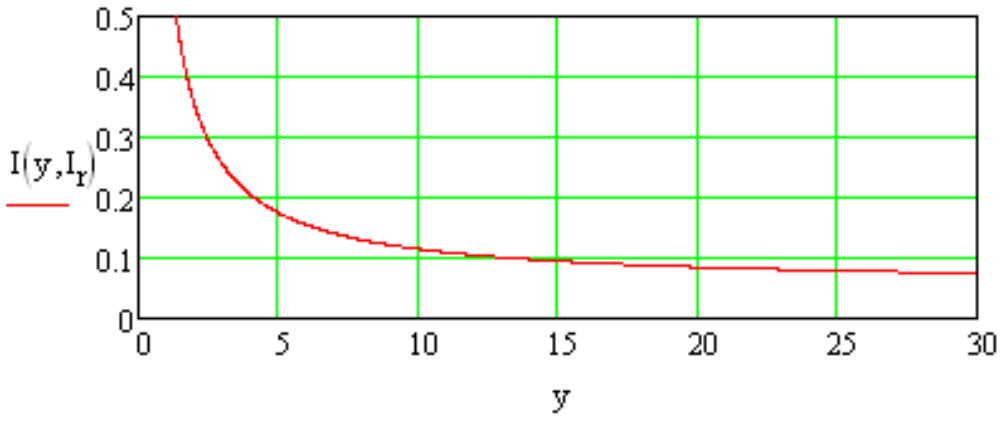

Figure 8.7: Turbulence Intensity (*I*) vs. Wind Speed (y), for a = 0.55 and b = 6

Figure 8.7 plots the turbulence intensity using two coefficient values, a = 0.55 and b = 6. The expected turbulence intensity in the longitudinal direction for a mean wind speed of 8 m/s is taken to be approximately 13%.

Equations (8.6) and (8.7) are tabulated in Table 8.1 using a range of values for coefficients a and b at 8m/s. The points highlighted in bold italics represent a low turbulence intensity (8.8%), normal turbulence intensity, 50th percentile (12.93%) and the 90th percentile turbulence intensity (14.4%) generally associated with wind turbine ultimate loading calculations.

	b	4	4.5	5	5.5	6
a						
0.250		7.5	8.1	***8.8***	9.4	10
0.300		8	8.6	9.3	9.9	10.5
0.350		8.5	9.1	9.8	10.4	11
0.400		9	9.6	10.3	10.9	11.5
0.450		9.5	10.1	10.8	11.4	12
0.500		10	10.6	11.3	11.9	12.5
0.550		10.5	11.1	11.8	12.4	13
0.600		11	11.6	12.3	***12.9***	13.5
0.650		11.5	12.1	12.8	13.4	14
0.700		12	12.6	13.3	13.9	14.5
0.750		12.5	13.1	13.8	***14.4***	15

Table 8.1: Turbulence Intensity Map

8.1.4.2 Simulating Energy Gain

Objective

In the absence of shear, one metric for establishing the amount of energy in turbulence is to calculate the ratio of actual energy captured in turbulence versus that energy captured under zero turbulence conditions. This calculation was done in Bladed using a shear-less wind field & assuming Class 1A wind.

Simulation Parameters

A group of simulations were running making different assumptions about the type of wind that the MRS would be operating in. This assumes a more normal 50 percentile turbulence distribution - more in keeping with average wind conditions rather than the 90 percentile conditions used for wind turbine design calculations. Simulation times were set at 610 seconds - with the first 10 transient seconds discounted from the result.

Normal Turbulence:

At $\overline{U}$ = 15m/s, I_1 = 10%, I_2 = 7%, I_3 = 5% (Normal Turbulence Model). α= 0, U_{ref} = 115m.

At $\overline{U}$ = 8m/s, I_1 = 12.9%, I_2 = 9.03%, I_3 = 6.45% (NTM), α = 0, Class Exp = 0.089, U_{ref} = 115m.

U_α = 0, U_φ = 0, U_Θ = 0

Where I_1 = longitudinal direction, I_2 = lateral direction, I_3 = vertical direction

Low Turbulence:

At $\overline{U}$ = 15m/s, I_1 = 6.8%, I_2 = 4.75%, I_3 = 3.39% (Normal Turbulence Model). α = 0, U_{ref} = 115m.

At $\overline{U}$ = 8m/s, I_1 = 8.8%, I_2 = 6.19%, I_3 = 4.42% (NTM). α = 0, U_{ref} = 115m.

Method

Groups of two types of simulations were run using the same MRS model previously defined within Bladed. The first, turbulent set, was run using various wind files

containing a 3D wind file of turbulent varying wind with fixed turbulence intensity values. As a counter-point a second constant speed 3D wind file (no shear) was created using the same average as the turbulent wind file and simulated within the model. To confirm that that any data was not adversely skewed by a particularly unfavourable wind seed, the simulation was run repeatedly using the same parameters but with different arbitrary wind seeds (seeds 1, 5, 8).

Limitations

There are several limitations to the proposed method that may impact on the validity of the results. Firstly, the relationship between instantaneous power and instantaneous wind speed at hub height is not exact - i.e. the system is not static. That is, for a given wind speed, the simulated output power will not always be what is predicted by the power curve alone due to the dynamics of the system. It is expected that these two values will never result in a ratio of 1.0 under any level of turbulence. There is not quick way of analysing the dynamics of the two systems from an energy gain ratio perspective. The only way to mitigate these effects is to complete the simulations using different levels of turbulence and seeing if the positive or negative energy gain effects are consistent.

Secondly, due to the simplistic nature of the auto-tuned controllers, a variation of a few percentage loss in energy gain may be a result of a poorly defined controller. It is expected that gains of less than 1.0 might be possible using a more refined controller. By the same logic, gains above 1.0 may be further enhanced by a properly tuned controller. It is hoped that these two effects would be approximately equal and therefore the use of simplistic auto-tuned controllers is not invalidating the results, but rather shifting them by a few percent.

Results

Figure 8.8 show the energy gain ratio in one of three 15 minute simulations each run with different seeds. It shows the apparent energy gain as a ratio caused by turbulence. In this case the simulated energy capture during the turbulent

simulations are compared to the predicted output if all turbines were capturing energy from a constant 8m/s wind.

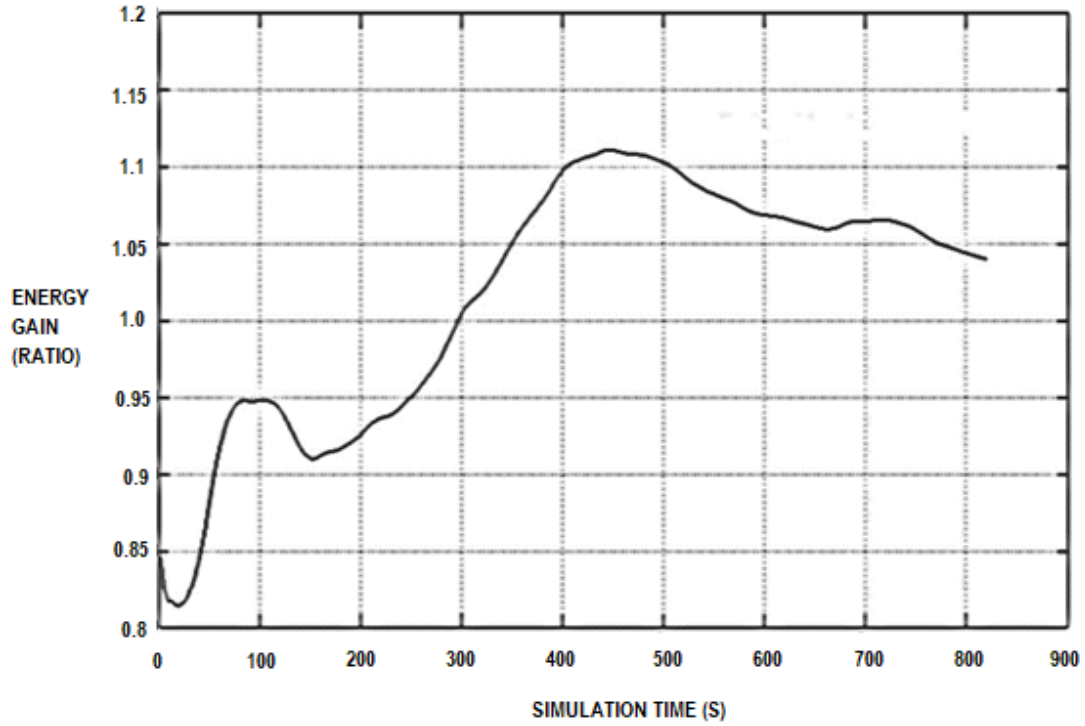

Figure 8.8: Energy Gain in Turbulence, 8m/s Average Wind (Seed 1)

The statistics for the three seeds are tabulated in Table 8.2 below:

Run #	Seed #	Sim. Time	Final Energy	Max Energy	Min Energy	Std. Dev.	Variance	$\bar{U}$ (m/s)	U_{max} (m/s)	U_{min} (m/s)
1	5	819s	1.0259	1.1275	0.9131	0.0555	0.0031	7.9969	8.9170	7.0193
2	1	819s	1.0401	1.1115	0.8147	0.0799	0.0064	8.0357	9.2369	7.0194
3	8	819s	1.0406	1.1596	0.9443	0.0508	0.0026	8.0341	9.3717	6.4833

Table 8.2: Energy Gain Statistics

Taking this data, the average net energy gain of the system in turbulence over a 15 minute period appears to be 3.55%. While it might be argued that the simulations are not long enough to be statistically significant there is some correlation between the theoretical additional energy contained in turbulence and that captured by the multi rotor system.

Significantly, while runs 2 and 3 appear to suggest additional energy capture due to turbulence they also correspond to average wind speeds that during the simulation

are marginally higher than the reference mean. This disparity occurs due to the artificial constraints on the simulation which attempts to average the wind speed out over the whole wind field and not just in the areas occupied by wind turbines. For example, in this case the wind field is 350m height by 382.5m wide corresponding to an area of 133,875m^2. However, the total combined swept area of the MRS is only 58,119m^2 or 43.4% of this total. The very selective nature of this sampling means there will inevitably be some deviation away from this mean during any given simulation length. This same constraint will also be apparent on the 20MW single rotor allowing for a direct comparison.

It is reasonable to assume that any feasible multi rotor system could not hope to capture all the additional energy within turbulence but that the added gain would likely increase with the number of rotors per given swept area.

This method was conducted using three different seeds for both the multi rotor system and the single 20MW rotor within the range of wind speeds 6-12 m/s. The results (shown in Table 8.3) seem to confirm that the multi rotor system will on average gain additional energy when operating in wind speeds below rated, with the advantage tailing off the closer the system comes to rated. On the other hand, they show that the single 20MW rotor is unable to capture any additional energy as a result of turbulence and in fact loses a significant amount of the turbulence potential at speeds below rated - with the disparity becoming less significant close to rated.

Two columns of data are presented:

The columns highlighted in green represent the energy gain ratio from the dynamic simulation versus the predicted output using the system average wind speed at each moment in time. This figure represents the advantage of rotor independence - i.e. this energy gain would be lost if all turbines were linked/clustered by rotor speed. For the single rotor, this simply represents a lag in the system between predicted output and actual output as a result of instantaneous hub wind speed.

The columns highlighted in red represent the energy gain ratio from the dynamic simulation versus a constant wind simulation - using the same mean wind speed. This column represents the additional energy captured from turbulence only.

		Energy Capture Ratios (After 600s)							
		Multi-Rotors (Final Time Step)		Multi-Rotors (Final Time Step)		Single Rotor (Final Time Step)		Single Rotor (Final Time Step)	
Wind Av (m/s)	Seed	Dynamic / Steady	Average 3 Seeds	Dynamic / Constant	Average 3 Seeds	Dynamic / Steady	Average 3 Seeds	Dynamic / Constant	Average 3 Seeds
6	1	1.00563		1.01105		0.90662		0.93064	
6	5	1.01014	1.00784	1.01556	1.01439	0.93658	0.93337	0.96622	0.95992
6	8	1.00776		1.01656		0.95692		0.98289	
7	1	1.00421		1.01099		0.91721		0.93743	
7	5	1.00865	1.00622	1.01366	1.01227	0.94682	0.94163	0.97165	0.96370
7	8	1.00580		1.01215		0.96087		0.98203	
8	1	1.00233		1.00854		0.93615		0.95135	
8	5	1.00631	1.00662	1.01124	1.01489	0.9547	0.96046	0.97258	0.97717
8	8	1.01124		1.02488		0.99054		1.00759	
9	1	1.00082		1.00498		0.94119		0.9467	
9	5	1.00426	1.00233	1.00740	1.00636	0.95846	0.95614	0.96631	0.96328
9	8	1.00192		1.00669		0.96877		0.97683	
10	1	0.99033		1.00278		0.9509		0.95075	
10	5	0.99644	0.99480	1.00684	1.00540	0.96783	0.96435	0.96847	0.96227
10	8	0.99762		1.00658		0.97431		0.9676	
11	1	0.98556		0.97526		0.97417		0.93966	
11	5	0.97552	0.97436	0.96199	0.96406	0.98921	0.98218	0.96219	0.95800
11	8	0.96199		0.95494		0.98316		0.97215	
12	1	0.955		0.99975		0.99937		0.97987	
12	5	0.99896	0.98378	0.998	0.99831	1.00929	1.00446	0.97912	0.97480
12	8	0.99744		0.99717		1.00471		0.9654	

Table 8.3: Final Energy Ratio Results NTM, 50th percentile (No Shear)

8.1.4.3 Energy Capture with Shear

A second and third group of simulations was carried out using the same turbulence data files but with modified values of shear. The objective of these additional groups of data is to show the effect that shear has, over and above normal turbulence, in energy capture ratios.

In the second group, the runs with average wind speeds of 6, 8, 10 and 12 m/s were re-run using a shear exponent of 0.06. A shear exponent of 0.06 would be considered very low by power production standards. The results from these runs are shown in Table 8.4 below.

	Energy Capture Ratios (After 600s)							
	Multi-Rotors (Final Time Step)		Multi-Rotors (Final Time Step)		Single Rotor (Final Time Step)		Single Rotor (Final Time Step)	
Seed	Dynamic / Steady	Average 3 Seeds	Dynamic / Constant	Average 3 Seeds	Dynamic / Steady	Average 3 Seeds	Dynamic / Constant	Average 3 Seeds
1	1.00787	0.99421	1.01342	0.99917	0.97431	0.95862	1.09975	1.05788
5	1.01219		1.01698		0.94069		1.10502	
8	0.96256		0.96712		0.96086		0.96886	
1	1.00430	1.00604	1.01052	1.01157	0.95523	0.95523	0.97076	0.97076
5	1.00837		1.01327		0.96803		0.97675	
8	1.00545		1.01092		0.94243		0.96477	
1	0.98550	0.98993	0.98650	0.99287	0.95503	0.96859	1.06112	1.02368
5	0.98955		0.99241		0.97207		1.03801	
8	0.99474		0.99970		0.97867		0.97193	
1	0.99830	0.99626	0.99830	0.99623	1.00115	1.00622	0.98265	0.97685
5	0.99636		0.99636		1.01132		0.98108	
8	0.99411		0.99403		1.00620		0.96682	

Table 8.4: Final Energy Ratio Results NTM, 50th Percentile (0.06 Shear)

In the third group, the same runs with average wind speeds of 6, 8, 10 and 12m/s were re-run using a shear exponent of 0.11. This shear exponent is commonly used to represent offshore wind farms in mild sea conditions. The result from these runs are shown in Table 8.5.

		Energy Capture Ratios (After 600s)							
		Multi-Rotors (Final Time Step)		Multi-Rotors (Final Time Step)		Single Rotor (Final Time Step)		Single Rotor (Final Time Step)	
Wind Av (m/s)	Seed	Dynamic / Steady	Average 3 Seeds	Dynamic / Constant	Average 3 Seeds	Dynamic / Steady	Average 3 Seeds	Dynamic / Constant	Average 3 Seeds
6	1	1.01412	1.01626	1.02010	1.02137	0.90662	0.93339	1.09473	1.05329
6	5	1.01840		1.02264		0.93660		1.10022	
6	8	-		-		0.95695		0.96492	
8	1	1.00430	1.00604	1.01052	1.01157	0.96655	0.94877	0.98847	1.02576
8	5	1.00837		1.01327		0.95474		1.07005	
8	8	1.00545		1.01092		0.92487		1.01876	
10	1	0.97631	0.98581	0.97551	0.98791	0.95090	0.96435	1.05652	1.01920
10	5	0.97964		0.98237		0.96784		1.03349	
10	8	1.00147		1.00581		0.97431		0.96759	
12	1	0.99950	0.98970	0.98490	0.99103	0.99938	1.00446	0.98091	0.97514
12	5	0.98970		1.00080		1.00929		0.97912	
12	8	0.97990		0.98740		1.00471		0.96540	

Table 8.5: Final Energy Ratio Results NTM, 50th Percentile (0.11 Shear)

It is not expected that a multi rotor system of this type would be employed in an onshore location and therefore the commonly used shear exponent of 0.14 was not investigated.

8.1.4.4 Discussion

The multi rotor system can capture more energy from turbulence than the less responsive 20MW single rotor. At speeds well below rated (6-8 m/s) the energy gain ratio compared to a constant wind speed is as much as +1.49% for the MRS compared to an energy loss of as much as -4% for the single rotor. Around rated wind speeds (9-12 m/s) the energy gain is negated and becomes a loss of as much as -2.5%. However, the single rotor also loses potential energy in this region of as much as 4%.

The multi rotor system captures additional energy in normal turbulence conditions below rated wind speeds. This is likely a result of the ability of individual's small rotors ability to accelerate or decelerate according to local wind conditions in order to maximize C_p to a much greater extent than the single rotor is able to do so. Shear plays an important role in this type of function as the distribution of many small rotors over an equivalent swept rating sees certain rotors operating above rated, while others below but overall results in a net positive energy gain compared to the single rotor.

This energy gain is partially reversed above rated, where the single rotor appears to fair better. This effect is a type of "ride through" that a large rotor is capable of enacting as a result of its momentum which allows it to stay above rated (maintaining electrical torque while decelerating) even under short wind speed dips below rated wind speed.

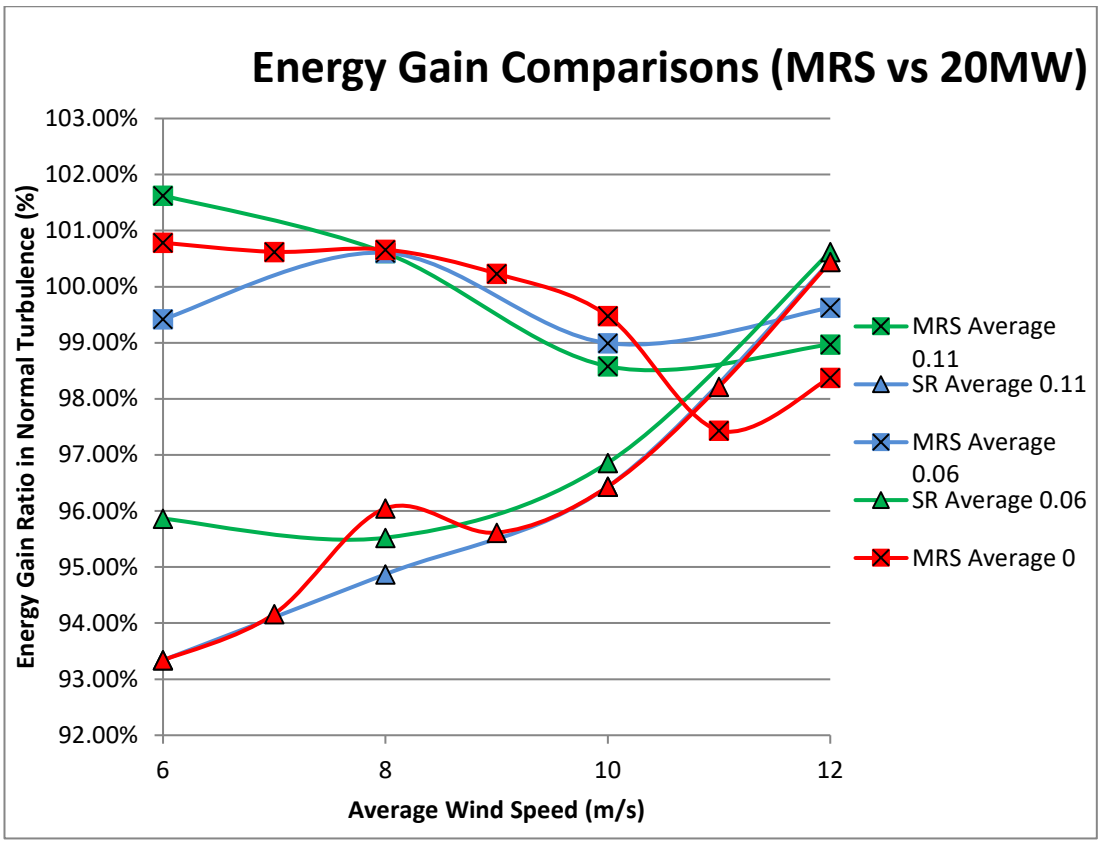

Figure 8.9: Energy Gain in Turbulent Wind with Varying Shear

8.1.4.5 Rotor Comparison for Wind Power Capture

To understand how a small rotor is better equipped to take advantage of turbulence first requires an examination of the key characteristics of both systems below rated power (i.e. in their variable speed region).

During the simulations, neither system achieves the required wind speed to reach their constant speed region whereby pitching is used to track C_p max, meaning that the rotor speed alone is the determining factor in the power produced. In the variable speed region, the controller is expected to allow the rotor speed to increase with increasing wind speed to maintain the correct tip-speed ratio and track the C_p-λ curve. The rate at which the rotor accelerates is dependent on aerodynamic torque, generator torque and rotor inertia

$$T_m - T_e = I \cdot \alpha \tag{8.8}$$

Acceleration requires a torque differential and this differential is created by the generator torque which lags behind aerodynamic torque. For a small rotor with low inertia, this ultimately means that acceleration can be quite rapid allowing for the rotor to achieve the optimum tip-speed ratio quickly. The larger rotor with a much higher inertia, while having higher torques ultimately accelerates slower meaning it often never reaches optimum rotor speeds within short periods of time. Figure 8.10 shows that the difference is quite significant.

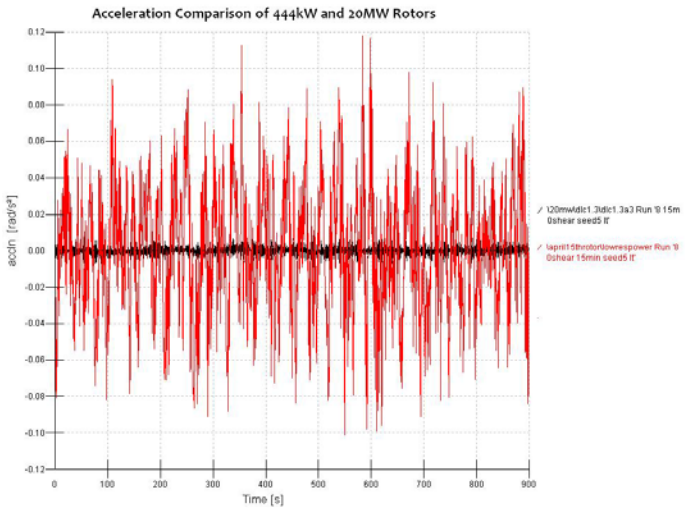

Figure 8.10: Acceleration Comparison

Figure 8.11 shows how the rotor speed of the large rotor varies in response to changing wind conditions (low turbulence) with a scaled power curve superimposed on top. What is immediately apparent from this graph is that there is a lag between wind speed changes and rotor speed and power output.

Figure 8.12 which shows the same simulation parameters but on the multi rotor system shows a much less pronounced lag between the three variables. The power output varies more as a result of localised gusting which the single large rotor is not capable of responding quickly enough to take advantage of.

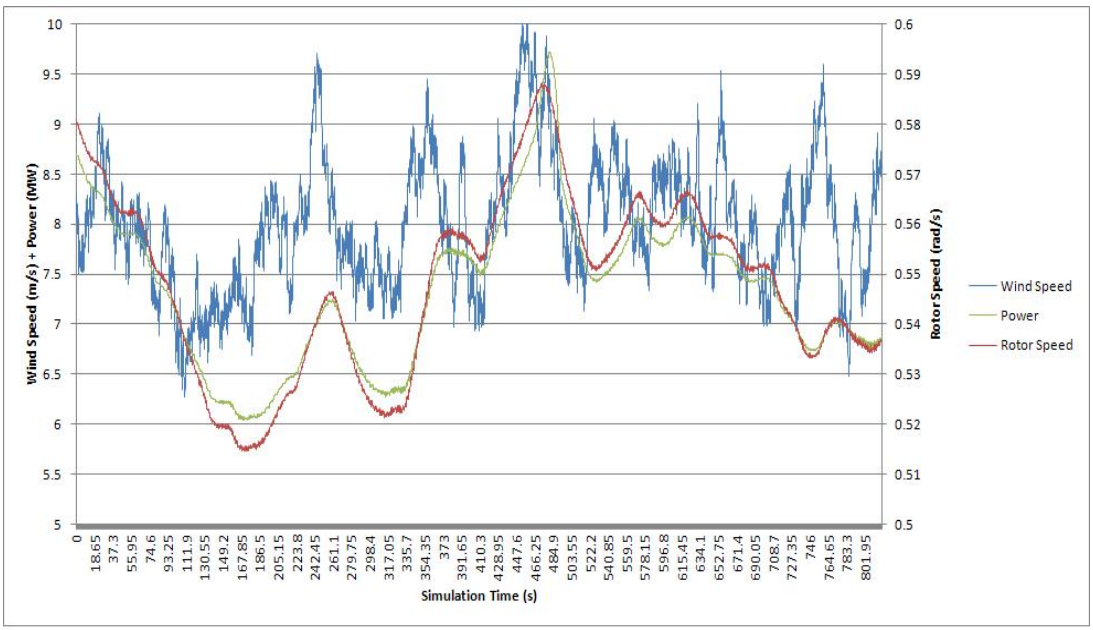

Figure 8.11: Large Rotor Simulation Parameters

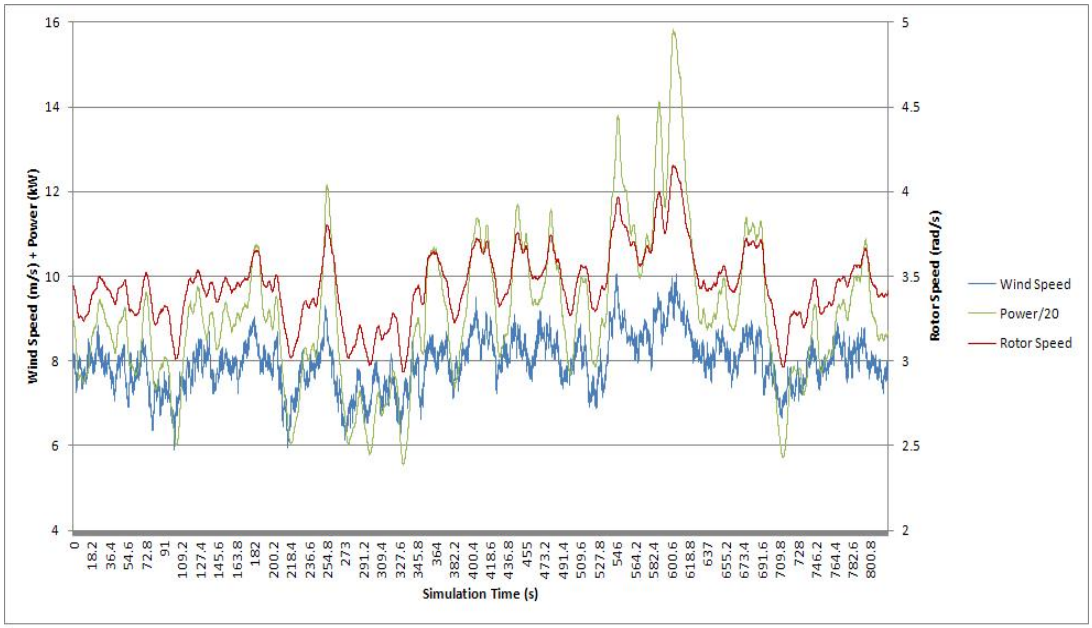

Figure 8.12: Small Rotor Simulation Parameters

8.1.5 Summary

Three different models have been run to investigate the way in which multi-rotor systems behave during normal power production compared to large equivalent single rotors.

The Standard Energy Capture Model from a purely statistical standpoint estimated a net benefit for the MRS of up to 14% over the course of a year at a site with mean wind speed of 9m/s.

The Bladed Energy Capture models both predict anything in the region of a 2-4% net benefit in energy capture for the MRS over an equivalent rated single-rotor at sites with wind speeds around rated (10.5m/s) under normal wind conditions.

The Turbulence Energy Capture model suggests a further gain of 1-2% in response to turbulent gusts which only the smaller rated MRS rotors can respond to.

It is not unreasonable to assume that in a real-world situation that a 45 rotor MRS could achieve a net energy gain of several percent over an equivalently rated large rotor. This added energy gain, providing that it is not offset by increased structural cost, will result in a lower cost of energy for multi-rotor systems. An evaluation of structural cost is now discussed.

CHAPTER IX - MULTI ROTOR COST ANALYSIS & COMPARISONS WITH EQUIVALENTLY RATED SINGLE ROTORS

9.1 INTRODUCTION

The penultimate chapter of this thesis is aimed at presenting the multi rotor system in economic terms in comparison to contemporary equivalent systems. Ultimately it is economics which will dictate the future of the MRS both from a research funding and commercialisation perspective. The objective is to present a cost analysis framework from which future multi rotor systems can be based on and which lies within the boundaries of what can be considered eminently plausible. This framework will take the form of a cost of energy (CoE) analysis and all that entails.

9.2 FACTORS AFFECTING COST

The initial capital expenditure (CAPEX) generally contributes the largest share of both onshore and offshore wind cost of energy. High upfront capital costs, even mixed with relatively lower operational costs can lead to uncompetitive electricity market prices in comparison to cheap coal and gas. If left to the market this lack of financial incentive towards highly desirable outcomes (governments attaining global renewable energy targets, a reduction in atmospheric pollution among other things) would result in a poor uptake from profit seeking firms. Wind energy plants in offshore environments are generally subsidised through financial incentives by local governments in the form of guaranteed unit purchase prices, carbon trading certificates and so on.

Consider that the UK subsidised CoE for offshore wind is about £69/MWh against £47/MWh for onshore wind (non-subsidised). Without these subsidies, the CoE offshore is estimated to be closer to £140/MWh around the UK coast [144]. Clearly the cost of offshore wind would be prohibitively expensive by a factor of almost 3 if not for these subsidies. The reliance on subsidies puts many wind farm developers in shaky territory. If subsidies were to fall or be removed entirely then it might be expected that offshore development would all but cease. There exists a strong incentive for the major components in CoE (i.e. O&M and ICC) to be reduced substantially if offshore wind is to survive and prosper in the future. One of the ways

in which this could comfortably be achieved is by a move towards larger ratings at individual offshore sites. Thus, the industry has moved towards investigating 7MW, 10MW and even potentially 20MW single unit ratings for off shore locations.

It is clear to see why offshore wind is more expensive than other forms of generation when considering the effect of turbine outages on O&M costs alone. When it comes to generic turbine faults, 75% of the faults on a wind turbine cause 5% of the downtime while the remaining 25% of the faults cause 95% of the downtime. These percentages are impacted strongly by the environment in which offshore wind turbines are placed.

Downtime onshore is dominated by a few large faults, many associated with gearboxes, generators and blades, requiring complex and costly replacement procedures. Being onshore, these failures can be repaired almost on demand and downtime is commensurately low. The 75% of faults causing 5% of the downtime are mostly associated with the electrical plant, the converter, electric pitch systems, control equipment and switchgear, whose defects are relatively easy to fix in an onshore environment. In an offshore environment, even the manual resetting of a switch or circuit breaker could take several days (if the weather is bad) and therefore every fault no matter how small is critical. The cost of offshore operations is profoundly affected by failure rate and downtime values. Generic failure rates offshore will be similar to onshore but downtime is hugely affected by the location of the offshore wind farm and its accessibility. This means that even small faults (which onshore account for only 5% of the downtime but 75% of the faults) is greatly increased in an offshore location [145].

9.3 HISTORICAL COST OF ENERGY

In the last ten years the costs of offshore wind energy have escalated dramatically, with capital expenditure costs doubling from approximately £1.5m/MW in the early 2000s to over £3.0m/MW in 2009. The increase in costs are attributed to many factors including: increased cost of planning permission, the movement into far offshore locations, a stretched supply chain and an increasing cost of borrowing.

In Denmark, the Vindeby offshore wind farm was completed in 1991 at a cost of £1.82m/MW, whilst Horns Rev (Denmark) was built for £1.05m/MW in 2002. North Hoyle (UK Round 1) was completed in 2003 at a reported cost of £1.35m/MW.

As of 2010 the industry consensus is that capital and energy costs are approximately £3m/MW and £150/MWh (un-subsidised) respectively, though there is a suggestion that the costs may have peaked or reached a plateau (being constant in 2009 and 2010). UK government research for example expects the cost of onshore energy to stabilise around £2.5/MW by 2020 [146].

It is believed that with favourably developments in a range of fields the cost of energy could come down to as low as £95/MWh, with £115/MWh a realistic target in the short term (by 2020). To achieve this target will require a capital cost reduction on the order of 17-18% at the minimum compared to 2010 levels.

9.4 CAPITAL EXPENDITURE

One of the largest contributions to total CAPEX cost outside of the wind turbine and tower are the foundations which may account for 20-35% of an offshore wind turbines capital cost - with the percentage increasing as turbines are routinely deployed in deeper water (> 20m).

Another capital cost that tends to take a larger proportion of the total costs is the grid connection which can account for around 15% of turbine CAPEX costs in shallow water and becomes higher as the generators move further offshore.

Figure 9.1 gives an indication of the breakdown of Capital Expenditure (CAPEX) costs as a percentage of the total costs for Round 1 Offshore Wind in the UK [148]. These values are broken down as follows: Development expenses: 2.5%, Preliminary and Management Works: 5%, Wind turbine, transformer and tower supply: 40%, Foundation supply: 18%, Offshore electrical supply: 6%, Wind farm monitoring system supply: 1.5%, Installation: 22%, Onshore electrical works: 5%. These values are only indicative values, and they will vary from system to system.

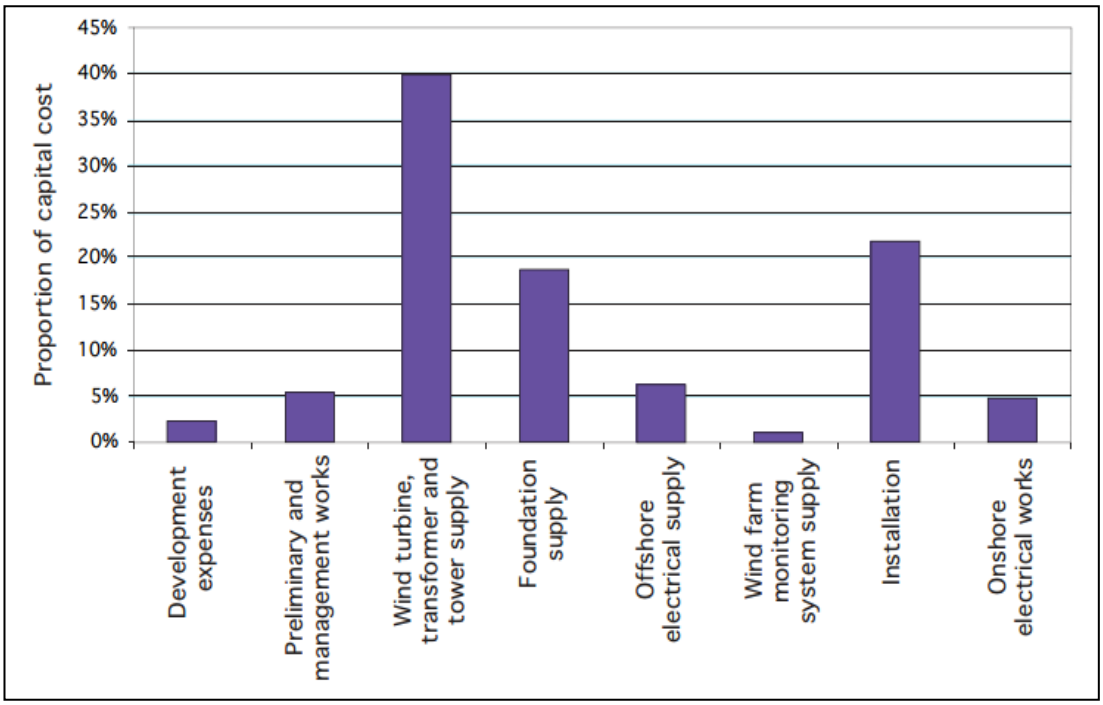

Figure 9.1: Offshore Cost Breakdown as a Percentage of Total (UK Round 1)

Turbine capital cost and balance of plants account for up to 70% of offshore capital costs, although only around 31% of this is actual material cost, with 26% apportioned to labour. It might be expected that a decrease in material cost in the multi rotor system might be offset by an increase in labour cost, because of the welding complexity involved in making the multi rotor space frame.

Much of the decrease in cost (as much as 20% of turbine costs) is expected as a result of the 'learning curve' seen as time progresses, development advances and economies of scale kick in [147].

9.4.1 Relationship Between Mass and Cost

9.4.1.1 Introduction

Early in this research product (after the initial 45 rotor concept) a rudimentary cost study was performed using speculative Figures based on various assumptions about the form of a future 20MW MRS. The costing was done on the assumption that *mass* is proportional to *cost* and with mass related to a fixed cost per unit energy according

to theoretical scaling laws - which were discussed in depth in Chapter 3. This costing was done as an initial sanity check for the multi rotor concept.

9.4.1.2 Basis of Comparisons

The analysis presented is all about technical differences affecting relative cost comparisons between different systems and does not depend on any absolute cost data.

First the 5MW reference wind turbine is up-scaled to 20 MW, essentially with similarity. Studies within the UPWIND project [14] suggest that it will be difficult to better this and rather a challenge not to do worse. If any improved technology can benefit the 20 MW design, then it would usually be applicable to the smaller 5 MW turbine, so preserving the comparison. An equivalent multi rotor system is then developed in this case based on 45 × 444 kW wind turbines with the same rated power (20 MW) and a spatial distribution in a triangular matrix having 6 rotors in the lowest row followed by 7,8,9,8,7 rotors on subsequent rows.

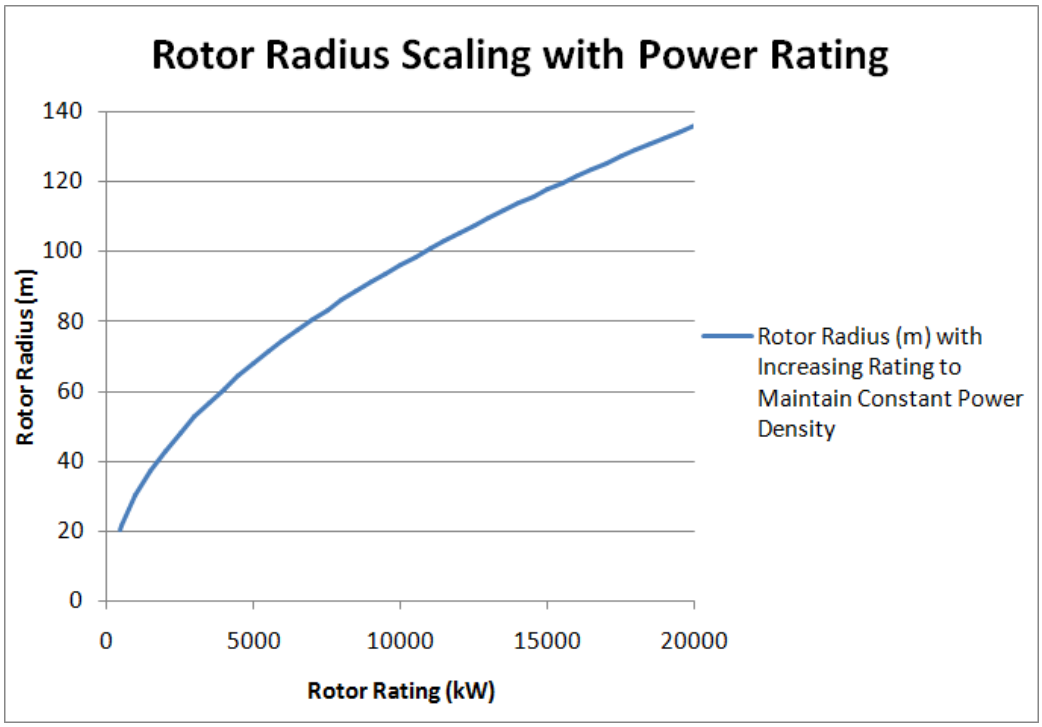

Figure 9.2: Rotor Size Scaling with Constant Power Density (350 W/m^2)

The UPWIND 20MW turbine developed was proposed to have the following characteristics, shown in Table 9.1. The 5MW reference machine and intermediate 10MW are also shown.

	Reference 5MW	Extrapolated	Extrapolated
Rotor Diameter (m)	126	178	252
Hub Height (m)	90	116	153
Max. Rotor Speed	12	9	6
Rotor Mass (tonnes)	122	305	770
Tower Top Mass	320	760	880
Tower Mass (tonnes)	347	983	2780
Predict. Elec. Prod	369	774	1,626

Table 9.1: UPWIND Design Reference Turbines

Some other interesting comparisons can be made between the UPWIND design and other notional designs defined by various research groups for tower (Table 9.2) and blades [89].

	Diameter	Rated Power	Tower Mass	Mass/ Power	Hub Height	Clearance	Clearance/ diameter	Power Density
	D [m]	P_r [MW]	M_t [t kg]	kg/kW	h [m]	c [m]	c/D	PD [W/m^2]
UPWIND 5MW	126.0	5	347	69.40	90	27.00	0.21	401.0
UoS 5MW	126.0	5	522.6	104.52	90	27.00	0.21	401.0
Samsung 7MW	171.2	7						304.1
UPWIND 10MW	178.0	10	983	98.30	116	27.00	0.15	401.9
DTU 10 MW	178.3	10	628.4	62.84	119.00	29.85	0.17	400.5
DTC 10MW	205.7	10	858	85.80	140.00	37.14	0.18	300.9
UPWIND 20MW	252.0	20	2780	139.00	153	27.00	0.11	401.0
UoS 20MW	258.0	20	9532.9	476.64	209	80.00	0.31	382.6
Averages				**129.56**		**36.43**	**0.19**	**374.11**

Table 9.2: Real World Tower Scaling Parameters (5-20MW)

One of the key points is that blade mass can vary wildly depending on the type of blade model used as scaling rules are not consistent, scaling either as the square or cube of diameter. This highlights a level of uncertainty in just how heavy a 20MW blade would be. The important consideration is that any 444kW blade should be able to benefit from the same scaling laws as the single 20MW rotor and therefore will

benefit just as much in downscaling. A blade mass of 550kg for the multi rotor 444kW machines has been used in this project.

9.4.1.3 Method

The single rotor and multi rotor systems are designed to give similar rated wind speed and annual energy capture at an offshore site with wind shear exponent of ~0.1. It is recognised that a wide range of wind shears may apply at some offshore sites depending on atmospheric stability and other factors.

Having set up comparisons with equal energy output, a cost of energy (CoE) evaluation is then based on a comparison of lifetime costs. It is assumed for the reference turbine that O&M costs amount to 30% of lifetime cost and that the initial capital cost is split 40% and 60% between wind turbine capital and balance of plant. In estimating the costs associated with the 20 MW multi rotor system, basic scaling with similarity is applied, with rotors for example scaling cubically and hence reducing in cost as $\frac{1}{\sqrt{n}}$.

The total weight is much less and the aggregate aerodynamic loads are less [156] for the multi rotor system than for the single rotor system. Nevertheless, the cost of the stub tower and lattice structure is taken as double the cost of the tower for a single 20 MW wind turbine.

Again, although there are no load increases and bearing sizes much reduced, the twin bearing yaw system cost is likewise doubled.

The cost of power conversion for the multi rotor system is also doubled.

The rotor sizes of the reference 5MW & 20MW designs and the smaller 444kW MRS designs have been scaled to achieve a consistent power density of 350 W/m^2.

These are basic assumptions that cannot be expanded upon without further study and have been chosen in that hope that they are conservative and do not artificially give the MRS a cost advantage.

This analysis necessarily does not do justice to the comparison that may evolve with more detailed engineering. For example, the relatively small turbines of the multi rotor system may advantageously be direct drive perhaps with a single collective pitch actuator and mechanical brake mounted off the generator stator for a second protection system.

Recent trends in offshore wind turbine design are towards larger rotors in relation to rated power or equivalently a reduction in power density. An industry average of around 400 W/m^2 (rated power/rotor swept area) is quite consistent with the Repower 5MW design with 126 m rotor diameter, for example [149]. The latest designs of Vestas and Siemens, perhaps acknowledging that offshore electrical costs are a much higher proportion of total life costs than on land, have moved towards reduced power density. The Vestas V164 and Siemens SWT 6-154 have power densities of 331 W/m^2 and 322 W/m^2 respectively.

This study adopts a power density of 350 W/m^2 on which basis reference 5 MW, 10MW and 20MW systems wind turbine is developed with a rotor diameter of 135m (Figure 9.2).

Cost fractions defining the relative costs of components in terms of life time costs are estimated using data from Jamieson [44]. Wind turbine prices have reduced in 2011 and a round number of €1000/kW has been used here as a basis for the ex-works capital cost of the wind turbine system alone.

For this study conducted in 2014, the projected cost per unit of installed capacity and cost of energy will be inflated to the year 2020 to provide a direct comparison to those Figures projected by the UK RAB using a flat inflation rate of 3% per year.

9.4.1.4 Results

It is possible to try at costing the multi rotor system without considering anything other than a combination of real-world data and the use of scaling laws. Table 9.3

represents an attempt at formulating the cost of a multi rotor system in comparison to 4 x 5MW single rotors and a single 20MW rotor using such a method.

The values within this Table were derived from representative scaling factors as taken from real world but commercially sensitive data provided by GL Garrad Hassan - and this was supplemented by theoretical scaling laws as described in Chapter 3. Note in this case that the large single 20MW rotor is not the one proposed in UPWIND, having a lower power density.

The foundation costs of 20 MW single rotor and multi rotor are taken as the same although the multi rotor system will be much lighter and hence have a higher fundamental frequency. The electrical costs within the wind farm and to grid connection are assumed to be the same but naturally more favourable for single 20 MW units of any type as compared to 20 MW realised as 4 × 5 MW wind turbines.

It may be evident from Table 9.3 that the multi rotor system lifetime cost is appreciably cheaper than for a single 20 MW rotor and less than for 4 × 5MW units. The multi rotor system has been rated at 20 MW to give direct comparisons with 5 MW and 20 MW single rotor systems. 20 MW rating, if not 10 MW, may be at an economic limit for the single rotor concept. However, there is no reason, rather additional benefit, in up-scaling the total capacity of the multi rotor system to total power ratings far beyond what may be practicable and economic with single rotors. As the principle would be to standardize on rotor size and simply increase the numbers of rotors, there can then be significant further cost reduction, quality and reliability enhancement arising from stable high-volume production.

Equation 8.1 describes the way the scaling rules are applied in Table 8.1.

$$N = Ref \times \left(D_N / D_{Ref}\right)^{DSF} \times \left(P_N / P_{Ref}\right)^{PSF} \qquad (8.1)$$

The reference design in this case is the 5MW machine with N representing the target design. The Diameter Scale Factor (*DSF*) is where appropriate 3.0 apart from the mechanical brakes and hydraulic systems which are scaled as 2 and 2.5 respectively. The Power Scale Factory (*PSF*) is 1 where appropriate and 0.2 for the control system.

MULTI ROTOR LIFE COST ASSESSMENT	Cost Fractions	Reference Design	Large Single Rotor	Equivalent Multi Rotor
No of rotors		1	1	45
Diameter @ 350 W/m²		135	270	40
Power rating [MW]		5	20	20
Rotor (€)	0.086	1542	12690	1892
Blades	0.052	920	7360	1097
Hub	0.022	398	3183	474
Pitch mechanism and bearings	0.013	224	2148	320
Drive train & nacelle (€)	0.157	2802	18588	7544
Low speed shaft	0.007	124	995	148
Bearings	0.004	68	547	82
Gearbox	0.053	939	7509	1119
Mechanical brake, HS coupling	0.001	10	41	41
Generator	0.020	348	1393	1393
Variable speed electronics	0.020	359	1435	2871
Yaw drive and bearing	0.004	75	597	89
Main frame	0.022	398	3183	474
Electrical connections	0.012	213	853	1023
Hydraulic system	0.002	44	246	37
Nacelle cover	0.013	224	1790	267
Control & Safety System (€)	0.002	36	47	1055
Tower (€)	0.035	622	622	1865
TURBINE CAPITAL COST (€)	0.281	5000	31947	12355
Foundations	0.163	2903	23225	23225
Installation	0.077	1375	11001	8801
Electrical and grid connection	0.129	2292	6417	6417
Sundry (survey, insurance and so on)	0.051	917	917	917
BALANCE OF PLANT COST (€)	0.420	7487	41560	39359
Parts	0.045	802	6416	1148
Labour	0.255	4545	9090	10908
O&M (€)	0.300	5347	15506	12055
TOTAL (costs € 1000)	1.000	**4 x 17834**	**89013**	**63770**
TOTAL (% of Base)		**80%**	**100%**	**71.6%**

Table 9.3: Lifetime costs comparison

9.4.1.5 Discussion

The results suggest that the structural capital expenditure cost of four 5MW rotors in an onshore location will cost ~ 80% of a single 20MW rotor. A 20MW multi rotor system can further reduce cost to ~89% of four 5MW rotors or ~ 71% of a 20 MW single rotor system. It is important to note that these fractions are independent of the predicted currency cost which will rise and fall based on various market influences.

9.5 OPERATION & MAINTENANCE COSTS

Operation and Maintenance costs (O&M) for offshore sites are in the range of 20-33% of overall electricity cost. There is a significant financial incentive for optimising

maintenance strategies irrespective of the type or size of the systems in question to improve turbine availability.

Availability is a function of component failure and the amount of time that the system is out of action because of a failure, it is strongly influenced by maintenance ship availability and most importantly by the sea state. This is most clearly seen by the effect of gearbox failure, which despite having low frequency accounts for more than 50% of downtime due to their requirement for a jack-up vessel. The control system on the other hand has the largest number of outages but as most can be fixed remotely account for only around 7% of downtime [150].

Most current maintenance ships can only safely operate in wave heights of around 1.5m. On a blustery winter's day in the North Sea wave heights can routinely exceed 2.5m. In the year 2009 the wind farm Egmond aan Zee had only 219 days in which maintenance could be carried out. Most sites typically depict a bath tub relationship when considering maintenance availability through the months Jan-Dec with the worst availability in winter months [150]. Specialised ships can operate in higher sea states but these are more expensive to commission which in turn increases the O&M cost and therefore the cost of energy (CoE).

In an onshore environment, the common approach for the maintenance of large wind farms is a combination of scheduled maintenance (1 or 2 visits per year) and reactive maintenance to restore components after their failure. On land, such an approach is deemed efficiently suitable by operators and can achieve availabilities in the region of 97% [151].

In an offshore environment, the maintenance statistics are markedly different. Due to a lack of operator experience operating in offshore locations or the failure of operators (who often lease wind farms under warranty) to share or make public failure databases have, in turn, left maintenance strategies severely lacking. An operator undertaking a maintenance strategy like that of an onshore site can result in comparatively poor availabilities only reaching 80%, with a wide variation (±10%) possible between wind farm sites [150][151].

The types of failure on a wind turbine are varied. This has led to renewed efforts by academics and industry to identify those components which impact critically on operations and compare them to alternatives quantitatively [152].

The accepted practice is to divide a wind turbine into various sub-systems that can then be characterised by their reliability and the amount of downtime they experience. The typical breakdown of subsystems is found in [153]

Typically, these subsystems are monitored over a period of a year at the site in question and the results presented in tabular format (Table 9.4). The example presented is for a total downtime (in hours) of 17.1% for a Norwegian 36 wind turbine site (V90 - 3MW), and is typical for an offshore wind farm [154].

	Lost MWh	% Lost MWh	# Stops	% Stops	Downtime (hrs)
Ambient	1335	2%	419	5.50%	474:25
Blade System	774	1.20%	88	1.20%	952:30
Brake System	107	0.20%	25	0.30%	75:53
Control System	4537	6.90%	2523	33.00%	3918:33
Converter	890	1.30%	228	3%	1173:42
Electrical	882	1.30%	69	0.90%	605:04
Gearbox	36713	55.60%	567	7.40%	30400:40
Generator	14920	22.60%	101	1.30%	11226:18
Pitch System	4382	6.60%	1599	20.90%	2633:41
Scheduled Service	919	1.40%	858	11.20%	1706:22
Yaw System	502	0.80%	1127	14.70%	203:55
Structure	44	0.10%	15	0.20%	48:52
Grid	0	0.00%	31	0.40%	520:54

Table 9.4 - Downtime as a Function of Wind Turbine Sub-System

The information is column 1 is presented in the form 'Lost MWh' - that is the electricity production lost due to downtime. This is a better metric than considering downtime alone as it accounts for both the downtime and the actual wind speed at that moment in time (i.e. utilises power curves). Hence, downtime occurring in low wind speeds results in a low number of lost MWh.

9.5.1 Availability and Failure Rates

There is always a concern that statistics might be skewed to favour one agenda over another. A study commissioned by GL Garrad Hassan for work-package one (WP1) of the Reliawind project [152] compared various wind turbine reliability data sets from multiple sources and investigations, such as: Reliawind, WindStats Germany, WindStats Denmark, the WMEP and LMK studies.

It concluded that while there is some spread between the relative reliability estimates of various sub-systems within the wind turbines the data sets were generally in good agreement. One of the key analyses from this investigation and of most prominent value in the context of multi rotor systems was the acknowledgment that turbine reliability reduces with increasing turbine rating and as such availability reduces.

The main limitation of the data sets is that they contain the average failure/availability values for multiple different brands/ratings of turbines at different sites. For example, the Reliability study concerns wind farms containing more than 12 turbines, each with individual ratings larger than 850kW (and operating for a minimum of 2 years) but other studies include turbine ratings as low as 50kW.

Figure **9.4** contains plots of the various data sets evaluated in the Reliawind study. The graph shows that the relationship is approximately linear up to ratings of 1MW (for which sufficient data exists) and that the relationship becomes less predictable at higher ratings. The suggestion from the data is that a turbine rated at 200kW is likely to fail half as often as one rated at 800kW though it is important to note that the study includes a multitude of different power electronics, controllers & transmission systems which are not readily comparable.

The German "250MW Wind Programme" [155] on the other hand is a study of machines the majority of which were below 1MW in rating. It is useful in evaluating the multi rotor concept, as any future MRS system will undoubtedly make use of turbines in the sub 1MW range.

Figure 9.3 shows the recorded failure rates for three categories of turbine rating: less than 500kW, between 500kW and 999kW and above 1000kW. This Figure depicts two important pieces of information, the first is that the smaller machines tend to maintain a more consistent failure rate independent of their operational age. This may be more a function of a larger data set (more turbines at sub 500kW rating) which tends to flatten out the failure rate data. The second observation is that the failure rates of the sub 500kW machines is around 60% of those in the 500-999kW bracket and around 25% of those in the 1MW and above category.

A third observation from the study (not shown in the graph) was that machines below 500kW in rating did not experience an increase in failure rates before their 15th year of operation. These Figures are significant as they show that the larger machines are less reliable [156].

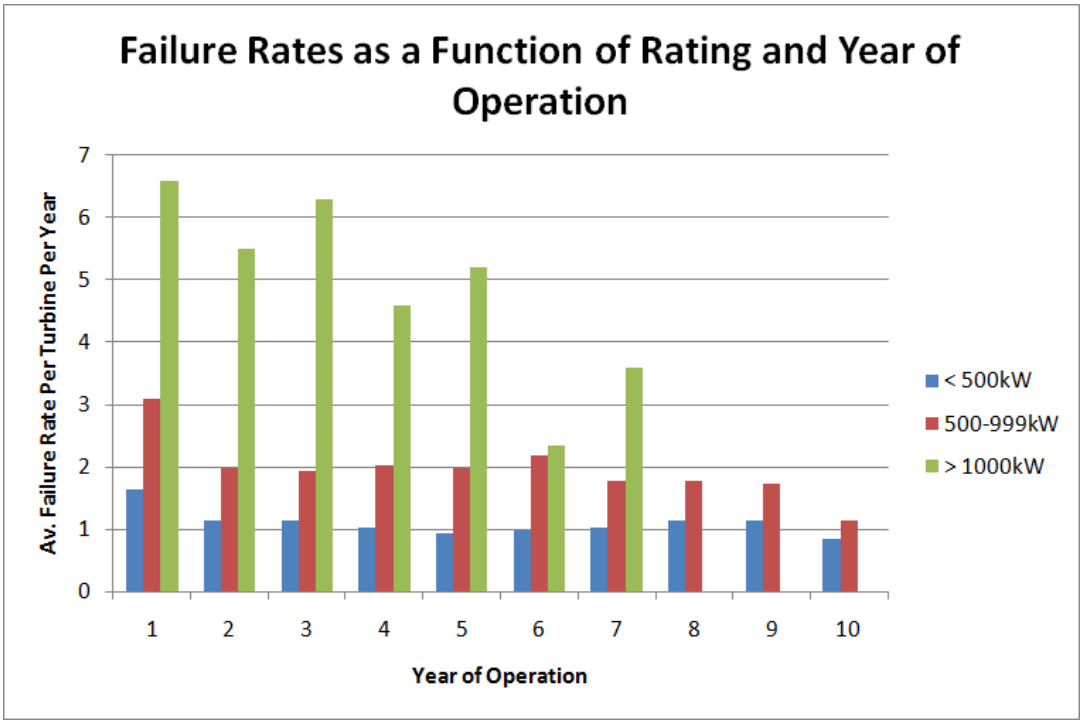

Figure 9.3: Failure Rates in the German 250MW Wind Program

While both main studies into operational failure rates suggest a moderate increase in reliability at lower turbine ratings, the GL GH review did note that there is a tendency

for reliability data from all manufacturers and operators to be under-reported. This means that individual points on the graph should be treated with a degree of scepticism and that the data only give indicative ranges of reliability.

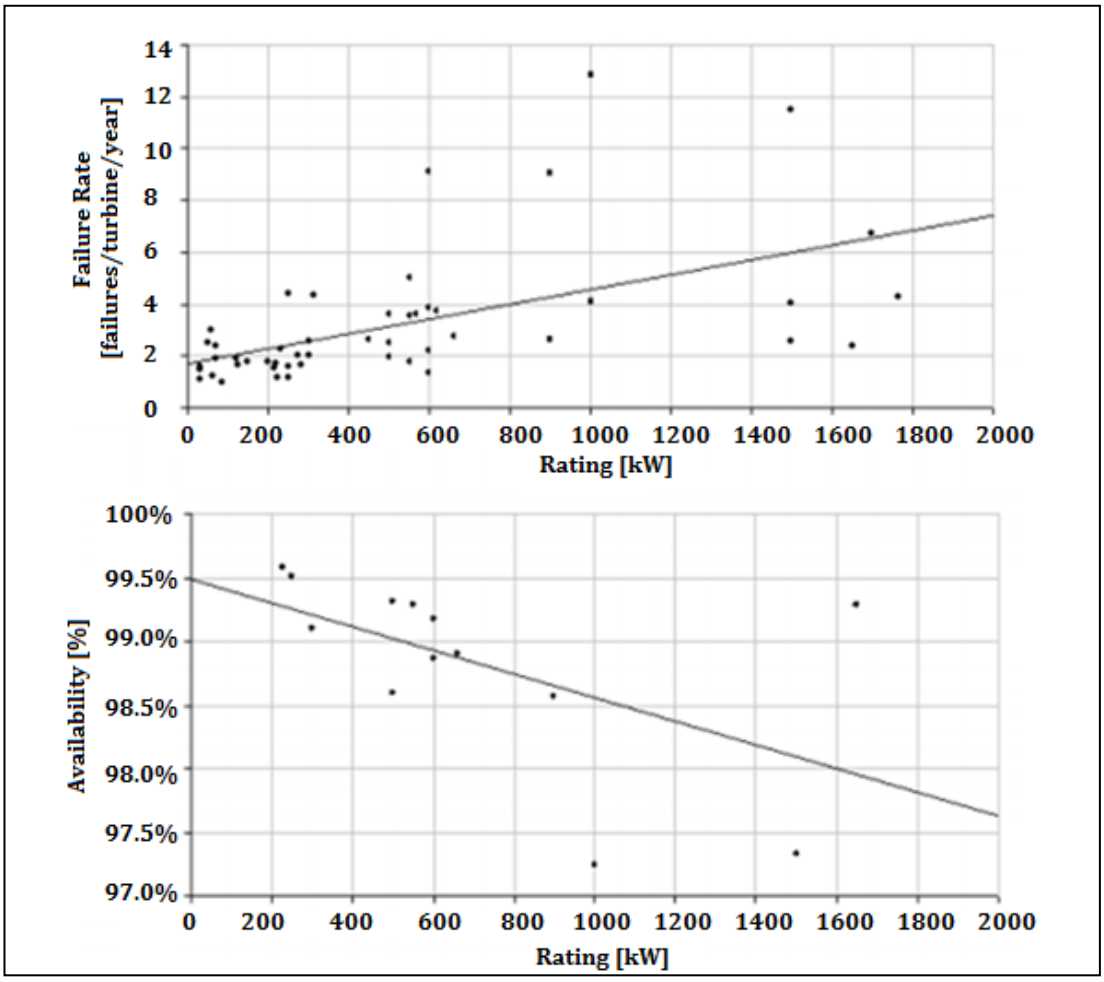

Figure 9.4 - Effect of Rating on Reliability of Sub-systems and Availability

From this real-world data, the MRS failure rate can be defined as something in the region of 2-3 failures per turbine per year or 90-135 failures per 20MW system per year. A 4x5MW system might suffer in the region of 6-8 failures per turbine per year for a total of 24-32 failures per 20MW system. It is difficult to extrapolate much beyond 5MW in any meaningful way therefore it is unknown how many failures a single 20MW rotor might suffer but it is very likely to be at-least the number of failures experienced with a 5MW machine (i.e. 24/32 failures).

Without considering the individual systems mean time to repair (MTTR) at this stage the total energy lost per system is defined as: *Rating x System Failure Rate x MTTR* or 59.94MTTR for the MRS, 160MTTR for the 4x5MW machines and 640MTTR for the single 20MW rotor.

For the three systems to have comparative energy loss over a year the MTTR could take on the ratio 106 hrs: 40 hrs: 10 hrs respectively. Given that manual and minor repairs typically make up 75% of the unscheduled maintenance on a 5MW machine and require at-least 40 hours as MTTR this means that the operators of an MRS can comfortably leave the repair of each 444kW single outage for up to 4.3 days before the system becomes uncompetitive in energy loss against a the 5MW systems and over 17 days before the system becomes uncompetitive in energy loss against a 20MW single rotor system.

A 17-day window per turbine repair is incredibly attractive from an O&M perspective as it would almost eliminate the need for any unscheduled maintenance meaning that short weather windows & vessel availability would no longer play a significant role in determining overall O&M costs.

9.5.2 O&M Modelling

9.5.2.1 Model Overview

The problem of failure and repair mechanisms/predictions for wind turbines is too complex to be adequately captured using analytical expressions and simulations are generally used to represent the process in the majority of studies. One model developed in the Wind Energy Doctoral Training Centre at Strathclyde University [154] has looked at simulating the repair and failure mechanisms for offshore wind farms using a stochastic process based on available failure rate data. The mean time to repair (MTTR) is determined using a representative time series for wave height and accounts for the availability of adequate repair windows. This approach is already taken in many commercial applications, however the use of an Auto-

Regressive (AR) time series model to generate a wave height time series with correlated wind speed time series is considered novel.

This new approach of using an AR model to represent meteo-ocean site conditions captures short term hourly correlations, medium term access windows of periods up to days and the annual distribution of site data which ultimately result in more realistic and accurate simulations. A Monte Carlo Markov chain failure model is used to simulate failure behaviour, which is the accepted norm amongst the wind industry at present.

The MTTR is implemented within the reliability simulation as a variable process, dependent on significant wave height. This approach automatically captures site characteristics including seasonality and allows for complex analysis using time dependent constraints such as working patterns to be implemented. A simple cost model was also developed to determine lost revenue as a function of both wind speed and turbine failure rates.

Preliminary investigations found that the influence of component reliability was key in determining overall turbine availability and associated power loss over and above any of the other components. In addition, the reliability data and predicted availability across a range of wind farm sizes (50-90 turbine) and individual turbine ratings (1-3MW) correlated strongly with reported real-world data.

This model, which has already been validated, will provide an excellent basis for a study of the multi rotor system O&M costs in comparison to other equivalent single rotor systems. It is hypothesised that any reduced failure rates of smaller rated machines compared to larger ones will result in a very positive O&M cost and overall reduction in CoE compared to alternative equivalently rated systems.

9.5.2.2 Model Parameters

The model allows for the adjustment of a great many parameters which will not be listed here. The crucial parameters that will be modified and tested against for the purposes of this study are:

1. Whether a Jack Up Vessel (JUV) is required. JUV are extremely costly, heavy lift vessels that are usually chartered on an as-needs basis due to their low world-wide availability. JUV are required for lifts above 200,000kg and can carry a limited number of heavy components.
2. The number of technicians employed for the purposes of affecting repairs amongst the wind farm.
3. The number of CTV's (construction & transport vessels) available for use to transport technicians to and from the wind farm and between turbines. This is the number of teams (each team consists of 2-4 men depending on the type of repair) that can be dropped off at each turbine site per hour. Having less sites per MW of installed capacity means less drop-offs.
4. The Medium and Major Repair corrective factor is a scale factor that is used to modify the amount of time taken to conduct a Medium or Major repair. Smaller turbines would require less time to repair by nature their smaller components many of which would not require special lifting equipment.
5. The failure rate as a ratio of the mean failure rate of 10 failures per turbine per year.

Then more generally for the model:

6. The probability of a fault which in turn activates a specific type of repair requirement, which is a function of pre-defined failure rates for each sub-system within the turbine. These values will be estimated using a scale factor and multiplied by the default probabilities (for a 3MW machine) already present in the model.
7. The power curve of the wind turbine used within the wind farm. Cut-out and cut-in wind speeds will be kept the same at 4m/s and 25m/s respectively for all the systems. Rated wind speed is assumed to occur at 10.8m/s.
8. The number of spares that the jack-up vessel can carry. The jack-up is only required for components weighing more than 200 tonnes meaning it would

only be required for 5MW systems and above and even then, only for components such as generators, new rotors and so on.

To make the comparison independent of turbine spacing, all systems other than the multi rotor system will have a standard turbine spacing of 5D. The multi rotor system, while not adequately captured within the sense of a wind farm will be set to have turbine spacing's of 10m given that all the rotors are located at a single site and there is no real way to simulate this within the confines of the current model.

The full details of the variable parameters set in each of the 8 models is shown in Table 9.5: **O&M Model Setup Parameters**

Model	A	B	C	D	E	F	G
# Turbines	45	45	4	4	2	2	1
Unit Rating (MW)	0.44	0.44	5	5	10	10	20
# Jack Up Spares	N/A	N/A	2	2	1	1	1
#Technicians	12	24	24	40	24	40	24
#CTV Turbine Vessels	1	2	2	2	2	2	2
#CTV Turbine Transfers	4	4	2	2	2	2	4
Repair Corrective Factor	0.9	0.9	1	1	1.1	1.1	1.2

Table 9.5: O&M Model Setup Parameters

9.5.3 Results

Table 9.6 presents the full comparison of the four systems, listing: the power produced by each system, the power lost due to failure downtime, the availability as a function of power curve, wind speed and failure rates, the total O&M costs in

millions, the direct O&M costs in millions, the total O&M CoE in £/MWh and the failure rate per turbine per year.

Failure Rate Scale Factor (Model Parameters)	Power Produced (MWh)	Power Lost due to Downtime (MWh)	Availability (%)	Total O&M Costs	Total Direct O&M Costs	Total O&M £/MW hr	Failure Rate / Faults Per Turbine per Year
0.2 (Model A)	2.03×10^6	5.01×10^4	97.32	55.5	50.9	27.33	2.26
0.2 (Model B)	2.03×10^6	5.11×10^4	97.35	85.9	81.3	42.21	2.27
0.30 (Model A)	2.02×10^6	6.47×10^4	96.75	58.7	52.9	29.11	3.21
0.30 (Model B)	2.02×10^6	6.39×10^4	96.81	88.2	82.5	43.74	3.25
0.43 (Model A)	1.99×10^6	8.73×10^4	95.80	63.1	53.3	31.68	4.62
0.43 (Model B)	2.00×10^6	8.44×10^4	95.97	93.2	85.6	46.52	4.63
1.43 (Model C)	1.81×10^6	2.73×10^5	88.04	130.3	105.7	71.79	15.72
1.43 (Model D)	1.79×10^6	2.96×10^5	87.00	70.35	43.7	39.23	15.60
1.55 (Model C)	1.79×10^6	2.91×10^5	87.19	140.5	114.3	78.56	16.76
1.55 (Model D)	1.78×10^6	3.175×10^5	86.06	74.44	45.9	42.04	16.93
1.60 (Model C)	1.78×10^6	3.1×10^5	86.43	146.9	118.9	82.61	17.19
1.60 (Model D)	1.75×10^6	3.34×10^5	85.34	76.89	46.7	43.83	17.41
2.5 (Model E)	1.64×10^6	4.45×10^5	80.68	110.7	70.65	67.47	26.44
2.5 (Model F)	1.583×10^6	5.08×10^5	78.03	78.2	32.53	49.93	26.82
2.94 (Model E)	1.575×10^6	5.1×10^5	78.05	120.1	74.45	76.25	30.54
2.94 (Model F)	1.483×10^6	6.0×10^5	74.02	89.73	35.73	60.48	31.05
3.14 (Model E)	1.555×10^6	5.3×10^5	77.08	124.15	76.4	79.82	32.04
2.5 (Model G)	1.69×10^6	3.925×10^5	82.39	72.25	36.95	42.78	27.04
2.94 (Model G)	1.635×10^6	4.55×10^5	79.77	80.13	39.45	49.14	31.35
4.65 (Model G)	1.42×10^6	6.65×10^5	70.50	110.23	50.45	77.69	47.73

Table 9.6: O&M Comparison (444kW, 5MW, 10MW, 20MW)

Note that this new analysis negates the effect of the increasing MTTR for the MRS artificially to reduce individual O&M costs on a per failure basis. As a result, the O&M costs are comparatively higher than they would be if properly optimised. It does show the improved per turbine failure rates and associated improvement in availability (in cases where each turbine is repaired as soon as possible) that the MRS competes with the 4x5MW system (Model D) with a maximum of 17 failures per year and the 1x20MW system (Model G) with maximum failure rate of 27 per year.

Further analysis suggests that the two most economic systems in an offshore environment are those with the least number of sites, in this case the MRS and the 20MW single rotor. This is not unexpected given the large amount of cost associated with launching both FSV and jack-up vessels at ratings of 5MW and above, which

make the 4 x 5MW and 2 x 10MW systems uncompetitive in comparison. The cheapest MRS option achieves a CoE in O&M of 27.33 £/MWhr, while the cheapest 20MW SR option achieves a CoE in O&M of 42.78 £/MWhr. These values will be carried into the CoE calculation in Section 9.6.

The two MRS and 20MW SR systems are balanced at the lower end of the failure probability spectrum because of the failure rates, which for the single rotor are only 27-31 per year but for the multi rotor system are essentially 2.27x45. As the simulation is not designed specifically for the multi rotor system, the model sends a repair vessel out to repair every single 444kW turbine fault even if it is uneconomic to do so. Therefore, the MRS system has a higher power production, a higher availability and yet a higher cost of O&M in comparison to the 20MW SR.

It is also very important to note that the 20MW single rotor only competes with the multi rotor if it is assumed that the failure rates similar to that of the 10MW rotor can be achieved. Achieving failure rates as low as this will require a mammoth leap in engineering skills/techniques, control systems and materials if it is to be realistic - likely beyond that even surmised by the UPWIND project. If the current failure rates are extrapolated out with even an optimistic outlook, the 20MW single rotor is sufficiently penalised to only have similar cost of energy (in O&M) compared to 4 x 5MW systems.

On the other hand, the multi rotor system can outperform any of the other systems in O&M cost without any new technologies or processes being used that are not already in use today. In addition, it still maintains several operation strategy outlooks that can be optimised - which are not available to the larger systems. This gives it very clear advantages in today's environment of rising offshore energy costs, increasing O&M costs and a demand for cheaper energy

9.5.3.1 Sensitivity to 'Scheduled Maintenance'

It is likely the multi rotor system could benefit from an increased scheduled maintenance regime which aims to catch major faults before they develop (more so that larger individual ratings). From a simulation perspective, this is modelled by increasing the number of hours devoted to scheduled maintenance for each machine per year.

While exact Figures are unknown, it would normally be expected that an increase in scheduled maintenance would result in a decrease in probability of unexpected faults or failures. To give this issue some consideration a sensitivity analysis of scheduled maintenance in conjunction with varying fault probabilities was conducted.

The results of this sensitivity analysis are presented in Table 9.7 and Figure 9.5.

Lost Revenue (£/MWh)							
20 MW MRS, 45 x 444kw Rotor		Ratio of Probability of Failure					
		0.7	0.8	0.9	1	1.1	1.2
Hours of Scheduled Maintenance	60		7.91	8.96	9.97	11.05	12.5
	90	7.55	8.65	9.53			
	120	7.88	8.92	10.15			

Table 9.7: Lost Revenue as a function of failure rate and scheduled maintenance hours

The results show that increasing the number of scheduled maintenance hours with a corresponding decrease in failure probabilities can achieve an increase in revenue as a result of less down-time providing the correct regime is chosen. For example, a decrease in failure rates of 30% brought about by a 50% or 100% increase in the number of scheduled maintenance would achieve a £2.12/MWh or £2.45/MWh reduction in CoE respectively.

It is very important to note that the current method of simulating the cost of operation and maintenance does not make use of one very important advantage available to the multi rotor system. That advantage is that it may be beneficial to run the whole array at less than maximum capacity (if 1 or more rotors has failed) until either a scheduled maintenance window arrives or more turbines fail (above a fixed percentage). The

reasoning behind this is that it is expensive to send a boat and technician crew out to a site to fix only (4.44/200) of capacity. CTV hire cost in most of these multi rotor simulations accounts for over 10.00 £/MWh of the O&M total. If it was only required to have access to these boats two-thirds of the time (say by having one on permanent standby and using a second boat only for scheduled maintenance) then the CoE could be reduced by several £/MWh. The exact reduction would of course depend on the amount of energy lost as a result of operating such a regime, which is something that would need verified through additional and repeated simulation.

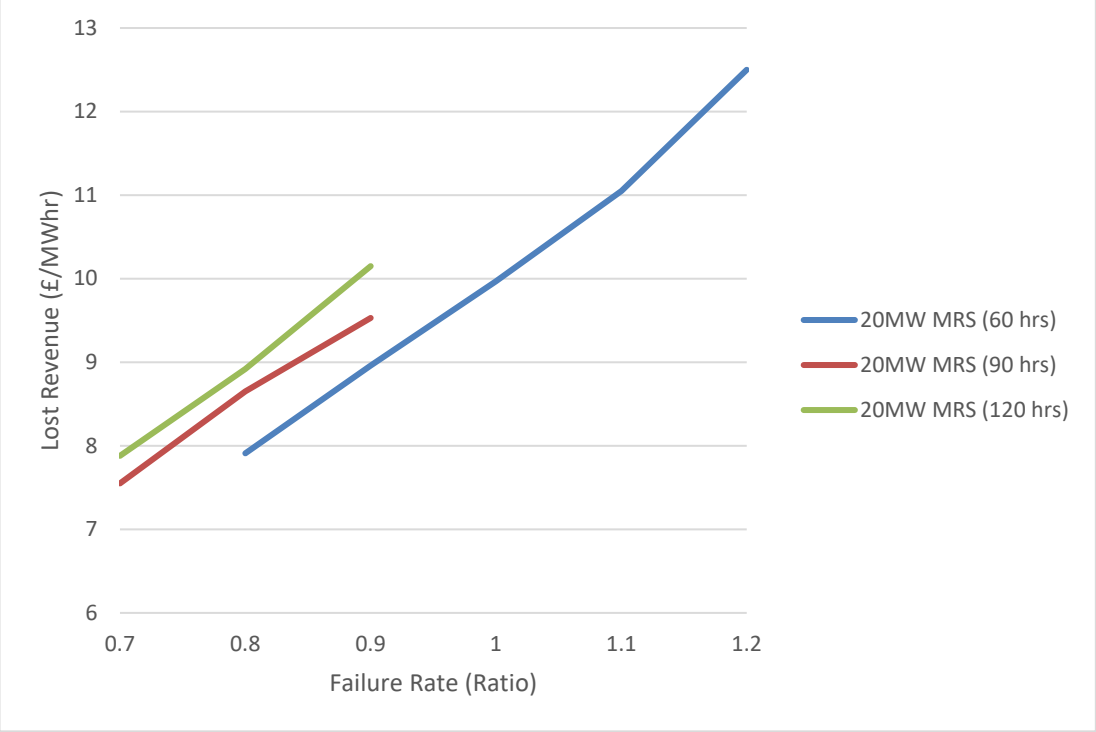

Figure 9.5: Effect of scheduled maintenance time on lost revenue. The ratio of default probabilities is defined as the ratio of the base probability (for a 3MW machine) vs. actual probabilities simulated on the 444kW rotors.

9.6 COST OF ENERGY MODELLING

9.6.1 Equation Form

The cost of energy equation can be expressed as:

$$CoE, £/kWh = \left(ICC \times FCR + O\&M(\lambda, MTTR)\right)/AEP\left(A(\lambda, MTTR)\right) \qquad (8.2)$$

where: *ICC* - the initial capital cost, *FCR* - the fixed charge rate, *MTTR* - is the mean time to recover (h), O&M - operation and maintenance cost (£), *AEP* - average energy produced (kWh), λ - is the failure rate, *A* - availability (%)

9.6.2 NREL Model

The National Renewable Energy Laboratory (NREL) in the United States has developed a tool which it uses to estimate the cost of wind-generated electricity [165]. The aim of the tool is to estimate the difference in cost of different scales of wind turbine, rather than provide a pricing tool by which to estimate real costs of energy. It is therefore perfectly suited to use within the scope of this project for the comparison of four scales of system.

The DOE/NREL scaling model was developed in spreadsheet form in 2006 (updated again in 2010) and uses simple scaling relationships to project the cost of wind turbine components and subsystems for different sizes and configurations of components. The model does not handle all potential wind turbine configurations, but rather focuses on those configurations that are most common in the commercial industry at the time of writing. This configuration focuses on the three-bladed, upwind, pitch-controlled, variable-speed wind turbine and its variants. While future multi rotor systems (and indeed any large-scale wind turbines) might benefit from moving away from these configurations the tool remains useful for a comparison study as of 2014.

The model is very simple in places unless a more sophisticated model of cost is available for that component. Most costs are derived from direct functions of rotor diameter, machine rating, tower height or some combination of these factors. More information about the methods used and initial cost data can be found in the cost model report.

It is important to note that the scaling relationships that the NREL model uses are not necessarily correct. Several of the scaling factors used in the model can be considered conservative - or rather, they reflect scaling with advancing technology rather than scaling with similarity. The results are treated with some caution and likely

underestimate the benefits of the multi rotor in comparison to large single rotor systems of equivalent rating.

9.6.3 Crawford Model (Learning Rates)

Currently the wind industry is non-homogenous in the extreme. There is no standard turbine commonly in use and the result is that ratings, component makeup and specifications vary wildly between wind farms. Turbine manufacturers are constantly adapting and competing on many different fronts, never settling on or standardising a design causing inherent inefficiencies. Standardisation of components allows for manufacturers to focus on mass production and achieve significant cost reductions as a result. Multi rotors, having many more rotors per MW of installed capacity can benefit immensely from component standardisation and the cost savings brought about by worker learning. The way in which workers learn and become more efficient at a task is considered the dominant factor in terms of short-run performance or productivity and the concepts are backed up by learning theory [98].

9.6.3.1 Learning Theory and the Learning Curve

The theory of the learning curve is based on the recognition that the time required to perform a task (or the effort expended) decreases as a worker gains experience. There are two types of learning curve models: the original Wright model which is referred to as the Cumulative Average Model and the Crawford model which is also known as the Incremental Unit Time (or Cost) model.

The concept of the learning curve was first introduced to the aircraft industry in 1936. [157] Wright described a basic theory for obtaining cost estimates based on repetitive production of airplane assemblies. Since then, learning curves (also known as progress functions) have been applied to all types of work from simple tasks to complex jobs and are often used to establish batch production costs in engineering. The underlying hypothesis is that the direct labour man-hours necessary to complete a unit of production will decrease by a constant percentage each time the production quantity is doubled. If the rate of improvement is 20% between doubled quantities,

then the learning percent would be 80% (100-20=80). While the learning curve emphasizes time, it can be easily extended to cost.

In Wrights model, the learning curve function is defined by:

$$Y = aX^b \tag{4.6}$$

where: Y - is the cumulative average time (or cost) per unit, X - the cumulative number of units produced, a - the time (or cost) required to produce the first unit, b - the slope of the function, i.e. log of the learning rate over log of 2.

The slightly more complex model, the Crawford model developed at Stanford University is defined by:

$$Y = aK^b \tag{4.7}$$

where: Y - is the incremental unit time (or cost) of the lot midpoint unit, K - the algebraic midpoint of a specific production batch or lot (average cost), with a and b the same as the Wright model.

Given that K is non-linear the algebraic expression (4.8) must be used:

$$K = \left[\frac{L(1+b)}{N2^{1+b} - N1^{1+b}}\right]^{-1/b} \tag{4.8}$$

where: K - the algebraic midpoint of the lot, L - the number of units in the lot, N_1 - the cost of the first unit in the lot minus 1/2, N_2 - the cost of the last unit in the lot plus 1/2.

To calculate the entire cost of the lot, Y is multiplied by the number of units produced.

The only way to establish which model is most accurate for a problem is to compare the results with real world data. In this case manufacturing data surrounding wind turbines is sparse to non-existent due to its commercially sensitive nature and relative infancy. The Crawford curve is more widely used in practice and thus will be the approach adopted here.

9.6.3.2 Learning Rates

The learning rate is usually determined by statistical analysis of actual cost data for similar products. The data is most readily available in mature industries which have been using mass production for several decades. The Cost Estimator's Reference Manual by Rodney Stewart [166] defines some comparative learning rate estimates that would likely bear strong similarities to the wind industry, these are: Aerospace = 85%, Shipbuilding = 80-85%, Purchased Parts = 85-88%, Raw Materials = 93-96%, Repetitive Welding Operations = 90%, Repetitive electronics manufacturing = 90-95%.

In the context of a wind energy high level costing analysis the concern is of learning rates at system level rather than component level. The systems are divided into 5 sections and their respective learning rates are estimated along with some reasoning:

- **Rotor and Nacelle** with associated focus on aerodynamics shares several aspects with the aerospace industry and therefore could take on a learning rate of **85%.**
- **Drive-train and generator** utilise well established technologies present in ship propulsion, aerospace and purchased parts and can comfortably assume a learning rate of **85%.**
- **Tower and foundations** involve more abstract forms of shipbuilding (in the marine environment sense), materials and the use of welding for a balanced learning rate estimate of **90%.**
- **Control systems and electronics** involve repetitive computerised construction and software installation and therefore can achieve a realistic **90%**.
- **The Balance of Plant** which arguably covers a multitude of different systems might realistically achieve a learning rate of **90%**, particularly in system electrical integration.

At this stage, these notional values need only be close representations of actual learning rates, providing that the same values are used for each of the systems evaluated a fair comparison can be made.

	20MW Single Rotor Crawford Curves			
	Standard 20MW	**Standard 20MW**	**Standard 20MW**	**Standard 20MW**
Unit Rating [MW]	**20**	**20**	**20**	**20**
System unit number	**1**	**10**	**100**	**1,000**
Total Rating [MW]	20	200	2,000	20,000
Turbine number	1	10	100	1,000
Rotor number	1	1	1	1
Rotor				
Blades	6,034,044	2,717,733	1,583,937	923,812
Hub	288,423	168,093	97,948	57,079
Pitch + Bearing	1,568,477	706,442	411,725	239,977
Spinner	67,513	39,347	22,927	13,361
TOTAL	**$7,958,457**	**$3,631,615**	**$2,116,538**	**$1,234,229**
Drive-train Nacelle				
LSS	1,334,416	777,698	453,168	264,081
Bearings	1,462,132	852,131	496,540	289,356
Brakes and Coup	39,787	23,188	13,512	7,874
Generator	5,756,825	3,355,078	1,955,018	1,139,276
Var Speed Elec	2,065,908	1,455,639	1,025,723	722,861
Yaw Drive	0	0	0	0
Main-Frame	68,968	48,595	34,243	24,132
Electrics	1,400,468	986,770	695,332	490,024
Hydraulics	328,517	109,889	52,366	24,934
Nacelle Cover	256,235	216,083	182,234	153,664
TOTAL	**$12,713,256**	**$7,825,069**	**$4,908,135**	**$3,116,202**
Control + Safety				
TOTAL	**$68,048**	**$57,385**	**$48,396**	**$40,808**
Tower				
TOTAL	**$6,471,811**	**$4,560,038**	**$3,213,254**	**$2,264,487**
Balance of Station				
Marinization	4,472,069	3,771,296	3,180,535	2,681,900
Transportation	136,450,451	115,068,665	97,043,561	81,829,335
Offshore Warranty	1,049,946	1,049,946	1,049,946	1,049,946
Support Structure	7,272,574	7,272,574	7,272,574	7,272,574
Port and Staging	484,838	484,838	484,838	484,838
Scour Protection	1,333,305	1,333,305	1,333,305	1,333,305
Electrical Interface	6,302,897	6,302,897	6,302,897	6,302,897
Installation	2,424,191	2,424,191	2,424,191	2,424,191
Offshore Permits	896,951	896,951	896,951	896,951
Personal Access	72,726	72,726	72,726	72,726
Surety Bond	6,017,503	6,017,503	6,017,503	6,017,503
TOTAL	**$166,777,451**	**$144,694,892**	**$126,079,027**	**$110,366,166**
SYSTEM COST	**$193,989,023**	**$160,768,999**	**$136,365,350**	**$117,021,892**
Cost per MW	**$9,699,451**	**$8,038,450**	**$6,818,268**	**$5,851,095**

Table 9.8: 20MW Single Rotor Costing

	Multi-Rotor Crawford Curves			
	Multi Rotor 20MW	**Multi Rotor 20MW**	**Multi Rotor 20MW**	**Multi rotor 20MW**
Unit Rating [MW]	**20**	**20**	**20**	**20**
System unit number	**1**	**10**	**100**	**1,000**
Total Rating [MW]	20	200	2,000	20,000
Turbine number	1	10	100	1,000
Rotor number	45	45	45	45
Rotor				
Blades	36,387	6,713	3912	2,281
Hub	8,885	2,121	1236	721
Pitch + Bearing	12,211	2,253	1313	765
Spinner	1,350	322	188	109
TOTAL	**$2,647,485**	**$513,424**	**$299,159**	**$174,421**
Drive-train Nacelle				
LSS	6,834	1,631	951	554
Bearings	2,317	553	322	188
Brakes and Coup	883	211	123	72
Generator	127,801	30,506	17777	10,364
Var Speed Elec	45,863	18,116	12768	8,998
Yaw Drive	0	0	0	0
Main-Frame	22,916	9,052	6380	4,496
Electrics	31,090	12,281	8655	6,100
Hydraulics	7,293	716	341	163
Nacelle Cover	9,800	6,236	5259	4,435
TOTAL	**$11,465,865**	**$3,568,562**	**$2,365,937**	**$1,591,617**
Control + Safety				
TOTAL	**$68,000**	**$43,520**	**$36,489**	**$30,773**
Tower				
TOTAL	**$6,331,095**	**$4,722,997**	**$2,500,783**	**$2,215,489**
Balance of Station				
Marinization	85,447	72,032	54,370	51,250
Transportation	22,154	18,676	14,097	13,288
Offshore Warranty	94,975	94,975	94,975	94,975
Support Structure	161,451	161,451	161,451	161,451
Port and Staging	10,763	10,763	10,763	10,763
Scour Protection	29,599	29,599	29,599	29,599
Electrical Interface	139,924	139,924	139,924	139,924
Installation	53,817	53,817	53,817	53,817
Offshore Permits	19,912	19,912	19,912	19,912
Personal Access	72,725	72,725	72,725	72,725
Surety Bond	40,660	40,660	40,660	40,660
TOTAL	**$32,914,215**	**$32,154,014**	**$31,153,163**	**$30,976,374**
SYSTEM COST	**$53,426,660**	**$41,002,517**	**$36,355,530**	**$34,988,673**
Cost per MW	**$2,671,333**	**$2,050,126**	**$1,817,777**	**$1,749,434**

Table 9.9: 20MW Multi rotor Costing

	10MW Single Rotor Crawford Curves			
	Standard 10MW	**Standard 10MW**	**Standard 10MW**	**Standard 10MW**
Unit Rating [MW]	**10**	**10**	**10**	**10**
System unit number	**2**	**20**	**200**	**2,000**
Total Rating [MW]	20	200	2,000	20,000
Turbine number	2	20	200	2,000
Rotor number	1	1	1	1
Rotor				
Blades	763381.9551	292,223	170,311	99,240
Hub	582569.5022	288,547	168,188	97,988
Pitch + Bearing	622590	238,327	138,900	80,937
Spinner	20254.11762	10,032	5,847	3,407
TOTAL	**$1,988,796**	**$829,129**	**$483,246**	**$281,571**
Drive-train Nacelle				
LSS	489,115	242,258	141,207	82,269
Bearings	431,281	213,613	124,511	72,541
Brakes and Coup	19,894	9,853	5,743	3,346
Generator	2,878,412	1,425,678	830,998	484,149
Var Speed Elec	1,032,954	655,100	461,627	325,277
Yaw Drive	0	0	0	0
Main-Frame	117,763	74,685	52,628	37,084
Electrics	700,234	444,088	312,935	220,504
Hydraulics	164,259	43,956	20,943	9,970
Nacelle Cover	130,220	104,320	87,977	74,187
TOTAL	**$5,964,131**	**$3,213,551**	**$2,038,569**	**$1,309,327**
Control + Safety				
TOTAL	**$68,048**	**$54,514**	**$45,974**	**$38,767**
Tower				
TOTAL	**$2,304,996**	**$1,461,829**	**$1,030,103**	**$725,843**
Balance of Station				
Marinization	1,939,498	1,553,732	1,310,325	1,104,932
Transportation	15,280,889	12,241,520	10,323,769	8,705,523
Offshore Warranty	2,154,997	2,154,997	2,154,997	2,154,997
Support Structure	3,636,287	3,636,287	3,636,287	3,636,287
Port and Staging	242,419	242,419	242,419	242,419
Scour Protection	666,653	666,653	666,653	666,653
Electrical Interface	3,151,449	3,151,449	3,151,449	3,151,449
Installation	1,212,096	1,212,096	1,212,096	1,212,096
Offshore Permits	448,475	448,475	448,475	448,475
Personal Access	72,726	72,726	72,726	72,726
Surety Bond	1,400,088	1,400,088	1,400,088	1,400,088
TOTAL	**$30,205,576**	**$26,780,441**	**$24,619,282**	**$22,795,643**
SYSTEM COST	**$40,531,548**	**$32,339,463**	**$28,217,173**	**$25,151,152**
Cost per MW	**$4,053,155**	**$3,233,946**	**$2,821,717**	**$2,515,115**

Table 9.10: 10MW Single Rotor Costing

	5MW Single Rotor Crawford Curves			
	Standard 5MW	**Standard 5MW**	**Standard 5MW**	**Standard 5MW**
Unit Rating [MW]	**5**	**5**	**5**	**5**
System unit number	**4**	**40**	**400**	**4,000**
Total Rating [MW]	20	200	2,000	20,000
Turbine number	4	40	400	4,000
Rotor number	1	1	1	1
Rotor				
Blades	879,261	286,112	166708	97158
Hub	88,855	37,408	21805	12706
Pitch + Bearing	248,543	80,876	47124	27464
Spinner	13,503	5,685	3314	1931
TOTAL	**$1,230,162**	**$410,080**	**$238,950**	**$139,259**
Drive-train Nacelle				
LSS	180,392	75,945	44268	25796
Bearings	127,954	53,868	31400	18297
Brakes and Coup	9,947	4,188	2441	1422
Generator	1,439,206	605,906	353181	205806
Var Speed Elec	516,477	294,753	207727	146370
Yaw Drive		0	0	0
Main-Frame	76,873	43,872	30918	21786
Electrics	350,117	199,812	140817	99223
Hydraulics	82,129	17,584	8377	3991
Nacelle Cover	67,213	51,156	43137	36382
TOTAL	**$2,850,308**	**$1,347,083**	**$862,267**	**$559,075**
Control + Safety				
TOTAL	**$68,048**	**$51,792**	**$43,674**	**$36,835**
Tower				
TOTAL	**$813,666**	**$464,359**	**$327,256**	**$230,593**
Balance of Station				
Marinization	811,977	617,995	521127	439523
Transportation	1,590,572	1,210,585	1020829	860977
Offshore Warranty	902,196	902,196	902196	902196
Support Structure	1,818,143	1,818,143	1818143	1818143
Port and Staging	121,210	121,210	121210	121210
Scour Protection	333,326	333,326	333326	333326
Electrical Interface	1,575,724	1,575,724	1575724	1575724
Installation	606,048	606,048	606048	606048
Offshore Permits	224,238	224,238	224238	224238
Personal Access	72,726	72,726	72726	72726
Surety Bond	440,578	440,578	440578	440578
TOTAL	**$8,496,738**	**$7,922,769**	**$7,636,145**	**$7,394,689**
TURBINE COST	**$13,458,923**	**$10,196,083**	**$9,108,292**	**$8,360,451**
Cost per MW	**$2,691,785**	**$2,039,217**	**$1,821,658**	**$1,672,090**

Table 9.11: 5MW Single Rotor Costing

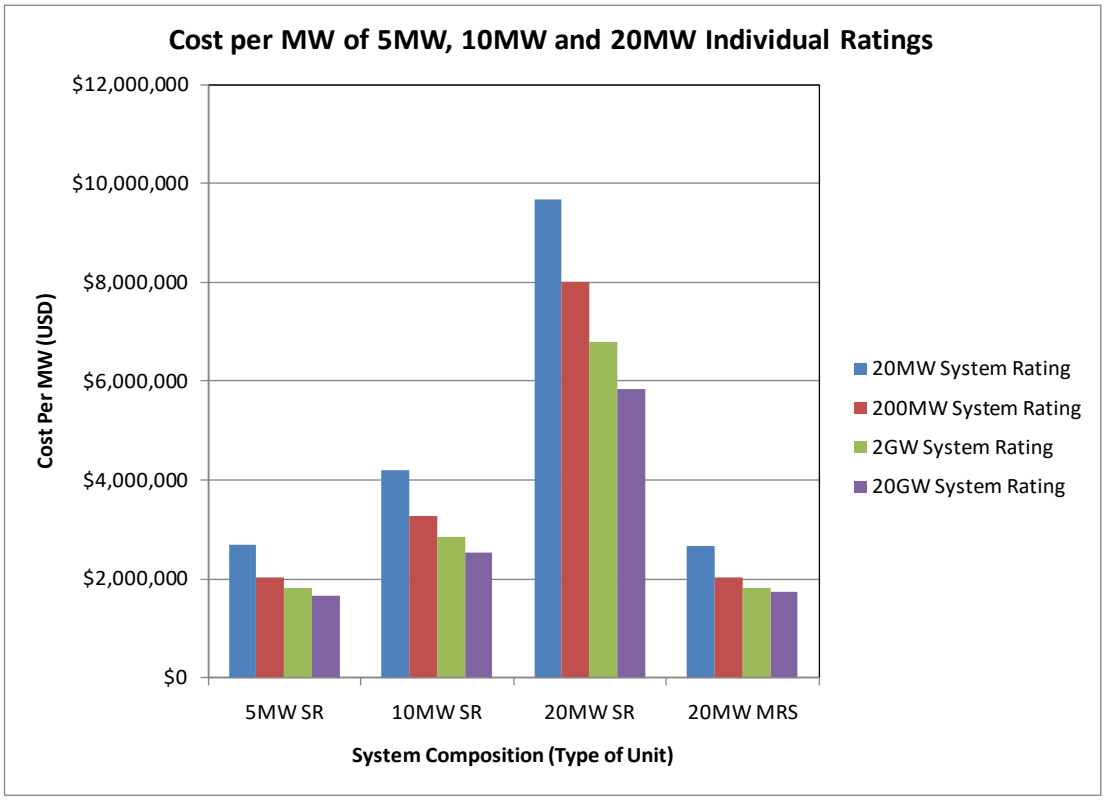

Figure 9.6: Total Cost per MW of Various Turbine Ratings with Increasing System Ratings

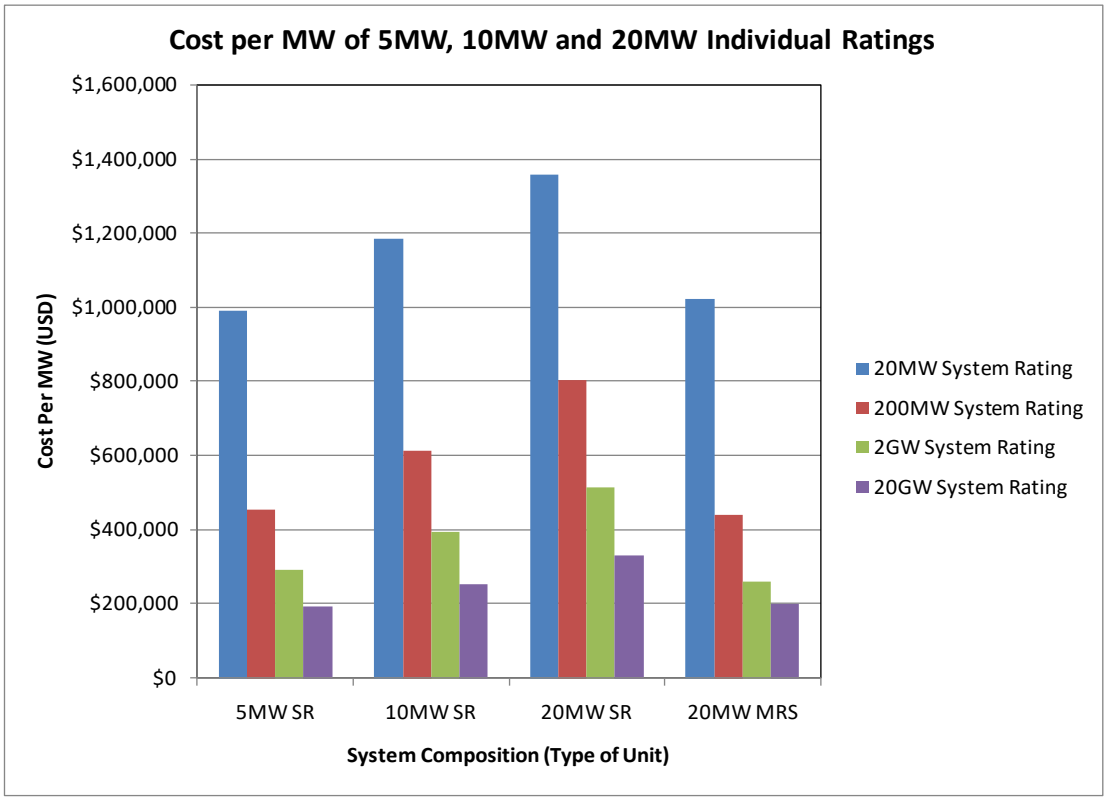

Figure 9.7: Reduced Cost per MW (Not including BOP)

Figure 9.6 represents the cost Figures for the rotor, drive-train, control-system, tower and balance of plant. The balance of plant arguably represents the cost areas of largest uncertainty. It includes such variables as: offshore permits, ports and staging, surety bonds, transportation and marinization. Though the model provides representative scaling equations to calculate these, it is perhaps more prudent to compare the systems without these. The largest Figure in balance of plant generally comes from the support structure which scales poorly with increasing rating. It is likely that any drive towards large individual ratings or multi rotors would result in much lower costs of support structure than existing scaling laws would predict. Figure 9.7 represents the cost analysis with balance of plant removed. Thus, it is possible to conclude that the multi rotor system makes significant savings in rotor, drive-train and tower costs alone to merit serious consideration at large MW scales, with savings of around 20% and 40% compared to two 10MW single rotors and a single 20MW rotor respectively.

Perhaps surprisingly is the fact that the 5MW system appears to match if not beat the multi rotor system at some scales (20MW and 2GW). This can be attributed to two reasons:

The first is that the NREL model scales with similarity and thus makes no account of changing technology with size. It has already been proposed that the small 444kW rotors could be further optimized such that they descend the scaling curves with a better than cubic relationship (in fact the NREL model empirical scaling factor is closer to a square law). In this case the multi rotor could comfortably make further savings over and above the already extensively developed 5MW machines.

The second reason can be attributed to the fact that the economies of scale work best on the order of a few hundred, with the gains decreasing as number of units increases. For example, there is only marginal net advantage to individual unit price of producing 20,000 units compared to 2,000 units. Thus, 5MW machines are already

achieving some economies of scale compared to larger rotors of 10MW or 20MW rating.

None the less, even this empirical scaling study suggests that the multi rotor system, even with several constricting factors (such as less than realistic scaling factors) appears to favourably compete with individual units of equivalent rating. This cost study will be tackled using another method in the next section to further confirm the results.

9.6.4 LCoE Cost Model (UoS)

9.6.4.1 Introduction

The final cost study is a summary of the adapted scaling model developed as part of this thesis and used to further the objectives of the Innwind project. It was modified internally at the University of Strathclyde. The objective of this study was to further investigate the predicted levelized cost of energy for a 20MW multi-rotor system versus that of 2x10MW single rotors. Modelling of the 10MW RWT is taken from a modified cost model provided as deliverable D1.23 of the Innwind Project (April 2014).

The main assumptions are a 1% improvement in availability (and associated increase in Capacity Factor) plus moderately cheaper overall CAPEX costs because of material savings in the MRS compared to equivalent single rotor systems. All the resulting costs are presented in 2012 Euro.

9.6.4.2 Results

A base case comparison of the LCoE evaluation of MRS and RWT is presented in Table 9.12.

Parameter (All include marinization and cost scaling factor where appropriate)	Wind Turbine System				Ratio (MRS/2x10MW turbines)
	Multi-rotor system wind turbines 20MW (45x444kW)		Single Turbines 2x10MW (20MW)		
	Single MRS rotor	All MRS rotors	Single 10MW	2x10MW	
Rotor System(s) cost (€)	**41,943**	**1,887,431**	**3,415,042**	**6,830,084**	**0.276**
Blades (€)	**24,615**	*1,107,668*	*2,174,323*	*4,348,646*	*0.255*
Hub (€)	**9,969**	*448,594*	*688,242*	*1,376,484*	*0.326*
Pitch mechanism (€)	**5,359**	*241,148*	*524,303*	*1,048,606*	*0.230*
Nose cone (€)	**2,000**	*90,021*	*28,173*	*56,346*	*1.598*
Drivetrain and Nacelle cost (€)	**132,693**	**5,971,175**	**7,041,092**	**14,082,184**	**0.424**
Low speed shaft (€)	**3,613**	*162,604*	*450,599*	*901,198*	*0.180*
Main bearing (€)	**2,520**	*113,386*	*547,098*	*1,094,196*	*0.104*
Gearbox (€)	**0**	*0*	*1,694,765*	*3,389,530*	-
Mechanical brake and couplings (€)	**988**	*44,444*	*25,955*	*51,910*	*0.856*
Generator (€)	**11,545**	*519,536*	*1,109,011*	*2,218,022*	*0.234*
Power electronics (€)	**49,110**	*2,209,931*	*1,290,417*	*2,580,834*	*0.856*
Bed plate (€)	**22,825**	*1,027,134*	*139,676*	*279,352*	*3.677*
Hydraulic and cooling system (€)	**7,121**	*320,428*	*187,104*	*374,208*	*0.856*
Nacelle Cover (€)	**1,621**	*72,959*	*142,964*	*285,928*	*0.255*
Electrical connections (€)	**33,350**	*1,500,752*	*876,315*	*1,752,630*	*0.856*
Yaw system (€)	**0**	*0*	*577,189*	*1,154,378*	-
Control/Condition Monitoring system (€)	**35,455**	**1,595,455**	**75,833**	**151,666**	**10.520**
Turbine Cost (excluding tower/support stucture) (€)	**210,090**	**9,454,061**	**10,531,967**	**21,063,934**	**0.449**
Support Structure/Tower (€)	**18,088,555**		**3,519,533**	**7,039,066**	**2.570**
Complete Turbine Cost including tower/spaceframe (€)	**27,542,615**		**14,051,500**	**28,103,000**	**0.980**
Balance of Plant (€)	**31,854,778**		**16,949,603**	**33,899,206**	**0.940**
Underwater Foundation system (€)	*18,154,552*		*9,496,800*	*18,993,600*	*0.956*
Offshore transportation (€)	*3,224,045*		*1,613,636*	*3,227,273*	*0.999*
Port and staging equipment (€)	*432,900*		*216,667*	*433,333*	*0.999*
Offshore turbine installation (€)	*3,246,750*		*1,625,000*	*3,250,000*	*0.999*
Offshore electrical I&C (€)	*6,796,530*		*3,401,667*	*6,803,333*	*0.999*
Scour Protection (€)	*0*		*595,833*	*1,191,667*	-
Turbine CAPEX (€)	**59,397,393**		**31,001,103**	**62,002,205**	**0.958**
Turbine CAPEX per MW Comparison					
Wind turbine capacity factor	**0.566**		**0.508**		**1.113**
Turbine Cost (Million€/MW)	**1.379**		**1.405**		**0.981**
Balance of Plant (Million€/MW)	**1.594**		**1.695**		**0.941**
Turbine CAPEX (Million€/MW)	**2.973**		**3.100**		**0.959**
500 MW Windfarm LCOE Comparison between MRS and 10 MW single wind turbines					
Power per wind turbine (MW)	*20*		*10*		*2.000*
Number of rotors per wind turbine unit	*45*		*1*		*45.000*
Number of wind turbine units	*25*		*50*		*0.500*
Availability (%)	*96*		*95*		*1.011*
Wake losses (%)	*7*		*9*		*0.778*
Wind farm capacity factor	*0.495*		*0.430*		*1.150*
Balance of Plant (Million€/MW)	*1.594*		*1.695*		*0.941*
Operation and Maintenance cost (€/MWh)	*24.45*		*28.12*		*0.870*
Annual Energy Production of wind farm (GWh/y)	*2169*		*1,886*		*1.150*
Windfarm (500 MW capacity) LCOE (€/MWh)	**78.03**		**91.77**		**0.850**

Table 9.12: Cost comparison between MRS and DTU 10 MW wind turbine.

The overall CAPEX reduction of MRS compared to RWT is rather small (4.2%) but within this, there are very large savings specifically in the rotor-nacelle systems (>60%). These for the single turbine concept are the high-risk components that are particularly demanding to develop at ever larger scale. With conservative O&M costs that give no credit to the quite different strategies that would apply to the MRS, the main source of net benefit to the MRS design is the higher capacity factor (or equivalently lower power density) that leads to increased energy capture per rated MW. The power density of the RWT could be decreased with a larger diameter rotor in which case the rotor and tower costs of RWT would rise and the advantage of the MRS would remain but appear much more in CAPEX than in energy output.

In the base case comparison presented here, it is seen that the LCoE model predicts a 15% reduction in LCoE for the MRS in comparison to the RWT.

Sensitivities to many input parameters (wake loss, aerodynamic loss, availability, O&M and so on) were also considered as part of the LCoE study.

9.6.4.3 Aerodynamic Loss Sensitivity

Aerodynamic losses present an interesting area, as the studies of NTUA [163] indicate that accelerated air flow in the spaces between rotors may increase the turbine power and wind farm capacity factor. At present, there is a likely performance gain and no sign of any penalty in aerodynamic performance of an MRS with very closely spaced turbines. Moreover, the analyses of NTUA suggested that an 8% power gain is maintained with the rotor spacing reduced from 5% of diameter to 2.5%. However, a secure position on aerodynamic performance estimates will not be achieved until the aerodynamic performance of complete structure and rotors has been simulated in a turbulent wind field over a range of the range of yaw angles associated with normal power production. It is almost certain that the MRS will have superior power performance to single large turbines in turbulent wind conditions and modelling/simulation predicts significant energy gains increasing markedly with increasing turbulence intensity.

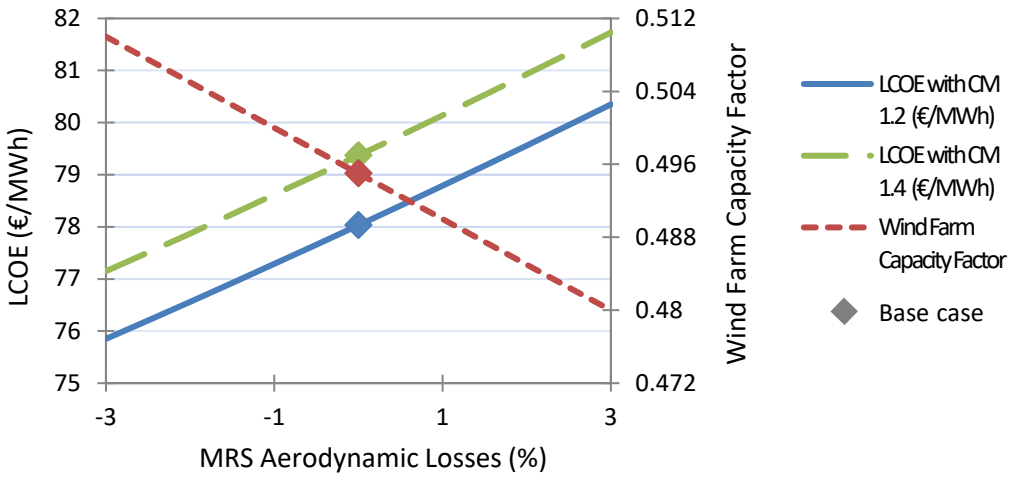

Figure 9.8: MRS LCoE sensitivity to MRS aerodynamic losses.

9.6.4.4 Wind Farm Availability Sensitivity

The availability of the wind farm (Figure 9.9) was varied between 93% and 97%.

Availability will depend on the reliability of the wind farm plant and scheduling of O&M. Offshore O&M is much restricted by availability of suitable weather windows with wave and wind conditions both influencing access and feasibility. The reduced urgency to perform maintenance on the multi rotor is advantageous as it reduced the importance of finding a weather window. In addition, the smaller rotors are likely to be more reliable overall. These factors combine to form a higher availability compared to single rotors of larger equivalent rating.

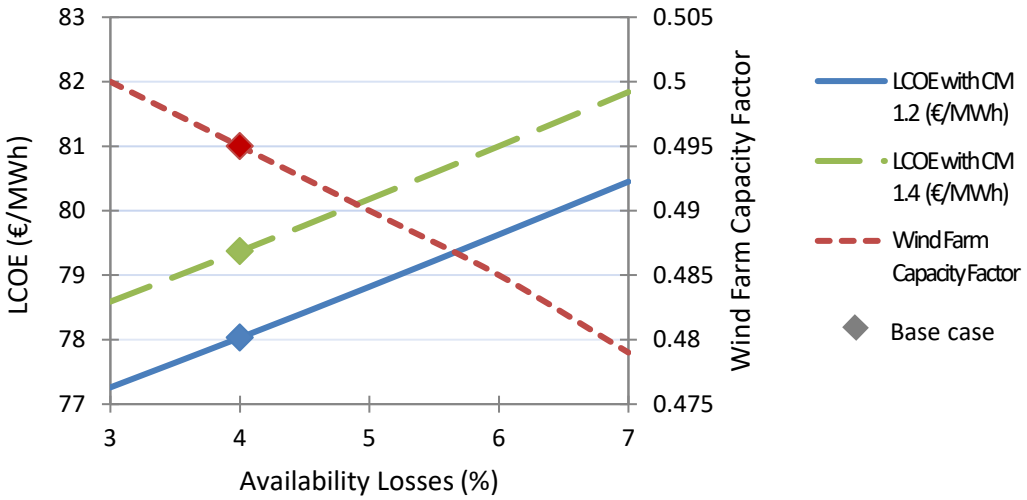

Figure 9.9: MRS LCoE sensitivity to availability.

9.6.4.5 O&M Sensitivity

O&M cost (Figure 9.10) is a very significant influence on LCoE and the choice of O&M model is often subject to debate. The main concerns are:

1. With MRS, there is no offshore installation of turbines and no use of large floating cranes or jack up vessels for rotor installation or rotor maintenance. The offshore activity comprises towing a complete assembly to site with connection of mooring lines and power cables.
2. There is little unscheduled maintenance directly associated with MRS. Obviously, any fault that compromises total power output or any fault with turbine interconnection and wind farm substation will need more urgent attention. This is not captured in the model.

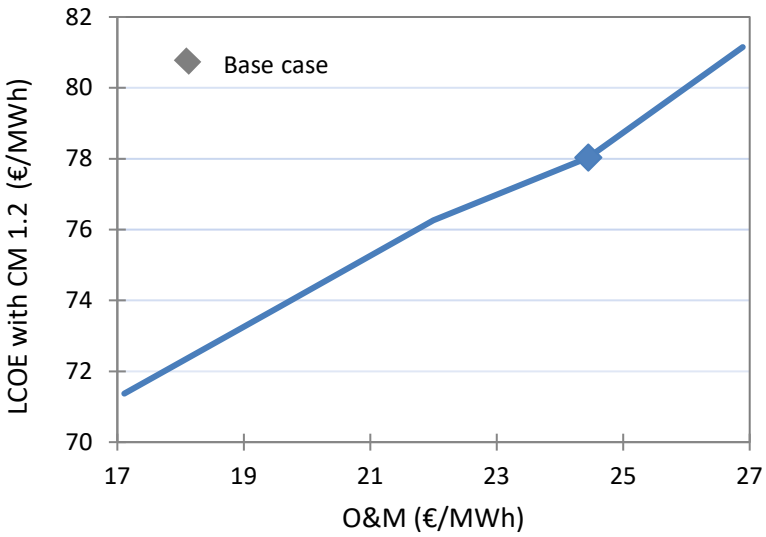

Figure 9.10: MRS LCoE sensitivity to O&M cost.

9.6.4.6 Turbine Cost Multiplier Sensitivity

The turbine cost multiplier (Figure 9.11) is based on scaling benefits, quantity production benefits and the use of robust existing technologies and material methods to enable cheaper parts to be manufactured. A sensitivity over a range of cost multipliers allows this effect to be observed in terms of LCoE. In an MRS, the turbines are a much smaller part of total costs than for the RWT and increasing cost multiplier by 17% from 1.2 to 1.4 increases LCoE by less than 2%.

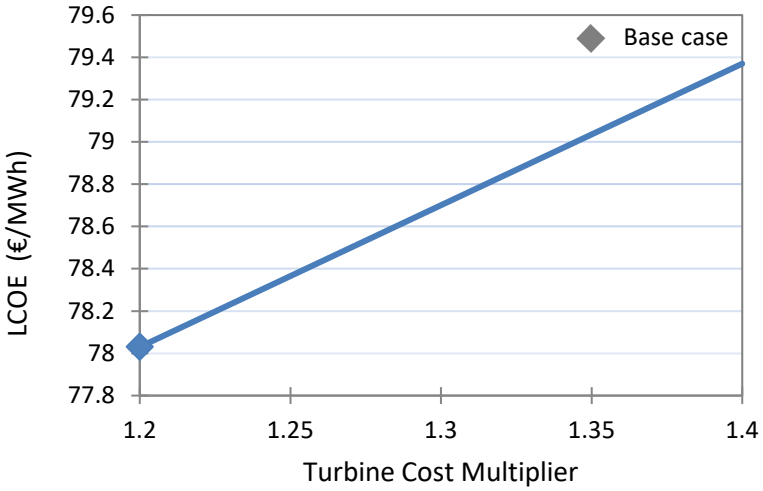

Figure 9.11: MRS LCoE sensitivity to turbine cost multiplier.

The turbine costs (Figure 9.11) are partly based on scaling rules and partly on historic models. Costs based on scaling have regard to the fact that rotor and nacelle costs are mostly fundamentally cubic with rotor diameter, as was discussed in Chapter 3. Commercial data often seems to violate this scaling but largely because components are compared at different stages of technology development. A key argument for the MRS is that most of the projected advantages from cubic downscaling of say rotor blade cost requires no further advance in technology, merely a rigorous application of best current materials and methods to component manufacture of turbines in the hundreds of kW range.

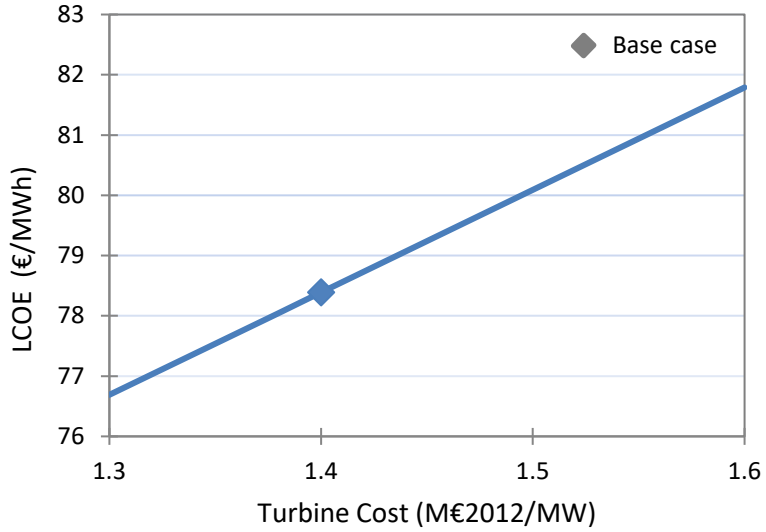

Figure 9.12: MRS LCoE sensitivity to turbine cost.

9.6.4.7 Structural Cost Sensitivity

The MRS structure cost (Figure 9.13) is based on general similarity to a jacket as a large welded space frame with a cost for structure joints included as discussed in Chapter 4. The cost value on the x-axis of Figure 9.13 is derived considering the ratio of cost of steel tubes per kg to cost in an all welded jacket structure. The cost per kg of jackets could decrease but this would require a demand driven development of automated processes for large welded joints.

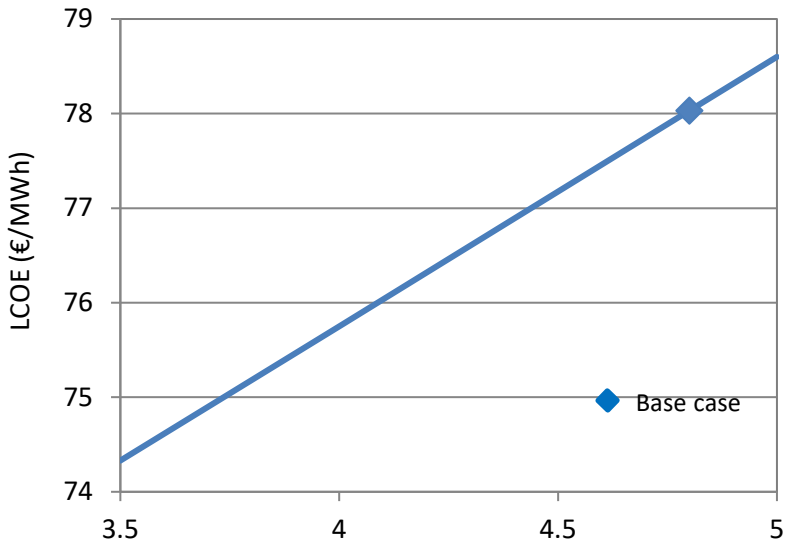

Figure 9.13: MRS structure cost (as jacket cost) per kg (€/MWh)

9.6.4.8 Power Rating Sensitivity

The power rating of the MRS individual units (Figure 9.14 and Figure 9.15) in relation to diameter may not be optimized. Power density (energy/area) is generally optimum at a lower value offshore than on land because total costs related to electrical output form a much larger proportion of CAPEX and of lifetime cost in the offshore situation. The MRS cost model would not readily adapt to a change of rotor diameter. However, as structure costs primarily relate to storm loading on the structure itself, the rated output of MRS may be reduced from the nominal 20 MW and, assuming no impact on structure cost, the cost impacts on electrical components and systems can be accounted.

Obviously as the MRS is de-rated, more systems are required to make up the total wind farm capacity (500 MW). An assumption was made that O&M costs rise in proportional to the number of systems making up wind farm capacity or equivalently that O&M costs were factored as (444 /P) where P is the unit turbine rating chosen. Figure 9.14 suggests that a unit de-rating to about 15 MW (power density 265 W/m^2) could further reduce LCoE. However, the LCoE modelling is too crude to have confidence in the precision of this assessment. There is general confirmation that the lower power densities now favoured by the industry for very large offshore turbines are appropriate.

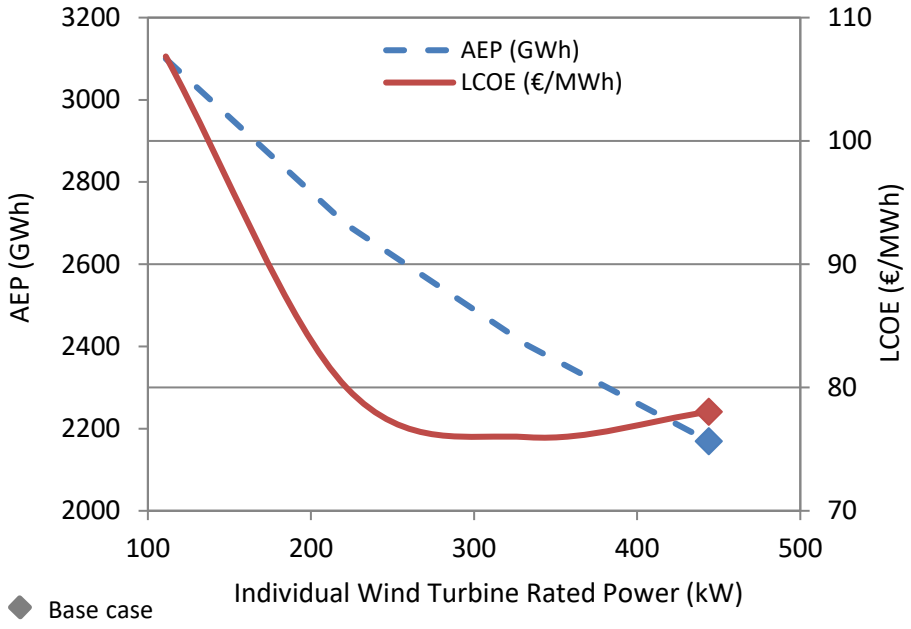

Figure 9.14: Individual Wind Turbine Rated Power (kW)

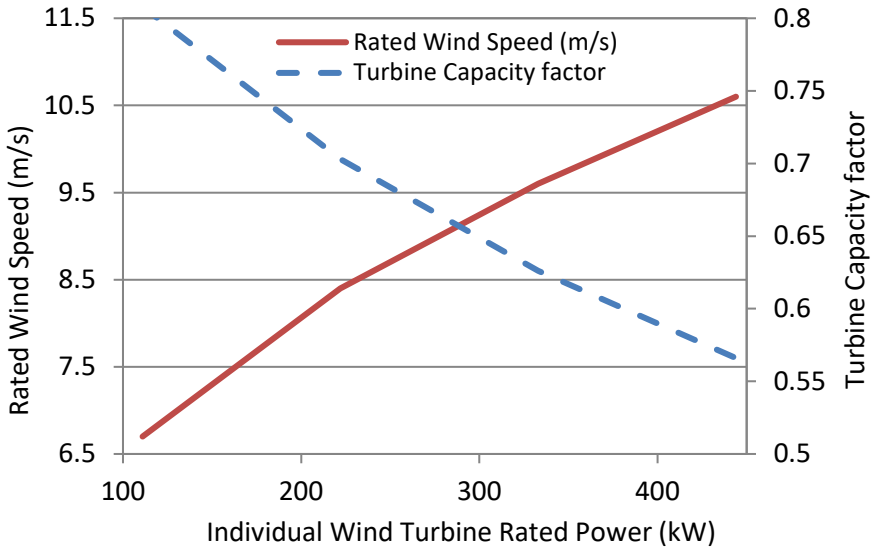

Figure 9.15: Individual Wind Turbine Rated Power (kW)

9.6.5 LCoE Sensitivity Study – DTU 10 MW wind turbine

The range of parameters investigated for MRS give some indication of sensitivities. To form a broad view of the range of overall advantage of MRS to RWT, some consideration is also given to cost sensitivities of the RWT. Wake loss, availability and turbine cost sensitivities are illustrated in Figure 9.16, Figure 9.17, Figure 9.18.

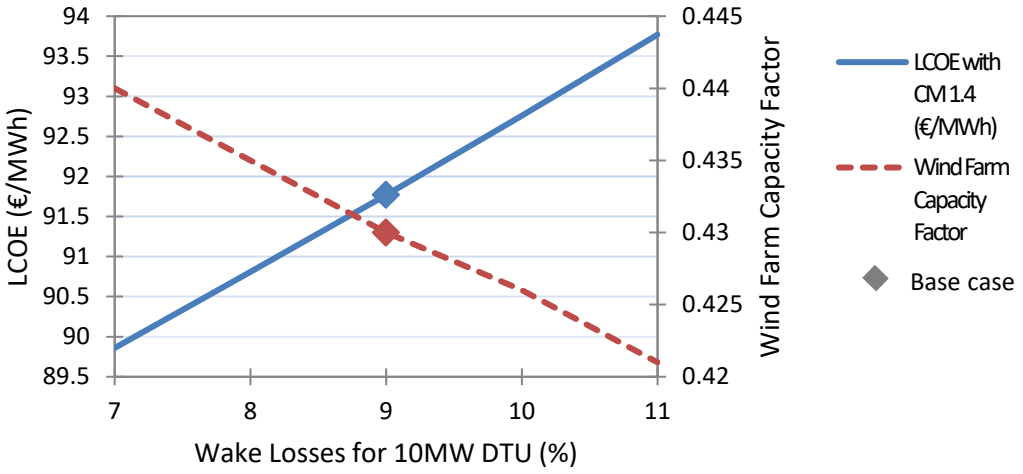

Figure 9.16: DTU 10MW LCoE sensitivity to wake losses.

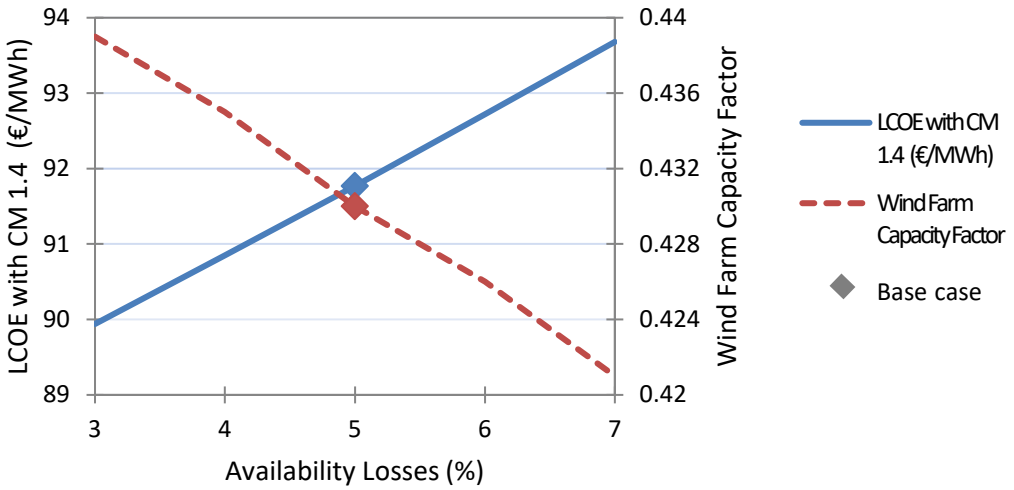

Figure 9.17: DTU 10MW LCoE sensitivity to availability losses.

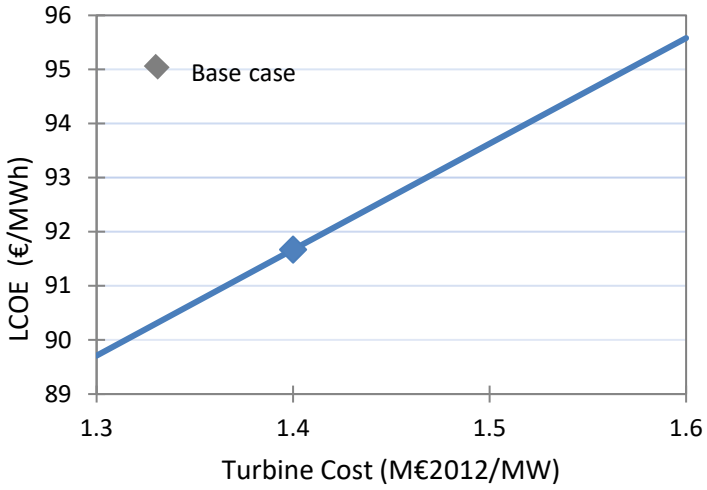

Figure 9.18: DTU 10MW LCOE sensitivity to turbine cost.

9.6.6 LCOE Sensitivity Comparison between MRS and DTU 10 MW RWT

The sensitivities of LCoE across defined ranges for the MRS and RWT are now directly compared (Figure 9.19). Best and worst-case scenarios for various factors (LCoE, O&M, AEP and Capacity Factor) are presented in Table 9.13, and Figure 9.20. The MRS is evaluated with a cost multiplier of 1.2 and 1.4 for comparison and the cost multiplier used in the rest of the study is set at 1.2.

The rather large range in best to worse case results of the MRS reflects various factors especially the lack of an approved O&M model for the MRS that would express the

impact of having no site assembly of turbines and the different pattern of site access requirements. The chosen ranges for "best" and "worst" are also somewhat arbitrary. They reflect considerations such as that, on the one hand, the MRS could gain about 10% power from rotor interactions and better turbulent wind power performance, whilst on the other hand, a significantly adverse impact from the "tower shadow" effects of the structure members, especially in yawed flow, which could cancel this benefit.

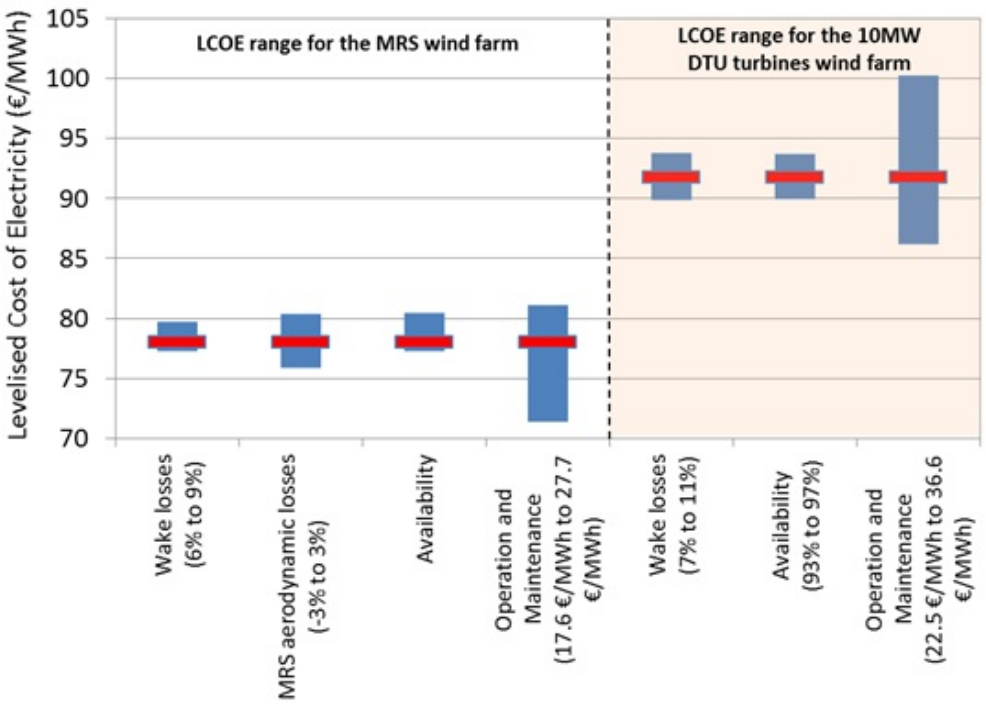

Figure 9.19: LCoE comparison.

		20 MW MRS				RWT - 10 MW DTU				
		Best case		Worst case		Best case		Worst case		Base case
		absolute value	*fraction of base case*	absolute value	*fraction of base case*	absolute value	*fraction of base case*	absolute value	*fraction of base case*	
LCOE	€/MWh	67.35	*0.73*	87.26	*0.95*	82.68	*0.90*	107.46	*1.17*	91.77
CAPEX	Million€/MW	2.97	*0.96*	2.97	*0.96*	3.10	*1.00*	3.10	*1.00*	3.10
O&M	€/MWh	16.27	*0.58*	29.25	*1.04*	21.56	*0.77*	41.11	*1.46*	28.12
AEP	GWh/y	2,281.83	*1.21*	1,994.54	*1.06*	1,968.39	*1.04*	1,806.05	*0.96*	1,886.35
Capacity Factor		0.52	*1.21*	0.46	*1.06*	0.45	*1.04*	0.41	*0.96*	0.43

Table 9.13: Best and worst-case scenarios with reference to the base case values of the 10MW DTU.

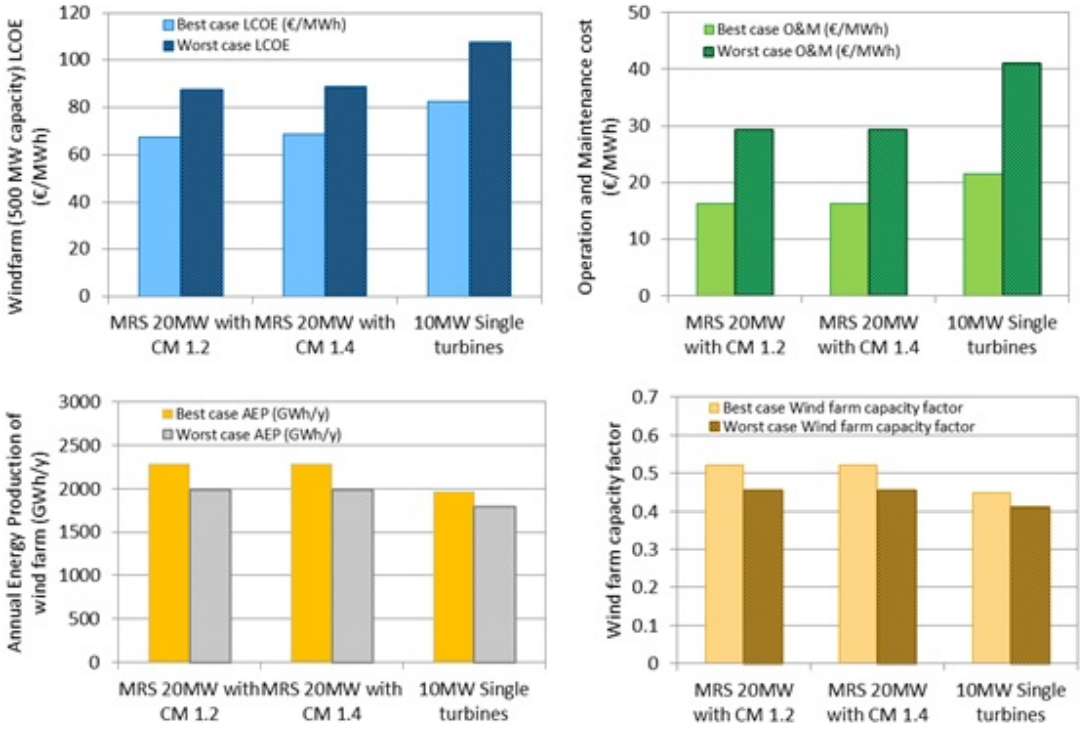

Figure 9.20: Best and Worst-case scenarios for each wind turbine LCoE, O&M costs, AEP and capacity factor.

CHAPTER X - THESIS CONCLUSIONS

10.1 OBJECTIVE OVERVIEW

This thesis set out to answer the question:

"are there are any systems that can provide for individual site ratings of upwards of 20MW but without an associated technological shift?"

The thesis answered this question in two parts. Initially this focussed on evaluating the wind energy design space, leading to a conclusion that rotating turbines provided the best technological and economic performance. It also identified that multi-rotor system could lead to lower cost of energy. The thesis then proceeded to validate that multi- rotors give a lower cost of energy than the equivalent larger single rotor devices at scales above 20MW.

A wide variety of alternative wind energy conversion systems have been investigated ranging from hydrodynamic water based systems to lighter than air kites. These systems were rated according to various parameters but mainly with the assumption that mass is closely related to cost and utilizing conventional scaling laws to predict their parameters if they scaled to 20MW. It was rapidly identified that the HAWT is among the top contenders when considering the efficiency and ease at which it converts wind potential energy into AC electricity. Scaling laws suggest that the move towards ever larger single unit ratings is imposing a financial penalty on LCoE which could be remedied using a more novel multi rotor system.

Multi rotors, utilising many small rotors on a single structure to achieve a larger unit rating have many benefits over large single rotors of equivalent rating, not least in mass scaling laws but also in redundancy, O&M, capacity factor, availability and so on. This study has investigated the multi rotor concept in depth, from the very limited data available to a point where it can now be considered a real contender for offshore wind at unit ratings of 20MW and beyond.

10.2 FINDINGS

As with any 'blue sky' research, there comes a degree of uncertainty with any findings. The nature of this study throws up a whole host of questions with very different potential answers - from the positive to the negative. Without further in-depth study, it cannot be said with 100% certainty that the multi rotor system out-performs single rotors of equivalent ratings - for example 4 x 5MW rotors. However, it can be said that the theory suggests that it should be the case when considering the effects of downscaling with similarity, turbine standardisation and single higher rated offshore wind generation sites. It implies that in up-scaling single rotors to 10MW and beyond, the structural cost begins to impede on any additional savings made using less, higher rated machines for a given wind farm power rating. The multi rotor system achieves higher single site ratings, but without these associated structural penalties and therefore is well placed to make use of O&M savings.

The cost of subsidised wind varies from between £69/MWh to £47/MWh for onshore wind depending on the source (non-subsidised). Without these subsidies, the CoE is estimated to be closer to £140/MWh. This study has shown that a 20MW system based as part of a wider 500MW wind farm could achieve a LCoE of £78.03/MWh, increasing individual unit capacity (through use of more turbines, not larger turbines per structure) could achieve LCoE of £77.88/MWh without subsidy. Larger single rotors based on conventional designs and scaled up to 10MW in accordance with current industry trends could achieve a LCoE of £91.77/MWh. It has therefore been shown that while moving to larger single ratings can result in lower cost of energy than currently seen in the industry, additional savings of 20-25% could be made by developing smaller unit capacities in single structures instead.

Actual CAPEX costs for a 20MW multi rotor system of 60 million Euros for a 20MW system compare favourably with 2 x 10MW single rotors based on the RWT design (Innwind) at 62 million Euros and 1 x 20MW single rotor based on the UPWIND design at 64.78 million. However, the true LCoE reductions come from an increase in energy capture prompted by reduced wake losses of a full percentage point [150],

increase energy capture per swept area because of rotor blockages (giving an 8% increase) and the ability to achieve higher capacity factors 0.495 instead of 0.435 due to the use of larger rotors for a given power rating (lower energy density). Overall these allow the multi rotor system to achieve a LCoE saving of around 15% over its single rotor equivalents at 2 x 10MW and 16% at 1 x 20MW.

These figures are not to be snuffed at and even if the multi rotor system developed here was found to have been optimistic in areas (though safety factors have been used in areas of uncertainty) then there is still plenty of scope for adjustment while maintaining a LCoE lead. Overall they provide a strong context for future study and expanded research into the concept.

The distributed nature of loading from multi rotors at a scale of 20 MW and greater (assuming larger systems have more rotors and not larger rotors) appears to lead to a structure which for Class 1 offshore sites will be designed by extreme wind loads on its own members and not by loading input from the rotors.

Fatigue load calculations for the MRS structure have yet to be completed but the very low load ranges resulting from total rotor loading strongly suggest that extreme storm loads rather than fatigue loading will drive structure design.

Initial results suggest that the current MRS concept can feasibly achieve the aim of 20MW rated power without being adversely limited by design critical loads, particularly extreme turbulent storm cases which often design limit large single rotors. The current space-frame and power-train mass is equivalent to a notional 20MW machine up-scaled from 5MW with similarity.

This suggests that the large CoE benefit of a MRS system associated with reduced rotor and drive train cost will not be significantly compromised by adverse structure cost.

Furthermore, the MRS system can take advantage of several factors that a single rotor cannot. For example, increased degrees-of-freedom, quicker response to varying

wind fields and importantly increased use of standardised components which help drive down the cost-of-energy.

10.3 LIMITATIONS & FURTHER STUDY

It is accepted the O&M model is not fully developed to support multi rotor systems in the context for which it has been used. However, the model has been verified independently as providing a good solution to O&M estimates for offshore single rotor machines in the region of 2-5MW for wind farms in excess of 80MW. O&M variation does significantly impact on LCoE for the multi rotor system, so it is important that this model be developed more fully in future work such that the LCoE can be presented with more certainty [174].

The cost model itself also relies on NREL data developed many years ago (2006) [175] for the scaling of various components of wind turbines. Many of these scale factors will now be out of date, as technology has progressed at a significant space in the last 8 years. While the final figures are outdated, it is hoped that the relative costs in relation to one another have remained fairly consistent and so each component is contributing an appropriate amount to the LCoE such that no single figure is outweighing the result.

In areas such as structural mass, rotor mass and electrical integration which have been areas developed throughout this study there have also been some liberties and assumptions taken that may not be accurate in the future. Where there has been uncertainty, the use of scale/safety factors have been provided in the hope that these figures err on the side of caution and do not unfairly benefit the conceptual multi rotor system over actual physical machines in use today - with figures based on years of commercial use.

The objective of this study was to investigate the multi rotor system from initial concept and first principles - i.e. that scaling laws should penalise single large rotors, while conversely benefiting the multi rotor system. These principles would in turn

lead to evidence that would suggest multi rotor systems, at-least at 20MW+ scale, can enable LCoE of energy reductions on the order of £60/MWh on today's 5MW machines and in excess of £10/MWh on large rotors of 10MW+. Such savings would allow subsidies for wind to be reduced (which is likely inevitable) and would lead to an uptake in wind as developers realise that the cost and profit from development is less reliant on government policy.

Secondly the study has shown that while single large rotors of 10MW+ can also see reductions in LCoE, the added structural cost imposed by scaling laws (even when conservative laws are used) punish them. LCoE reductions of £45-50/MWh might be expected and it is this saving which has prompted developers to begin utilising ever increasing single machine ratings.

10.4 SUMMARY

The multi rotor system has developed from a concept touted in the 1980's by one of the pioneers of wind energy systems, Heronemus. It was consigned to the history books until developments more recently have finally pushed the industry towards seeking large unit capacities at a single site in an attempt to lower costs of energy. Thus the multi rotor concept has resurfaced as possibly the only contender to the conventional single rotor horizontal axis wind turbine at ratings of 20MW+ in off-shore locations and indeed the theory suggests that CoE will in all likelihood be significantly reduced as a result. Indeed, there are arguments that the final ratings for multi rotors could well be expected to exceed 40MW at a single site given the fact that scaling the system only involves multiples of the existing parameters as opposed to negatively affecting scaling laws.

With the introduction of the multi rotors into the Innwind project as part of a wider EU review into the development of future wind energy systems, the multi rotor has finally gained some much needed traction. It is hoped that this thesis will help aid in that process and help provide a starting point for future research into this exciting concept.

10.5 REFERENCES

[1] **World Bank** (2013) *World Development Indicators, Energy Use Per Capita.* Available at: http://www.google.com/publicdata?ds=wb-wdi&met_y=eg_use_pcap_kg_oe&tdim=true&dl=en&hl=en&q=world+energy+usage#ctype=l&strail=false&nselm=h&met_y=eg_use_pcap_kg_oe&scale_y=lin&ind_y=false&rdim=country&ifdim=country&tdim=true&hl=en&dl=en (Accessed: 5 August 2013).

[2] **U.S. Energy Information Administration** (2010) *International Energy Outlook 2010.* Available at: http://205.254.135.24/oiaf/ieo/pdf/0484(2010).pdf (Accessed: 5 August 2013).

[3] **World Bank** (2013**)** *Alternative and Nuclear Energy (% of total energy usage).* Available at: http://data.worldbank.org/indicator/EG.USE.COMM.CL.ZS/countries/1W?display=graph (Accessed: 5 August 2013).

[4] **Page, D.** (2010) *Energy For Keeps.* 3rd ed. Chapter 1. California: Energy Education Group.

[5] **Burton, T., Sharpe, D., Jenkins, N. and Bossanyi, E.** (2010) Chapter 1. *The Wind Energy Handbook,* 3rd Ed. John Wiley & Sons, Ltd.

[6] **Price, T., Blyth, J.** (1839-1906) *Oxford Dictionary of National Biography.* Available At: http://www.oxforddnb.com/public/dnb/100957.html. (Accessed: 9th August 2013)

[7] **Vestergaard, J., Brandstrup, L., and Goddard III, R.** (2004) *A Brief History of the Wind Turbine Industries in Denmark and the United States.* South East USA: Academy of International Business.

[8] **Johnson, G.,** (2001) *Wind Energy Systems.* Manhattan: Prentice Hall.

[9] **Gipe, P.** (1995) *Wind Energy Comes of Age.* p77-78. John Wiley and Sons

[10] **Irena.** *GWEC: 30 years of policies for wind energy.* Available at: https://www.irena.org/DocumentDownloads/Publications/GWEC_Denmark.pdf (Accessed: 20th March 2015)

[11] **Krohn, S.** (2002) *Danish Wind Turbines: An Industrial Success Story.* Available at: http://www.vindselskab.dk/media(483,1033)/Danish_Wind_Turbine_Industry,_an_industrial_succes_story.pdf (Accessed: 5th August 2013)

[12] **D.G. Randall Trans, A. Betz** (1966) *Introduction to the Theory of Flow Machines*. Pergamon Press, Oxford.

[13] **Harrison, R., Hau, E., and Snel, H.** (2001) *Large Wind Turbines: Design and Economics*. Chapter 3. John Wiley and Sons.

[14] **EWEA.** (2012) *The European offshore wind industry - key trends and statistics 2012*.

[15] **European Wind Energy Association**. (2011) *UPWIND 2011, Design limits and solutions for very large wind turbines.* March Edition. (Brussels).

[16] **Burton, T., Sharpe, D., Jenkins, N. and Bossanyi, E.** (2010) Chapter 1. *The Wind Energy Handbook,* 3rd Ed. John Wiley & Sons, Ltd.

[17] **Wind Energy Division, Riso** (2010) *The World of Wind Atlases - Wind Atlases of the World.* Available at: http://www.windatlas.dk/ (Accessed: 7th August 2011)

[18] **Intellicast** (2011) *Jet Stream Wind Map*. Available at: http://www.intellicast.com/National/Wind/JetStream.aspx. (Accessed: 8th August 2011)

[19] **Noord, M., Beurskens, L. and de Vries, H.** (2004) *Potentials and Costs for Renewables Electricity Generation - A Data Overview.* Amsterdam: ECN

[20] **Esker, D.** (2009) *Galileo's Square Cubed Law and Why Size Matters.* Available at: http://www.coloradocast.org/userfiles/Size%20Matters.pdf (Accessed: 8th August 2011)

[21] **Engler, N.** *The Nature of Wood - Wood Strength.* Available at: http://workshopcompanion.com/KnowHow/Design/Nature_of_Wood/3_Wood_Strength/3_Wood_Strength.htm (Accessed: 8th August 2011)

[22] **Menet, J. and Bourabaa, N.** (2004) *Increase in the Savonius' Rotors Efficiency via a Parametric Investigation.* Valencia: EWEC 2004

[23] **Ragheb, M.** (2011) *Vertical Axis Wind Turbines.* Available at: http://mragheb.com/NPRE%20475%20Wind%20Power%20Systems/Vertical%20Axis%20Wind%20Turbines.pdf (Accessed 10th February 2014) Illinois: University of Illinois

[24] **Wahl, Mats.** (2007) *Designing an H-rotor type Wind Turbine for Operation on Amundsen-Scott South Pole Station.* PhD Thesis, Uppsala University.

[25] Parsons, D & Chatteron, J. Carbon Brainprint Case Study: Novel Offshore Vertical Axis Wind Turbines. (2011). Cranfield University.

[26] **Boatner, B.** (2010) *Vertical axis wind turbine with articulating rotor. United States Patent 7677862* Available from Wind Engineering 415/4.2.

[27] **Helix Wind** (2009) *Harnessing Wind Power to Provide Custom Renewable Energy Solutions.* Available at: http://www.helixwind.com/download/media107_1_HLXW_EIO_09-09-2009.pdf (Accessed 5th Septemeber 2011)

[28] **Zannetti, L., Gallizio, F. and Ottino, G.** (2007) *Vortex Capturing Verical Axis Wind Machine.* Journal of Physics, Vol. 1 Conference Series 75. doi:10.1088/1742-6596/75/1/012029.

[29] **Kogaki, T.** (2004) *Performance Improvement of Airfoils for Wind Turbines by the Modified Vortex Generator.* EWEC: AIST, 2004.

[30] **Kocivar, B.** (1977) *Tornado Turbine Reaps Power from a Whirlwind.* Popular Science. Vol. January.

[31] **Windrich, J and Fricke, J.** (1983) *Extraction of Power from a Tornado.* Solar Energy, Vol. 32. Wurzburg.

[32] **Wikipedia** (2011) *George Pocock,* Available at: http://en.wikipedia.org/wiki/George_Pocock_(inventor) (Accessed at: 8th October 2011)

[33] **KiteGen** (2009) *KiteGen Research, KiteGen.com.* Available at: http://www.kitegen.com/en/?page_id=7 (Accessed 10th August 2009)

[34] **Tesla, N.** (1913) *Fluid Propulsion.* Patent 1,061,142. United States Patent Office.

[35] **Fuller, H.** (2010) *Wind turbine for generation of electric power,* Patent 7695242, 415/2.1. United States Patent Office.

[36] **Hau, E.** (2006) *Wind Turbine: Fundamentals, Technologies, Application, Economics.* 2nd Edition. Birkhauser.

[37] **Kentfield, J.** (1992) *The delta-wing bladed rotor concept.* Journal of Wind Engineering and Industrial Aerodynamics, Volume. 39, p405-416. Amsterdam.

[38] **Schefter, J.** (1983) *Energy Experts Pick 5 Wild Windmills.* Popular Science. (June, 1983)

[39] **Scott, D.** (1983) *Tip-Vane Windmill Doubles Output Efficiency.* Popular Science. (September, 1983)

[40] **Venturi Wind** (2011) *Venturi Wind Turbines.* Available at: www.venturiwind.com (Accessed on: 15th August 2011).

[41] **Garvey, S.** (2010) *Structural Capacity and the 20MW Wind Turbine.* Power and Energy, Proc. IMechE, Vol. 224.

[42] **Gipe, P.** (2001) *Vortec Closure No Surprise. Wind-Works.org.* Available at: http://www.wind-works.org/articles/vort_closure_hend.html (Accessed at: 10th August 2011)

[43] **Conrad, J.** (2010) *Wind Turbine Designs - The 11 Most Interesting.* Available at: http://gcaptain.com/the-most-interesting-wind-turbine-designs?3397 (Accessed 14th August 2011)

[44] **Thompson, Kalee** (2008) *Ten Times the Turbine.* Popular Science (May, 2008).

[45] **Jamieson, P and Jaffrey, A.** (1995) *Advanced Wind Turbine Design.* Wind Energy, Vol. 16. John Wiley and Sons.

[46] **Crawford, C and Platts, J.** (2008) *Updating and Optimization of a Coning Rotor Concept.* Journal of Solar Energy Engineering. June 2008. doi:10.1115/1.2931497

[47] **Nakafuji, D.** (2001) *Active Load Control for Airfoils using Microtabs.,* Japanese Journal of Physical Science and Engineering, Vol. 123, November 2001

[48] **Williams, J, Butler, S. and Wood, M.** (1963) *The Aerodynamics of Jet Flaps.* Bedford: The Ministry of Aviation Aeronautical Research Council.

[49] **Mamou, M and Khalid, M.** (2007) *Steady and unsteady flow simulation of a combined jet flap and Coanda jet effects on a 2D airfoil aerodynamic performance.* Ottawa: Revue des Energies Renouvelables

[50] **Craft, T. Iacovides, H. and Launder, B.** (2010) *Dynamic Performance of Flettner Rotor with and without Thom Dics.* MACE. Manchester: Turbulence Mechanics Group.

[51] **California Energy Commission** (2003) *Counter Rotating Wind Turbine System.* P500-03-055F, PIER.

[52] **Shen, W., Zakkam V., Sorensen, J. and Appa, K** (2007) *Analysis of Counter-Rotating Wind Turbines.* Journal of Physics, Vol. 1 Conference Series 75.

[53] **Burton, T., Sharpe, D., Jenkins, N. and Bossanyi, E.** (2010) *The Wind Energy Handbook.* Edition 3, Chapter 4: Aerodynamics of Horizontal Axis Wind Turbines. John Wiley and Sons Ltd.

[54] **European Wind Energy Association** (2008) *Wind Energy: The Facts: Airborne Turbines.* Routledge: EWEA

[55] **Roberts, B., Shepard, D.** (2007) *Harnessing High Altitude Wind Power.* IEEE Energy Conversion. Vol. 22. p136-144. Sydney.

[56] **Buckley, R. *et al.*** (2008) *Design of a One Kilowatt Scale Kite Power System.* Worcester: Worcester Polytechnic Institute.

[57] **J., Hyung-Jo and L., Seung-Woo.** (2011) *The experimental validation of a new energy harvesting system based on the wake galloping phenomenon.* Dajeon: Smart Mater. Struct. , Vol. 20.

[58] **Donga, S., Song-Yul, C. and Dong-Joo, K.** (2007) *Analysis of piezoelectric materials for energy harvesting devices under high-g vibrations.* Issue 10R, Japanese Journal of Applied Physics, Vol. 46.

[59] **Priya, S., Chih-Ta, C., Fye, D., and Zahnd, J.** (2005) *Piezoelectric Windmill: A novel solution to remote sensing.* Issue 3, Arlington: Japanese Journal of Applied Physics, Vol. 44.

[60] **Sivadas, V and Wickenheisera, A.M.** (2011) *A study of several vortex-induced vibration techniques for piezoelectric wind energy harvesting.* Washington: Proc. of SPIE. Vol. 7977.

[61] **J., Hyung-Jo and L., Seung-Woo.** (2011) *The experimental validation of a new energy harvesting system based on the wake galloping phenomenon.* Dajeon: Smart Mater. Struct. , Vol. 20.

[62] **Ovejas, V J and Cuadras, A.** (2011) *Multimodal piezoelectric wind energy harvesters.* Smart Material Structures, Vol. 20. doi:10.1088/0964-1726/20/8/085030

[63] **Schmidt, H. V.** (1992). Dusseldorf: Ultrasonics Symposium 897

[64] **Paraschivoiu, I.** (2002) *Wind turbine design: with emphasis on Darrieus concept.* Polytechnic International Press. Canada.

[65] **Williams, P., Lansdorp, B. and Ockels, W.** (2007) *Optimal Cross-Wind Towing and Power Generation with Tethered Kites.* Delft: AIAA Guidance, Navigation and Control Conference. August 2007.

[66] **Ockels, W.** (2001) *Laddermill, a novel concept to exploit the energy in the airspace.* Delft: Aircraft Design, Vol. 4

[67] **Lloyd, M.** (1979) *Crosswind Kite Power.* Journal of Energy, No. 3. Vol. 4.

[68] **Fletcher, C., Honan, A., and Sapuppo, J.** (1983) *Aerodynamic Platform Comparison for Jet-Stream Electricity Generation.* Journal of Energy, Vol. 7

[69] **Lang, D.** (2005) *Electrical Power Generation Using Kites.* Seattle: Drachen Foundation.

[70] **Hobbs, S.** (1986) *A Quantitative Study of Kite Performance in Natural Wind with application to Kite Anemometry.* Cranfield: Cranfield University.

[71] **Goela, J. *et al*.** (1985) *Wind Loading Effects on a Catenary.* Journal of Energy Vol. 21.

[72] **Riegler, G., Riedler, E and Horvath, E.** (1981) *The Transformation of Wind Energy by High Altitude Power Plant (HAPP).* Colorado Springs: Terrestrial Energy Systems Conference, December 1981

[73] **Kling, A.** (1975) *Wind Driven Power Plant.* Patent 4,073,516 United States Patent Office.

[74] **Fry, C.** (1978) *Wind Driven, High Altitude Power Apparatus.* Patent 4,165,468. United States Patent Office.

[75] **Benoit, W.** (1982) *Lighter Than Air Wind Energy Conversion System Utilising a Rotating Envelope.* Patent 4,450,464. *United States Patent Office.*

[76] **Layton, D. M.** (1985) *Basic Aerostatics - A Tutorial.* New York: AIAA

[77] **Wikipedia**. *LZ129 Hindenburg* Available at: http://en.wikipedia.org/wiki/LZ_129_Hindenburg (Accessed 25th August 2011).

[78] **Colozza, A and Dolce, J.** (2005) *High-Altitude, Long-Endurance Airships.* Ohio: NASA/TM—2005-213427

[79] **Musial, W., Butterfield, S. and McNiff, B.** (2007) *Improving Wind Turbine Gearbox Reliability.* European Wind Energy Conference. Milan: NREL/CP-500-41548.

[80] **Minardi, J., Lawson, M. and Williams, G.** (1976) *Electrofluid Dynamic (EFD) Wind Driven Generator.* Division of Solar Energy, Energy Research and Development Administration. COO/4130-77/1

[81] **Minardi, J. and Lawson, M.** (1984) *Conceptual Design of an Electrofluid Dynamic Wind Energy System.* Dayton: Solar Energy Research Institute

[82] **Djairam, D.** (2008) *The Electrostatic Wind Energy.* Delft: University of Delft

[83] **Wikipedia** (2010) *Biography, Johann Bessler and the Bessler wheel.* Available at: http://en.wikipedia.org/wiki/Johann_Bessler (Accessed on 25th August 2011).

[84] **Symon, K.R. (2008)** *Mechanics.* 2nd edition. Chapter 3. University of Wisconsin. Addison-Wesley.

[85] **Jamieson, P.** (2011) *Innovation in wind turbine design.* Volume 2. Chapter 15. John Wiley and Sons ISBN: 9780470699812 (Glasgow)

[86] **European Wind Energy Association**. (2004) *Wind Power Economics: Wind Energy Costs*. Investment Factors.

[87] **Jamieson, P., and Branney, M.** (2012) *Multi-rotors: a solution to 20MW and beyond?* EnergyProcedia Deepwind2012 Proc. Conf. Volume 24 pp. 52-59 (Trondheim).

[88] **Bazant**, **Z.P.** (1999) *Size Effect on Structural Strength: A Review*, Archive of Applied Mechanics, volume 69, p703-725.

[89] **Burton, T., Sharpe, D., Jenkins, N. and Bossanyi, E.** (2010) Chapter 2. *The Wind Energy Handbook,* 3rd Ed. John Wiley & Sons, Ltd.

[90] **Gamesa.** (2009) *Gamesa partners with MTorres on blade venture*. Windpower Monthly Magazine, May 2009.

[91] **Windenergie.** (1999) *Bundesverband WindEnergie*. ISBN 3-9806657-0-4

[92] **Chaviaropoulos T., Lekou D. and Sieros G.** (2011) *Cost Models Applied to Blades*. UPWIND Project, Presentation Work Package 1B4.

[93] **Unknown**. (2008) *Windraftanlagen Markt. Issues from 1997 to 2007*. Published Sun Media GmbH.

[94] **Tavner P.J, Xiang J.P. and Spinato, F**. (2006) *Reliability analysis for wind turbines.* Wind Energy Journal - Edition 10, p1-18.

[95] **Smulders P.T., Orbons S. and Moes C**. (1984) *Aerodynamic Interaction between Two Wind Rotors set next to each other in one Plane.* EWEC (Hamburg).

[96] **Ransom, D., Moore, J. J., and Heronemus-Pate, M**. (2010) *Performance of wind turbines in a closely spaced array.* Renewable Energy World**,** Volume 2:3, pp. 32-36.

[97] **Stewart, R.D., Wyskida, R.M. and Johannes, J.D.** (2010) *Cost Estimator Reference Manual*. 2nd Edition. John Wiley and Sons. ISBN: 978-0-471-30510-1.

[98] **Nordtank.** (2013) *Nordtank Stall Regulated 600kW Wind Turbine.* Available at: http://www.4coffshore.com/windfarms/turbine-nordtank-ntk-600-43-tid34.html (Accessed: May 2013).

[99] *Learning Theory Calculator.* Available at: http://maaw.info/LearningCurveSummary.htm (Accessed June 2014)

[100] **Harman**, **K. G.** (2010) *Availability and Operating Efficiency - How well do wind farms actually perform?*, RenewableUK 2010, (Glasgow)

[101] **NordzeeWind**. (2007-08) *Wind Farm Egmond aan Zee Operations Report 2007; OWEZ_R_000_20081023 Wind Farm Egmond aan Zee Operations Report 2008; OWEZ_R_000_200900807;*

[102] **Innwind.EU** (2014) *Innovative Turbine Concepts - Multi-Rotor System.* Deliverable Report for Innwind.EU Task 1.33.

[103] **Jamieson, P., and Branney, M.** (2012) *Multi-rotors: a solution to 20MW and beyond?*

EnergyProcedia Deepwind2012 Proc. Conf. Volume 24 pp. 52-59 (Trondheim).

[104] **Germanischer Lloyd**, *Guideline for the Certification of Wind Turbines,* Edition 2003 (Hamburg 2003).

[105] **International Electro-mechanical Comission**, (2005-08) *International Standard: IEC61400-1* Chapter 6; Design Load Cases. 3rd, Edition 05-08.

[106] **International Electro-mechanical Comission.** (2005-08) *International Standard: IEC61400-1.* Chapter 7; Structural Design. Page 33-45. 3rd, Edition 05-08.

[107] **DNV GL,** *Bladed,* Edition 4.4 - Available at: http://www.gl-garradhassan.com/en/software/GHBladed.php (Accessed: December 2013)

[108] **DTI/BERR**. (2011) *Offshore wind capital grants scheme annual reports.*

[109] **Valpy, B. B. A.** (2010) *How to Improve the Cost of Energy from Offshore Wind - Technology Perspectives*, RenewableUK 2010, (Glasgow)

[110] **O.D.E. Limited**. (2006) *Study of the Costs of Offshore Wind Generation*, Department of Trade and Industry. URN NUMBER: 07/779

[111] **Tavner, P.** (2012) *Offshore Wind Turbines; Reliability, availability and maintenance.* Renewable Energy, Series 13.

[112] **NordzeeWind**. (2009) *Wind Farm Egmond aan Zee Operations Report 2009,* OWEZ_R_000_20101112.

[113] **Wilkinson, M.R., Spinato, F. and Hendriks, B.** (2010) *Report on the Wind Turbine Reliability Profiles, Technical Report.* Reliawind Project deliverable: D.1.3

[114] **Lange, M., Wilkinson, M. and van Delft, T.** (2011) *WIND TURBINE RELIABILITY ANALYSIS.* Work Package 1, EU Reliawind Project. GL Garrad Hassan.

[115] **Yanhui, F. and Tavner, P**. (2010) *Introduction to Wind Turbines and their Reliability and Availability.* Bathtub Curve, Side 3. EWEC (Warsaw)

[116] **Jamieson, P**. *Future Vision of the Technology*. Presentation to US, DOE Deepwater Wind Energy Workshop. (Washington DC 2004).

[117] **Ministry of Defence; Aeronautical Research Council**, (1971) *Cumulative Damage in Fatigue with Particular Reference to the Effects of Residual Stresses.* CP No 1185

[118] **Burton, T., Sharpe, D., Jenkins, N. and Bossanyi, E.** (2010) *The Wind Energy Handbook Ed.3.* Chapter 2; Wind Resource. John Wiley and Sons, Ltd, 2010.

[119] **Renewable Advisory Board.** (2010) *Value breakdown for the offshore wind sector.* Section 5.1.3.

[120] **European Wind Energy Association**. (2009) *The Economics of Wind Energy*. Page 9.

[121] **CIGRÉ,** (2004) *Guide on Economics of Transformer Management*, Working Group A2.20, CIGRÉ Document 248.

[122] **Andrew R Henderson**, (2009) *Optimising Redundancy of Offshore Electrical Infrastructure Assets by Assessment of Overall Economic Cost.* European Offshore Wind Energy Conference (Stockholm).

[123] **Tavner, P.** (2012) O*ffshore Wind Turbines; Reliability, availability and maintenance.* Renewable Energy Series 13. Chapter 2

[124] **Muljadi, E. and Butterfield, C.P.** (1999) *Pitch-Controlled Variable-Speed Wind Turbine Generation.* IEEE Industry Applications Society Annual Meeting.

[125] **Chen, Z. and Spooner, E.** (1998) *Grid interface options for variable-speed, permanent-magnet generators*, IEE Proc. Electrical Power Appl., vol. 145, no. 4, pp. 273-283.

[126] **Ribrant, J. and Bertling, L. M.** (2007) *Survey of failures in wind power systems with focus on Swedish wind power plants during 1997–2005*. IEEE Trans. on Energy Convers., vol. 22, no. 1, p167-173.

[127] **Hasnaoui, O., Bejhadj, J. and Elleuch, M.** (2013) *Direct-Drive Permanent Magnet Synchronous Generator Wind Turbine Investigation.* Journal of Electrical Systems.

[128] **Mahersi, E., Khedher, A. and Faouzi M.,** (2013) *The Wind Energy Conversion System Using PMSG Controlled by Vector Control and SMC Strategies*. International Journal of Renewable Energy Research, Vol. 3, No. 1.

[129] **ABB Group.** (2013) *Energy Efficiency Cost of Losses.* Available at: http://www02.abb.com/global/zaabb/zaabb011.nsf/bf177942f19f4a98c1257148003b7a0a/478b6c8571f1e111c1257b7200381db1/$file/energy+efficiency+applied+to+transformers.pdf (Accessed July 2014)

[130] **Mitchell, B.** (2014) *An Introduction to Materials Engineering and Science: For Chemical and Material Engineers*. Appendix 8, Wiley Publishing, ISBN 0-471-43623-2

[131] **Federal Industry.** *Aluminium to Copper Comparison Chart.* Available at: http://www.federalindustrialsales.com/pdf%20files/alum-copper.pdf (Accessed June 2013)

[132] **Poore, R. and Lettenmaier, T.** (2000) *Alternative Design Study Report: WindPACT Advanced Wind Turbine Drive Train Design Study.* Section 4.11.1. NREL Report. Available at: http://www.nrel.gov/docs/fy03osti/33196.pdf (Accessed June 2013)

[133] **Elliot, D., Jones, C. and Finney, S.** (2013) *Offshore wind farm cluster based DC collection network – operation and design considerations.* Wind Energy Centre for Doctoral Training.

[134] **European Wind Energy Association**. (2009) *The Economics of Wind Energy*. Page 10-13.

[135] **Power Engineering Society General Meeting.** (2005) *Effect of low voltage ride through (LVRT) characteristics on voltage stability*. pp 1901-1907

[136] **Matevosyan, J. Ackermann, T. and Bolik, S.** (2004) *Comparison of International Regulations for connection of wind turbines to the network.* In Nordic Wind Power Conference, (Goteborg).

[137] **Yang, J.** (2011) *Fault Analysis and Protection for Wind Power Generation Systems.* Chapter 3. PhD Thesis. University of Glasgow.

[138] **Causebrook, A., Atkinson**, **D. J. and Jack**, **A. G.** (2007) *Fault ride-through of large wind farms using series dynamic braking resistors.* IEEE Trans. Power Syst., vol. 22, no. 3, pp. 966-975.

[139] **Muljadi, E. and Butterfield, C. P.** (2001) *Pitch-controlled variable-speed wind turbine generation*, IEEE Trans. Ind. Appl., vol. 37, no. 1, pp. 240-246.

[140] **Smulders, P. T., Orbons, S. and Moes, C.** (1984) *Aerodynamic interaction of two rotors set next to each other in one plane*. EWEC Proc. Int. Conf. pp. 529-533 (Hamburg)

[141] **McCormick, B.** (1979) *Aerodynamics, Aeronautics, and Flight Mechanics*. p. 24, John Wiley & Sons, Inc.

[142] **Jensen, P.** (2014) *Innovative Turbine Concepts - Multi-Rotor System. Deliverable 1.3.3.* EU 7th Framework program.

[143] **NREL** (2013) *Cost of Wind Energy Review.* (Accessed March 2015).

[144] **Mast, E.H., van Kuik, G.A. and Zaaijer**, **M.B.** (2013) *Offshore Wind Energy Policies and their Effects: Experiences in Denmark and the UK and prospects for the Netherlands*. Wind Energy Research Group, DUWIND, TUDelft.

[145] **Renewable Advisory Board.** (2010) *Value breakdown for the offshore wind sector: A report commissioned by the RAB.* Available at: https://www.gov.uk/government/uploads/system/uploads/attachment_data/file/48171/2806-value-breakdown-offshore-wind-sector.pdf (Accessed: March 2015)

[146] **EWEA.** (2014) *Wind Power Economics: Wind Energy Costs - Investment Factors*.

[147] **Tegen, S., and Lantz, E.** (2011) *Cost of Wind Energy Review.* National Renewable Energy Laboratory, Technical Report.

[148] **Vaughan, N.** *Economics of Wind Farms*, Alternative Energy Institute.

[149] **Manwell, J.F., McGowan, J.G. and Rogers, A.L.** *Wind Energy Explained: Theory, Design and Application.* Chapter 11: Wind Energy System Economics. p531.

[150] **Jonkman, J., Butterfield, S., Musial, W. and Scott, G.** (2009) *Definition of a 5-MW Reference Wind Turbine for Offshore System Development.* Technical Report NREL/TP-500-38060.

[151] **Tavner, P.** (2012) *Offshore Wind Turbines; Reliability, availability and maintenance.* Renewable Energy Series 13. Chapter 3.

[152] **Hahn, B., Durstewitz, M. and Rohrig, K.** (2011) *Reliability of Wind Turbines, Experiences of 15 years with 1,500 WTs*. Institute fur Solare Energieversorgungstechnik (Kassel, Germany)

[153] **Wilkinson, M.R., Spinato, F. and Hendriks, B.** (2010) *Report On the Wind Turbine Reliability Profiles, Technical Report*. Project deliverable: Reliawind D.1.3.

[154] **Lange, M., Wilkinson, M. and van Delft, T.** *WIND TURBINE RELIABILITY ANALYSIS*.

[155] **Dinwoodie, I., Quail, F. and McMillan, D.** (2012) *Analysis of offshore wind turbine operation and maintenance approach using a novel time domain meteo-ocean modelling approach*. Proceedings of ASME Turbo Expo (Copenhagen)

[156] **Langiss, O.** (2006) *The German 250-MW-Wind-Program, Centre for Solar Energy and Hydrogen Research* (Baden-Wurttemberg).

[157] **Billington, R.** (1970) *Power System Reliability Evaluation*. Gordon and Breach, (New York)

[158] **Wright. T,P.** (1936) *Journal of the Aeronautical Science.*

[159] **Gonzalez-Longatt, F., Wall, P. and Terzija, V.** (2011) *Wake effect in wind farm performance: steady-state and dynamic behaviour.* Renewable Energy Journal, p1-10.

[160] **Vattenfall.** *Kentish Flats* Available at: http://www.vattenfall.co.uk/en/kentish-flats.htm (Accessed: August 2014)

[161] **4Coffshore.** *Wind Speed Database of 10 year Mean Wind Speeds Recorded at all Major Offshore Wind Farms* - Available at: http://www.4coffshore.com/windfarms/windspeeds.aspx (Accessed: August 2014)

[162] **Burton, T. (2010)** *The Wind Energy Handbook Ed.3.* Chapter 4; Costing. John Wiley and Sons.

[163] **Fingersh, L., Hand, M. and Laxon, A.** (2006) *Wind Turbine Design Cost and Scaling Model.* Technical Report, NREL/TP-500-40566

[164] **Jensen, P.** (2014) *Innovative Turbine Concepts - Multi-Rotor System.* Deliverable 1.3.3. EU 7th Framework program.

[165] **Dinwoodie, I.** (2014) *Modelling the Operation and Maintenance of Offshore Wind Farms.* PhD Thesis. University of Strathclyde.

[166] **Fingersh, L., Hand, M. and Laxson, A.** (2006) *Wind Turbine Design Cost and Scaling Model.* Technical Report. National Renewable Energy Laboratory.

[167] **Stewart, R.D., Wyskida, R.M. and Johannes, J.D.** (2010) *Cost Estimator Reference Manual*. 2nd Edition. John Wiley and Sons. ISBN: 978-0-471-30510-1.

[168] **Jamieson, P., Chaviaropoulos, P. K., and Voutsinas, S.** (2015) *Large Scale Offshore Wind Energy Systems, the Multi-Rotor Solution.* EWEA Offshore 2015.

[169] **Salta, O.** *Tools of Nanotechnology.* Current Nanoscience, No. 1, Vol. 1.

[170] **Gaskell, S.** (1977) *Electrospray: Principles and Practice.* Journal of Mass Spectrum, Vol. 32

[171] **Higuera, F.** (2003) *Flow Rate and Electric Current Emitted by a Taylor Cone.* Madrid: Journal of Fluid Mechanics, Vol. 484.

[172] **Rohner, T. C., Lion, N. and Girault, H.** (2006) *Electrochemical and Theoretical Aspects of the Electrospray Ionisation.* Journal of Physics and Chemistry, Vol. 6.

[173] **Wilm, M.S. and Mann, M.** (1994) *Electrospray and the Taylor-Cone theory, Dole's beam of macromolecules at last?* Heidelberg: International Journal of Mass Spectrometry and Ion Processes, Vol. 136

10.6 APPENDIX A

Piezo Electric Theory

That is, given:

$$D = \varepsilon \cdot E \tag{3.46}$$

Where; D is the electric charge density displacement, ε the permittivity of the material and E the electric field strength.

And:

$$S = s \cdot T \tag{3.47}$$

Where; S is the applied strain, s the compliance of the material and T the applied stress.

These can then be combined into the so-called coupled equations of which the strain-charge form is:

$$\{S\} = [S^E]\{T\} + [d^t]\{E\} \tag{3.48}$$

$$\{D\} = [d]\{T\} + [\varepsilon^T]\{E\} \tag{3.49}$$

Where; $[d]$ *is the matrix for the direct piezoelectric effect,* $[d^t]$ *is the matrix for the converse piezoelectric effect, superscript E represents a zero or constant electric field and superscript T represents a zero or constant stress field.*

In terms of material properties and variables, the key objects are defined by a series of four piezoelectric constants, the most applicable of which is defined as:

$$d_{ij} = \left(\frac{\partial D_i}{\partial T_j}\right)^E = \left(\frac{\partial S_j}{\partial E_i}\right)^T \tag{3.50}$$

This coefficient defines the relationship between differential charge and stress under a constant or zero electric field and differential strain and electric field under a constant or zero stress. These coefficients are defined by the composition of the material in question, for example, Lead zirconium titanate (PZT) has one of the highest d_{31} coefficients; $320\ x\ 10^{-12} m/V$.

The electromechanical coupling coefficient, k, characterises the efficiency of the conversion process from mechanical to electrical energy in the direct piezoelectric effect and the electrical to mechanical energy conversion in the inverse piezoelectric effect. For PZT, the coupling coefficient has a value, k_{31} = 0.44, meaning that at maximum, 44% of the mechanical energy will be transferred to electrical.

After the application of a force, the polarization of the crystal leads to an accumulation of charge according to the following expression:

$$Q = d \cdot F \tag{3.51}$$

Where; Q is the charge, F is the force and is a vector quantity and d is a 3x3 matrix of piezoelectric coefficients.

Forces along the x-axis produce charges along the x, y and z axis, with the charge along the x-axis given by the d_{11} coefficient of the d matrix, the charge along the y-axis given by the d_{21} coefficient and so on.

As previously mentioned, a piezoelectric transducer works by creating a voltage drop across two points in the structure, in essence acting as a capacitor. Therefore the normal equations for both the capacitance of the device and the voltage drop can be defined thus;

$$C = \frac{\varepsilon \cdot \varepsilon_0 \cdot A}{d} \tag{3.52}$$

Where; C is the capacitance of the device, ε and ε_0 the material permittivity and permittivity of a vacuum respectively, A the area of material forming the "capacitor plates" normal to the voltage differential vector and d the distance between the plates

And:

$$V = \frac{d_{33} \cdot L \cdot F}{\varepsilon \cdot \varepsilon_0 \cdot A} \tag{3.53}$$

Where; L is the thickness of one plate and F the force applied

From this it is clear that should a designer wish to increase the voltage across the device then they would need to reduce its capacitance through a reduction in the plate area.

Piezoelectric devices can be modelled as a capacitor from a circuit analysis point of view, assuming that an electrode is attached to either side of the material.

A piezo-electric device differs from a typical electrical power source in that its internal impedance is capacitive rather than inductive and it can inherently handle mechanical motion of varying amplitude. As with any removal of energy from a system, the use of piezo-electrics acts to dampen a systems vibration.

A piezo-electric element can be modelled as a sinusoidal current source, I_p in parallel with its internal capacitance C_p. As the frequency of oscillation is directly coupled to the current generated, the instantaneous current equation is simply:

$$i_p(t) = I_p \cdot sin(\omega \cdot t) \tag{3.54}$$

Where; I_p - the maximum current amplitude as determined by the level of mechanical excitation (A), ω - is the frequency of vibration (Hz), t – is the time (s)

Therefore there is a requirement for rectification from AC-DC such that the power can be adequately harnessed. In-fact, it is found that there is some voltage, V_{rect_opt} at which optimum power transfer occurs and this occurs at electrical resonance. The voltage at which this occurs is found by;

$$V_{rect\_opt} = \frac{I_p}{2 \cdot \omega \cdot C_{pzt}} \tag{3.55}$$

Where; C_{pzt} – is the capacitance of the piezo-electric transducer

With the electrical power harvested then being;

$$P = V_{rect} \cdot \bar{I} = V_{rect} \cdot \frac{2}{\pi} \cdot \left(I_p - \omega \cdot V_{rect} \cdot C_{pzt}\right) \tag{3.56}$$

This equation shows that for maximum power production, the piezo-electric device should be of maximum capacitance and also be driven by a rapidly changing force (in order to increase the frequency of vibration and increase the rectified voltage).

10.7 APPENDIX B

The electro-spray method is the preferred way of imparting a charge on to the liquid and the most crucial technological hurdle to the development of EHD systems. It allows for the release of droplets of fixed diameter and charge density and also provides an electrostatic force that is used to expel the droplets into the wind.

The charge species can consist of water, ethanol or other saline or aqueous solutions. The choice of which will depend on sustainability, desired surface tension, dielectric constant and so on. The charging of the species is based on the principle of ionization, whereby molecules are converted into an ion by adding or removing charged particles; such as electrons or other ions.

At rest, no activity is witnessed in an electro spray system due to the lack of a significantly strong electric field to drive the vaporization of solvent at the tip of the capillary. The threshold electric field across the capillary at which emission begins is then (3.28):

$$E_{init} \approx \sqrt{\frac{2 \cdot \gamma \cdot cos\theta_0}{\varepsilon_0 \cdot r_c}} \tag{3.28}$$

Where: r_c is the radius of the emitter orifice (m), θ_0 is the cone half angle in degrees, γ is the surface tension of the liquid, ε_0 the vacuum permittivity of the solvent.

By varying this applied voltage, the electric field at the emitter, E_{ES} can be increased till formation of the Taylor cone (Figure 0.1) (3.29):

$$E_{ES} = \frac{2 \cdot V_{ES}}{r_c \cdot ln\left(\frac{4d}{r_c}\right)} \tag{3.29}$$

Where: V_{ES} is the applied voltage in V and d is the distance between the emitter orifice and the counter electrode in m.

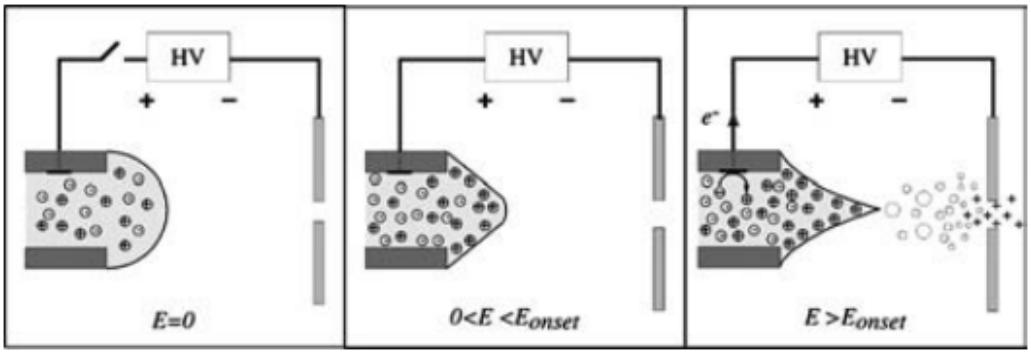

Figure 0.1 - Formation of the Taylor Cone and Jet Emission

The surface convection current begins to become important when these conditions change in the transition region and beyond, and eventually it dominates over the conduction current and is the only transport mechanism left when the jets break into drops.

The conservation equation for the free surface charge is:

$$\frac{dI_s}{dx} = 2 \cdot \pi \cdot r_s \cdot k \cdot {E_n}^i \sqrt{(1 + {r_s}'^2)} \tag{3.30}$$

With;

$$I_s = 2 \cdot \pi \cdot r_s \cdot v_s \cdot \sigma \tag{3.31}$$

And;

$$\sigma = \varepsilon_0 \left(E_n - \beta \cdot {E_n}^i\right) \tag{3.32}$$

Where: I_s is the free surface charge in A, x is the distance along the symmetry axis in m, v_s is the velocity of the liquid at the surface in m/s, r_s is the radius of the surface cross-section in m, k is the electrical conductivity of the liquid and ${E_n}^i$ is the component of the electric field normal to the surface at the liquid side, E_n is the electric field in the gas, β is the dielectric constant of the liquid, and σ is the surface charge density .

The space charge in the droplet is dependent on the electric field in both the capillary/liquid and the dielectric constant of the liquid. The resultant current is a function of these (through space charge) and the radius of the cross section which is

reliant on the formation of the Taylors cone, under the condition that electrostatic force exceeds that created by the inward force due to surface tension;

The resulting plume of charged airborne droplets are then accelerated towards the counter electrode due to the electric field. Once airborne, the liquid droplets structural integrity becomes dependant on the struggle of surface tension with the electrostatic repulsion that results from the solvated ions. Up to a point, known as the Rayleigh limit, surface tension will hold the repulsive forces in check and prevent droplet fragmentation. Continuous shrinkage of the droplet size due to evaporation gradually brings the charges closer together, increasing the repulsion proportionally. Eventually the Rayleigh limit is overcome and the droplet undergoes Columbic explosion (fission).

The theoretical maximum amount of charge that the droplet can hold before fission (fragmentation) occurs can be quantified by;

$$q_r = 8 \cdot \pi \sqrt{\varepsilon_0 \cdot \gamma \cdot r^3} \tag{3.33}$$

Where: r is the radius of the droplet in m, γ is the surface tension and ε_0 the vacuum permittivity of the solvent.

Though generally the Rayleigh limit is reported to be only 70% of this value. Experimental work carried out by EWICON show a clear degradation in the charging efficiency (Figure 0.2) for increasing water droplet diameter suggesting that losses may be a significant factor.

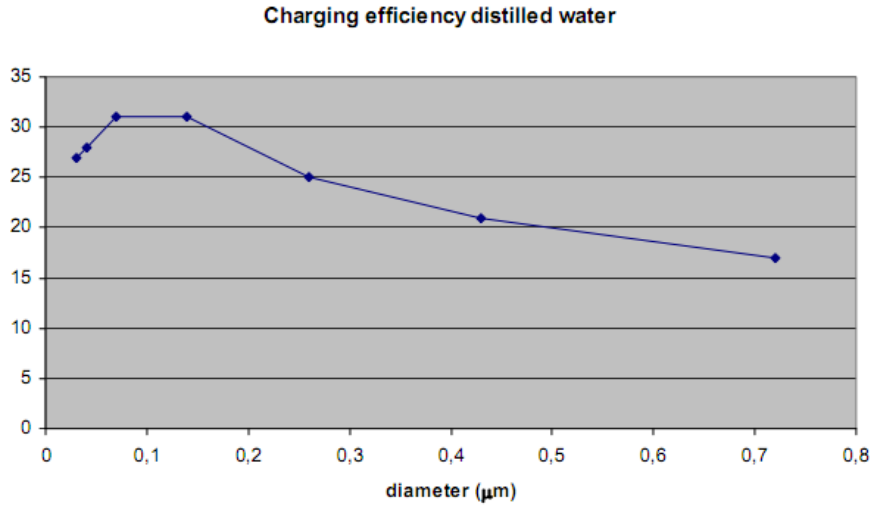

Figure 0.2 - Charging Efficiency as a Function of Droplet Diameter

10.7.1.1 Space Charge

The radius of the jet of liquid expelled from the Taylor cone is given by:

$$r_s = \left(\frac{\rho}{4 \cdot \pi^2 \cdot \gamma \left[\left(\frac{V_a}{V_T} \right)^2 - 1 \right] tan\left(\frac{\pi}{2} - \theta \right)} \right)^{\frac{1}{3}} \cdot \left(\frac{dv}{dt} \right)^{\frac{2}{3}} \tag{3.34}$$

Where: r_s the radius of the emission region at the tip of the Taylor cone, θ the cone angle, $\frac{dv}{dt}$ is the flow rate, ρ is the density of the liquid, V_a is the voltage applied.

The size, charge and initial velocity as well as the rate at which the droplets are ejected, all depend on the voltages on the electrodes, the geometrical configuration of these electrodes and the flow rate of the liquid. The droplet which holds the charge must be of small enough mass to maximise charge/mass but large enough to survive a circuit of the EHD without first evaporating. The breakup of a stream of liquid into droplets is a result of the Plateau-Rayleigh instability; i.e. liquids, by virtue of surface tension, tend to minimize their surface area.

Of primary concern is to ensure that the device can generate as much energy as it takes to run; there is a requirement of energy to charge the species, pump liquid and pressure spray into particles of miniature proportions. Fortunately the process of ionization in the electro-spray is near enough 100% and due to the size of the

capillaries maintaining liquid pressure can be achieved through gravity alone. The only other requirement for energy is that of maintaining a potential difference across the device (if configured) and also the force driving the particles must also be greater than that exerted by the potential differences of the device and the ion charge.

For the acceleration of a particle in an electric field, the equation is defined as:

$$a = \frac{q \cdot \bar{E}}{m} \tag{3.35}$$

Where; a is the acceleration of the particle in m/s², q is the charge on the particle in C, E is the electric field strength in V/m and m is the mass of the particles in kg.

The wind then moves charged particles through an opposing electrostatic field - it is this moving of the charged particle against a force gradient that gives the particle potential energy through the relationship;

$$dU = q \cdot dV \tag{3.36}$$

The opposing force of the electrostatic field can then also be defined as:

$$F_e = q \; x \; E \tag{3.37}$$

Where; F_e is the electrostatic field force.

Assuming that the droplets formed can approximately described by a sphere, then the drag force on a sphere given by creeping flow is:

$$F_d = 3 \cdot \pi \cdot \mu \cdot U \cdot d \tag{3.38}$$

Where: d is the diameter of the sphere in m, μ the dynamic viscosity of the fluid, U relative wind speed in m/s.

Thus relative motion of the particle would be achieved when $F_e > F_d$.

There is the possibility of leaving a small particle behind in the case of droplet evaporation (salt crystals or oils) to retain charge and provide adequate area such that the wind may act against the particle. This may occur naturally as a result of negatively charged particles attracting positive particles of dust, sand, in the air.

Alternatively, a liquid that does not evaporate readily could be used. The evaporation of the droplet is a function of temperature pressure and relative humidity. This suggests it may be better suited to the upper atmosphere where temperatures are coolest.

Some typical values of surface tension are shown in Table 0.1:

Condition	**Surface Tension (γ)**
Water @ 0C	75.64
Water @ 25C	71.97
Mercury @ 15C	487
Sucrose (+55%) + Water @ 20C	76.45
Sodium Chloride 6.0M Solution @ 20C	82.55

Table 0.1 - Surface Tension of Solutions

In general, inorganic salts increase surface tension in which case each droplet can hold more charge.

Every wind speed has a set of operational conditions (field strength, droplet charge) that will maximise the energy extracted. Thus, there is a requirement for wind speed measurement, active control and ambient temperature, pressure and humidity.

The space charge in a system consisting of one type of charge will find that the 'cloud' of charges will try and tear apart and likewise charges entering the system will be repelled by their neighbours. This will limit the device to some artificial power output as the charge density becomes too great for the wind drag force to over-come.

The field strength from space charge in the shape of an infinite wall is described by:

$$E = \frac{\rho \cdot L}{2 \cdot \varepsilon} \tag{3.39}$$

Where: ρ is the charge density, L the thickness of the charge wall in m, ε the universal permittivity constant of free space.

10.7.1.2 Droplet Size

Controlling the droplet size itself is difficult as only the flow rate and stream width can be controlled. Actual droplet formation will depend on the complex interaction

of surface tension, charge and wind dynamics. There is a reason to believe that the active use of fission may be desirable.

Consider the extreme case of a single droplet of radius 0.2m, the volume is; 0.0335m^3. The cross-sectional area presented to the wind is; 0.251m^2.

Now if this droplet was broken down into five mono-droplets through fission then the volume of each becomes; 0.0067m^3 and the total cross-sectional area presented by all five droplets is now; 0.43m^2.

These five droplets present a large cross-sectional area against the wind and therefore will be able to extract 41.6% more energy. This effect is depicted in Figure 0.3.

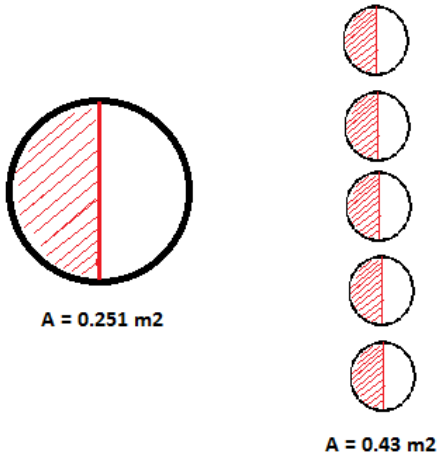

Figure 0.3 - Effect of Droplet Fission on Active Area

To some extent, this effect will happen naturally as some of the solvent evaporates and forces the charge into closer proximity. But it may be that some optimum level of charge will be found for stream jet diameters which will maximise the cross-sectional area for a specific wind speed and energy capture.

10.8 APPENDIX C

10.8.1.1 GENERAL CHARACTERISTICS OF ROTOR AND TURBINE

Rotor diameter	40.5516	m
Number of blades	3	
Teeter hinge	No	
Hub height	227.064	m
Offset of hub to side of tower centre	0	m
Tower height	226.05	m
Tilt angle of rotor to horizontal	0	deg
Cone angle of rotor	0	deg
Blade set angle	0	deg
Rotor overhang	2.32467	m
Rotational sense of rotor, viewed from upwind	Clockwise	
Position of rotor relative to tower	Upwind	
Transmission	Direct drive	
Aerodynamic control surfaces	Pitch	
Fixed / Variable speed	Variable	
Diameter of spinner	0.730676	m
Radial position of root station	0.675776	m
Extension piece diameter	1.02718	m
Extension piece drag coefficient	1	
Cut in wind speed	4	m/s
Cut out wind speed	25	m/s

10.8.1.2 BLADE CHARACTERISTICS

Blade length	19.6051	m
Pre-bend at tip	0.00	m
Pitch control	Full span	

10.8.1.3 BLADE MASS

Blade 1 Mass Integrals (No ice)

The blade mass assumes use of best-technology, i.e. carbon composites to achieve a light weight design well within the realms of current engineering capability. While generally speaking turbines are tested for structural survivability under ice conditions, the objective of this project is not to design the rotors themselves and therefore there is no requirement for ice to be included in the mass totals.

Blade Mass	550	kg
First Mass Moment	3547.77	kgm
Second Mass Moment	37801.7	kgm^2
Blade inertia about shaft	42846.8	kgm^2

10.8.1.4 HUB MASS AND INERTIA

Mass of hub	1500	kg
Mass centre of hub	0	m
Hub inertia: about shaft	150	kgm²
Perpendicular to shaft	0	kgm²
Total Rotor Mass	3285	kg
Total Rotor Inertia	128825	kgm²

10.8.1.5 BLADE GEOMETRY

Distance along blade	Distance along pitch	Chord (m)	Aerodynamic Twist (deg)	Thickness (%)	Neutral axis (x) (m)	Neutral axis (y) (m)	Neutral axis, local	Neutral axis, local
0	0	0.835	13	100	0.0469	-0.0099	0	50
0.583271	0.58	0.835	13	100	0.10853	-0.0124	0	50
1.16328	1.16	0.93	13	85	0.10640	-0.0121	0	47
1.74411	1.74	1.116	13	64	0.0754	-0.0086	0	38
2.32451	2.32	1.302	13	50	0.0542	-	0	33
2.90506	2.9	1.393	13	40	0.029	-0.0033	0	29
4.64507	4.64	1.393	9	30	0.0246	-	0	29
6.38508	6.38	1.254	5.231	25	0.0191	-	0	29
8.13508	8.13	1.116	3.045	22	0.014	-9.55E-	0	29
9.87509	9.87	0.93	1.571	19	0.00929	-5.03E-	0	29
11.6151	11.61	0.835	0.509	17	0.00633	-2.6E-	0	29
13.3551	13.35	0.744	-0.293	15	0.00396	-1.14E-	0	29
14.8151	14.81	0.649	-0.826	13	0.00241	-4.83E-	0	29
15.9751	15.97	0.605	-1.186	12	0.00147	-1.92E-	0	29
17.1351	17.13	0.51	-1.498	12	6.59E-	-4.6E-	0	29
18.0051	18	0.463	-1.707	11.5	2.24E-	-5.87E-	0	29
18.5851	18.58	0.42	-1.836	11	0	0	0	29
19.3451	19.34	0.277	-1.993	11	0.00123	-2.95E-	0	29
19.6051	19.6	0.013	-2.044	11	8.37E-	-2.92E-	0	29

10.8.1.6 BLADE MASS DISTRIBUTION

Centre of mass (x) (%)	Centre of mass (y) (%)	Mass/unit length (kg/m)	Polar intertie/unit length (kgm)	Radii of gyration ratio	Mass axis orientation (deg)
0	50	181.322	0	1	13
0	50	61.9053	0	1	13
0	47	55.6001	0	0.85	13
0	38	46.4192	0	0.64	13
0	33	39.1646	0	0.5	13
0	29	39.1593	0	0.4	13
0	29	34.9637	0	0.3	9
0	29	33.0505	0	0.25	5.231

0	29	28.8502	0	0.22	3.045
0	29	24.6456	0	0.19	1.571
0	29	20.6347	0	0.17	0.509
0	29	17.386	0	0.15	-0.293
0	29	13.7565	0	0.13	-0.826
0	29	11.4634	0	0.12	-1.186
0	29	9.93529	0	0.12	-1.498
0	29	9.3618	0	0.115	-1.707
0	29	8.97998	0	0.11	-1.836
0	29	6.87808	0	0.11	-1.993
0	29	4.2034	0	0.11	-2.044

10.8.1.7 DIRECT DRIVE GENERATOR

It is proposed to use a variable speed permanent magnet synchronous generator (PMSG). These types of generator can achieve a lightweight compact design, which is one of the key considerations for any multi rotor space frame design.

Generator mass	1500	kg
Distance between generator and hub centres of	1.2	m
Inertia: about shaft	150	kgm²
Inertia: perpendicular to shaft	150	kgm²

10.8.1.8 NACELLE GEOMETRY

The nacelle drag coefficient is taken nominally to be 1.6, though this value will depend on the final shape of the nacelle and whether the nacelle is aerodynamically shaped. Ultimately it should not have noticeable bearing in the results.

Nacelle width	1.2	m
Nacelle length	2	m
Nacelle height	1.2	m
Nacelle drag coefficient	1.6	

10.8.1.9 NACELLE MASS

Nacelle mass	6500	kg
Nacelle centre of mass lateral offset	0	m
Nacelle centre of mass above tower top	0.702807	m
Nacelle centre of mass in front of tower axis	0	m
Yaw inertia (about tower axis)	9928.9	kgm²
Nodding inertia (about CoG)	0	kgm²
Rolling inertia (about CoG)	0	kgm²
Total Tower-head Mass	11285	kg
Total Yaw Inertia: 0° azimuth	94140.9	kgm²
Total Yaw Inertia: 90° azimuth	94140.9	kgm²

10.8.1.10 DRIVE TRAIN

Direct drive transmission		
Position of shaft brake	Low speed	(Gearbox End)
Generator inertia	100	kgm²
Gearbox inertia	0	kgm²
Low speed shaft	Flexible	

10.8.1.11 GENERATOR CHARACTERISTICS

Lowest rotational speed for the rotor and low-speed shaft is approximately 1 rad/s to achieve rated output.

Generator model	Variable	
Power electronics time constant	0	s
Maximum generator torque	460800	Nm
Minimum generator torque	0	Nm
Phase Angle	0	deg

10.8.1.12 ELECTRICAL LOSSES

Shaft power (kW)	Power loss (kW)
24.15	2.612
36.83	2.711
52.06	2.885
70.1	3.169
91.06	3.601
114.72	4.278
142.14	5.076
173.62	5.999
209.44	7.062
249.87	8.284
295.21	9.68
345.71	11.273
401.67	13.076
463.21	15.121
481.82	15.567
500	16.5

10.8.1.13 POWER PRODUCTION CONTROL

Variable Speed Pitch Regulated Controller	Dynamic	
Minimum generator speed	26.42	rpm
Optimal mode quadratic speed-torque gain	4562.5	Nms²/rad²
Optimal mode maximum generator speed	46.63	rpm
Generator torque set point	94030	Nm
Above-rated generator speed set-point	46.63	rpm
Minimum pitch angle	0	deg
Maximum pitch angle	90	deg

Pitch direction	to Feather	
Speed transducer time constant	0	s
Power transducer time constant	0	s
Maximum negative pitch rate	-8	deg/s
Maximum positive pitch rate	8	deg/s

10.8.1.14 PI TORQUE CONTROL

Controller values are simple placeholders defined by the auto-tune function in Bladed and therefore are in no way optimised for this system. This lack of tuning will ultimately lead to higher loads than perhaps otherwise possible. This is not considered an issue in the design phase whereby the structure will be designed to operate in as high a load as possible and where a negative impact on loading could be seen as adding a buffering region in terms of structural capacity.

Proportional gain	158249	Nms/rad
Integral gain	83248.5	Nm/rad
Desaturation time constant	0	s

10.8.1.15 GAIN SCHEDULE (gain divisor)

Constant value	1

10.8.1.16 PI PITCH CONTROL

Proportional gain	0.222774	s
Integral gain	0.171883	
Desaturation time constant	0	s

10.8.1.17 GAIN SCHEDULE PITCH (gain divisor)

Lookup Table based on	pitch
Pitch (rad)	Gain divisor
-0.017453	1
0.087266	1
0.610847	4.99643
1.5708	4.99643

10.8.1.18 NORMAL STOP CALCULATION

Pitch rate for stopping	6	deg/s
Final pitch angle	90	deg
Rotor speed for parking brake application	-100	rpm

10.8.1.19 EMERGENCY STOP CALCULATION

Emergency pitch trip mode	Grid loss	
Emergency pitch rate	12	deg/s

Final pitch angle	90	deg
Emergency brake trip mode	Grid loss	
Rotor speed for parking brake application	0	rpm

10.8.1.20 SHAFT BRAKE CHARACTERISTICS

Brake Number: 1

Note: The required braking torque from rated approximate 100kNm, the braking torque used for the simulation is 80% higher than this and therefore may be too high and so may exaggerate braking strength.

Maximum brake torque	181845	Nm
Shaft brake ramp time	1	s

10.8.1.21 SAFETY SYSTEM

Circuit number 1

Pitch action	Yes
Disconnect generator	No
Disconnect yaw drive	No
Apply shaft brake 1	No
Apply shaft brake 2	No
Apply shaft brake 3	No
Apply generator brake	No

Trip	Level	Delay	Circuit
Generator over speed	1650 rpm	0 s	1
Rotor over speed	51.295 rpm	0 s	1
Emergency pitch rate demand		6	deg/s

10.8.1.22 IDLING SIMULATION

Pitch angle for idling	90	deg
External controller	No	

10.8.1.23 PARKED LOADS SIMULATION

Pitch angle for parking	90	deg
Rotor azimuth when parked	0	deg
External controller	No	

10.8.1.24 PITCH ACTUATOR

External DLL	False	

Input Demand	Position	
Frequency (?)	0.9999992	Hz
Damping (?)	0.8	-
End Stops	False	
Limit Switches	True	
Bearing Friction	False	
Rate Limits	False	
Minimum	0	deg/s
Maximum	0	deg/s
Acceleration Limits	False	
Minimum	0	deg/s²
Maximum	0	deg/s²
Maximum	90	deg
Minimum	-2	deg
Individual Pitch Control	False	
Single Actuator	False	
Demand set by external controller	False	
Rate calculated according to	Constant	
Rate Demand	6.000002	deg/s
Minimum	0	
Maximum	0	
Actuator Drive Details	None	

10.9 APPENDIX D

Generator Side Full Load Fault Current:

Assumes: Y connected, 690V L-L, 0.9 p.f, P_{rated} = 444kW, S_{rated} = 493kVA, X = 0.15

$$I_{ph} = {S}/{V_L} = {P_{rated}}/{(\sqrt{3} \times V_L \times p.f)} = {444k}/{(\sqrt{3} \times 690 \times 0.9)} = 412.5A$$

$$Full\ Load\ Fault\ Current = {I_{ph}}/{X} = {412.5}/{0.15} = \mathbf{2750}\boldsymbol{A}$$

Transformer Secondary Full Load Fault Current:

Assumes: 690/6000 VAC, 0.9 p.f, S_{rated} = 2000kVA, X = 0.06

Single Stage… $I_{L-pri} = {S_{rated}}/{V_L} = {2000k}/{690} = 2898A$

Two Stage… $I_{L-pri} = {S_{rated}}/{V_L} = {500k}/{690} = 724A$

Single Stage… Primary Fault Current $= I_{L-pri} \times X = 2898 \div 0.06 = \mathbf{48.3kA}$

Two Stage… Primary Fault Current $= I_{L-pri} \div X = 724 \div 0.06 =$ **$12.06kA$**

$$N_P/N_S = V_P/V_S = 690/6000 = 0.115 = a$$

Single Stage… $I_{L-sec} = I_{L-pri} \times a = 2898 \times 0.115 = 333.3A$

Two Stage… $I_{L-sec} = I_{L-pri} \times a = 724 \times 0.115 = 82.36A$

Single Stage… Secondary Fault Current $= I_{L-sec} \div X = 333.3 \div 0.06 =$ **$5.55kA$**

Two Stage… Secondary Fault Current $= I_{L-sec} \div X = 82.36 \div 0.06 =$ **$1372.7A$**

10.10 APPENDIX E

DLC 1.2 Overview;

Fatigue loads are aggregated using Miners Rule over the full expected lifetime of the MRS. To achieve this requires the time-dependent load data for each degree of freedom to be binned/grouped together and weighted by the probability distribution of wind speed vs. time. To establish the appropriate load information, simulations must be run at various operational wind speeds and the results collated. It is possible to limit the number of runs to encompass only a few wind speed bins, for example every 4m/s from cut-in wind speed (normally this would be every 2m/s but limits to simulation time prevent this).

DLC 1.3 Overview;

The extreme turbulent model (ETM) encompasses high turbulence intensity coupled with normal operating wind speeds. Ideally this would be run at wind speed intervals in the same manner as DLC1.2 but examination of the rotor thrust curve shows that the peak loading will occur during the upper limit of operation (between rated speed and cut-out) and therefore turbulent simulations at both these mean speeds usually suffice.

Standard practice for a single rotor is to run 6 or more seeds per wind speed to ensure that a single favourable or unfavourable run does not unduly effect the design considerations and this is the approach taken in this instance. However, as the multi rotor already has an averaging effect (as the wind does not remain coherent over the whole array) there is an argument that this is not necessary. In addition, to reduce simulation time, the seeded runs will look at only look at a 1-minute ultimate wind speed disposition within a 10-minute turbulence file.

Key Simulation Parameters;

- Simulation Time: 60s, Wind Shear Exponent: 0.14, Rotor Azimuths: Equal
- Wind Speed: 11 m/s (6 seeds) & 25 m/s (6 seeds)
- Kaimal Spectrum Parameters; Longitudinal: 340.2m, Lateral: 113.4m, Vertical: 27.72m, Coherency: 340.2, Decay: 12.
- Wind Parameters; Y Points: 39, Z Points: 26, Y Width: 382.5m, Z Height: 350m, Time: 600s, F: 13.65Hz

DLC 1.4 Overview;

The extreme change of direction (ECD) simulation encompasses an extreme gust coinciding with a wind direction change. These two effects occur over a short time period (10.5 seconds) to cause a sharp spike in various loads throughout the rotor and tower. The effect of azimuth and rotor direction of rotation has a larger part to play when considering the effects of both a positive and negative direction change. This effect may be less noticeable on the smaller individual multi rotors and also due to the fact that in reality they would likely be counter rotating – offering some degree of symmetry whichever way yaw error occurs.

The whole system should perform a stop under the conditions of maximum yaw misalignment which is usually set according to individual wind speeds, with linear interpolation applied between the points. For example;

Wind Speed	0	5	10	35
Yaw Error	60	60	45	30

Key Simulation Parameters;

- Simulation Time: 45s, Wind Shear Exponent: 0.14, Rotor Azimuths: Equal
- Wind Speed: 11 m/s, Gust speed: +6.67m/s, Start Time: 30s, Period: 10.5s
- Wind Direction: 0 deg, Direction Change: +65.45 deg, Start Time: 30s, Period: 10.5s
- Normal Stop: 6.79s seconds into event.

DLC 2.3 Overview;

The extreme operating gust case is similar to the ECD case of DLC1.4 but without a direction change. Instead it is assumed that there is an electrical fault (causing emergency shutdown) during the transient period of the gust that combines to cause increased loading on the structure. The equation that determines the gust shape (second order Gaussian probability) causes the 'Mexican hat' form meaning that there is a reduction of wind speed immediately preceding and following the maximum spike. By phasing the point at which the fault occurs in relation to the gust, various potential for maximum loading can be evaluated.

Key Simulation Parameters;

- Simulation Time: 45s, Wind Shear Exponent: 0.14, Rotor Azimuths: Equal
- Wind Speed: 11 m/s, Gust speed: +6.67m/s, Start Time: 30s, Period: 10.5s
- Wind Direction: 0 deg
- Emergency Stop: 0s, 2.45s, 4s & 5.35s into gust

DLC 4.2 Overview;

DLC4.2 refers to a normal stop under an extreme operating gust. There are two instances in which such a condition might occur; either the localised wind speed exceeds a pre-defined maximum causing the stop logic within the controller to initiate a stop or the coincidental planned or unplanned stoppage of a wind turbine during an unpredictable extreme gust. In both conditions the controller is designed to operate in such a way as to minimize loading on the rotor and thereby avoid any potential damage.

The coincidence of a normal stop with an extreme operating gust is one that can normally be avoided if the control system has measurement of the incident wind field. However, the standard dictates that the rotor and structure should still be designed to cope with such a load case.

DLC4.2 has the essentially the same simulation parameters as DLC2.3 but utilising a normal stop as opposed to emergency stop. In this load case the control requirement is less demanding and therefore designed to reduce loading.

Key Simulation Parameters;

- Simulation Time: 45s, Wind Shear Exponent: 0.14, Rotor Azimuths: Equal
- Wind Speed: 11 m/s, Gust speed: +6.67m/s, Start Time: 30s, Period: 10.5s
- Wind Direction: 0 deg

Emergency Stop: 0s, 2.45s, 4s & 5.35s into gust

DLC 6.1 Overview;

The 50-year gust is an event that has such low probability that it may occur on average once every 50 years. It is commonly assumed that over a typical turbine lifespan of 20 years the chances of the 50-year gust occurring during another major fault or extremely unfavourable event are almost negligible and for all intents and purposes the combination of the two need not be designed for. Instead, the design standard dictates that the only other condition that need be met is a yaw misalignment of plus or minus 15 degrees.

Key Simulation Parameters;

- Simulation Time: 65s, Wind Shear Exponent: 0.14, Rotor Azimuths: Equal
- Wind Speed: 70 m/s, Event Start Time: 30s, Period: 10.5s
- Starting Yaw: 0 deg, Yaw Misalignment: -+15 deg

DLC 6.2 Overview;

The second case of the 50-year gust assumes that the yaw system is non-operational. In the case of a single rotor this would usually be a result of grid loss – though in the multi rotor on a water bearing the effect of such a condition is less clear. The standard dictates that the extreme wind may come from other unfavourable yaw angles and that the system may be aligned unfavourably. As such the simulation is run at various points around a full 360 degrees around the structure. In this case only the negative angles are shown as these represent higher ultimate loading than positive angles - as discussed in the previous section.

Key Simulation Parameters;

- Simulation Time: 90s, Wind Shear Exponent: 0.14, Rotor Azimuths: Equal
- Wind Speed: 70 m/s, Start Time: 20s, Period: 10s
- Wind Direction: 0 deg, Wind Change: -45, -60, -90, -120, -180 deg

DLC 6.3 Overview;

The final simulation of DLC6.3 is a 1 year gust of 50m/s coinciding with an extreme yaw misalignment which in this case is considered to be +- 30 degrees. This simulation, which on its basis would appear to be less impactful than DLC6.2 is included for completeness.

Key Simulation Parameters;

- Simulation Time: 65s, Wind Shear Exponent: 0.14, Rotor Azimuths: Equal
- Wind Speed: 50 m/s, Start Time: 30s, Period: 10.5s

Wind Direction: 0 deg, Wind Change: -+30 deg

10.11 APPENDIX F

Wind Farm Overview	
Number of Turbines	45
Wind Farm Life (Yrs)	20
Wind Turbine Rating (kW)	444.17
Total Failure Rate (excl. remote resets)	4.63
CTV Travel Distance to Wind Farm (km)	10.18

Resources Overview	
Number of CTVs	2.00
Number of Staff	24
Helicopter Used	No

Availability and Production Overview	
Availability Absolute	95.97%
Availability Exluding Scheduled Maintenance	97.34%
Availability OEM Responsibility	99.72%
Power Produced (MWhr)	2.00E+06
Power Lost Due to Downtime (MWhr)	8.44E+04

	Units	MWhr
	Currency	£
Costs Overview	(m£)	(£/MWhr)
Lost Revenue	7.6	3.79
Transport Costs	26.2	13.07
Staff Costs	38.4	19.16
Repair Costs	21.0	10.50
Fixed Costs	0.0	0.00
Total O&M Costs	93.2	46.52
Total Direct O&M Costs	85.6	42.73

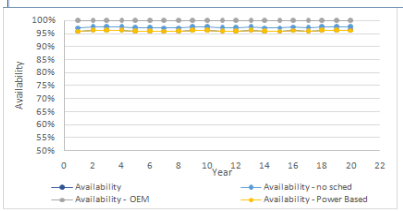

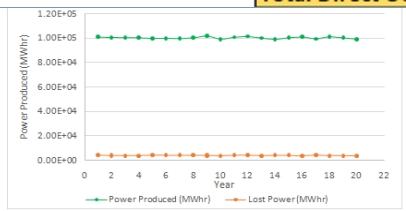

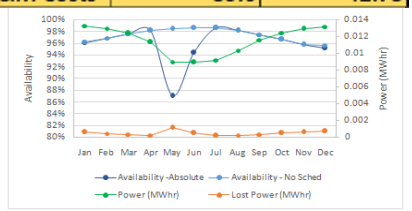

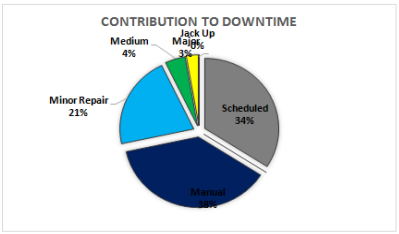

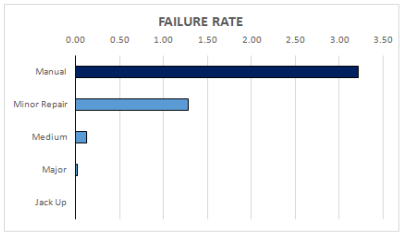

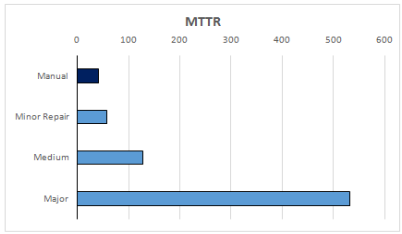

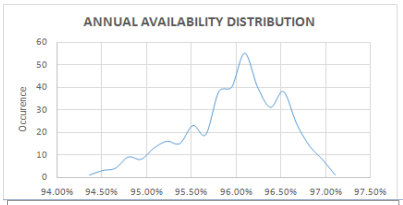

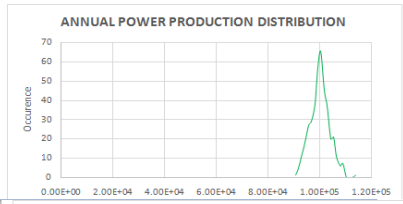

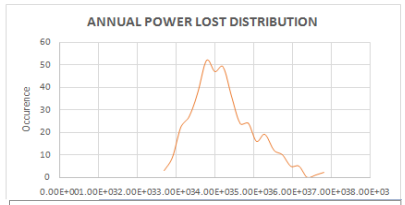

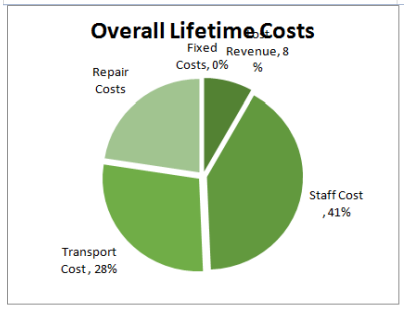

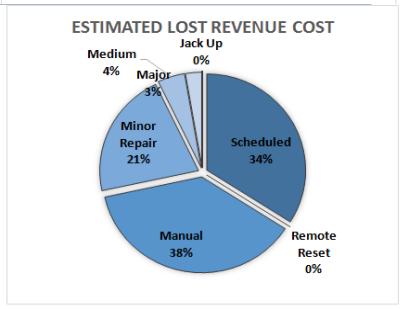

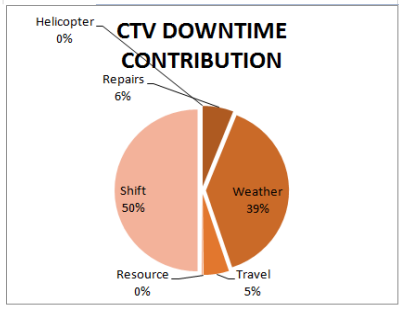

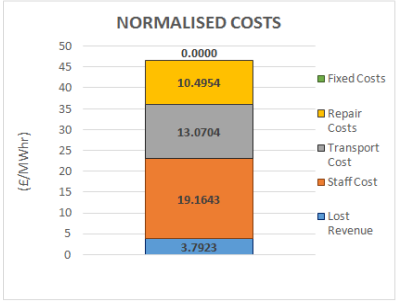

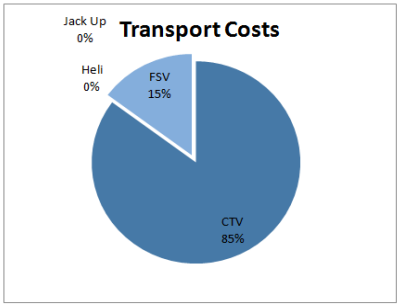

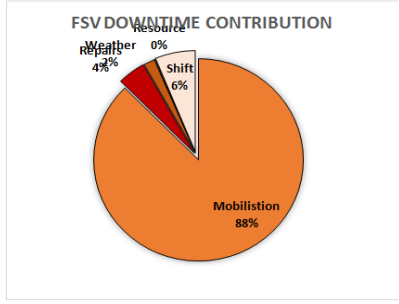

Figure 0.4: 20MW MRS Pessimistic (Scale Factor: 0.433)

Wind Farm Overview	
Number of Turbines	45
Wind Farm Life (Yrs)	20
Wind Turbine Rating (kW)	444.17
Total Failure Rate (excl. remote resets)	3.25
CTV Travel Distance to Wind Farm (km)	10.18

Resources Overview	
Number of CTVs	2.00
Number of Staff	24
Helicopter Used	No

Availability and Production Overview	
Availability Absolute	96.81%
Availability Exluding Scheduled Maintenance	98.18%
Availability OEM Responsibility	99.80%
Power Produced (MWhr)	2.02E+06
Power Lost Due to Downtime (MWhr)	6.39E+04

	Units	MWhr
	Currency	£
Costs Overview	(m£)	(£/MWhr)
Lost Revenue	5.8	2.85
Transport Costs	24.6	12.18
Staff Costs	38.4	19.03
Repair Costs	19.5	9.67
Fixed Costs	0.0	0.00
Total O&M Costs	**88.2**	**43.74**
Total Direct O&M Costs	**82.5**	**40.89**

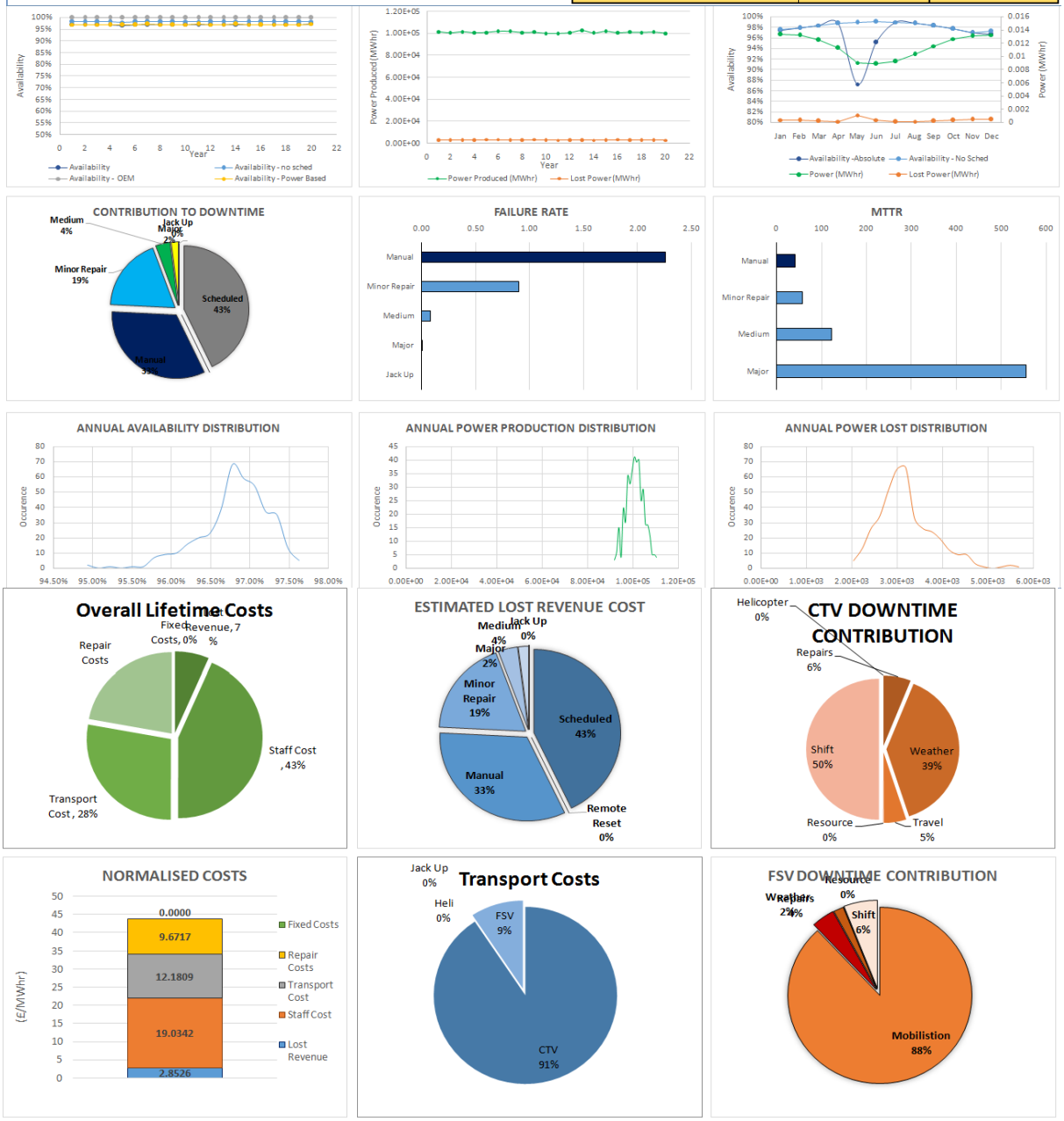

Figure 0.5: 20MW MRS Standard (Scale Factor: 0.3)